Electrospun Scaffolds to Promote Tendon Tissue Regeneration in Rotator Cuff Tears

A dissertation submitted to the University of Oxford in partial fulfilment of the requirements for the degree of

Doctor of Philosophy



Edward Thomas Stace

Balliol College
Nuffield Department of Orthopaedics, Rheumatology and Musculoskeletal Science
University of Oxford
Trinity Term 2018

Supervisors: Professor Andrew Carr, Associate Professor Stephanie Dakin, and Associate Professor Sarah Snelling

Declaration

I certify that this thesis is a true and honest account of my own research, which was conducted ethically and the results obtained are genuine. Where I have drawn on the work, ideas, and results of others, this has been appropriately acknowledged in the thesis.

Edward Thomas Stace

Abstract

Improving rotator cuff repair outcomes is an important unmet healthcare need. Rotator cuff tear surgical outcomes have not improved despite the development of advanced biomaterials and surgical techniques in the last few decades. Biomaterials used in repair have generally been adopted from use in other tissues, not tested and developed for the specific needs of human rotator cuff disease.

The aim of this thesis was to investigate biomimetic, synthetic, polydiaxanone electrospun scaffolds specifically in the context of rotator cuff disease. The thesis hypothesises that electrospun scaffolds replicating native fibrous tendon ECM structures will promote tendon fibroblast attachment, proliferation and result in increased matrix deposition. It also hypothesises that biomimicry will induce immune cell responses conducive to tendon healing.

This study reveals important results for the future design and evaluation of biomaterials for tendon and other tissues.

Firstly, polymer and electrospinning parameters were investigated to ensure repeatable, homogenous fibre production. Polydiaxanone supplier, batch and resin storage conditions had significant effects on electrospun fibres. Whilst fibre diameter and alignment could be rescued through electrospinning parameter modification, the different polymer chemistry and altered parameters required to produce scaffolds from degraded resin potentially creates scaffolds with differential biological effects.

Secondly, diseased tendon fibroblasts exhibit significant differences in attachment, proliferation and gene expression when cultured on electrospun fibres compared to healthy tendon fibroblasts. Biomaterial evaluation using fibroblasts from diseased tendon will lead to more applicable results and development of more appropriate treatments.

Thirdly, although the response of tendon fibroblasts to different scaffold configurations was relatively blunted for both healthy and diseased phenotypes, in contrast biomimetic fibre diameters resulted in significant differences in immune cell attachment, which may be advantageous for tissue regeneration.

Finally, adsorbed protein coronas on the scaffold surface can be functionalised to further direct immune cell and to a lesser extent, tendon fibroblast responses.

In conclusion, the relative sensitivity of immune cell populations to biomimetic materials opens a novel immunomodulation strategy for biomaterial augmentation of rotator tendon cuff repair. Future work should explore the relationship between immune cell populations and tendon fibroblasts as a strategy to promote endogenous healing and improved patient outcomes.

Acknowledgements

Word says there are 392,571 characters in this thesis. There are also probably 392,571 characters who've left their mark on it but aren't actually in it. Thanking everyone who has been part of this thesis and my journey through Oxford in one page is tough. I have truly been surrounded by incredible, supportive and clever people. This work is as much yours as it is mine. I couldn't have done it without you.

The Carr group is a fantastic place to be doing research. This starts at the top. Prof, you've been supportive, understanding and encouraging in the right ways at the right times. Sarah and Steph, how you've managed to put up with me I don't know, but, I do know I wouldn't have been able to put up with my DPhil without you. To everyone else, Pierre, Tonia, Hayley, Jo, Bridget, Kim, Anne, Louise, Lucy, Rich, Henry, Wataru, Muzzy, Roxanna, Nav, Jolet and Mat, thank you for making the Botnar home.

To the Trans-Siberian crew who started it all, to my flatmates in the Crowded House, in the Eagles Nest and Charlie, Chris and Sara, to OULRC who took an eighth of me, to OUBC who built it back on and to OUCCC who gave me an excuse to run from my thesis, to Balliol, to the Rhodes Trust, to the staff and students at the Botnar, the NOC and LIMA, and to all the friends who fit into the puzzle in some other way, thank you.

As always, my family have been beside me, reading things they don't understand but being entirely supportive anyway. What I wrote in my Rhodes application 6 years ago is still true, it is your support and guidance that has got me here.

I really have, at times, put all of my heart and all of my head into this thesis and I am proud of what I have achieved. Sadly, it seems these parts of me cannot repair rotator cuff tears. Fortunately, there are smarter, better scientists who will continue to look for treatments to improve the lives of people suffering from rotator cuff tears. To the Carr group of now and in the future I wish you good luck and good results! After all, I need you to succeed, all the pipetting has definitely given me some sort of tendinopathy.

I may not be leaving with a first, a full blue or a wife, but a DPhil, two and a half half blues and a girlfriend who'll move to the other side of the world for you isn't too bad.

Thank you Oxford, it's been a blast.

Contents

Declaration ..... **ii**

Abstract ..... **iii**

Acknowledgements ..... **iv**

Contents ..... **v**

Chapter 1 Introduction **1**

1.1 Overview 1

1.2 The significance of rotator cuff tears 1

1.3 The structure and function of the rotator cuff 2

1.3.1 Anatomy of the shoulder and rotator cuff 2

1.3.2 Structure of rotator cuff tendon 4

1.3.3 The enthesis 9

1.4 Rotator cuff tendon response to injury 10

1.5 Rotator cuff tendinopathy and tears 11

1.6 Rotator cuff tear treatment 15

1.6.1 Non-surgical rotator cuff tear treatment 15

1.6.2 Surgical rotator cuff tear treatment 16

1.7 Biomaterials currently available for augmenting rotator cuff tear repair 18

1.7.1 Biologic patches 18

1.7.2 Synthetic patches 19

1.7.3 Biosynthetic patches 20

1.7.4 Rotator cuff tear treatment summary 20

1.8 Ideal biomaterial properties for augmenting rotator cuff tear repair 21

1.9 Targeting cell-material interaction 23

1.9.1 Mechanisms of cell-material interaction 24

1.9.2 Biophysical cues used to influence cell-material response 26

1.9.3 Biomaterial fabrication strategies that allow tuning of biophysical cues 26
1.10 Electrospinning 28
1.10.1 Introduction and background 28
1.10.2 The electrospinning system 29
1.10.3 The electrospinning process 30
1.10.4 Electrospinning balances electrostatic force and surface tension 32
1.10.5 Advances in electrospinning 35
1.10.6 Polydioxanone storage conditions and breakdown 43
1.10.7 Summary 44
1.11 Current electrospun materials for rotator cuff tear repair and tendon tissue engineering 45
1.12 Electrospun fibre effects on cell populations involved in tendon healing .. 47
1.12.1 Tendon fibroblast response to electrospun fibres 48
1.12.2 Tendon progenitor stem cell population response to electrospun fibres 51
1.12.3 Immune cell population response to electrospun fibres 51
1.12.4 Endothelial cell response to electrospun fibres 53
1.12.5 Summary of cell responses to electrospun fibres 54
1.13 Summary 55
1.14 Aims 56
1.15 Hypotheses 57
Chapter 2 Fabrication of biomimetic electrospun scaffolds 58
2.1 Abstract 58
2.2 Introduction 58
2.3 Aims 59
2.4 Hypotheses 59
2.5 Materials and methods 60

2.5.1 Electrospinning protocol 60
2.5.2 Homogeneity within electrospun scaffolds 63
2.5.3 Consistency of electrospun scaffolds produced from the same solution 63
2.5.4 Consistency of electrospun scaffolds produced from different solutions of the same concentration 64
2.5.5 PDO supplier effects on electrospun fibre fabrication 64
2.5.6 PDO batch effects on electrospun fibre fabrication 64
2.5.7 PDO resin storage effects on electrospun fibre fabrication 64
2.5.8 Fibre diameter optimisation 67
2.5.9 Fibre alignment optimisation 67
2.5.10 Pyridine effect on electrospun fibre fabrication 68
2.5.11 Final electrospun biomimetic scaffold production parameters 69
2.5.12 Effect of altered fibre diameter and alignment on scaffold surface roughness and local mechanical properties 70
2.5.13 Scaffold porosity, pore size and thickness characterisation 70
2.5.14 Scaffold statistical analysis 71
2.6 Results 72
2.6.1 Homogeneity and consistency of electrospun scaffolds 72
2.6.2 PDO supplier effects on electrospun scaffold fabrication 77
2.6.3 PDO batch effects on electrospun scaffold fabrication 77
2.6.4 PDO resin storage condition effects on electrospun fibre fabrication 78
2.6.5 Fibre diameter optimisation 82
2.6.6 Fibre alignment optimisation 84
2.6.7 Pyridine effect on electrospun scaffold fabrication 86
2.6.8 Biomimetic electrospun scaffolds used for *in vitro* experiments 89
2.6.9 Evaluation of electrospun fibre roughness and local mechanical properties 90

2.6.10 Scaffold porosity and pore size characterisation 90
2.7 Discussion 91
2.7.1 Consistency and homogeneity of electrospun scaffolds 91
2.7.2 Parameter effects on electrospun scaffolds in a purpose-built electrospinning set up 96
2.7.3 Pyridine effect on electrospun scaffold fabrication 97
2.7.4 Final biomimetic scaffold production 98
2.8 Conclusions 100
Chapter 3 Biophysical effects of electrospun fibres on tendon fibroblast and peripheral blood mononuclear cell biology 102
3.1 Abstract 102
3.2 Introduction 102
3.3 Aims 104
3.4 Hypotheses 104
3.5 Materials and methods 105
3.5.1 Electrospun scaffold fabrication and preparation 105
3.5.2 Tendon fibroblast acquisition, expansion and assessment 106
3.5.3 Effect of fibre alignment on healthy tendon fibroblasts 110
3.5.4 Effect of fibre diameter on tendon fibroblasts derived from healthy and diseased tendon 111
3.5.5 Peripheral Blood Mononuclear Cell response to electrospun scaffold diameter 112
3.5.6 Statistical analyses 115
3.6 Results 116
3.6.1 Effect of fibre alignment on tendon fibroblasts from healthy tendon 116
3.6.2 Effects of fibre diameter on tendon fibroblasts derived from healthy and diseased tendon 121

3.6.3 Effects of fibre diameter on PBMCs 129
3.7 Discussion 134
3.7.1 Fibre alignment supports tendon fibroblast proliferation, morphology and matrix gene expression 135
3.7.2 Tendon fibroblast response to electrospun fibre diameter is more dependent on disease phenotype than fibre diameter 138
3.7.3 Electrospun fibre diameter affects PBMC sub-population attachment 144
3.8 Conclusions 146
Chapter 4 Functionalisation of electrospun scaffolds through modulation of the adsorbed protein corona 148
4.1 Abstract 148
4.2 Introduction 148
4.3 Aims 151
4.4 Hypotheses 151
4.5 Materials and methods 152
4.5.1 Electrospun fibre diameter and alignment effects on protein corona formation 152
4.5.2 Characterisation of protein coronas formed through functionalisation of electrospun fibres with different biological fluids 154
4.5.3 Tendon fibroblast response to electrospun fibres functionalised through biological fluid treatment 154
4.5.4 PBMC response to electrospun fibres functionalised through biological fluid treatment 156
4.5.5 Statistical analysis 157
4.6 Results 158
4.6.1 Electrospun fibre diameter and alignment effects on protein corona formation 158

4.6.2 Biological fluid treatment effects on protein corona formation 166
4.6.3 Biological fluid functionalisation effects on healthy and diseased tendon fibroblasts 169
4.6.4 Biological fluid functionalisation effects on PBMC populations 174
4.7 Discussion 178
4.7.1 Protein corona formation on electrospun fibres is affected by mean fibre diameter 179
4.7.2 Diameter dependent protein corona results in the context of previous tendon fibroblast and PBMC experiments 182
4.7.3 Electrospun scaffold biological fluid functionalisation effects on tendon fibroblast and PBMC populations 184
4.8 Conclusions 189
Chapter 5 Discussion 191
5.1 Overview 191
5.2 Thesis aims and hypotheses 191
5.3 The significance of rotator cuff tendon tears 193
5.4 The potential of electrospun scaffolds as biomaterials for rotator cuff repair 194
5.5 Biophysical parameters of electrospun fibre scaffolds can regulate cell biology but this regulation is dependent on cell type and cell disease state 197
5.6 Biological fluid adsorption creates unique protein coronas on electrospun scaffolds capable of modulating tendon fibroblast and PBMC-scaffold interactions 200
5.7 Limitations 203
5.8 Future work 204
5.9 Implications of this thesis 205
5.10 Summary 206
Chapter 6 References 208
Chapter 7 Appendices 225

Appendix A: Additional information for Chapter 2 225

Appendix B: Additional information for Chapter 3 227

Appendix C: Additional information for Chapter 4 231

Appendix D: List of suppliers 235

List of Figures xii

List of Tables xvii

Abbreviations xviii

List of Figures

Figure 1-1. Significant anatomical features of the right shoulder 3

Figure 1-2. Structure of the rotator cuff of the right shoulder 4

Figure 1-3. The hierarchical structure of tendon provides significant mechanical strength 6

Figure 1-4. The specialisation of layers of rotator cuff tendon 7

Figure 1-5. The structure of the enthesis 10

Figure 1-6. Tendon healing is a complicated, tightly regulated process 13

Figure 1-7. Characteristic changes observed in diseased tendon matrix 14

Figure 1-8. Schematic depicting rotator cuff tears and selected biomaterial repair strategies 17

Figure 1-9. SEM images comparing the structure of tendon ECM, synthetic and biologic scaffolds 18

Figure 1-10. Schematic depicting how the changing scale of biophysical features can affect cell-material interaction 25

Figure 1-11. SEM images of tendon ECM and electrospun fibres 27

Figure 1-12. Number of articles published by year relating to electrospinning ... 29

Figure 1-13. Schematic depiction of a simple electrospinning circuit and a commercial electrospinning device 30

Figure 1-14. Schematic depiction of the stages of the electrospinning process 32

Figure 1-15. SEM images showing the effect of electrostatic force and surface tension balance on resultant electrospun fibres 33

Figure 1-16. μCT images of multi-filament yarn and simple extruded suture 39

Figure 1-17. Schematic depiction of a complex electrospinning system used to produce multi-zoned scaffolds for ligament repair 41

Figure 1-18. The BioPatch biomaterial for rotator cuff repair 46

Figure 1-19. The interplay between biomaterials and cell populations governs the tendon healing response after injury and biomaterial implementation 55

Figure 2-1. ImageJ measurement protocol of fibre diameter and angle 62

Figure 2-2. Homogeneity of electrospun fibres from different areas within the same scaffold..... 73

Figure 2-3. Consistency of electrospun scaffolds produced from the same solution over consecutive weeks..... 74

Figure 2-4. Consistency of electrospun fibres produced from different PDO solutions of the same concentration..... 76

Figure 2-5. Effect of PDO supplier on electrospun fibre fabrication..... 77

Figure 2-6. Effect of PDO batch on electrospun scaffold fabrication 78

Figure 2-7. The effects of resin storage conditions over time on electrospun fibre diameter 80

Figure 2-8. The relationship between PDO concentration with diameter and viscosity of control solutions..... 81

Figure 2-9. Change in PDO crystallinity of PDO resin stored in different conditions over 6 months 82

Figure 2-10. Effect of selected influential parameters on electrospun fibre diameter 83

Figure 2-11. Effect of temperature and humidity on electrospun fibre diameter. 84

Figure 2-12. Effect of collector speed on fibre alignment..... 85

Figure 2-13. Effect of voltage on electrospun fibre alignment 86

Figure 2-14. Effect of pyridine on electrospun fibre diameter, alignment and distribution width..... 87

Figure 2-15. Effect of pyridine concentration on electrospun fibre diameter and scaffold morphology 88

Figure 2-16. The 5 scaffolds produced for subsequent *in vitro* experiments 89

Figure 2-17. Reproducibility of the 5 scaffolds produced over 3 years for *in vitro* evaluations..... 90

Figure 3-1. Electrospun scaffolds with random and aligned fibres were fabricated with conserved mean fibre diameters..... 117

Figure 3-2. Healthy fibroblast attachment rates to random and aligned

electrospun scaffolds were similar but notably lower compared to TCP..... 118

Figure 3-3. Metabolic activity increased for healthy tendon fibroblasts cultured on random and aligned scaffolds more than on TCP 119

Figure 3-4. Aligned electrospun scaffolds promote an elongated morphology more than random scaffolds and TCP after 7 days culture..... 120

Figure 3-5. Fold change in gene expression differs for tendon fibroblasts cultured on random and aligned electrospun fibres for 7 days 121

Figure 3-6. Fibre diameter and alignment were conserved across the 3 scaffolds used to assess healthy and diseased tendon fibroblast response to changes in diameter 122

Figure 3-7. Attachment to electrospun scaffolds is dependent on fibroblast disease phenotype but not fibre diameter 123

Figure 3-8. Metabolic activity increased significantly over 21 days culture for fibroblasts derived from diseased tendon compared to healthy tendon on electrospun scaffolds irrespective of fibre diameter..... 124

Figure 3-9. Morphology of fibroblasts from healthy tendon after 14 days culture on electrospun fibre scaffolds of 300nm, 1000nm and 4000nm diameters..... 125

Figure 3-10. Fold change in gene expression for tendon fibroblasts after 14 days culture on electrospun scaffolds is different for fibroblasts derived from healthy compared to diseased tendon 126

Figure 3-11. Fold change in gene expression changes after 14 days for healthy and diseased tendon fibroblasts cultured on electrospun fibres of different diameters..... 127

Figure 3-12. *IL6* fold change in expression for tendon fibroblasts derived from healthy versus diseased tendon over 21 days culture on different diameter electrospun scaffolds 128

Figure 3-13. Fold changes in the expression of selected cell attachment genes was similar for healthy and diseased fibroblasts cultures on electrospun scaffolds for 24 hours 129

Figure 3-14. Fold changes in inflammatory gene expression was not significantly

influenced by diameter for PBMCs seeded on electrospun scaffolds for 24 hours 131
Figure 3-14. PBMC flow cytometry gating strategy 132
Figure 3-15. Graphs of selected PBMC populations showing fibre diameter dependent cell attachment of PBMCs over 24 hours. 134
Figure 4-1. Electrospun scaffolds used to examine fibre diameter and alignment effects on protein corona formation. 159
Figure 4-2. Stacking of electrospun fibres distorts scaffold morphology 160
Figure 4-3. Overlay of the intensity of proteins detected on serum adsorbed aligned, 1000nm electrospun scaffolds and a reference protein database 162
Figure 4-4. Principal component analysis of protein coronas formed on electrospun scaffolds with different mean diameters 163
Figure 4-5. Heat map of proteins detected at significantly different intensities in protein coronas formed on electrospun scaffolds of different mean diameters 165
Figure 4-6. Principal component analysis of proteins from blood, serum, plasma and synovial fluid and the resultant protein coronas formed on adsorption to identical 1000nm, aligned electrospun scaffolds. 167
Figure 4-7. Heat map of proteins detected at significantly different intensities in the coronas formed through incubation of electrospun scaffolds in biological fluids. 168
Figure 4-8. Attachment rates of tendon fibroblasts from healthy and diseased tendon to electrospun scaffolds functionalised with coronas adsorbed from different biological fluids 170
Figure 4-9. Metabolic activity of tendon fibroblasts isolated from healthy tendon and diseased tendon on electrospun scaffolds functionalised with coronas adsorbed from different biological fluids 171
Figure 4-10. Fold changes in gene expression of tendon fibroblasts cultured for 7 days on electrospun scaffolds functionalised with coronas adsorbed from different biological fluids 173

Figure 4-11. Fold changes in gene expression of PBMCs cultured for 24 hours on electrospun scaffolds functionalised with biological fluids..... 175

Figure 4-12. Plots of selected PBMC sub-populations following culture on electrospun scaffolds functionalised with biological fluids over 24 hours 177

Figure 5-1. Rotator cuff tendon response to implanted electrospun biomaterials is dependent on biophysical cues, biochemical stimuli and multiple cell populations 207

Figure A-1. The effects of PDO resin storage conditions on solution viscosity over time 225

Figure B-1. Tendon fibroblasts derived from diseased tendon display increased metabolic activity when cultured on TCP compared to fibroblasts from healthy tendon..... 227

Figure B-2. The fold change in gene expression is different for tendon fibroblasts derived from healthy and diseased tendon on TCP after 14 days culture..... 228

Figure B-3. Gene expression changes for tendon fibroblasts from healthy and diseased tendon cultured for 21 days on different diameter electrospun ... 229

Figure B-4. Accutase lifting efficacy of PBMCs from electrospun fibre scaffolds 230

Figure C-1. Heat map of proteins detected at significantly different intensities in the coronas formed through treatment of electrospun scaffolds in biological fluids 231

Figure C-2. Fold changes in gene expression of PBMCs cultured on electrospun scaffolds functionalised with biological fluids for 4 hours 234

List of Tables

Table 1-1. Biophysical cues used to manipulate cell biology 26

Table 1-2. System and process parameters modulated in electrospinning to affect fibre diameter, alignment and topography 34

Table 2-1. Electrospinning parameters used to fabricate scaffolds for homogeneity experiments 63

Table 2-2. Parameters used for the electrospinning of scaffolds from PDO stored in different conditions 65

Table 2-3. Electrospinning parameters and the tested range of each parameter to determine the effect on electrospun fibre diameter 67

Table 2-4. Final electrospinning parameters for electrospun scaffolds used in the *in vitro* experiments of this thesis 69

Table 3-1. Assays used to assess the effects of alignment on healthy tendon fibroblasts 111

Table 3-2. Assays used to assess the effects of diameter on tendon fibroblasts isolated from healthy and diseased tendon 112

Table 3-3. Antibodies used for PBMC flow cytometry experiments 115

Table 3-4. Summary statistics of the fibre diameter and alignment of the electrospun scaffolds used to assess PBMC responses to electrospun scaffolds 130

Table A-1. The effects of electrospinning parameters on fibre diameter 226

Table B-1. Primer sequences used for gene expression analysis 227

Abbreviations

ADLs	Activities of Daily Living
AFM	Atomic Force Microscopy
μCT	Micro-Computer Tomography
D10	DMEM/F12 with 10% FBS and 1% PS
D50	DMEM/F12 with 50% FBS and 1% PS
DMEM/F12	Dulbecco's Modified Eagle Medium: Nutrient Mixture F-12
DSC	Differential Scanning Calorimetry
ECM	Extra-Cellular Matrix
EMA	European Medicines Agency
EU	European Union
FBS	Fetal bovine serum
FDA	Food and Drug Administration (US)
FSC-A	Forward Scatter Area
FSC-H	Forward Scatter Height
FTIR	Fourier Transformation Infra-Red spectroscopy
GAG	Glycosaminoglycan
HFIP	1,1,1,3,3,3-Hexafluoro-2-propanol
ISO	International Standards Organisation
LTE	Low Temperature Electrospinning
MFR	Melt Flow Rate
NSAIDs	Non-Steroidal Anti-Inflammatory Drug
PBMC	Peripheral Blood Mononuclear Cell
PBS	Phosphate Buffered Saline
PCL	Polycaprolactone
PDO	Polydioxanone
PLGA	Poly(lactic-co-glycolic acid)
PLLA	Polylactic acid
PMA	Pre-Market Approval
PRP	Platelet Rich Plasma

PS	Penicillin-streptomycin
PU	Polyurethane
PVA	Polyvinyl alcohol
RCT	Rotator Cuff Tear
cRPMI	RPMI supplemented with 10% FBS, 1% PS and 2mM L-glutamine
RPMI	Rosewell Park Memorial Institute 1640 media
SEM	Scanning Electron Microscopy
SIS	Small Intestine Submucosa
SPM	Scanning Probe Microscopy
SSC-A	Side Scatter Area
SSC-H	Side Scatter Height
SSC-W	Side Scatter Width
TCP	Tissue Culture Plastic
TERM	Tissue Engineering and Regenerative Medicine
UK	United Kingdom
USA	United States of America
XRD	X-Ray Powder Diffraction

Chapter 1 Introduction

1.1 Overview

This chapter has three aims:

I. To highlight the burden of rotator cuff tendon disease, and investigate the limitations of biomaterials currently used to augment surgical repair,

II. To consider the key characteristics of an ideal biomaterial tailored for repairing torn rotator cuff tendons,

III. To review the current knowledge of cell-material interactions with electrospun scaffolds.

1.2 The significance of rotator cuff tears

Rotator Cuff Tears (RCTs) are a globally significant cause of shoulder pain, reduced work capability and barrier to Activities of Daily Living (ADLs). Whilst, not every patient with a RCT will progress to surgery, pain and disability from RCTs result in more than 300,000 repair operations in the United States of America (USA) and 10,000 in the United Kingdom (UK) annually [1]. In the UK, surgical repair rates increased by 500% from 2001 to 2010 [2]. As RCTs affect 15% of 60 year olds and up to 50% of 80 year olds [3,4], the demographic shifts expected from an ageing population will only exacerbate the burden of RCT related pain, disability and surgery [5,6]. This pressure on health services is magnified by the rising cost of RCT surgery, with a 300% increase occurring between 2001 and 2013 alone [7].

The detail of RCT repair surgery is covered in section 1.6.2 (Surgical rotator cuff tear treatment). At this stage, it is sufficient to highlight that such surgery involves using sutures and scaffolds to promote reattachment of the torn tendon to the bone. However, recent

research has cast doubt on the effectiveness of such RCT operations, suggesting surgical treatment fails in 40% of patients within 12 months of treatment [8]. Depending on the population undergoing surgery, this failure rate has been reported to be as high as 94% [9]. Failed repair and re-tearing are correlated with poor functional outcomes [10]. In contrast, less than 5% of patients undergoing total hip replacement will experience implant failure within 10 years of implantation [11]. RCT repair outcomes are evidently significantly worse compared to other biomaterial-treated conditions.

Whilst the reasons for the low success rates of RCT surgery are multifactorial, a major concern addressed in this thesis, is that the biomaterials currently used to facilitate RCT repair are inadequate [3], as discussed in section 1.7 (Biomaterials currently available for augmenting rotator cuff tear repair). Despite the considerable research and numerous advances in surgical materials and surgical techniques over a 30 year period from 1980 to 2012, surgeons and researchers have failed to improve the rate of successful surgical outcomes [12].

RCTs already cause significant pain, disability and strain on health systems. Present conservative and surgical treatment strategies are ineffective in ensuring acceptable long-term patient outcomes. Changing population demographics and increased treatment expectations will only further increase the burden of RCTs in the future [13,14]. These pressures drive the urgent development of superior RCT treatments to mitigate the costs, both financial and physical, for individuals, clinicians, and health systems.

1.3 The structure and function of the rotator cuff

1.3.1 Anatomy of the shoulder and rotator cuff

The human shoulder has evolved to perform complex, coordinated upper limb movements in a number of planes. The shoulder comprises four joints: the acromioclavicular joint, the sternoclavicular joint, the scapulothoracic joint and the glenohumeral joint (Figure 1-1).

The glenohumeral joint is the main articulating surface of the shoulder and the site of rotator cuff action. At this joint, there is low bony congruence between the humerus and glenoid fossa in order to enable the wide range of motion needed at the shoulder [15]. However, to maintain shoulder stability and ensure the humerus is not displaced during movement, a number of soft tissue structures have developed. These include a fibrocartilaginous labrum to increase the articular surface without the concrete restriction of bone tissue, extensive ligaments to limit excessive movement, and specialised muscles to actively stabilise the shoulder in multiple planes of movement. These specialised muscles are collectively termed the rotator cuff and are the most important contributor to shoulder stability.

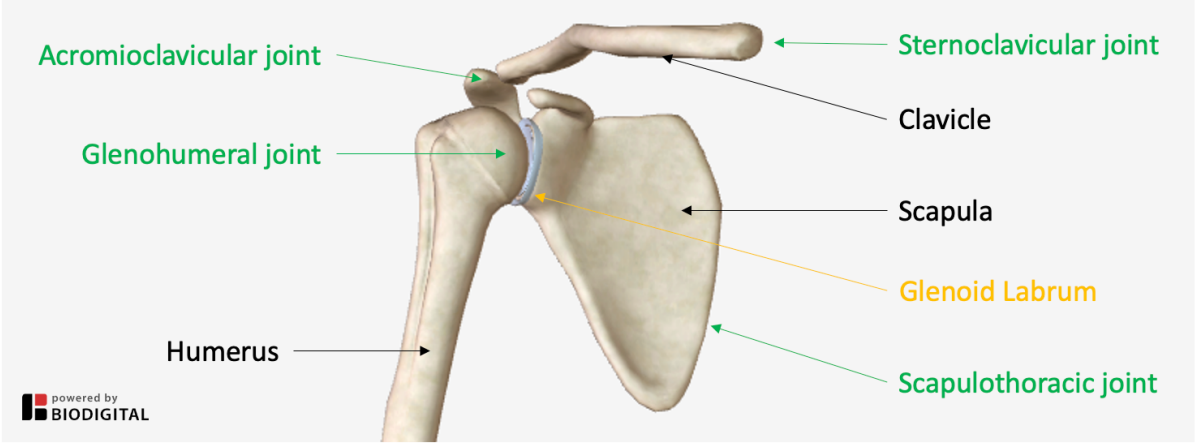


Figure 1-1. Significant anatomical features of the right shoulder, anterior view.

The shoulder is a complex structure made from 3 bones (black) forming 4 joints (green) with a number of supportive soft tissue structures (yellow - NB ligaments not shown for clarity of other structures). Figure adapted from HUMAN, powered by BioDigital [16].

The rotator cuff is comprised of 4 muscles and tendons, which originate from the scapula and insert into the proximal humerus. These are the supraspinatus, infraspinatus, subscapularis, and teres minor (Figure 1-2). As the tendons pass over the glenohumeral joint, they blend together to form a common cuff, enveloping the humeral head. This common tendon is where

rotator cuff tendon tears occur. The tendon to bone transition occurs through a gradual transition termed the enthesis as discussed in section 1.3.3 (The enthesis).

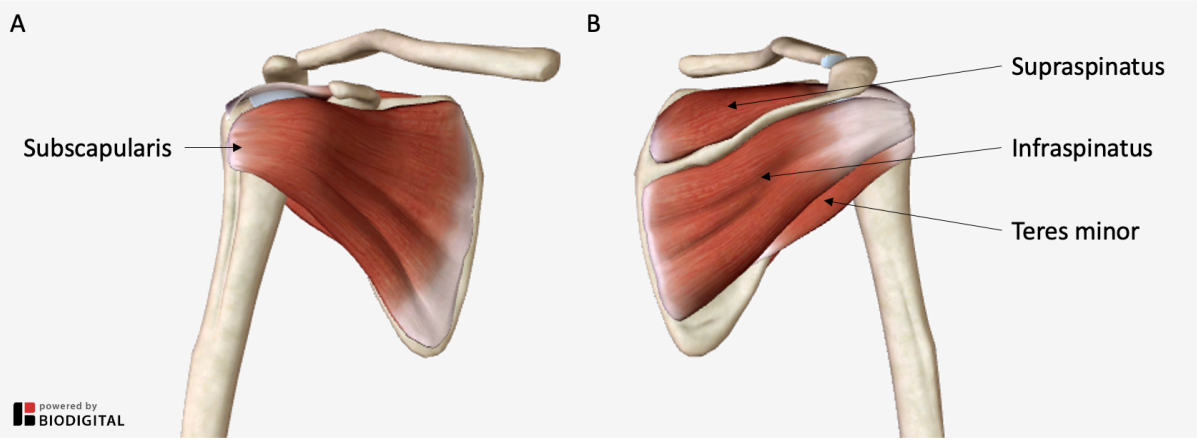


Figure 1-2. Structure of the rotator cuff of the right shoulder, anterior view (A) and posterior view (B).

The rotator cuff is made up of 4 muscles which originate from the scapula, envelop the glenohumeral joint and insert into the head of the humerus. Figure adapted from HUMAN, powered by BioDigital [16].

The synergistic action of muscle groupings work to actively maintain shoulder stability and an appropriate position of the humeral head on the glenoid fossa. Connections between the muscles and static ligaments allow the rotator cuff to tension the shoulder capsule and ligaments, reducing ligamentous laxity and further increase stability [17].

In addition to their roles in shoulder stability, rotator cuff muscles are important initiators of shoulder motion. The supraspinatus begins abduction, the infraspinatus powers external rotation, while the subscapularis provides an important component of internal rotation [18]. Disruption of these structures can consequently cause significant dysfunction and impair quality of life.

1.3.2 Structure of rotator cuff tendon

Tendon tissue has a number of structural elements, both micro- and macroscopic, to permit successful force transmission from muscle to bone, controlling movement and providing

stability at articular surfaces [19]. These are reviewed here with the context of biomaterials and Tissue Engineering and Regenerative Medicine (TERM) in mind. The hierarchical division which exists in tendon is complex. Even further subspecialisation is found depending on both the position along the length of the tendon towards the enthesis, and the depth into the tendon tissue. Designing a material which can recreate this biological complexity and promote specialised tissue transitions is challenging, but crucial, to ensure appropriate tendon healing.

1.3.2.1 Hierarchical structure of rotator cuff tendon

Microscopically, the first important feature of tendon structure and its subsequent function is the relatively acellular nature of tendon tissue, with Extra-Cellular Matrix (ECM) making up 85% of the dry weight of tendon [19,20]. In addition, tendon tissue is largely avascular, un-innervated and has limited lymphatic drainage. This reduces weakness in the tissue from structural elements not capable of withstanding the high mechanical forces experienced in physiological tendon loading.

The ECM is comprised of collagen fibers, elastin, ground substance, inorganic components and water. However, collagen accounts for the majority (up to 80%) of the ECM matrix. Tendon collagen is largely Type I collagen, deposited in a multi-hierarchical structure of increasing size to confer considerable strength [21] (Figure 1-3). The intracellular processing of collagen polypeptides is complex and only covered in sufficient detail to illustrate how transmission of force is supported from the molecular level of collagen through to level of tendon [22-25].

Type I collagen is a 3 stranded right handed super-helix made up of 2 α-1 chains and 1 α-2 chain [26]. The chains in collagen have a unique recurring amino acid triplet motif, Glycine-X-Y, to facilitate interaction between the chains. The X is commonly proline and the Y commonly lysine [25]. The glycine amino acid is relatively small enabling the three chains to come close together within the superstructure to facilitate cross-linking [26]. The proline causes kinks in the

individual polypeptide chains forcing a left handed helix conformation. This twist increases potential crosslinking and binding sites over a fixed distance to increase the strength of the collagen. The lysine residues can undergo hydroxylation, along with proline residues, to facilitate cross-linking between collagen chains and further promote strength [25]. Enzymatic and non-enzymatic glycosylation of peptides during intra-cellular processing provide sugar groups to facilitate another layer of covalent cross linking between collagen chains [24].

Following assembly, the procollagen superhelix is secreted through exocytosis. Upon cleavage of the N-terminus (ADAMTS2) and C-terminus (BMP-1), an insoluble tropocollagen molecule is formed [26]. These 280-300nm long, 1.5nm wide units self-assemble in a quarter staggered array to form collagen fibrils. Cross-linking between tropocollagen molecules occurs as previously described between collagen alpha chains [20,23].

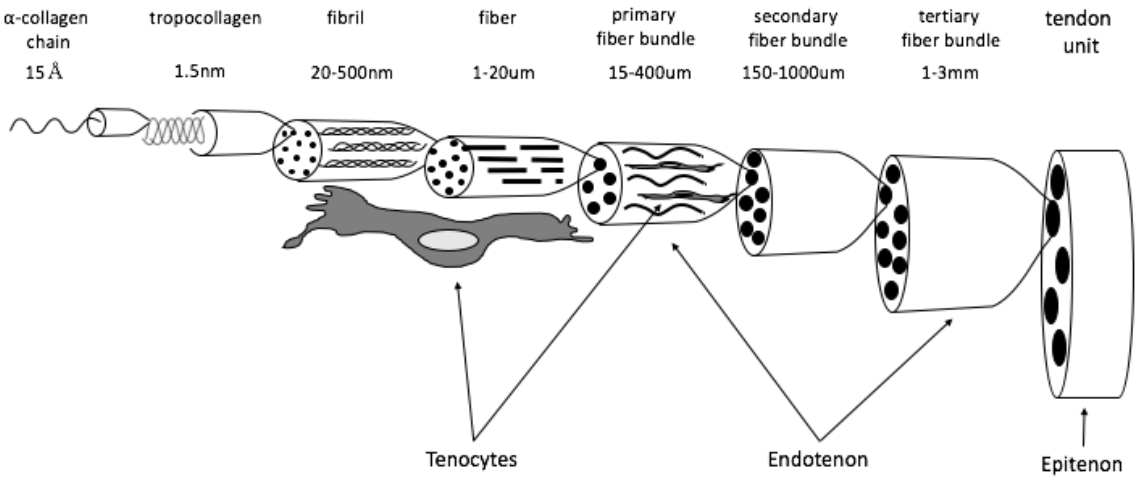


Figure 1-3. The hierarchical structure of tendon provides significant mechanical strength.

Collagen is a complex molecule with specialisations in structure, both spatial and biochemical, that facilitates significant crosslinking within and between collagen chains. This hierarchy perpetuates up through larger tendon structure components, which generates a robust tissue, capable of force transmission from muscle to bone in the face of demanding mechanical forces. Tenocytes are found between collagen fibers, where they interact with the fibril and fibre-sized elements of collagen and other elements of tendon ECM. Endotenon and epitenon connective tissue layers reduce friction and provide conduits for vasculature, lymphatic, and nervous elements. Adapted from Wang 2006 [28].

Collagen fibrils have a distinctive 67nm axial periodicity, contributing to the characteristic banding and crimp patterns of tendon fibers seen on histology. Fibrils range in diameter from 20nm-500nm depending on tissue and tendon function [28]. Collagen fibrils can extend micrometres in length [23,29]. Whilst fibrils are often deposited longitudinally, they can form spiral, plait and crossed formations depending on the directional force requirements [30].

Fibrils are assembled into fibres (1-20um in diameter). Fibres are bundled together to form a primary fibre bundle or sub-fascicle. Sub-fascicles coalesce to form a secondary fiber bundle or fascicle. These subsequently unite to form tertiary fiber bundles. Tertiary fiber bundles unite to form a tendon unit. Tendon units combine over various levels and sizes to form a functional tendon [19].

1.3.2.2 Layer specialisation of rotator cuff tendon

In addition to this hierarchical arrangement, the rotator cuff tendon is highly specialised depending on the location in the tendon as shown in Figure 1-4. Histologically, the rotator cuff has been divided into 5 layers with variation in the arrangement of tendon fibrils, fibers, and fascicles in each layer, depending on the position along the tendon length or depth [31].

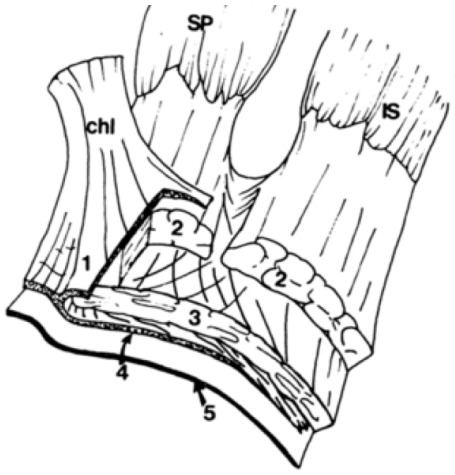


Figure 1-4. The specialisation of layers of rotator cuff tendon.

Tendon is a multi-component structure with various layers of complexity to reinforce and facilitate its function. It is not yet possible to engineer biomaterials with such complicated

structural variation. The numbers 1, 2, 3, 4, 5 denote histologically discrete layers of the rotator cuff tendon from superficial to deep. SP: Supraspinatus, IS: Infraspinatus; CHL: Coracohumeral ligament. Adapted from Clark 1992 [31].

The primary, secondary and tertiary fiber bundles are separated by a thin layer of endotenon. This layer acts as a loose connective tissue to allow rotator cuff tendons to move within other tissues of the shoulder joint with less friction. The epitenon performs a similar function at the level of tendon units. The epitenon contains the small amount of vasculature, lymphatic and nervous tissue present in tendon. An additional layer of paratenon overlies the most superficial epitenon surface and also reduces friction between the rotator cuff tendons and other tissues of the shoulder [32].

Tendon tissue is innervated by nerve fibres which cross the myotendinous junction forming a plexus within the paratenon. Most nerve fibres terminate on the surface of the tendon with some nerve endings penetrating through the epitenon and into the endotenon. This penetrating fibres play an important role in the Golgi Tendon Reflex. Specialised afferent nerve fibres are interlinked with collagen fibres of both muscle and tendon at the myotendinous junction. Compression of these fibres with increasing muscle contraction leads to a spinal cord level reflex to modulate the force of muscle contraction to prevent injury from overloading.

1.3.2.3 Non-collagenous components of rotator cuff tendon matrix

A number of important non-collagenous components also facilitate rotator cuff function. Elastin is present to enable passive tendon recoil following movement between tendon tissue structures. Proteoglycans with glycosaminoglycan (GAG) side chains are highly hydrophilic molecules that pull water into tendon tissue to facilitate lubrication between tendon structures and resist compression [33]. Furthermore, proteoglycans are involved in collagen fibrillogenesis and maturation [34].

1.3.2.4 Cellular components of rotator cuff tendon

Within healthy tendon matrix, the predominant cells (90-95%) are tendon fibroblasts or tenocytes. These cells make up less than 5% of the volume of tendon tissue [35]. Healthy tendon fibroblasts have a highly elongated cell shape and are distributed throughout the tendon matrix [36]. They are connected by gap junctions and communicate based on biochemical, mechanical, and biophysical cues to ensure appropriate production and maintenance of the tendon matrix [26,37]. However, tendon fibroblasts are sparse, slow to divide and have low collagen turnover rates [38], furthermore few tendon-progenitor stem cells exist in the matrix, limiting the ability of tendon tissue to heal quickly [39].

There are a small number of chondrocytes at the enthesis, capillaries and arterioles running within the epitenon, and synoviocytes in the synovial lining. There are also a small number of resident macrophages [40]; however, in the context of injury and inflammation of the rotator cuff, the immune response is driven from peripheral cells recruited to the site at the time of injury [41]. It is likely that it is recruited peripheral immune cell populations which govern the inflammatory reaction that occurs after biomaterial implantation for rotator cuff repair [42]. This important inflammatory response is detailed in section 1.12.3 Immune cell population response to electrospun fibres.

1.3.3 The enthesis

The enthesis connects the rotator cuff tendon to the humerus. This site is commonly affected in rotator cuff tears. The enthesis is a complex transition from tendon to bone matrix, enabling successful force transmission as shown in Figure 1-5. The enthesis is classified into 4 zones: tendon fibers, fibrocartilage, mineralised fibrocartilage and bone [43,44]. In these zones, collagen, GAG, mineralisation composition and cell type varies significantly to form a functional transition. When repaired surgically, tendon fibers of the tendon edge are brought directly into contact with the bone [44,45]. This arrangement fails to recreate the complex native

transitional structure evolved to offload force appropriately. The relative weakness of this new tendon-bone transition may contribute to the high treatment failure rates [46].

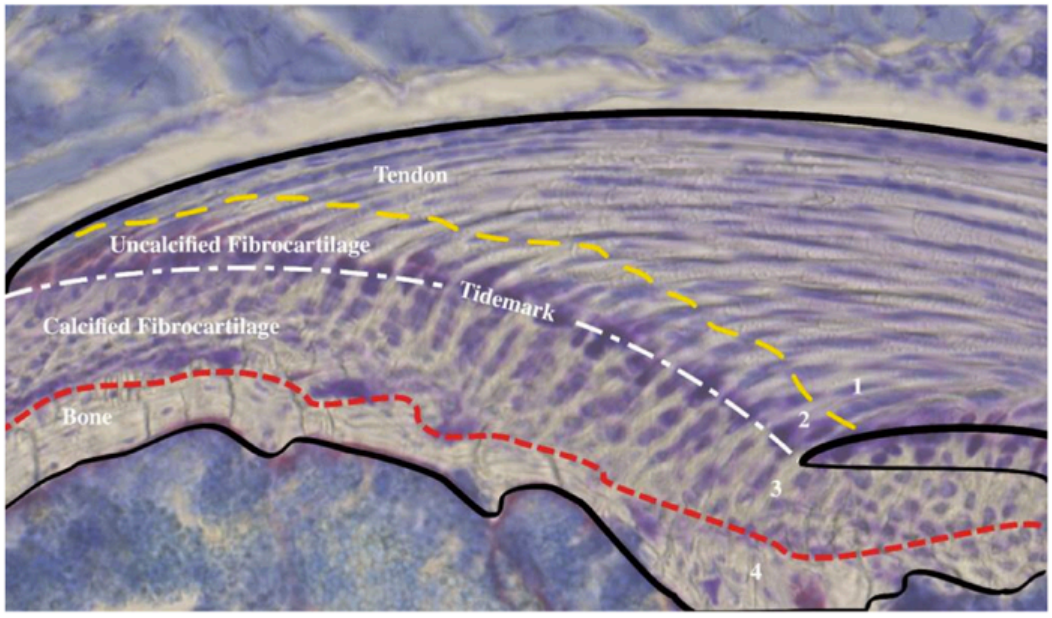


Figure 1-5. The structure of the enthesis.

The transition from tendon bone tissue is a gradual but highly specialised transition through 4 distinct histological layers from tendon matrix to uncalcified fibrocartilage, calcified fibrocartilage and finally bone matrix. Biomaterial repair will need to recreate this functional transition to promote adequate healing. Adapted from Apostolakos 2014 [47].

1.4 Rotator cuff tendon response to injury

Following trauma healthy tendon can successfully heal through inflammation/resolution, proliferation, and remodelling. These are carefully balanced and orchestrated processes, with successful healing dependent on injury site, size and many biological factors [48].

The inflammatory phase (hours to days) is characterised by tissue injury triggering the release of chemotactic factors and subsequent recruitment of peripheral inflammatory cell populations to the injury site [49]. Neutrophils and macrophages break down and degrade the damaged matrix. The proliferative stage (days to weeks) results from increased proliferation

of intrinsic tendon fibroblasts and increased tendon matrix production [50]. This is supported by a relative increase in vascularisation [51]. At this stage, immature tendon matrix is deposited, with high collagen III and proteoglycan contributions [52]. During remodelling (weeks to years), tendon fibroblasts respond to physiological stimuli from biomechanically loading. This leads to slow increases in collagen I production, increased alignment of deposited collagen components and reduced cellularity [53]. This final tendon tissue does not completely replicate un-injured tendon matrix with some differences in protein content but affords more function than scar tissue [54]. Resolution of the inflammatory component to tendon injury also occurs gradually over the same time scale as remodelling.

In the context of rotator cuff tears where tissue fails to heal appropriately, a number of factors are believed to contribute to the initial injury as well as the failed healing response. These include anatomical, vascular, genetic and inflammatory components and are reviewed in detail in section 1.5 (Rotator cuff tendinopathy and tears). However, it is important to highlight that there are fundamental pathways which exist to heal tendon damage and that these could be harnessed to improve rotator cuff repair outcomes.

1.5 Rotator cuff tendinopathy and tears

Rotator cuff tendinopathy is a descriptive term for a number of conditions which can affect the rotator cuff. This spectrum ranges from inflamed, fibrotic, and ultimately torn tissue. RCTs can occur in any of the 4 rotator cuff tendons but occur most commonly in the supraspinatus tendon. The aetiology behind rotator cuff tears is complicated, but is being increasingly probed and understood [24,40,55-57]. This new research is helping to drive the direction of biomaterials research.

A number of models have been put forward to explain the cascade of healthy tendon matrix to weakened tissue and ultimately, to tendon tearing. Tendinopathy is in reality a multi-

factorial condition resulting from the interplay between these various aetiologies (Figure 1-6). These include:

- Anatomical – This theory proposes that the impingement of the supraspinatus tendon on the coracoacromial arch during shoulder movement leads to focal, repeated tissue damage and initiates tearing [58].
- Vascular – This concept is grounded in hypovascularity at a critical zone or 'watershed area' of the supraspinatus tendon, 1cm proximal to the insertion, corresponding with the site of many small rotator cuff tears [59,60]. Additionally, doppler ultrasounds of this area in torn tendon reveals increased vascularity in this area, potentially in an attempt to promote healing [61].
- Genetic – Whilst no allele or polymorphism has been directly linked to rotator cuff pathology [62], siblings of patients with a full thickness rotator cuff tear are 4.6 times more likely to develop full thickness tears than controls [63]. Progression of tear size is also more likely to occur in patients with siblings who also have rotator cuff tears [64].
- Overuse – This model suggests that repeated loading and unloading of the tendon leads to microscale damage at a rate exceeding endogenous healing mechanisms [65]. This theory is supported by over-use models in animals [66]. In contrast, unloading and immobility of tendon tissue also leads to reduction in tendon volume and changes in composition [67]. Tendon is clearly a dynamic tissue with physiological homeostasis dependent on balanced mechanical stresses.
- Age related degeneration – This idea proposed that the degeneration of tissue over time gradually accumulates until weakened tissue ruptures in response to physiological loading [68]. This theory is not supported by recent research. Whilst age is a definite risk factor for rotator cuff tear incidence, there are elderly patients who have intact rotator cuff tendons, suggesting age is simply confounding other factors that underlie the changes in tendon biology that cause tendon damage.

- Inflammation – Whilst the role of inflammation in tendinopathy and tendon is debated in the literature, increasing evidence shows that inflammatory cells are present and inflammatory pathways are activated in tendinopathy and torn tendon [69-72]. Dysregulated resolution in the responses to injury can lead to sustained inflammation [55] and fibrosis with the deposition of relatively weakened scar tissue [73]. Additionally, tendon fibroblasts from rotator cuff tears have an inflammatory memory, displaying primed responses to inflammatory stimuli, suggesting previous inflammatory exposure [40,55,74]. Whilst surgery reconnects bone and tissue, current biomaterials have no deliberate effect on the chronic inflammation and failed resolution processes involved in tendinopathy. To promote effective healing, biomaterials may need to influence and 'reset' this inflammatory imbalance in order to promote healthy, mechanically sound tendon tissue deposition.

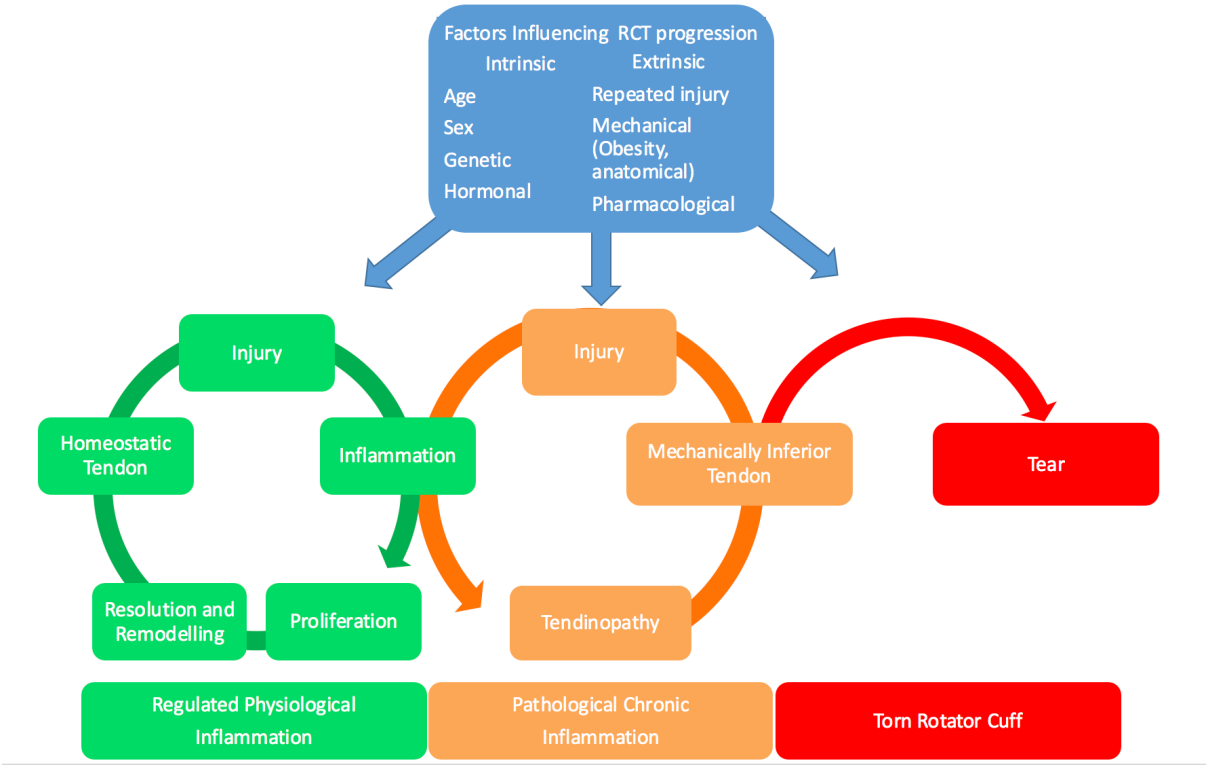


Figure 1-6. Tendon healing is a complicated, tightly regulated process.

Small scale tendon damage can be repaired through endogenous healing mechanisms (green). However, this healing ability is subject to intrinsic and extrinsic factors (blue). In the case of tendinopathy, combinations of these factors prevent endogenous healing and establish a

chronic inflammatory response (orange). These changes propagate a cycle with immature and inflamed matrix relatively more susceptible to further injury and inflammation. Ultimately, this tissue becomes structurally impaired to a point where physiological loading leads to rupture (red). At this point, tendon cannot heal without intervention. Tearing prevents mechanical loading of the tendon tissue, an important physiological input for regulating tissue homeostasis. Without this loading, over time, rotator cuff tendons retract from the enthesis and undergo fatty infiltration and other phenotypic changes further affecting tendon biomechanics and precluding healing.

Irrespective of aetiology, there are characteristic changes within tendinopathic and torn rotator cuff tendon tissue in comparison to healthy tendon (Figure 1-7) [75]. Factors of particular importance for this thesis and rotator cuff repair biomaterials include; reduction in fibril diameter; disorganised fiber orientations and more heterogeneous fiber diameters [24]; rounded less elongated cell morphology [76]; increased vascularity [61]; increased GAG content [24]; reduced collagen content with altered collagen types and increased cross linking [24]. Ultimately tendinopathic tissue is weaker, leading to tendon tears under physiological loads [73,77].

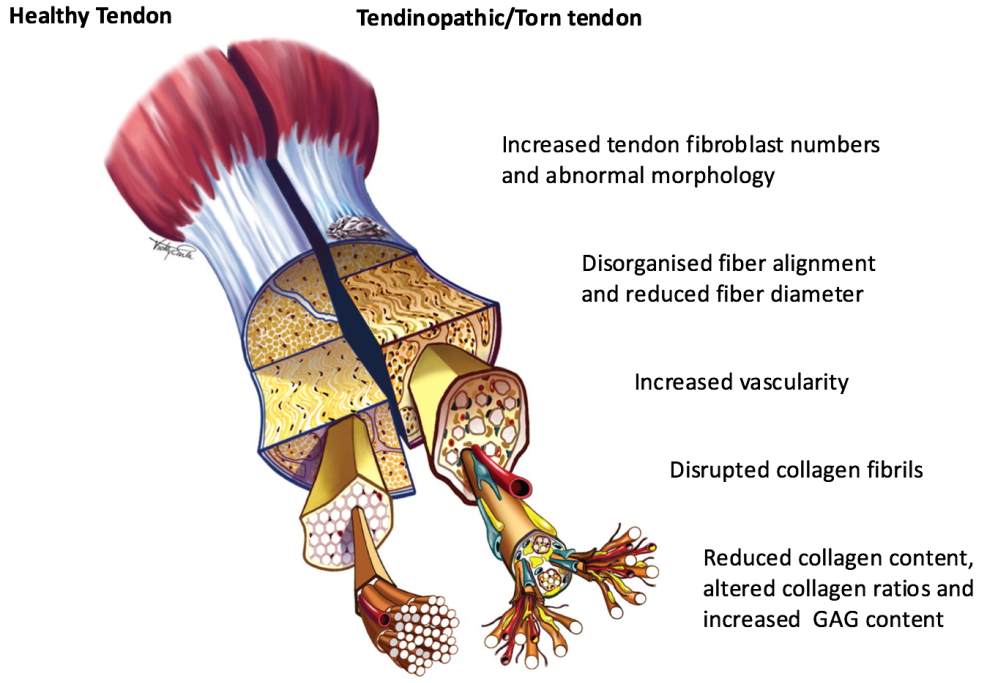


Figure 1-7. Characteristic changes observed in diseased tendon matrix.

Tendon tears occur in the context of weakened tendinopathic tissue characterised by disordered ECM, hypercellularity and increased vascularity. Adapted from Bruckner 2002 [78].

Whilst these tears can be painful and disabling as previously described, it is important to note that not all rotator cuff tears cause pain or disability [4]. Furthermore, the degree of pain or dysfunction does not correlate with the extent of the tear [79]. These factors suggest there is another layer of complexity to rotator cuff disease of which we are currently unaware.

The pathogenesis of healthy rotator cuff tendon to tendinopathic tissue and finally, to tendon tears is chronic, occurring over years [80]. Acute tears are biologically and mechanically different injuries to chronic rotator cuff disease, occurring as a result of extreme force. Whilst biomaterials developed for use in chronic rotator cuff tears may have a role in acute tear treatments, acute tears are not directly considered as part of this research.

1.6 Rotator cuff tear treatment

1.6.1 Non-surgical rotator cuff tear treatment

Initial rotator cuff tear treatment adopts a non-surgical approach. Analgesia and physiotherapy can reduce pain and improve function. For some patients, these treatments are enough to return their shoulder function back to, or very close to, a normal level of function with no further escalation of treatment required [81].

Analgesia is commonly achieved through corticosteroid injections and oral analgesia, particularly non-steroidal anti-inflammatory drugs (NSAIDs). The use of NSAIDs is controversial, with *in vitro* and animal evidence suggesting the impact from these medications on bone healing and physiological inflammation potentially worsens long term outcomes [82-84]. A randomised controlled trial comparing NSAID effects with other classes of medication for pain after repair has been completed but not reported (NCT02153177). No published human study has looked at the effects of NSAID on tear progression.

Whilst steroid injections have shown short term benefit [85,86], recent studies have raised concerns about the effects of corticosteroids on long-term tendon outcomes [87,88]. Platelet rich plasma (PRP) therapy [89] and cell therapies [90] have also been trialled with no definite evidence of benefit, and in the case of PRP treatment, suggestions of worse outcomes [91,92].

1.6.2 Surgical rotator cuff tear treatment

Surgical rotator cuff repair aims to oppose the free edge of the tendon back to its insertion on the humeral head and maintain compression while the tendon and bone can fuse (Figure 1-8). The procedure was first performed in 1911 [68]. Surgical technique has greatly advanced with the deployment of arthroscopic shoulder surgery, new suture techniques, and new types of materials. As mentioned earlier, however, these surgical advances have not influenced successful repair outcomes with 40% of repairs still failing within 12 months [8].

The earliest form of RCT repair involved passing a single row of sutures through the tendon and into a bone tunnel to provide fixation of the tendon insertion back to its original footprint (Figure 1-8C). Invention of suture anchors allowed fixation of the tendon to the bone without bone tunnels. To improve fixation and compression, a double row of sutures passing through the free edge of the tendon evolved to place more compression over the footprint (Figure 1-8D). A modification of this technique sees the lateral row of suture anchors being placed further laterally outside of the tendon footprint. This minimises damage and invasion of the footprint by sutures as well as increasing the compression over the footprint [93].

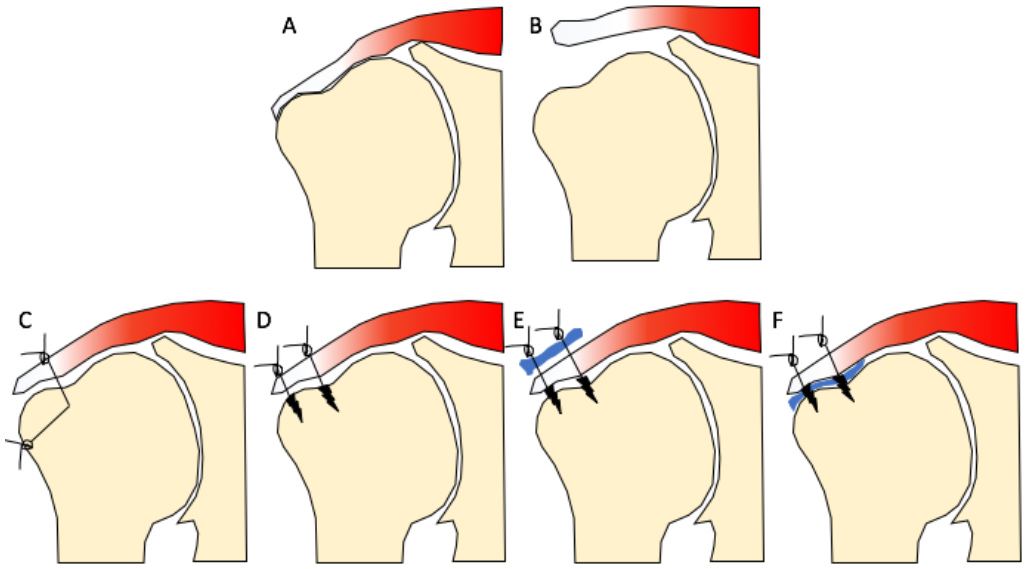


Figure 1-8. Schematic depicting rotator cuff tears and selected biomaterial repair strategies.

The rotator cuff normally inserts on to the humeral head (A). When this is torn, the tendon can lift and retract from its footprint on the humerus (B). Traditional suture technique uses a single row of sutures passed through the tendon into bone tunnels for fixation and compression of the tendon free edge back on to the humerus (C). Double row sutures with bone anchors allow for increased compression of the free edge without the need for bone tunnels (D). Overlay biomaterial positioning (E) sees a biomaterial placed over the top of the repair site. Interpositional implants (F) are inserted between the tendon and bone at the site of the tendon footprint.

Whilst numerous iterations of suture anchors and suture materials have been developed for use in conjunction with these techniques, no single surgical material has been shown to make a difference in clinical outcome in a large, well-designed human trial. Additional augmentation strategies have been trialled, including stem cell treatments and PRP. Whilst some studies have found improved healing with PRP, a meta-analysis showed no benefit in pain, function, and re-tear rate after 1 or 2 years follow up [94].

Patch repair augmentation involves using an additional biomaterial at the re-attachment site. This enables increased compression and fixation of the free edge of the tendon. This is most commonly performed through placement of the biomaterial over the top of the repair, an

onlay technique (Figure 1-8E). A biomaterial can also be inserted between the tendon and bone in an interposition technique (Figure 1-8F).

1.7 Biomaterials currently available for augmenting rotator cuff tear repair

There are over 20 biomaterials currently used for the augmentation of rotator cuff repair. These can be classified as biologic, synthetic or biosynthetic. No class of biomaterial currently captures the biophysical aspects of native tendon matrix (Figure 1-9)

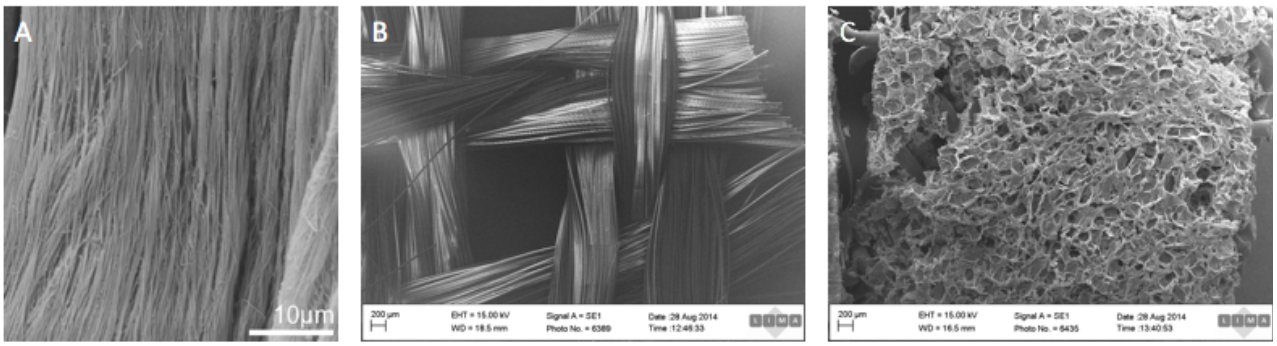


Figure 1-9. SEM images comparing the structure of tendon ECM, synthetic and biologic scaffolds.

This figure shows an SEM image of tendon matrix (A – scale bar 10um), adapted from Youngstrom 2013 [95], compared to the structure of a synthetic scaffold, 50x (B) and a biologic scaffold, 50x (C), scale bar 200um. Even with the differences in magnification, the difference in size and regularity of these foreign materials. Panels B and C adapted from Smith 2016 [96].

1.7.1 Biologic patches

Biologic grafts are the most popular graft type used. This is likely grounded in the belief that native ECM contains advantageous biochemical and biophysical cues to promote cell attachment, proliferation and tissue deposition [97].

Biologic materials are prepared from allograft, xenograft, and autograft tissue. Allograft materials, prepared from human cadaveric dermal tissue, are the most common form.

Different companies produce these materials with various methods to sterilise, decellularise, cross-link, and reduce the antigenicity of the tissue. However, these same processes also induce damage to the molecular epitopes and physical structure of the scaffold [96], potentially mitigating the expected benefits. The exact processes use proprietary techniques, making evaluation of the exact effects on ECM components difficult for researchers.

Xenograft patches are sourced from porcine dermis and small intestine submucosa (SIS) and subjected to similar treatment processes as allograft materials prior to use. Xenograft materials have been less popular following the recall of Restore™ (Depuy, Indiana, USA), a porcine SIS derived graft, after two studies demonstrated adverse outcomes related to this material [98,99].

Autograft patches from fascia lata and biceps tendon have been described but are not commonly used.

1.7.2 Synthetic patches

Current synthetic scaffolds have been designed to provide mechanical support and have often been repurposed for use in tendon following development for use in other tissue types [100-102]. These patches predominantly use non-degradable polymers, which assist in load transmission and suture retention, but make no attempt to actively support and influence the underlying healing process. The materials were developed to be 'bio-inert', meaning they interacted or affected cell behaviour as minimally as possible.

Synthetic scaffolds are often produced from fibers and combined through weaving, braiding and other techniques. The fibers have large diameters (from 10s to many 100s of micrometres) not representing natural tissue components and are arranged without the longitudinal alignment seen in collagen fibers. Furthermore, permanent or very slow degrading polymers prevent physiological load transmission through the forming tendon tissue. As tendon tissue is dynamic and responsive to strain [67,103], this long term disruption of mechanical loading may impair tendon healing and strength.

1.7.3 Biosynthetic patches

Biosynthetic scaffolds attempt to functionalise a synthetic material. Coating or combining a synthetic material with naturally occurring molecules could harness the theoretical biomolecular benefits from biological grafts in conjunction with the mechanical advantages of synthetic materials. This also reduces the risk of antigenicity, infection and batch variation associated with pure biologic grafts. The current synthetic patches use bovine collagen (BioFiber-CM (Tornier, Minnesota, USA)), and equine pericardial ECM (OrthADAPT PR (Pegasus Biologics, California, USA)) so infection and antigenicity issues persist but are lowered than pure processed biological tissue. However, these materials still rely on synthetic fibers, which do not replicate the size or alignment of natural tendon matrix.

1.7.4 Rotator cuff tear treatment summary

The techniques and biomaterials currently used as adjuncts for tendon repair are ineffective. Irrespective of the material or technique, successful repair rates remain static at 40% [8]. Additionally, whilst *in vitro* studies [96,97,104], *in vivo* animal studies [105-107] and some observational human studies [108-110] suggest improvements in the mechanical, vascular or biological nature of patch-augmented tendon repairs, there is no large, well-designed clinical trial showing benefit of any one material.

This is perhaps not surprising given that these materials are re-purposed from use in other tissues, including chronic foot ulcers, hernia repair and genitourinary surgery. Commercial rotator cuff repair materials are not designed for use in a highly specialised tissue operating at the extent of its physiological limits. The issue of inappropriate re-purposing of materials is a major concern in other fields of tissue engineering [101] and has led to recent changes for device regulation and approval in Europe (EU 2017/745 regulations) and the USA (PMA/510K approval pathways). This reflects research that 16% of surgical meshes on the market gained approval based on equivalence with materials which have been recalled due

to serious adverse events [100]. Re-thinking and re-engineering biomaterials tailored for use in the highly specialised rotator cuff anatomy is required to improve patient outcomes.

1.8 Ideal biomaterial properties for augmenting rotator cuff tear repair

The next generation of biomaterials for rotator cuff repair must possess certain characteristics. First and foremost, any biomaterial must be safe. Secondly, the biomaterial must be effective and improve patient outcomes. This efficacy will be determined by ensuring the scaffold has the appropriate gross mechanical, biological, and biophysical attributes to facilitate tendon healing. Additionally, the implant must be easy to use, affordable, and large-scale production of homogenous implants must be possible [111-113].

Tissue Engineering and Regenerative Medicine (TERM) provides several avenues towards such a treatment. TERM attempts to use a triad of scaffolds, cells and bioactive molecules alone or in combination to restore biological function [114,115]. Of these approaches, scaffold treatments herald the most potential to produce a biomaterial that truly satisfies the requisite characteristics of a biomaterial to improve rotator cuff tear healing.

Cell-based treatments can either involve *ex vivo* culture of cells on materials in a bioreactor to generate functional tissue for implantation or involve seeding a cell population onto a scaffold at the time of implantation. However, due to a lack of understanding of the relevant cell biology and immature 3-dimensional perfusion culture systems, cell-based strategies to generate functional tissue *ex vivo* are unlikely to produce treatment strategies to help patients with torn rotator cuff tendons in the near future. Cell-seeded approaches are also unlikely to succeed with issues around cell sourcing, expansion and the long-term safety of cell re-implantation yet to be resolved [116-119]. Even if the technical issues around cell-based TERM could be resolved, such treatment would be extremely limited in accessibility due to the cost and the availability of specialist facilities capable of producing such treatments.

It is worth noting, however, that both *ex vivo* and *in vivo* cell-based TERM applications require a scaffold to support the cell population. Thus developments made in pursuit of pure scaffold-based treatments may also have a role in cell-based treatments in the future. In the meantime, using the body as a bioreactor and cell source for scaffold-based therapeutic strategies has more potential to produce meaningful advances in rotator cuff tear treatments.

Bioactive molecules can be delivered to a target site to influence cell biology and improve healing. Given the incomplete understanding of changes in cell biology relevant to healing in tendon, the selection of an appropriate molecule or molecules is challenging. Furthermore, delivery of a molecule at the right concentration over an appropriate time period is challenging. Any bioactive molecule based treatment also faces increased regulatory challenges, development costs and time taken to reach the patients in need of improved treatments [120]. However, looking ahead, incorporation of bioactive molecules for delivery within a scaffold provides several advantages. Biomaterial-based administration enables localized delivery to minimize adverse effects, tailored delivery kinetics to reduce the need for multiple treatments as well as an ability to deliver combinations of bioactive molecules spatially and temporally to better influence cell biology [121,122].

Biomaterial-based treatments are much more promising. Currently available synthetic materials already satisfy several of the defined characteristics for an ideal rotator cuff repair biomaterial. Compared to biologic scaffolds, synthetic scaffolds remove the risk of antigenicity and immune response to allograft and xenograft materials. They also remove the risk of infection associated with allograft and xenograft materials. Avoidance of xenograft tissue increases patient acceptability. Specific production and quality control mechanisms eliminate concerns around supply and processing variation. Furthermore, using degradable materials can also reduce the chronic inflammatory response to the biomaterial and reduce the risk of bacterial infection with degradation removing potential biofilm formation and bacterial reservoirs [123].

However, current synthetic biomaterials for RCT repair have been adopted from other tissue applications and aim to solely approximate the torn edge of the rotator cuff tendons to the humerus. They aim to allow passive healing of the tendon or to permanently provide a material structure to replace tendon function. This is ineffective, with healing occurring through scar tissue formation, not the deposition of highly specialised tendon matrix. The resulting scar tissue is not mechanically robust and is unable to withstand physiological forces, leading to re-rupture and treatment failure.

A smart, deliberately designed synthetic biomaterial is a significantly different proposition building on the advantages of the currently available biomaterials. This is because specific, intelligent engineering can harness the power of biophysical cues to actively influence underlying cell populations in targeted ways to affect cell biology.

1.9 Targeting cell-material interaction

Biomaterials designed to generate a deliberate cell material response are increasingly possible. No longer is the connection between cell and matrix viewed as passive but is appreciated as a dynamic, bidirectional and powerful relationship [124]. The relationship between cells and their physical surroundings in the ECM, specifically the biophysical cues ECM can impart, is particularly relevant to this thesis. This is also made possible through a deepened understanding of tissue healing and the cellular, molecular and physical regulators of these pathways. In concert with this broadened understanding of tissue repair and the biophysical effects of materials on cell biology, material fabrication techniques have advanced greatly.

These advances allow a novel generation of biomaterials with great specificity in their biophysical profiles, in order to deliver the biophysical cues that target endogenous cell processes to support the healing of native tissue. These bioactive materials will facilitate tissue regeneration and supersede older bio-inert materials designed and used to replace native

tissue [125,126]. Furthermore, these biomaterials can employ biomimicry, that is replicating the biophysical stimuli found in native tissue to recreate a niche that favourably drives cell biology [127].

1.9.1 Mechanisms of cell-material interaction

Cell-material interactions are dependent on biophysical and biochemical stimuli. Adhesion contacts convey biophysical information. Adhesion contact is a term for the cell-matrix attachments largely occurring between cell-surface integrins and their matrix receptors [128]. As adhesion contacts increase in number, type and space, significant information about the matrix is transferred through to the nucleus via the cytoskeleton and other intracellular signalling pathways [129]. This biophysical information is synthesised with other inputs (e.g. biochemical stimulation, inflammatory state, cell-cell signalling) to dictate the cell-material response. Whilst the underlying mechanism may be similar between cell types, the actual response depends on cell type [130,131]. This response can, however, be manipulated.

Upon implantation or exposure to biological fluids, biomaterials adsorb a surface layer of proteins and other bioactive molecules. This biochemically active, adsorbed layer is termed the corona. Corona formation and its role in cell response is reviewed in more detail in Chapter 4. However, it is important to highlight firstly, that biomaterial properties affect the chemical composition of the adsorbed corona and secondly, that biomaterial surface properties also affect the conformation of the adsorbed proteins. The protein composition and protein conformation have important effects on cell-material interaction.

The distribution of the adsorbed corona proteins is also important. Changes in biomaterial topography and configuration introduce a 3 dimensional structure to the spatial distribution of cell adhesion molecules (Figure 1-10). This distribution is important in dictating cell response.

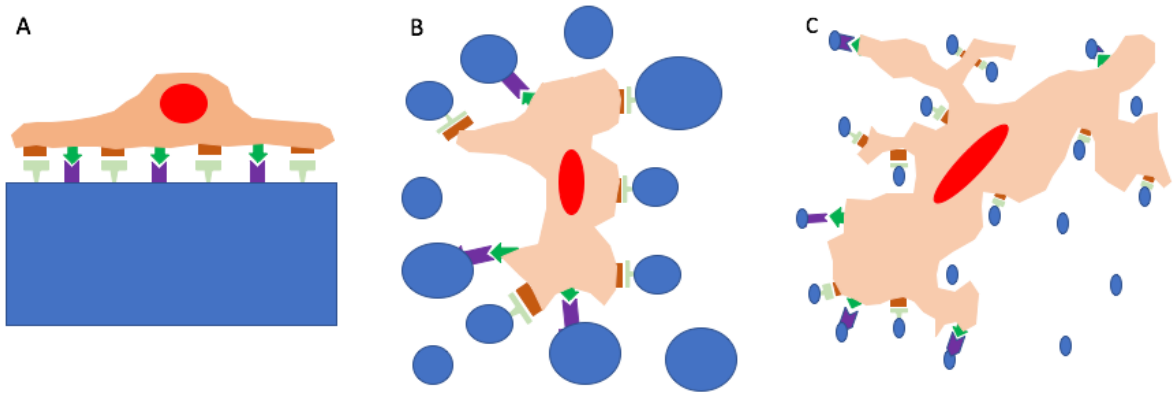


Figure 1-10. Schematic depicting how the changing scale of biophysical features can affect cell-material interaction.

On a macroscopically flat surface (A), proteins are adsorbed over the surface. Cells interact with these proteins adopting a flattened morphology unseen in native tissues. Presentation of attachment sites in a spatial distribution, result in more natural 3D cell conformations (B). Further still, nanoscale materials (C) allow more precise control in the spatial arrangement of matrix adhesions, the resultant cell shape, and the intra-cellular chemical and cytoskeletal response. Although, not depicted in this figure, scaffold stiffness also dictates cell response.

When a cell encounters a biomaterial and the adsorbed corona, it first forms a focal complex. Focal complex formation is dependent on appropriate cell surface proteins (predominantly integrins), their ligands in the matrix and the physical stability of the cell in the matrix. Under the right conditions, a focal complex will enlarge to form a focal adhesion anchoring the cell in to the biomaterial. Focal adhesions can progress to fibrillar adhesions further cementing cell-material connections. Maturation through matrix adhesion formation from focal complex to focal adhesion to fibrillar adhesion, is accompanied by changes in the integrin composition and connection with cytoskeletal elements [128].

Matrix stiffness is another biomaterial facet involved in the response to cell attachment molecules. Stiffness is important because when cells contract against the matrix through adhesion contacts, the relative deformation generates information about the surrounding matrix to influence cell response.

The information sensed through cell-material interactions exacts effects on cell biology through direct mechanisms and biophysical epigenetic regulation [132,133]. Biophysical epigenetic regulation can influence the cell response in two ways. Firstly, the cytoskeleton links focal adhesions with the nucleus. Intrinsic cytoskeletal forces thus transmit information about the surrounding matrix directly to the nucleus, leading to nuclear deformation, chromatin rearrangement and exposure of transcription sites to directly influence gene expression. Secondly, the formation of adhesion contacts in time and space leads to activation and suppression of associated intracellular signalling pathways [134-136].

1.9.2 Biophysical cues used to influence cell-material response

Biophysical cues from biomaterials have been used to direct cell differentiation [137-138], cell adhesion [139], cell proliferation [139], matrix production [140], affect immune response [141-143] and even replace molecular signals required to induce pluripotency [133]. This highlights the importance of the biophysical control of cell response as an important intrinsic material property to be considered in TERM research. Biophysical cues used to influence cell behaviour are listed in Table 1-1.

Table 1-1. Biophysical cues used to manipulate cell biology

Surface chemistry	Alignment/anisotropy
Surface hydrophobicity	Porosity/pore size
Surface charge	Local mechanical properties
Surface roughness	
Surface topography	

1.9.3 Biomaterial fabrication strategies that allow tuning of biophysical cues

Various biomaterial fabrication techniques exist to harness biophysical cues including; molecular self-assembly [144,145], freeze drying [146], phase separation [147], 3D printing [148,149] and electrospinning. Electrospinning has shown promising results in laboratory, animal models

and early stage human clinical trials. Electrospun materials are in or have been developed for use as scaffolds in a variety of tissue types including tendon [150], cornea [151,152], skin [153], cardiac muscle [154,155], bone [156] and in other applications as bone fillers [157], as functionalised coatings of other implants [158], in stem cell expansion [159,160] and for *in vitro* organogenesis [161].

Electrospun materials are particularly encouraging for rotator cuff tear repair for a number of reasons. Firstly, electrospun materials can recreate the micro and nano structure of native fibrous tendon ECM (Figure 1-11). This biomimicry could engage underlying cell biology pathways to promote intrinsic biological healing mechanisms. Secondly, electrospinning can employ a wide range of materials and additives to generate materials that are physically, chemically and biologically suited to tendon. Furthermore, electrospun materials can undergo considerable mechanical, biophysical, and biological property modification following manufacture, in order to further functionalise electrospun fibers. These materials can also be engineered to degrade at tailored rates, to enable functional tissue to form and mature as it experiences normal physiological loading as the material degrades, without foreign material compromising normal tissue integrity. Finally, electrospinning is affordable, scalable and accessible, accentuating commercial viability.

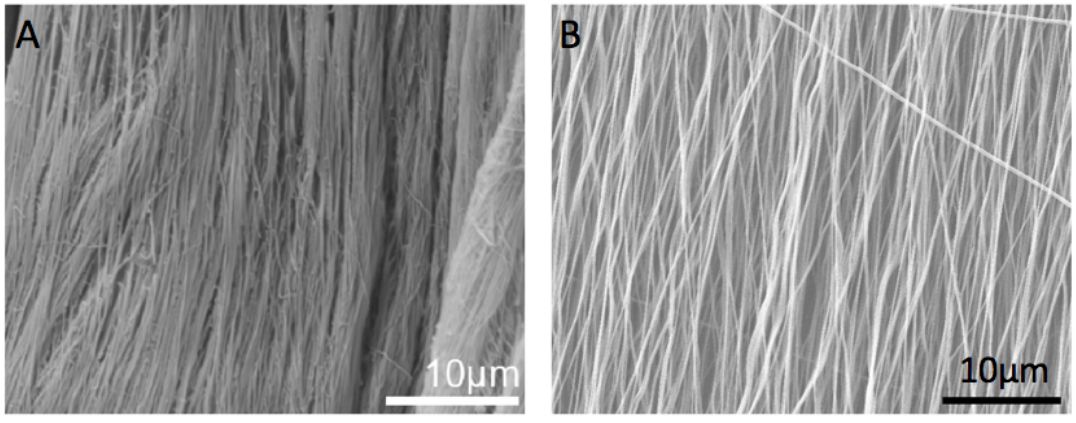


Figure 1-11. SEM images of tendon ECM and electrospun fibers.

Tendon ECM has a highly aligned, fibrous structure made up of collagen fibers (A), adapted from Youngstrom 2013 [95]. Electrospinning is able to recreate the diameter and alignment of such fibers (B) (own image). Scale bars 10um.

1.10 Electrospinning

1.10.1 Introduction and background

Electrospinning has progressed significantly since Boys first electrospun fibrous materials in 1887 [162]. Electrospun materials are now poised to play a significant role as biomedical implants [8,121,157], tissue engineering scaffolds [152,161], stem cell expansion systems [159,160], drug delivery [122,163], wound dressings [153], and bioactive coatings of other materials [158]. Electrospinning also has the potential to facilitate *in vitro* research without the cell phenotype loss experienced in static, 2-dimensional culture systems which limits generalisability of results to *in vivo* applications [161,164,165].

Electrospinning became an active biomedical research area following the generation of nanofibers in 1995 [166]. This timing was significant as cell biologists were beginning to fathom the active, bi-directional relationship between cell and ECM [167-170]. The ability to create nanofibre scaffolds over the same scale of native ECM components, vary these in deliberate ways and mimic the fibrous nature of ECM shared between multiple tissue types triggered significant interest in electrospinning as a biomaterial research area [171]. Continued breakthroughs in electrospinning techniques and advances in established protocols have sustained interest in the biomaterial applications of electrospinning (Figure 1-12) [172]. However, electrospinning's potential remains to be translated successfully into widely available commercial products.

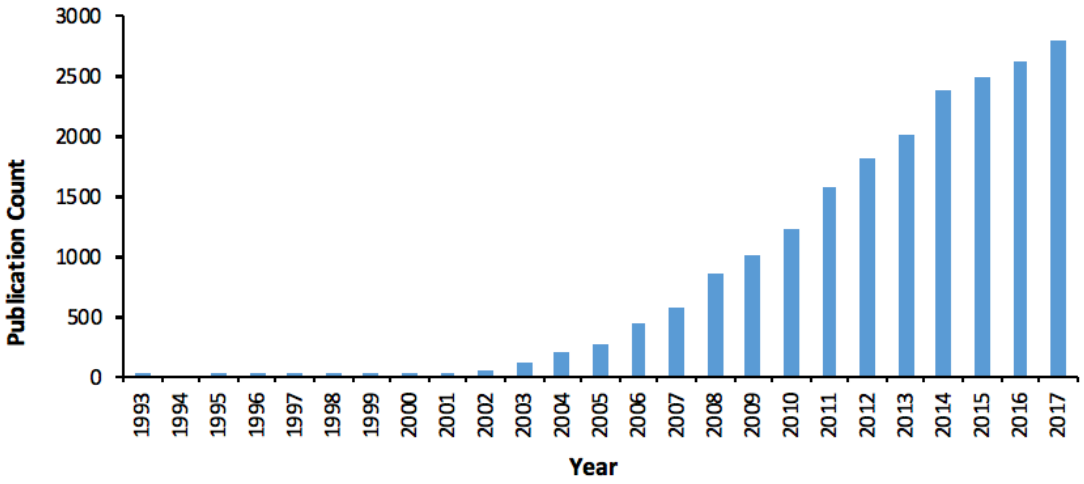


Figure 1-12. Number of articles published by year relating to electrospinning

The generation of electrospun nanofibers in 1995 instigated a sustained and near exponential increase in scientific paper publications relating to electrospinning, particularly within biomedical research. Produced using Web of Knowledge.

This section introduces the principles behind electrospinning, selected advances in electrospinning relevant to biomaterial fabrication for tendon biomaterial TERM and examines the current state of electrospun biomaterials being developed for use in RCT repair and selected other relevant applications.

1.10.2 The electrospinning system

Electrospinning uses electrostatic force to draw a polymer solution towards a collector. As the volatile solvent evaporates, polymer molecules entangle as a long continuous fibre. This fibre is then deposited on a collector. 5 key components are required to enable simple electrospinning (Figure 1-13).

1. A polymer solution made up in a volatile solvent,
2. A pump to deliver polymer solution into the system,
3. A spinneret/nozzle to feed solution into an electric field,
4. A high voltage power source to create the electric field,

5. A collector to receive the polymer fibres.

To help maintain the consistency of electrospun fibers, electrospinning is usually performed inside a chamber where temperature, humidity and airflow can be regulated. This also reduces exposure of the operator to the toxic solvents released during the electrospinning process.

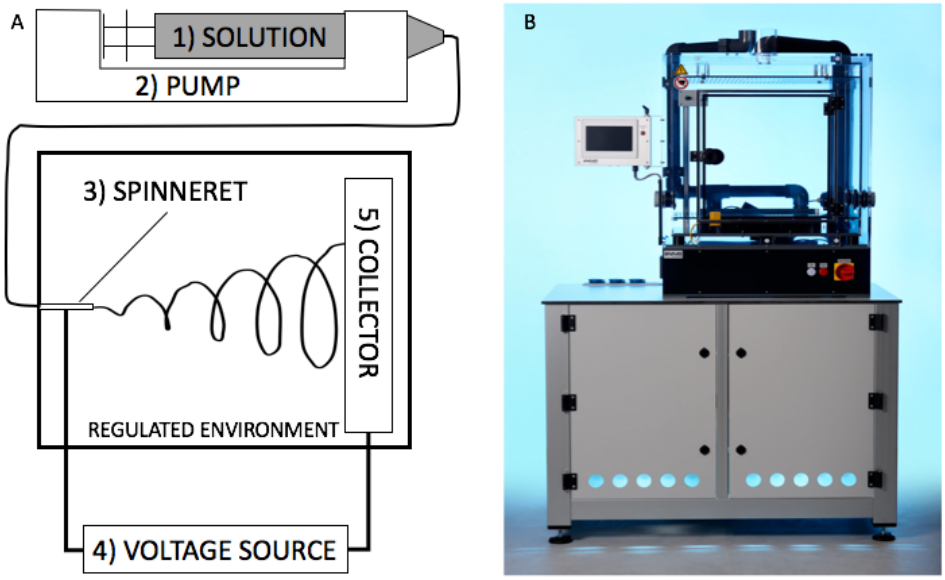


Figure 1-13. Schematic depiction of a simple electrospinning circuit (A) and a commercial electrospinning device (B).

This figure shows how electrospinning components fit together schematically (A) and how these are combined in real life in the commercially available electrospinning machine used for electrospinning in this thesis (B). Photo reproduced from IME promotional material [173].

1.10.3 The electrospinning process

The electrospinning process is best broken into 5 parts in order to understand the process and how it can be modified. These 5 parts are depicted in Figure 1-14.

1. Shear stress induced chain elongation – passage through the spinneret leads to shearing which promotes the elongation and alignment of polymer chains arriving at the nozzle tip (1).

2. Charging of the solution – the applied voltage induces charge separation within the polymer solution. Uncompensated ions accumulate at the fluid surface (2).
3. Formation of the Taylor Cone – the charge separation and resultant repulsion builds at the fluid surface until it exceeds the surface tension and viscous forces of the polymer solution, driving formation of a conical shape with an electrically driven jet (2). This is known as the Taylor Cone and is essential for researchers as a gauge for the process, as it is often the only visible part of electrospinning to monitor the process.
4. Jet thinning – From the Taylor cone, an initial linear jet is formed. As this jet accelerates towards the collector, charge repulsions within the solution take effect. This induces bending and deformation of the jet. The complex bending or whipping instability helps to stretch out entangled chains (3). As the fiber is drawn out in length towards the collector, the volatile solvent continually evaporates with inter-molecular chain entanglements maintaining fiber stability (4).
5. Fiber collection – Fibers are deposited onto a grounded collector in a randomly orientated fashion with diameter following a normal distribution (5). Complicated collectors can be used to modify the morphology of the resulting fibers, as discussed in section 1.10.5 (Advances in electrospinning).

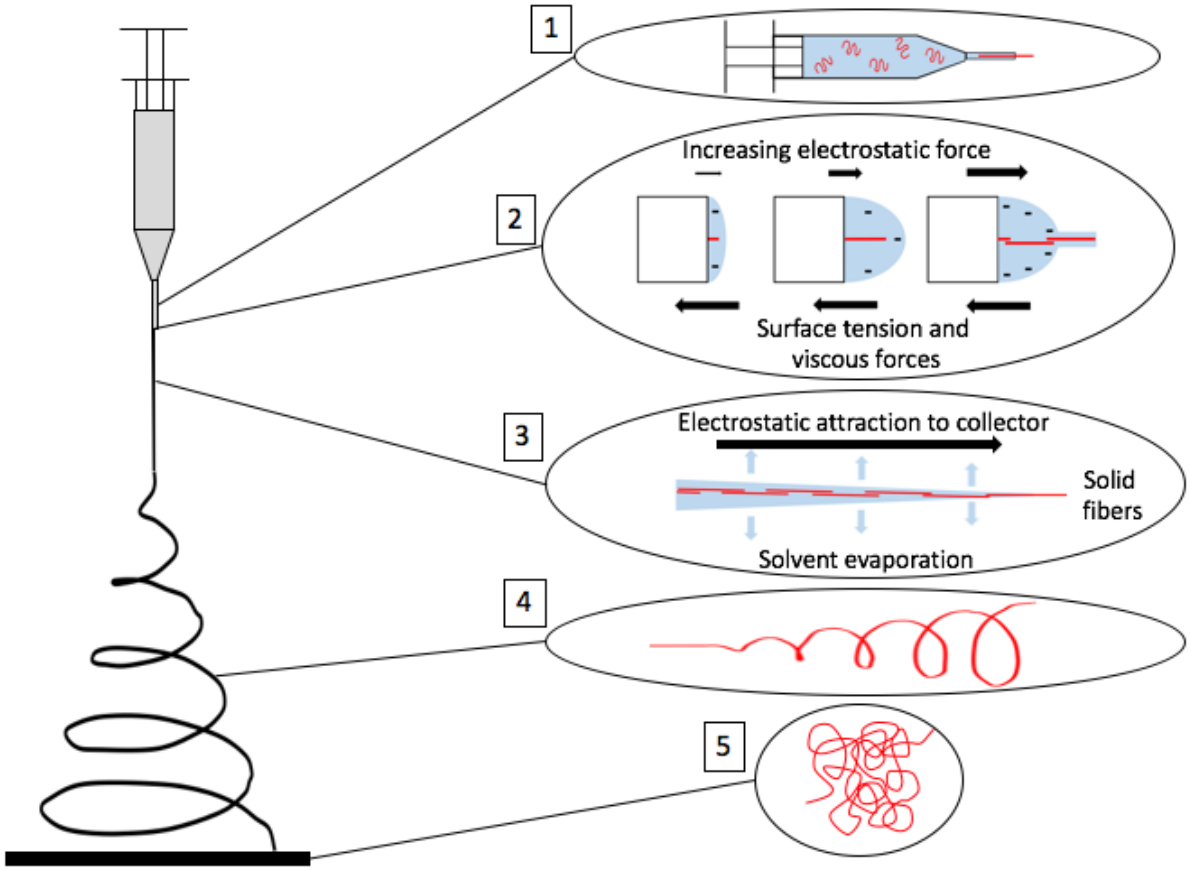


Figure 1-14. Schematic depiction of the stages of the electrospinning process.

Polymer chains are randomly dispersed throughout the solution but elongate when subjected to shear stress as they are pumped into the electric field (1). Charge separation builds on application of electrostatic force until it is sufficient to overcome the surface tension and viscous forces of the solution, establishing the Taylor Cone (2). During transit towards the collector, charge repulsions induce complex instability and whipping, stretching polymer chains (3). Throughout this time, volatile solvent evaporates is evaporating, leaving behind polymer chains held together through inter-molecular interactions (4). Randomly orientated fibers are deposited on the grounded collector (5).

1.10.4 Electrospinning balances electrostatic force and surface tension

The balance between electrostatic force and surface tension is crucial for electrospinning (Figure 1-15). When the surface tension of the polymer solution is balanced with the applied electrostatic force, polymer chain entanglements can form appropriately in order to allow a stable jet and continuous electrospun fibers (B). If insufficient electrostatic force is applied, surface tension can pull the solution together once ejected from the nozzle, resulting in small

droplets ((A) electrospraying – a technique with other biomedical applications). If the electrostatic force is too great, multiple Taylor cones can form, along with increased branching and cross linking causing irregular fiber deposition (C).

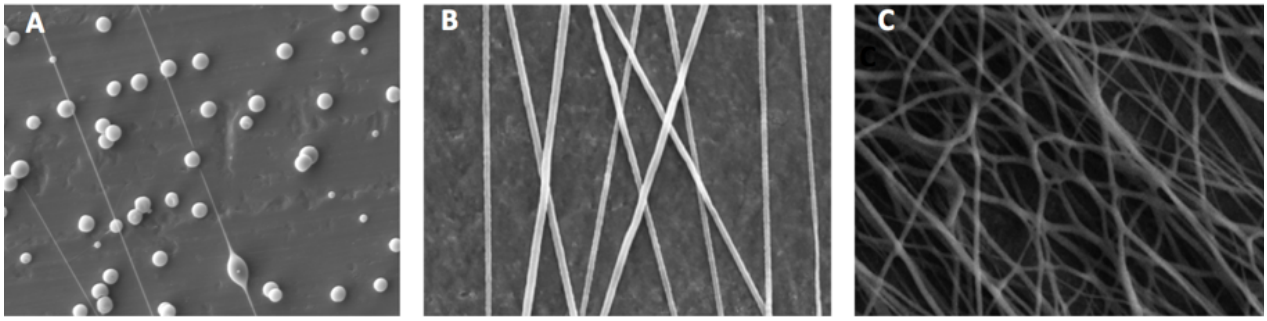


Figure 1-15. SEM images showing the effect of electrostatic force and surface tension balance on resultant electrospun fibers.

Insufficient electrostatic force allows surface tension to pull solution into beads and droplets (A). Balanced forces result in smooth homogenous fibers (B). Sufficiently great electrostatic force results in multiple jet electrospinning and more irregular fiber deposition (C).

Within each electrospinning system, parameters can be manipulated to change electrospinning behaviour and the resulting fibers [174-177]. These changes include topography, diameter and alignment. Whilst there is debate in the literature about how to group different electrospinning variables, this thesis will define parameters as system or process parameters (Table 1-2). Generally, system parameters are considered as things which cannot be changed once electrospinning has commenced. Process parameters, however, could theoretically be fine-tuned during the electrospinning process.

Table 1-2. System and process parameters modulated in electrospinning to affect fiber diameter, alignment and topography.

System parameters			
Polymer (176, 178) -Material -Molecular weight -Concentration	**Nozzle (180, 184)** -Material -Diameter -Distance to collector	**Solvent (179,181)** **Salts/additives (182)**	**Collector (184)** -Type -Material **Temperature (183)** **Humidity (183)**
Process parameters			
Flow rate (179)	**Voltage (177, 179)**	**Collector motion**	**Gas/Solvent parallel flow**

A detailed discussion of each parameter effect can be found in the literature as indicated in Table 1-2 [176-184]. However, a change to a process and a system parameter and the effects on electrospun fiber diameter, a main aim of this thesis, are reviewed to help illustrate the principles behind electrospinning.

If electrospinning of a polymer occurs over a longer nozzle-collector distance (system parameter), there is increased time for charge repulsion to act and increase whipping instability. This results in more drawn-out fibers, narrowing the mean diameter. The effect of increasing the distance is limited by solvent vaporisation. Once all solvent has evaporated and the polymer exists in a solid state, not an aqueous phase, whipping instability will not draw polymer chains past each other. For this reason, a less volatile solvent (system parameter) which increases the time spent in an aqueous phase can also reduce fiber diameter, as polymer chains can be drawn out for a longer time during their passage from nozzle to collector before solidifying. However, if the solvent is insufficiently volatile, fibers may accumulate on the collector in a semi-liquid state. This can lead to ribbons and more amorphous sheet formation, rather than discrete fibers.

Increasing the applied voltage (process parameter) can also have marked effects on electrospinning behaviour (Figure 1-15). Increasing the voltage induces more charge

separation and whipping instability, ultimately reducing fiber diameter. However, this also has limitations. Once the applied voltage crosses a threshold, complicated multi-jet electrospinning is induced, leading to irregular fiber patterns.

Whilst each parameter can be considered individually, in reality they are interlinked. Changing the solvent will lead to altered viscosity, conductivity and vaporisation, all parameters which in their own right will affect electrospinning. Significant work has been done to model the electrospinning process and how changes in parameters can affect resultant fibers [185]. However, these models cannot reliably demonstrate the observed outcomes of more complex electrospinning set-ups. Machine learning and complicated neural networks are being developed to allow in silico modelling to improve reliability and reduce the time and cost of producing desired electrospun scaffolds [186,187].

1.10.5 Advances in electrospinning

This section details advances in electrospinning technique to create chemically, biophysically or mechanically more advantageous materials for tendon repair.

1.10.5.1 Increasing the range of electrospun fibrous material

Traditional solvent-based electrospinning has limitations: polymers must be soluble in an appropriately volatile solvent, polymers and any added components must be stable in harsh solvents, and using such toxic solvents necessitates precautions. Harnessing the benefits of electrospun fibers in combination with the benefits of other polymers and materials could, however, generate biomaterials better suited for use in different tissue applications. Consequently, a number of techniques have evolved to increase the range of substrates and materials suitable for electrospinning.

Adding metals, ceramics and nanoparticles to polymer solutions allows fabrication of fibers with these components evenly distributed throughout the polymer fibers. In the case of nanoparticles these can directly influence the mechanical properties [188]. With metals [189],

ceramics [190] and salt additives [191], post-fabrication treatments can fuse these added components while removing the polymer to generate fibrous materials of altered base chemistries conveying mechanical or biomolecular advantages.

Melt electrospinning utilises molten polymers not polymer solutions. This facilitates the generation of biomimetic fibers from semi-crystalline polymers. This is important as different polymer materials have significant effects on cell biology [137,192]. For example, polypropylene has a long history of use as a biomaterial because of its favourable material and chemical properties [193,194]. However, problems resulting from other fabrication techniques, particularly those related to inflammatory reactions stemming from unnatural surface sizes and mechanical properties, may underlie the recent failings of polypropylene materials [195]. Melt electrospinning is now able to generate scaffolds combining the favourable material properties of polypropylene with the benefits of biomimetic fibers, specifically matching the scaffolds surface size and mechanical properties to those of native tissue.

Co-axial spinning allows for the electrospinning of a core/sheath fiber [196]. It is also possible to create tri-partite fibers [197]. Co-axial fibers can combine favourable materials. For example, Chen *et al* manufactured collagen coated polyurethane fibers [198]. PIEC cells attached and proliferated significantly more greatly on these materials than on polyurethane fibers alone. PIEC cell attachment and proliferation was also greater on co-axial collagen/polyurethane fibers than on polyurethane functionalised through collagen adsorption following electrospinning. This suggests that it is not merely the presence of collagen directing cell biology, but the more biomimetic nature of fibrous collagen produced through electrospinning that underpinned the greater attachment and proliferation.

1.10.5.2 Bio-active molecule functionalisation of electrospun fibres

Whilst changing the base chemistry of electrospun fibers has extended the applications for electrospinning in biomaterial fabrication, combining additives can also promote biological

activity to broaden electrospun fiber uses. These include cells [199], drugs [200], growth factors, proteins and nucleic acids [201]. However, many of these additives are insoluble or unstable in the volatile solvents used in electrospinning. Furthermore, direct blending into solution often leads to burst release of the additive on exposure of the scaffold to solution, limiting use.

Electrospinning advances can avoid these issues. Emulsion electrospinning uses an emulsifying agent to create small volumes of the insoluble material within the polymer which are released as degradation of the polymer occurs [202]. Selection of the polymer, solvent and emulsification agent gives considerable control over the rate of delivery of the target molecule. Co-axial fibers can also be used to control delivery of biological molecules. Inclusion of a target molecule in the sheath, core, or both components, can change the timescale of delivery of a molecule from a single material.

Electrospinning can provide spatial and temporal control over delivery of multiple biologically active moieties from scaffolds. Development of electrospun materials capable of delivering biologically active molecules in different areas, at different times are under development [121]. Such materials are limited not only by the capabilities of electrospinning but by an immature understanding of the required patterning of tissue biology drivers.

1.10.5.3 Enhancing the nano-scale biophysical cues of electrospun scaffolds

Surface roughness and topography can exact significant effects on cell biology. Surface roughness can be modified through alterations of humidity and temperature used in the electrospinning environment. Changing the relative humidity impairs solvent vaporisation and has been used to create pits [203] and longitudinal grooves [204] in electrospun fibres. Post manufacture laser processes have also been applied to electrospun fibers to form pits of more deliberate sizes and spatial arrangements [205]. Nano-lithography techniques, stamping, and salt leaching have also been used to impose various nanoscale patterns and features onto electrospun fibers [206].

1.10.5.4 Enhancing the micro-scale biophysical cues of electrospun scaffolds

Of particular relevance to tendon tissue engineering is the alignment of electrospun fibers. Without modification of the collection system, fibers are deposited randomly as a mesh. Various techniques have been developed to give control over the arrangement of fibers. The simplest and most commonly used technique is the use of a rotating collector. With increased rotational speed, the whipping instability is overcome to deposit fibers in aligned scaffolds. This can also be achieved through a rotational nozzle [207]. Patterned collectors have also been used where some areas are relatively insulated, leading to preferential deposition of fibers in pre-designed patterns. Not only can this promote fiber alignment and patterning, but it can also be used to introduce deliberate pore sizes and porosity to a scaffold.

Achieving adequate porosity and pore size to facilitate cell invasion is a major issue for successful tissue engineering. Low temperature electrospinning (LTE) uses temperatures below freezing to generate ice crystals between fibers as they form on the collector. Post-spinning treatments remove the crystals to leave a scaffold with increased porosity [208]. A more controllable method has since been developed through the simultaneous spinning of two fiber populations [209]. Two polymer solutions are electrospun from two nozzles to create a scaffold comprised of a target fiber population and a sacrificial fiber. The scaffold is then immersed in a solvent selected to dissolve only the sacrificial polymer. Alterations in the ratio of target to sacrificial fiber population allows for manipulation of the final scaffold porosity.

Altering the porosity of the scaffold affects other aspects of biomaterial function. *In vitro* testing of a high porosity scaffold showed significant cell invasion [210]. On implantation in an *in vivo* rat rotator cuff tear model, however, cell invasion was not greater than a non-porous control material. The porous scaffold was unable to withstand the physical forces during surgical implantation, those experienced *in vivo*, or both, collapsing down to a porosity and pore size which no longer facilitated cell invasion.

Even if porosity is high, a minimum pore size is required to allow cells to move through the scaffold as the nucleus, the largest cell organelle, has limits on how much it can deform. Improving pore size has been achieved through formation of nanoyarns [211], with laser treatments [205], or through the use of patterned collectors, as previously described.

1.10.5.5 Producing macro-scale electrospun materials

As surgical implants and tissue engineering scaffolds progress, the need to consider biomaterials in 3D becomes increasingly important. This has been achieved through a variety of methods during electrospinning as well as through post-manufacture modifications.

Complicated collection systems, building on the same principles of 2D patterned collectors, have been used to develop 3D structures, including pipes and bifurcated tubes [212].

Electrospun fibers can also be combined after production into more complicated structures. Electrospinning of fibers into long filaments enables combination into yarns [213]. This combines the biophysical stimuli of biomimetic fibers with increased porosity to promote cell invasion and higher surface area to volume ratios to promote degradation or increase exposure of cells to biophysical or added bioactive stimuli (Figure 1-16).

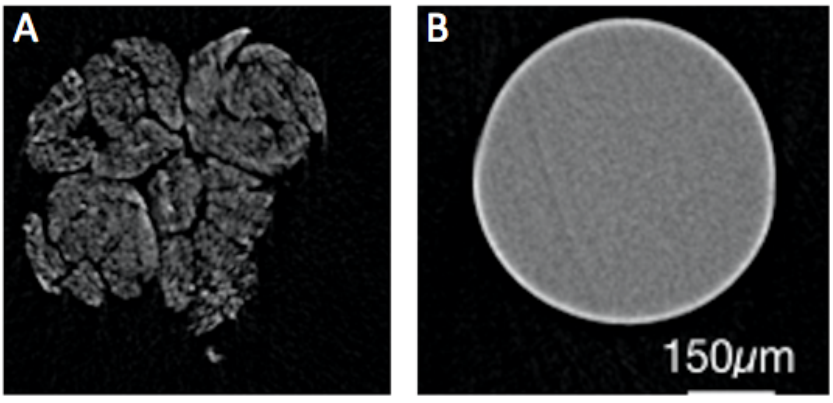


Figure 1-16. μCT images of multi-filament yarn (A) and simple extruded suture (B).

These μCT slices show the increase in porosity achievable through electrospun fibers. This porosity aims to facilitate cell invasion and matrix deposition to order to improve the speed and strength of tissue repair.

Electrospun materials are fragile and require suitable mechanical properties to withstand implantation as discussed. Fabricating electrospun scaffolds capable of surviving these processes can, however, be challenging. As electrospun fibers form on the collector, the collector becomes relatively insulated. This means that surface fibers may differ significantly from the deeper fibers in their biophysical properties, particularly diameter and alignment. To overcome the differences between fibers, multiple thinner, uniform layers can be combined to create thicker, uniform scaffolds [150]. In a similar fashion, electrospun fibers can be layered onto other material types as coatings to harness biophysical cues and functionalise materials with mechanical advantages [158].

1.10.5.6 Producing electrospun materials with specialised zones

As discussed, the enthesis is a complex zone with transitions through 4 distinct histological zones. Biomaterials will need to mimic these transitions to optimise the chances of optimised healing and tissue regeneration. Samavedi *et al* combined multiple advances in electrospinning to create a multi-zoned surgical implant for patella ligament repair [214], a similar tissue transition to the enthesis. Using 2 polymer solutions, 3 electrospinning nozzles, carefully positioned shields and 2 collection methods, a single electrospun scaffold was formed with 3 distinct zones (Figure 1-17). The zones differed in material composition and fiber alignment. The outer bone areas were comprised of random, stiffer fibers in order to replicate a bone niche, and a softer, aligned fiber inner component to recreate ligament tissue. The transitional areas between the zones had both configurations and types of fibers, hoping to assist with more specialised cell phenotypes in the enthesis.

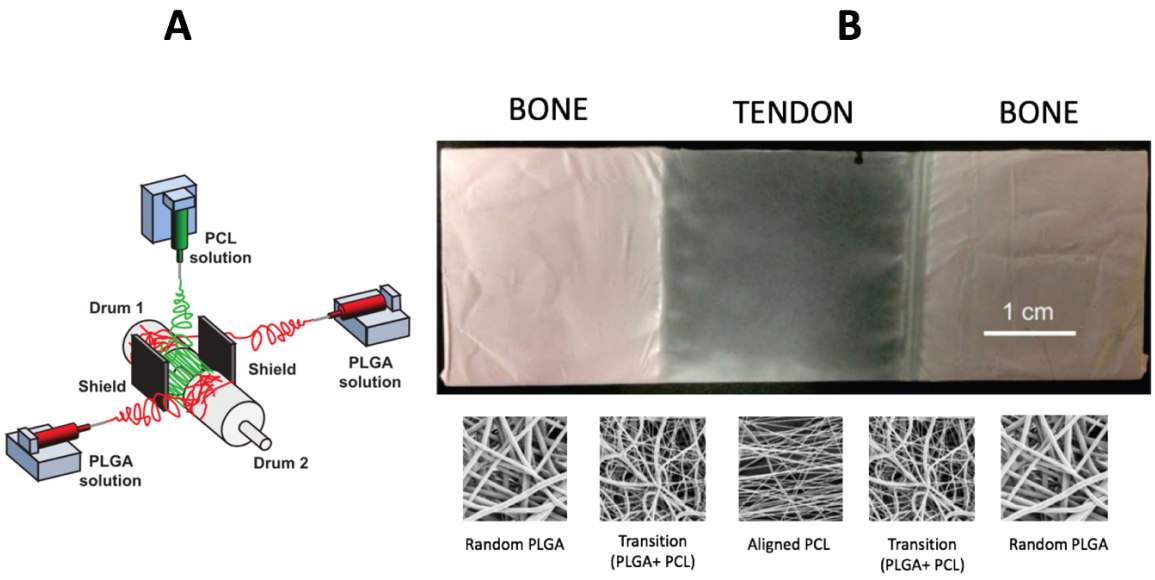


Figure 1-17. Schematic depiction of a complex electrospinning system used to produce multi-zoned scaffolds for ligament repair.

This figure shows a schematic representation of a complex electrospinning system (A). This shows the use of multiple nozzles spinning multiple solutions, shields to focus fiber deposition in targeted zones, and multiple collectors of different types. The resulting scaffold (B) had 3 distinct zones with SEM micrographs showing the random poly(lactic-co-glycolic acid) (PLGA) fibers suited to bone tissue formation and the aligned polycaprolactone (PCL) component used to promote tendon formation. The transition zones with both fiber populations may play an important role in engineering an appropriate entheseal response [214].

1.10.5.7 Enhancing the mechanical properties of electrospun scaffolds

Biomaterials face a range of mechanical challenges upon implantation. Firstly, the material must be able to withstand implantation and perform its macroscale mechanical property function [215]. Secondly, the material must be able to favourably encourage local cell interaction with appropriate microscale or local mechanical properties. Adequate macro mechanical properties must be combined with biomimetic local mechanical properties to ensure an implant can promote appropriate healing [195].

In the context of RCT repair, macro-mechanical properties refer to whether an implant can return to a useable state following the handling during implantation, can withstand the forces applied during fixation with sufficient resistance to prevent suture pull-through, and can

withstand forces transmitted through the implant during physiological loading. These macroscale properties have been improved through altered polymer selection or additives [188,216], nanoyarn reinforcement [211], combination products [190], annealing [217] and cross linking [218] treatments. However, manipulation of the mechanical properties impacts on other biologically important considerations, including degradation rates and the local mechanical properties [217].

Local mechanical properties, or micromechanical properties, describe the mechanical properties experienced by cells interacting with the material. Differences in these local mechanical properties are powerful and able to direct the differentiation of stem cells down separate lineages [138]. Manipulation of the local mechanical properties of biomaterials is more difficult and less reported in the literature than assessment of macro mechanical properties. The impacts of such modifications, however, are potentially significant in enhancing patient outcomes, with the mismatch between local mechanical properties of native tissue and biomaterials implanted into these environments raised as a potential contributor to poor surgical outcomes [195].

1.10.5.8 Enhancing the surface bioactivity of electrospun scaffolds

On implantation and in *in vitro* use, biomaterials interact initially with the surrounding fluids, drawing a complex mix of ions, proteins and other molecules to the surface of the biomaterial to form an adsorbed layer [219]. Cell populations then invade into this created niche, responding to both the molecules in the surrounding layer and to the spatial arrangement of these molecules in the adsorbed interface.

These interactions can be thought of in two groups: those relating to the concentration or activity of these molecules, and those relating to the spatial association of the molecules. Advances in material fabrication techniques and post-fabrication modifications make it possible to influence both the concentration and spatial distribution of molecules to provide

avenues for engineering favourable cell responses. These can be manipulated through changes to material hydrophobicity, charge and surface chemistry during or after the electrospinning process. However, separation of these effects is challenging, as they are inter-connected: changing the base material can change the hydrophobicity and charge of the fibers.

It is important to highlight that the responses to biomaterials are cell-type specific, necessitating detailed research of target cell types with the proposed biomaterials. For example, increasing biomaterial hydrophobicity from 0^{o} to 60^{o} promotes fibroblast attachment [131] but reduces osteoblast attachment [130].

Modification of electrospun fiber hydrophobicity, charge and chemistry can be achieved through wet chemical treatments [220], plasma treatments [221] and radical polymerization methods [222]. Plasma treatment is limited to the more superficial layers of an electrospun scaffold, but wet chemical treatment can penetrate through the entire thickness of a scaffold. These treatments alter the functional groups present on the surface of the material, predominantly altering the number and ratio of amine, hydroxyl, or carboxyl groups. These changes increase or decrease protein binding [223] as well as altering protein conformation [224] with subsequent influences on cell adherence [225,226] and cell morphology [227]. Wet chemical treatment is easily performed on highly porous electrospun scaffolds, to further functionalise electrospun biomaterials for tailored uses.

1.10.6 Polydioxanone storage conditions and breakdown

Biomaterial fabrication extends upstream from fibre production to the storage and condition of the initial polymer. However, unlike the breakdown and degradation of polymer materials *in vitro* and *in vivo*, these aspects have not been well studied and documented in the literature [215]. Whilst some of the *in vitro* research can be drawn on to consider the effects of polydioxanone (PDO) storage conditions, no literature on the effect of PDO storage or other polymers prior to electrospun manufacture is available.

Degradation of PDO occurs predominantly through hydrolytic breakdown. Awareness of the effects of hydrolytic degradation during fabrication are documented, with publications advising heat treatments to reduce potential water vapour effects on resulting materials [228]. Packaging and storage of polymer biomaterial products, in line with ISO standard 11607, also involves treatments to remove water vapour prior to sealing in highly impermeable products to minimise hydrolytic breakdown. Given that these effects are well known and documented, it is surprising that less attention has been paid to the pre-manufacture storage of PDO.

Polymer chains exist in either crystalline or amorphous states. Crystalline areas are dense regions which act as crosslinks, promoting mechanical properties. Hydrolytic breakdown of polymer chains disrupts the crystalline areas, leading to the break down and eventually degradation of the material. PDO exists as a semi-crystalline material, meaning crystalline areas are found within amorphous regions. Increasing the proportion of polymer in a crystalline state will increase the mechanical properties. Related to this, increasing the crystalline proportion results in slower degradation as there are less sites for water molecules to hydrolyse [215]. Consequently, hydrolytic breakdown of the polymer prior to fabrication will impact upon electrospinning as well as lead to weaker, faster degrading electrospun fibers, potentially jeopardising implant integrity before adequate healing can occur.

1.10.7 Summary

Electrospinning is capable of producing a new generation of biophysically active biomaterials. These materials can harness and deliver powerful biophysical cues to direct cell responses and engage intrinsic healing potential. Over and above the generation of biomimetic fibers, technical advancements enable chemical and physical modifications of electrospun scaffolds to further engineer cell responses. Electrospun materials are inexpensive to produce, can be produced at scale, face a lower regulatory threshold and mitigate the risks associated with allograft and xenograft materials. Accordingly, considerable research time and funding is

being channelled into clinical translation of these products for RCT repair, other tissue applications, as well as scientific applications.

1.11 Current electrospun materials for rotator cuff tear repair and tendon tissue engineering

Currently there are no commercially available electrospun materials for rotator cuff tear repair. As previously mentioned, a large scale clinical trial proving the theoretical benefits of electrospun scaffolds in any tissue type is yet to occur. There are in the literature, however, electrospun fibre scaffolds in various stages of development looking to take advantage of the biomimicry and potential of electrospun fibres. These include the BioPatch (University of Oxford), the BioYarn (University of Oxford) and BioWick™ (Cayenne Medical, Scottsdale, AZ, USA) [231]. These 3 separate products are trying 3 different approaches to use electrospun fibres to deliver biophysical, biomimetic cues to support tendon healing.

The BioYarn is a multi-filamentous structure comprised of nanoyarns (Figure 1-16) [213,229]. The braiding of these filaments creates a porous environment to facilitate cell ingrowth and tissue deposition while also providing biomimetic cues from the electrospun fibres. The BioYarn is to be used in the place of conventional sutures. Presently to generate a material strong enough to perform this role, the BioYarn diameter is larger than a conventional extruded suture of the same strength. Clinical trials have been approved for this product with manufacture of the implants for the study underway. Further research and development to reduce the BioYarn diameter through advanced electrospinning techniques may reduce the tissue damage incurred through insertion of a larger diameter suture at the enthesis, increasing chances of successful healing.

The BioPatch is a multicomponent biomaterial with approval for clinical trials following favourable results in extensive *in vitro* and *in vivo* animal studies (Figure 1-18) [150,230]. The

BioPatch is designed for use in an onlay augmentation of rotator cuff repairs (Figure 1-8). Mechanical strength is provided by a woven component of 120μm diameter fibres, while the aligned 1μm electrospun fibers are positioned on the surface of the tendon to provide biophysical cues. A proprietary thermoplastic layer annealing technique has been generated to preserve pore size and porosity while generating an electrospun fibre layer thick enough to support and steer invading cell populations. PDO, the polymer used for both components, is degradable, allowing physiological load transmission to the deposited tissue over time to promote maturation and remodelling into more functional tendon tissue.

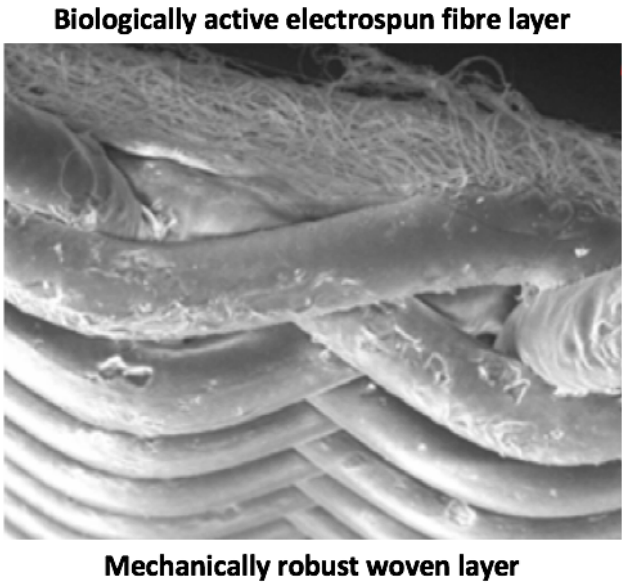


Figure 1-18. The BioPatch biomaterial for rotator cuff tendon repair.

The BioPatch has a multi-layered electrospun fibre layer to provide biophysical cues (top) and a woven component to provide mechanical strength (bottom).

BioWick™ is another electrospun scaffold designed for rotator cuff repair. Unlike the BioPatch, the BioWick is designed to be used as an interpositional augmentation biomaterial. The BioWick is comprised solely of PLGA electrospun fibres. The exact size and distriburtion of these fibres has not been published. Strength is provided through the stronger PLGA chemistry. However, this may lead to local mechanical properties non-compatable with

tendon fibroblast biology or longer degradation times which impair the remodelling of deposited tissue. Recruitment to a clinical trial (NCT03199391) is underway following approval based on animal studies [231].

For all three of these products, optimisation of fibre alignment, diameter and local mechanical properties with tendon fibroblasts from diseased rotator cuff tendon could further increase the positive effects of these products and improve tissue healing and patient outcomes.

1.12 Electrospun fibre effects on cell populations involved in tendon healing

The biological response of cells to biomaterial cues is cell type specific [130,131]. Accordingly, we must consider the effects of biophysical cues from electrospun fibres on the individual cell populations central to tendon healing. These include tendon fibroblasts, immune cells, endothelial cells and tendon-progenitor stem cells.

Whilst this section considers cell response to deliberately altered biophysical cues, specifically fibre alignment, diameter and stiffness, it is important to highlight that alterations in electrospinning parameters to change these biophysical cues may also affect biomaterial surface properties. Surface hydrophobicity and charge can be affected by alterations in electrospinning parameters, affecting the adsorbed corona. Cell responses may be attributed to changes in the biophysical property, but potentially be confounded by unintended alterations in other properties.

In the context of RCT repair, this is important because fibroblasts are sensitive to hydrophobicity and charge. Fibroblasts are most adherent to and most proliferative on biomaterials with mid-range hydrophobicities [131]. Fibroblast morphology and gene expression are also dependent on biomaterial hydrophobicity [131,232]. Fibroblasts also show

increased attachment [233], increased proliferation [234] and increased collagen [235] on charged polymers. However, in these experiments [131, 232-235] the changes in biomaterial hydrophobicity and charge was deliberate and over considerable ranges, much greater changes than those expected to occur as unintended consequence when altering other biophysical parameters.

1.12.1 Tendon fibroblast responses to electrospun fibres

1.12.1.1 Tendon fibroblast response to altered fibre alignment

The literature on the response of tendon fibroblasts to fibre alignment is limited. However, fibre alignment has significant impacts on fibroblasts derived from other tissues. Whilst the response of tendon fibroblasts may differ from fibroblasts derived from other lineages, the differences are likely minimal given the conserved nature of response between ligament [236], dermal [237], conjunctival [238] and cell-line fibroblasts [239,240] across species and over different polymer types. Tendon fibroblast sensitivity to alignment is also observed across other topographical features. Aligned grooves have also been shown to maintain tendon cell phenotype and affect matrix production [202,241].

Alignment did not affect proliferation of anterior cruciate ligament derived fibroblasts cultured on random and aligned polyurethane (PU) nanofibres for 7 days [236]. This was consistent with NIH 3T3 fibroblasts seeded on PLGA scaffolds [239]. Zhong *et al* however noted lower attachment and greater proliferation on aligned collagen scaffolds over 7 days culture compared to random scaffolds [238].

The adopted morphology of fibroblasts is also proportional to fibre alignment. Bashur *et al* cultured NIH 3T3 fibroblasts on 4 PLGA electrospun scaffolds varying in alignment, revealing a relationship between the elongation of the cell and increasing fibre alignment. This relationship between fibre alignment and altered morphology has also been shown in L929 fibroblasts on PLLA fibres [240] and in conjunctival fibroblasts on collagen fibres [238].

Matrix production is also sensitive to fibre alignment. ACL fibroblasts seeded on aligned PU fibres showed significantly increased collagen production compared to random fibres [236]. Additionally, the quality of deposited collagen, as assessed by second harmonic generation microscopy, and strength of the deposited matrix, as assessed by tensile testing, produced by human dermal fibroblasts after 21 days culture on PCL fibres was dependent on fibre alignment [242]. Aligned fibres induced aligned collagen fibres better mimicking native collagen arrangements and increased tissue strength.

1.12.1.2 Tendon fibroblast response to altered fibre diameter

Tendon fibroblasts are sensitive to electrospun fibre diameter with demonstrated effects on matrix production, morphology and proliferation. Lower diameter fibres (0.32μm) induced greater proliferation, increased collagen secretion and higher proteoglycan deposition than larger diameter fibres (1.8μm). The larger fibres however increased expression of tendon fibroblast markers supporting fibroblast phenotype [140]. Bashur *et al* showed fibre diameters of 3.6μm induced larger aspect ratios or increased elongation of NIH 3T3 fibroblasts than 0.14μm fibre scaffolds [239].

Studies have reported on the relative effects of fibre diameter and alignment on cell populations, describing the relative strength of one variable over the other. Cardwell *et al* showed that the effects of diameter elicited greater responses in gene expression of C3H10T1/2 stem cells than fibre alignment [243]. Other papers have suggested the interaction is mutually dependent with fibroblasts only showing responses to altered alignment when diameter was above a critical threshold [244].

1.12.1.3 Tendon fibroblast response to altered local fibre mechanical properties

While the effect of stiffness on cell function has been well researched in some cell lineages and biomaterial types, the effects of electrospun fibre stiffness on tendon fibroblast function are not well characterised. There are two reasons for this. Firstly, determination of stiffness of

fibres below a micron is technically challenging. Secondly, tendon fibroblast response to stiffness is a less active research area than the role of stiffness in biomaterials for other tissue types like bone, where stiffness has been shown to play an important role in bone tissue formation and osteogenic differentiation. Nevertheless, some research exists on other fibroblast populations which may be applicable to tendon fibroblast responses on electrospun fibres.

It has been shown that fibroblasts proliferate and spread more on stiffer materials [245]. Fibroblasts also migrate in a graduated fashion towards stiffer substrates [246]. Furthermore, they regulate their cytoskeletal stiffness in response to their environment [247]. Tendon fibroblasts have also been shown to maintain their phenotype on stiffer scaffolds. The rate of tendon fibroblast matrix turnover is also sensitive to stiffness with more compliant or softer scaffolds promoting matrix breakdown and turnover [248].

Preferential migration, attachment, proliferation and gene expression would suggest matrix stiffness and other local mechanical properties are an important consideration for biomaterial biophysical impacts, a property not currently considered in commercially available materials.

1.12.1.4 Tendon fibroblast response to altered surface roughness

Surface roughness has also been shown to affect fibroblast behaviour. One study has shown that increased roughness can decrease total fibroblast attachment [249], while the strength of the adherent fibroblasts is greater on rougher surfaces [250]. Surface roughness also impacts upon fibroblast gene expression [251]. The response to roughness appears to have a threshold. Whilst not conducted on electrospun fibres, the response of fibroblasts to nano-grooves was limited by a threshold of 35nm. Fibroblasts displayed morphological and alignment differences as groove size decreased from 1000nm down to 35nm. However, below 35nm these differences in cell morphology and alignment were not observed [252].

1.12.2 Tendon progenitor stem cell population response to electrospun fibres

Tendon-progenitor stem cells exist in very low numbers in mature tendon [39]. Their contribution to tendon healing is uncharacterised with cell lineage tracing in animal models suggesting the increase in tendon fibroblasts comes from proliferation of pre-existing tendon fibroblasts, particularly those found in the paratenon [50,54]. Research suggests stem cells are, however, similarly responsive to biophysical cues provided by biomaterial scaffolds with aligned electrospun fibres supporting the proliferation and the subsequent differentiation of tendon derived stem cells [253].

Significant literature has examined the effects of electrospun fibres on other stem cell populations but these results are difficult to generalise to tendon progenitor stem cell responses. For example, electrospun fibres have been used to both promote differentiation of Neural Stem Cells [254] but maintain potency of Mesenchymal Stem Cells [159].

Stem cells in other tissues and disease states are known to perform immunomodulation roles [255]. Tendon progenitor stem cells could have a role in tendon healing and biomaterial response in this more indirect but important pathway. Without further research of tendon progenitor stem cell specific responses to electrospun fibre biophysical cues, and their relative contribution to tendon healing, it is not possible to develop electrospun fibres which deliberately target and moderate tendon progenitor stem cells to optimise tissue response.

1.12.3 Immune cell population response to electrospun fibres

The immune response to biomaterial implants in tendon has been linked to subsequent surgical outcomes [99,256]. Chronic inflammation affects tissue healing [257] and has been linked to biomaterial failure in human genitourinary surgery [258]. More pronounced inflammatory responses to biomaterials in animal tendon models have been linked to increased repair failure rates [107]. Biophysical cues from the implant could target the immune response, an important early determinant of tissue healing and successful biomaterial implantation [259].

Upon implantation, the biomaterial induces a foreign body response, a specific type of chronic inflammatory response resulting in the formation of a fibrotic capsule and macrophage-derived foreign body giant cells [257]. The macrophages differentiate from monocytes from peripheral blood that are attracted chemotactically to inflammation and tissue injury at the surgical site. The macrophage response is a key determinant of the long term immune reaction. Depending on the chemical, biological and physical nature of the biomaterial, macrophages may drive chronic inflammation and fibrosis or promote healing and resolution of inflammation [260].

Electrospun fibre biophysical properties have significant effects on macrophages with potential implications for improved tissue healing. Fibre alignment has been shown to have an effect *in vitro* and *in vivo*. *In vitro*, macrophage adhesion to aligned PCL scaffolds was significantly lower than random PCL scaffolds. *In vivo*, the fibrotic capsule thickness was significantly thinner around aligned fibres than around random fibres with cell invasion into aligned but not random fibre scaffolds [261].

Other research has suggested that fibre diameter impacts more on macrophage function than fibre alignment. Macrophages seeded on nanofibre PLLA scaffolds demonstrated lower pro-induction of pro-inflammatory genes responses than microfibre scaffolds. The differences between aligned and random scaffolds of the same diameters did not induce this same reduction in gene expression [143]. These studies have used different polymers which potentially explains the conflicting results as polymer material chemistry has been shown to independently affect macrophage function [262,263].

Further work has shown that fibre diameter influences macrophage phenotype with thicker (5-6µm) PCL fibres promoting M2 phenotypes compared to thinner (700nm) fibres eliciting an M1 bias [141]. Whilst simplified, macrophages can be considered across a spectrum from M1 (pro-inflammatory) to M2 (anti-inflammatory) [264]. M2 macrophages are seen as beneficial in

long term biomaterial responses [259]. Similar results were found with larger diameter PDO fibres promoting M2 phenotypes. This work went on to show that pore size was another important biophysical biomaterial property to manipulate macrophage function [265].

Macrophages are also sensitive to other biophysical cues. Increased pro-inflammatory signatures were induced with increasingly stiff scaffolds *in vitro*. Furthermore, the degree of fibrosis correlated with increasing stiffness *in vivo* [266]. Topographical groove dimensions have also promoted M2 macrophage phenotypes [267]. Hydrophilic surfaces have also been shown to promote giant cell apoptosis and down-regulate pro-inflammatory cytokines [262,263].

Dendritic cells [268] and neutrophils [269] are other important immune cells in the foreign body response with function differing according to biophysical inputs. Dendritic cells play an important role in innate immune response and immunomodulation through their effects on T Cell populations. Neutrophils also play a role in the initial inflammatory response. However, unlike other cells involved, neutrophils are less affected by biophysical cues. Neutrophil response, for example, does not differ with altered matrix stiffness like macrophage response [269].

The biomaterial effects on different immune cell populations and the interplay between these populations are complex. However, they must be considered in parallel to promote tissue healing ahead of chronic inflammation and fibrosis.

1.12.4 Endothelial cell response to electrospun fibres

The role of angiogenesis and vascularisation in tendon healing varies in health and disease. Avascular healthy tendon tissue develops an increased vascular network in rotator cuff tendinopathy as seen on ultrasound [61]. In other tissue types, the endothelial response has been tightly linked to the immune response [270,271] with pro-angiogenic factors released from immune cell populations in the acute phase of inflammation promoting vascularisation [51]. The

extent of endothelial response is also directly related to the capacity for successful tissue healing [272,273].

The effects of electrospun scaffolds on endothelial cells are not fully characterised but they are evidently sensitive to biophysical cues. It has been shown that 6μm PLGA fibres initiated greater attachment of human umbilical vein endothelial cells than 12μm fibres. However, no difference in proliferation or prostacyclin secretion, a marker of cell function, was noted over the different electrospun fibre diameters [274]. Additionally, endothelial cells are sensitive to PCL fibre alignment, demonstrating greater adherence strength with increasing alignment [275].

Angiogenesis is linked with both acute and chronic inflammation, and tissue healing. As endothelial cells are responsive to electrospun fibre biophysical cues, further research should be undertaken to characterise this relationship and determine optimal biophysical parameters for a favourable angiogenic response suited to tendon tissue.

1.12.5 Summary of cell responses to electrospun fibres

Currently, it is not known which cell population is the most important driver of biomaterial response for tendon healing. Successful healing is likely an orchestrated response from contributions of different cell types varying over the lifecycle of the implant and subsequent tissue maturation. Furthermore, it remains to be shown exactly what a favourable response for each cell type might be. However, biophysical cues can be used to have significant influence over the biology of tendon fibroblast, macrophage, endothelial cell and other cell types involved in tendon healing to tailor supportive cell-material interactions.

While the response of each cell type differs with individual biophysical stimuli, ultimately, healing is a complex relationship both between individual cell types and the biomaterial, and different between cell types (Figure 1-19). The interaction and communication between different cell types is also influenced by biophysical properties. For example, the relationship between immune cell response and tendon fibroblasts is sensitive to alignment. Tendon

fibroblast responses to inflammatory cues imparted from macrophage co-cultures, are dependent on electrospun scaffold alignment [276]. Ultimately, cell material responses cannot be considered in isolation but as part of a tissue response.

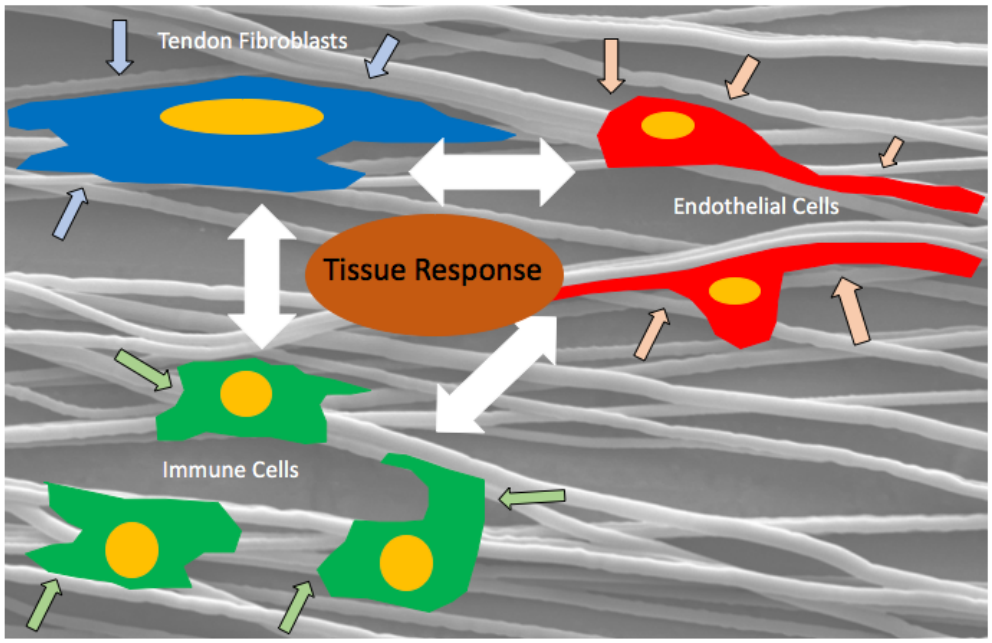


Figure 1-19. The interplay between biomaterials and cell populations governs the tendon healing response after injury and biomaterial implantation.

Tendon cell populations interact with a biomaterial in cell-specific ways. Only selected important populations are shown in this figure. Tendon fibroblasts are in blue, immune cell populations in green and endothelial cells in red. The lighter coloured arrows represent the different relationship between each cell population and the underlying electrospun scaffold. The individual cell populations also interact as indicated by the white arrows. The overall tissue response is a function of all these individual interactions. Tendon progenitor stem cells are not included in this figure as their contribution to tendon healing is uncharacterised. Research must generate an understanding of how cell populations interact and how to steer this interaction towards positive healing outcomes.

1.13 Summary

This chapter has outlined the burden of RCTs and the poor treatment outcomes to contextualise this thesis. The structure of the rotator cuff was analysed from the molecular to the macro level to illustrate how the complex hierarchical structure confers tendon function. This structure can be disrupted and instigate tendinopathic changes in tendon cell

populations and extracellular matrix, giving rise to rotator cuff tears. Current treatment strategies were then reviewed and potential explanations for the low success rate visited.

Having outlined the unmet clinical need, the requirements for a new generation of RCT repair materials were stipulated, specifically safety and efficacy. Compared to materials already available, new biomaterials must actively influence and support cell populations to promote healing. Potential treatment avenues were explored with scaffold based strategies identified as holding considerable advantages over cell and bioactive molecule based therapies.

Electrospun materials were studied in detail because their biomimetic fibre structure can deliver powerful biophysical stimuli to cell populations directly involved in repairing tendon to promote healing. Finally, the effects of electrospun fibres on cell populations relevant to tendon healing were reviewed.

1.14 Aims

This thesis aims to generate a range of biomimetic electrospun scaffolds varying in fiber diameter, fiber alignment and local mechanical properties. These materials will be tested with tendon fibroblasts and peripheral blood mononuclear cells (PBMCs), important cell populations for tendon healing, to evaluate their potential to influence cell biology. Furthermore, functionalisation of electrospun scaffolds through biological fluid pre-exposure will be explored. Specifically, this thesis aims to:

1. Generate a range of biomimetic scaffolds approximating different hierarchical levels of tendon structure to provide biophysical cues similar to native tendon ECM.
2. Compare and contrast the response of fibroblasts from healthy and diseased tendon to the same biomimetic scaffolds.

3. Determine if a particular scaffold type provides biophysical cues to promote tendon fibroblasts from diseased tendon to adopt a profile more similar to fibroblasts from healthy tendon.
4. Investigate the attachment and response of PBMCs to biomimetic scaffolds in order to determine if scaffold types influence inflammatory response.
5. Investigate whether functionalisation of biomaterials through biological fluid exposure can modify the PBMC and tendon fibroblast response to scaffolds.

1.15 Hypotheses

1. Tendon fibroblast populations will attach, proliferate and produce more tendon matrix on electrospun fibers approximating those of native collagen fibrils.
2. Diseased tendon fibroblasts will revert to a more 'healthy' phenotype as assessed by changes in gene expression favouring tendon matrix production and reduced inflammation when exposed to biomimetic biophysical cues.
3. Peripheral blood mononuclear cells will demonstrate increased expression of inflammatory genes when cultured on electrospun fibres not replicating native ECM components.
4. Functionalisation of electrospun fibres through adsorption with biological fluids will moderate tendon fibroblast and PBMC attachment and gene expression.

Chapter 2 Fabrication of biomimetic electrospun scaffolds

2.1 Abstract

2.1.1 Background

Biomimetic scaffolds have the potential to influence cell-material responses and improve tissue healing. This chapter examines the consistent fabrication of such electrospun scaffolds. Biomimetic scaffolds comprised of aligned fibres with diameters of 300nm and 4000nm were made to represent native tendon matrix components. Aligned fibre scaffolds with diameters of 1000nm and 2000nm and a random fibre scaffold with a 1000nm diameter were produced to represent non-naturally occurring matrices.

2.1.2 Materials and methods

A systematic characterisation of electrospinning parameter effects on fibre production was undertaken, along with an assessment of the homogeneity and consistency across electrospun scaffolds. Combinations of various electrospinning parameters and the use of pyridine as a solution additive were tested to enable successful production of target scaffolds.

2.1.3 Results

Consistent and homogenous electrospinning was possible, however PDO supplier, batch and storage conditions have significant impacts on electrospun fibre fabrication. Pyridine has pronounced effects on electrospinning allowing significant reductions in fibre diameter whilst largely preserving fibre alignment and morphology. The targeted scaffold morphologies were produced.

2.1.4 Conclusions

Electrospinning allows homogenous and consistent fabrication of target fibrous scaffolds. Pyridine is a significant addition to the electrospinning toolkit to produce biomimetic PDO fibres at the range of collagen fibrils. Techniques to evaluate the local mechanical properties and surface material properties of electrospun fibres must be developed to examine if these bioactive conditions change unintentionally with altered electrospinning parameters. Furthermore, accurate and reliable assessment of these effects would allow their use as a deliberately changeable biophysical cue to further manipulate cell-material responses.

2.2 Introduction

Electrospun biomaterials are positioned to play an important role in the next generation of deliberately engineered bioactive medical implants. Electrospinning can generate safe scaffolds with the required mechanical, chemical and biophysical properties to improve rotator cuff repair outcomes as discussed in sections 1.8 (Ideal biomaterial properties for augmenting rotator cuff tear repair), 1.9 (Targeting cell-material interaction) and 1.10

(Electrospinning). Electrospun materials are particularly promising candidates because of the biomimetic potential to harness and engage powerful biophysical cues to influence cell biology in a targeted manner. This chapter outlines the methods developed to consistently produce homogenous electrospun scaffolds of the targeted fibre diameters and alignments to mimic collagen fibrils and fibres. The results are then reported followed by a discussion of these results in the context of this thesis as well as within the wider field of electrospun biomaterials.

2.3 Aims

1. The primary aim of this chapter is to produce consistent, homogenous electrospun PDO scaffolds over a range of diameters approximating important hierarchical divisions of tendon ECM. Specifically, these are aligned scaffolds with a diameter less than 500nm, 1000nm, 2000nm and 4000nm and a random scaffold of 1000nm. 500nm approximates the top end of collagen fibril size and 4000nm approximates collagen fibre size. The BioPatch is currently fabricated using 1000nm fibres.
2. To enable this, the effect of PDO supplier, molecular weight and storage conditions on homogenous electrospinning will be investigated.
3. This chapter also aims to characterise how the surface roughness, local mechanical properties, porosity and pore size are affected during the fabrication of the target scaffolds.

2.4 Hypotheses

1. Electrospinning will enable consistent and homogenous production of fibrous scaffolds.

2. PDO supplier and molecular weight will affect electrospinning behaviour and subsequent scaffold properties.
3. Long term PDO storage in recommended storage conditions will not affect electrospinning behaviour and subsequent scaffold properties.
4. Manipulation of system and process parameters in different combinations will enable generation of target scaffold diameters and alignments.
5. Surface roughness, local mechanical properties, porosity and pore size will be influenced by changes in fibre diameter and alignment.

2.5 Materials and methods

2.5.1 Electrospinning protocol

2.5.1.1 PDO solution preparation

Solutions were prepared for electrospinning through the dissolution of PDO resin (multiple suppliers, see section 2.5.5 (PDO supplier effects on electrospun fibre fabrication)) in HFIP (Apollo Scientific Ltd, Cheshire, UK) to obtain required concentrations (% w/v) of PDO solution. Solutions underwent gentle agitation on a roller at room temperature for at least 12 hours to ensure the PDO resin had completely dissolved prior to solution use.

2.5.1.2 Electrospinning process

Solutions were electrospun using an IME electrospinning device (IME Technologies, Spaarpot, the Netherlands). A PHD 2000 syringe pump (Harvard Apparatus, Kent, UK) delivered PDO solution to a single stainless steel nozzle at appropriate flow rates. The nozzle was used in static and translocating functions.

A voltage was applied between the nozzle and the grounded collector, positioned a fixed distance from the nozzle tip. The collector was used in rotating or static roles depending on

the required scaffold type. Electrospinning took place in an environment-controlled chamber at 20 °C and 30% humidity unless otherwise stated. Electrospinning was undertaken for various times depending on application.

2.5.1.3 Scanning Electron Microscopy image acquisition

10mm by 10mm areas were cut from electrospun scaffolds. Samples were mounted on aluminium stubs (Agar Scientific, Essex, UK) using carbon tape (Agar Scientific). These were gold/palladium coated for 105 seconds (SC7620 Mini Sputter Coater, Quorum Technologies, Laughton, UK). Scanning Electron Microscope (SEM) images were acquired using a EVO LS15 SEM (Zeiss, EVO LS15, Oberkochen, Germany) at multiple sites of the mounted sample at magnifications ranging from 50-10,000x. Sufficient images were taken to give greater than 50 fibres for measurement for a single area or scaffold.

Acquired images were analysed using ImageJ software as shown in Figure 2-1 (WS Rasband, National Institutes of Health, Bethesda, USA). Each image was calibrated appropriately using the scale bar (A). Measurements were acquired at 200% to improve accuracy (B). Each image was scanned from left to right, measuring all fibres consecutively (C) to generate a measurement of diameter.

This measurement of diameter also created an angle measurement for each fibre from the axis of the image (D). This was perpendicular to the fibre direction. To transform this angle measurement to the long axis direction of the fibre, 90^{o} was added to each fibre angle measurement (E). For each individual image, a hypothetical mean long axis was calculated over all measured fibres. The deviation from each individual measurement from the mean angle was calculated for analysis of alignment. Fibre alignment is a circular statistic requiring separate statistical analysis techniques. These are detailed in section 2.5.14 (Scaffold statistical analysis).

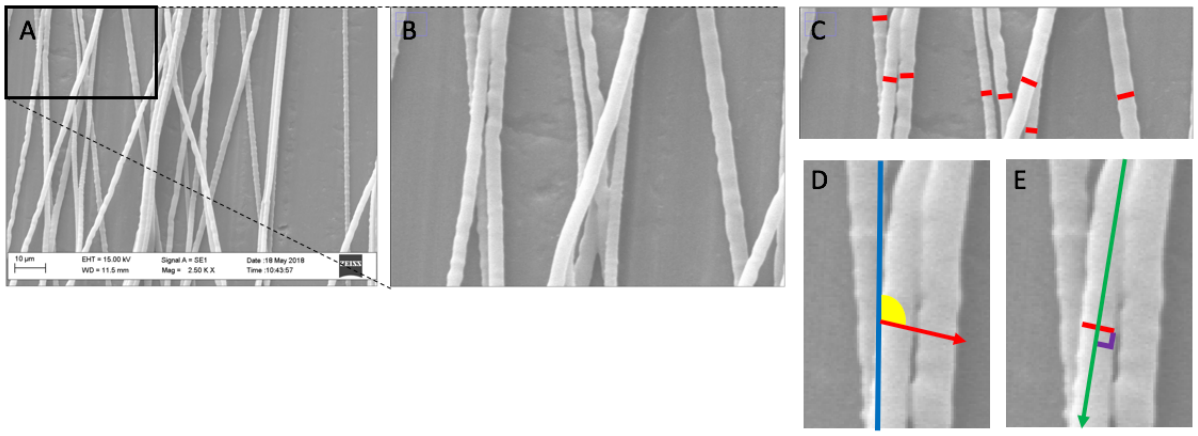


Figure 2-1. ImageJ measurement protocol of fibre diameter and angle.

Original SEM images were imported into ImageJ and calibrated individually against the scale bar, bottom left (A). To minimise measurement error, measurements were taken at 200% magnification (B). All visible individual fibres were measured across the entire image, shown by red lines, scrolling from left to right along the top border of the image (C). ImageJ calculates the angle of a measurement relative to the axis of an image (D). Addition of 90 ^{o} to this measured angle transforms the measured angle into the long axis of the fibre (as shown in green) relative to the image axis (E). The superimposed lines have been added in Microsoft PowerPoint to show more obvious approximations of more accurate measurements taken using ImageJ.

2.5.1.4 PDO solution viscosity measurement

Dynamic viscosity was measured using a ViscoPad R viscometer fitted with a TR8 spindle (Fungilab, Barcelona, Spain). Given the sensitivity of viscosity to temperature fluctuations, all measurements were undertaken in a room, air-conditioned to 18 ^{o}C overnight prior to measurement.

7.2ml of solution was measured into a purpose-built steel container. The spindle was then lowered carefully into the solution. The container and spindle were then fixed to the viscometer and submerged into water in a beaker to further ensure a consistent temperature environment. Solutions were left to sit for 5 minutes to allow air bubbles to float to the surface of the solution.

Viscosity was actively measured for 5 minutes as depending on viscosity, it could take up to 3 minutes to reach a steady state. Consequently, only data generated from the measurements between 4 and 5 minutes was analysed.

2.5.1.5 PDO solution conductivity measurement and analysis

The conductivity of PDO solutions was measured using a SevenCompact S230 meter fitted with an InLab741 ISM probe (Mettler Toledo, Leicester, UK). All conductivity measurements were obtained in a room, air conditioned over night to 18 ^{o}C. PDO solutions were left to sit for 2 minutes prior to the probe being immersed and conductivity measured.

2.5.2 Homogeneity within electrospun scaffolds

A PDO solution was prepared as previously described. This was electrospun at the parameters outlined in Table 2-1. From the resultant scaffold, three 10 mm x10 mm areas were cut, spanning the width of the material. Fibres were measured and analysed as per the protocols previously described in section 2.5.1.3 (Scanning Electron Microscopy image acquisition).

Table 2-1. Electrospinning parameters used to fabricate scaffolds for homogeneity experiments.

Electrospinning parameter	Value	Electrospinning parameter	Value
Concentration	7 %	Voltage	7 kV
Flow rate	1 ml/hr	Temperature	20 °C
Nozzle diameter	0.8 mm	Humidity	30 %
Nozzle movement	Static	Time	60 min
Collector Distance	20 cm		
Collector speed	2000 rpm		

2.5.3 Consistency of electrospun scaffolds produced from the same solution

A PDO solution was prepared as previously described. This was electrospun at the parameters outlined in Table 2-1 at baseline and then at 7 and 14 days. From the resultant

scaffolds, three 10mm x10mm areas were cut, spanning the width of the material. Fibres were measured as per the protocol previously described in section 2.5.1.3.

2.5.4 Consistency of electrospun scaffolds produced from different solutions of the same concentration

3 PDO solutions were prepared as previously described. These were electrospun at the parameters outlined in Table 2-1. From the resultant scaffolds, three 10mm x10mm areas were cut, spanning the width of the material. Fibres were measured using the protocol previously described in section 2.5.1.3.

2.5.5 PDO supplier effects on electrospun fibre fabrication

7% PDO solutions were prepared from three different suppliers (Polymed (Anderson, SC, USA), Evonik Nutrition and Health Care GMbH (Essen, Germany), Riverpoint Medical (Portland, OR, USA)) as previously described. 3 solutions were made up from each supplier and electrospun for 10 minutes as per Table 2.1. Samples were prepared and mounted for SEM as in section 2.5.1.3.

2.5.6 PDO batch effects on electrospun fibre fabrication

Riverpoint PDO is delivered in individual lots of 100g characterised by the supplier with a melt flow rate (MFR). This is a surrogate measurement to molecular weight. The MFR of individual batches ranged from 1.2 to 18.1g/10min. 3 solutions were made up of PDO resin with MFRs of 1.2, 2.9 and 5.1g/10min. These were electrospun under controlled conditions and underwent viscosity testing.

2.5.7 PDO resin storage effects on electrospun fibre fabrication

Given the difficulties experienced trying to recreate electrospun scaffolds over time, the effects of storage conditions were examined. Different suppliers dictated a variety of storage conditions to maintain polymer stability over time. To explore the effects of different

suggested storage conditions, fresh PDO (from the same batch and MFR) was stored in the following conditions (in triplicate):

Solution: 8g PDO made up into 100ml solution with HFIP, sealed and stored at 20 ^{o}C.

Room conditions: 8g placed in glass containers, sealed and stored at 20 ^{o}C.

Vacuum: 8g placed in glass containers, unsealed and stored in a vacuum chamber at 20 ^{o}C.

Freezer: 8g placed in glass containers, sealed and stored at -8 ^{o}C.

Incubator: 8g placed in glass containers, unsealed and stored in an incubator at 37 ^{o}C, 100% humidity, 5% CO_2 and 21% O_2.

At baseline (0 months), 10ml of each of the PDO solutions was taken for measurement of viscosity and conductivity and to be electrospun as previously described. At time points of 1 month, 2 months, 4 months and 6 months, this testing was repeated for the PDO stored in solution. For comparison and interpretation of the magnitude of storage condition effects, 0, 3, 6, 7, 9, 12 and 15% solutions were made up at baseline and subjected to the same viscosity, conductivity and electrospinning assessments.

At 1 month, 2 months, 4 months and 6 months, 0.8g aliquots of PDO resin were taken from each storage condition to make up 8% PDO solutions in triplicate. These solutions were also tested with the same protocols. All electrospinning was conducted at the same parameters throughout the duration of the study as stipulated in Table 2-2.

Table 2-2. Parameters used for the electrospinning of scaffolds from PDO stored in different conditions.

Electrospinning parameter	Range	Electrospinning parameter	Range
Concentration	8 %	Voltage	7 kV
Flow rate	1 ml/hr	Temperature	20 °C
Nozzle diameter	0.8 mm	Humidity	30%
Nozzle movement	Static	Nozzle material	Metal
Collector Distance	20 cm	Foil surface	Shiny
Collector speed	1500 rpm	Time	10min

To examine the effects of storage condition on PDO at the molecular level, PDO resin was subjected to Differential Scanning Calorimetry (DSC) interrogation. DSC can give a phenomenological understanding of changes in crystal sizes and morphologies and an overall crystallinity of a polymer by comparison with a 100% crystalline sample [277-279]. This crystallinity has been correlated with macro mechanical properties in unpublished research within the Carr laboratory group.

DSC testing of the PDO resin occurred at baseline and at 1 and 6 months for PDO resin stored in the test conditions. For PDO stored as a solution, this involved measuring out 1ml of solution and allowing solvent evaporation to generate thin films of PDO. These were cut up into small pieces to resemble the size and weight of provided PDO granules.

10mg of PDO resin for each condition was sealed into weighed TZero aluminium pans (TZero Aluminium, TA Instruments, Hertfordshire, UK) along with a reference pan. DSC was performed using a differential scanning calorimeter (Q2000-1275 Differential Scanning Calorimeter (TA Instruments, Hertfordshire, UK)) set at a heating cycle beginning at 25 ^{o}C and increasing at 10 ^{o}C per minute up to 140 ^{o}C. PDO has a known melting point of 110 ^{o}C and glass transition point of -10 ^{o}C [280]. The sample was held at 140 ^{o}C for 2 minutes before cooling back to 25 ^{o}C at the same rate. A second heating and cooling cycle was then performed with the same settings. Analysis and measurements were made on the thermogram of the first heating cycle to calculate sample crystallinity at 0, 1 and 6 months, as well as generate inferences over changes occurring in the amorphous and crystalline phases of the material.

Crystallinity was calculated as a percentage using the following formula;

$$X = (Hf/Hf[100\%]) \times 100$$

where X is sample crystallinity (%), Hf is the measured heat of fusion (J/g) and Hf[100%] is the theoretical fusion of a 100% crystalline PDO material (141.2J/g) [280].

2.5.8 Fibre diameter optimisation

The effects of selected parameters on electrospun fibre diameter were examined in order to generate a range of diameters corresponding to collagen fibril (500nm) through to collagen fibre (4000nm) size. While testing one parameter, every other parameter was held at the value in bold as listed in Table 2-3. However, the effect of temperature and humidity was however assessed using a 6.5%, not 8% solution.

Table 2-3. Electrospinning parameters and the tested range of each parameter to determine the effect on electrospun fibre diameter.

Electrospinning parameter	Range	Electrospinning parameter	Range
Concentration	5 - 6.5 – **8** %	Voltage	6 - **8** - 11 kV
Flow rate	0.5 – **1** – 4 ml/hr	Temperature	**20** - 38 °C
Nozzle diameter	0.4 - **0.8** mm	Humidity	25 – **30** - 80 %
Nozzle movement	**Static** or translocating (10mm/s)	Nozzle material	**Metal** or plastic
Collector Distance	15 – **20** - 25 cm	Foil surface	Dull or **shiny**
Collector speed	1 – **2500** rpm	Time	1 - **20** - 60 min
Solvents (plain and in 1:9, 1:5, 1:1 ratios with HFIP)	Chloroform, Dichloromethane, Dimethylformamide	Salts	NaCl, CaCl2

2.5.9 Fibre alignment optimisation

The effects of collector speed and voltage on fibre alignment were explored in detail. These two parameters were selected based on previous experimental results and published literature.

2.5.9.1 Collector speed effect on fibre alignment

7% PDO solution was prepared as previously described. This solution was electrospun as described in Table 2-2 with collector speeds ranging from 1 to 2500 rpm. The collector diameter is 10cm. The solutions were electrospun for 10 minutes. Samples were prepared and mounted for SEM as described in section 2.5.1.3.

2.5.9.2 Electric field strength effect on fibre alignment

7% PDO solution was prepared as previously described. This solution was electrospun as described in Table 2-2 with voltages of 7, 8, 9, 10, 11 and 25kV. The solutions were electrospun for 10 minutes. Samples were prepared and mounted for SEM as described in section 2.5.1.3.

2.5.10 Pyridine effect on electrospun fibre fabrication

Favourable parameter settings in various combinations failed to consistently produce the targeted fibre diameters below 500nm. Pyridine was trialled in an attempt to reduce fibre diameter. Pyridine (Sigma, Dorset, UK) was added at 100ppm to a 7% PDO solution prior to mechanical agitation for 12 hours. This solution along with a control 7% solution with no pyridine were electrospun at the settings in Table 2-2 for 20 minutes. 3 areas from each of the produced scaffolds were then prepared and analysed through SEM as previously described to examine the effects on fibre diameter and alignment.

To further investigate the effect of pyridine on electrospinning behaviour, pyridine was added at 10 and 200ppm to 7% PDO solutions. These solutions, along with the 100ppm pyridine solution, were then electrospun for 20 minutes at the parameters in Table 2-2, except at a reduced flow rate of 0.25 ml/hr to eliminate dripping and maintain a stable Taylor Cone. Areas from these scaffolds were also analysed under SEM to examine the effects on diameter. The viscosity and conductivity of these solutions were also measured as previously described.

Macroscopically, the addition of pyridine created a broader distribution of fibres over the collector. To quantify this effect, the distance of fibre deposition was measured across the width of the scaffold with a ruler, perpendicular to the axis of the fibres.

2.5.11 Final electrospun biomimetic scaffold production parameters

Various permutations of different system and process parameters were trialled to manufacture the desired range of electrospun scaffolds, both in terms of diameter and in alignment. Table 2-4 stipulates the final parameters involved in spinning each scaffold type.

Table 2-4. Final electrospinning parameters for electrospun scaffolds used in the *in vitro* experiments of this thesis.

Scaffold Type	300 nm aligned	1000 nm aligned	2000 nm aligned	4000 nm aligned	1000 nm random
PDO concentration	7 %	8 %	10 %	13 or 14 % (dependent on PDO lot)	8 %
Pyridine concentration	100 ppm	0 ppm	0 ppm	0 ppm	0 ppm
Flow Rate	0.25 ml/hr	0.75 ml/hr	1 or 1.1 ml/hr (dependent on PDO lot)	3 ml/hr	0.5 ml/hr
Voltage	7 kV	7 kV	7 kV	7 kV	7 kV
Collector speed	2000 rpm	1500 rpm	1500 rpm	1500 rpm	5 rpm
Time	3 h	4 h	3 h	1 h	4 h

To ensure scaffold thicknesses were as equal as possible, the duration of electrospinning was initially varied to match the weight of electrospun PDO deposited. However, this was not practically possible, and durations were ultimately determined by the shortest time that produced a scaffold able to support the cell suspension to *in vitro* experimentation.

For each experiment, fresh scaffolds of each type were produced as contemporaneously as possible (within 7 days) and stored in a desiccator to prevent hydrolytic breakdown prior to use. The time period between manufacture and use in experiments was minimised as much as possible, ranging from 1 to 4 weeks.

2.5.12 Effect of altered fibre diameter and alignment on scaffold surface roughness and local mechanical properties

10mm by 10mm areas were cut from electrospun scaffolds and carefully mounted on a glass slide to achieve as flat a surface as possible. Samples were attached with carbon tape or a thin layer of epoxy resin.

Scanning Probe Microscopy (SPM) was performed on an MFP-3D Atomic Force Microscope (Asylum Research, High Wycombe, UK) with an AC160TS probe (Olympus, Japan). Nano-mechanical mapping and loss-tangent measurements were performed with a tip correction factor derived from a known PDO suture modulus (Ethicon, USA). Areas were randomly selected with the surface roughness and loss tangent acquired over a chosen area.

The size of this area was determined by fibre diameter. Blanket scanning resulted in poor tip-sample interaction distorting results. Focused areas were instead selected on the top, providing relatively more accessible surface where the contact between the tip and scaffold material was optimal.

2.5.13 Electrospun scaffold porosity, pore size and thickness characterisation

Porosity and pore size measurement were undertaken using a mercury intrusion technique. An AutoPore IV 9500 mercury porosimeter (Micromeritics Instrument Co, Norcross, GA, USA) with a max pressure range of 33,000 psia and a measureable pore size range of 0.005um to 360um. Electrospun scaffolds (weight ranges trialled were between 20mg and 100mg) from the 5 target scaffolds were placed in the penetrometer (s/n = 14, 3 bulb, 0.412 stem, powder). The penetrometer was first passed through the low-pressure port to evacuate gases from the penetrometer, then backfilled with mercury before finally through the high-pressure port. Samples were run with a mercury filling pressure of 0.49 psia and an equilibration time of 10 s based on in house protocols. Experimentation was trialled with 2 repeats of each scaffold, one thinner (20-30mg) and one thicker scaffold (80-100mg).

2.5.14 Scaffold statistical analysis

Statistical analysis of fibre diameter was performed with GraphPad Prism v7 software (GraphPad Software Inc, California, USA). Statistical testing between scaffold types was performed using methodologies suited for the number of scaffolds. For testing for statistical differences in mean diameter of two scaffolds, an unpaired, two-tailed t test with Welch's correction was used. For testing more than two scaffolds, a one-way ANOVA with Tukey's multiple comparisons testing was used. Statistical significance was taken at $p<0.05$.

These same statistical analyses were used to assess differences in PDO solution viscosity, PDO solution conductivity and PDO resin crystallinity dependent on the number of comparisons.

For assessment of the effects of storage conditions on PDO solution viscosity and mean fibre diameter, a two-way ANOVA with Tukey's multiple comparisons testing was performed comparing storage conditions at each time point. For fibre diameter assessment, incubator stored PDO was excluded from the analysis because no useful scaffold could be formed.

Statistical analysis of fibre alignment was performed with PAST3 v20 (Oyvind Hammer, Natural History Museum, University of Oslo). Different software and testing was needed because angle measurement analysis requires circular statistic techniques. A circular arrow plot was created using axial distributions to overlay all fibre angles through a central point. This enabled calculation of the angular deviation and Rayleigh's R value. This R value is a measure of preferential alignment of a population of angles. In the context of electrospun fibre scaffolds, a value of 0 means uniform dispersion of fibre axes and a value of 1 implies complete orientation of all fibre axes. For this thesis, an $R>0.9$ was deemed an aligned fibre scaffold and an $R<0.1$ was deemed a random fibre scaffold.

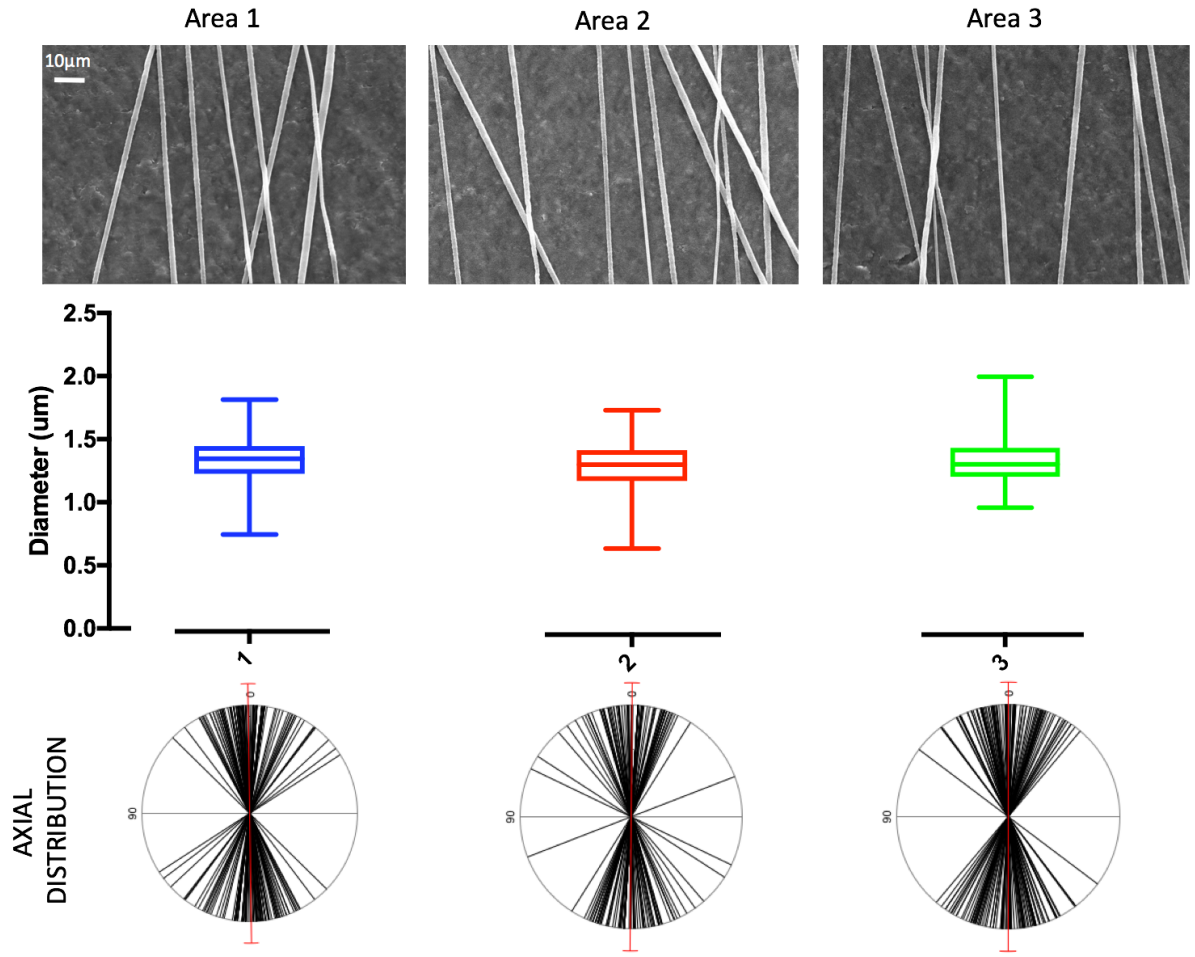
2.6 Results

2.6.1 Homogeneity and consistency of electrospun scaffolds

Identical scaffolds were required over a 3 year period for the research in this thesis. Establishing the ability to consistently produce homogenous scaffolds from different solutions at different times was fundamental to enable this. PDO degradation with time could change scaffold surfaces and biophysical cues confounding experimental results. Similarly, scaffold to scaffold variation from inconsistent fabrication could also limit the interpretation and application of results.

2.6.1.1 Homogeneity of areas within the same electrospun scaffold

Electrospun scaffolds were homogenous within the same scaffold. Representative images of three areas taken from within a single scaffold are presented in Figure 2-2 along with box and whisker plots of fibre diameter, fibre angle distribution and summary statistics. There were no significant differences in the mean diameter of the 3 areas of the scaffold. The angular deviation and Rayleigh's test for uniform direction were also nearly equal across all 3 areas.



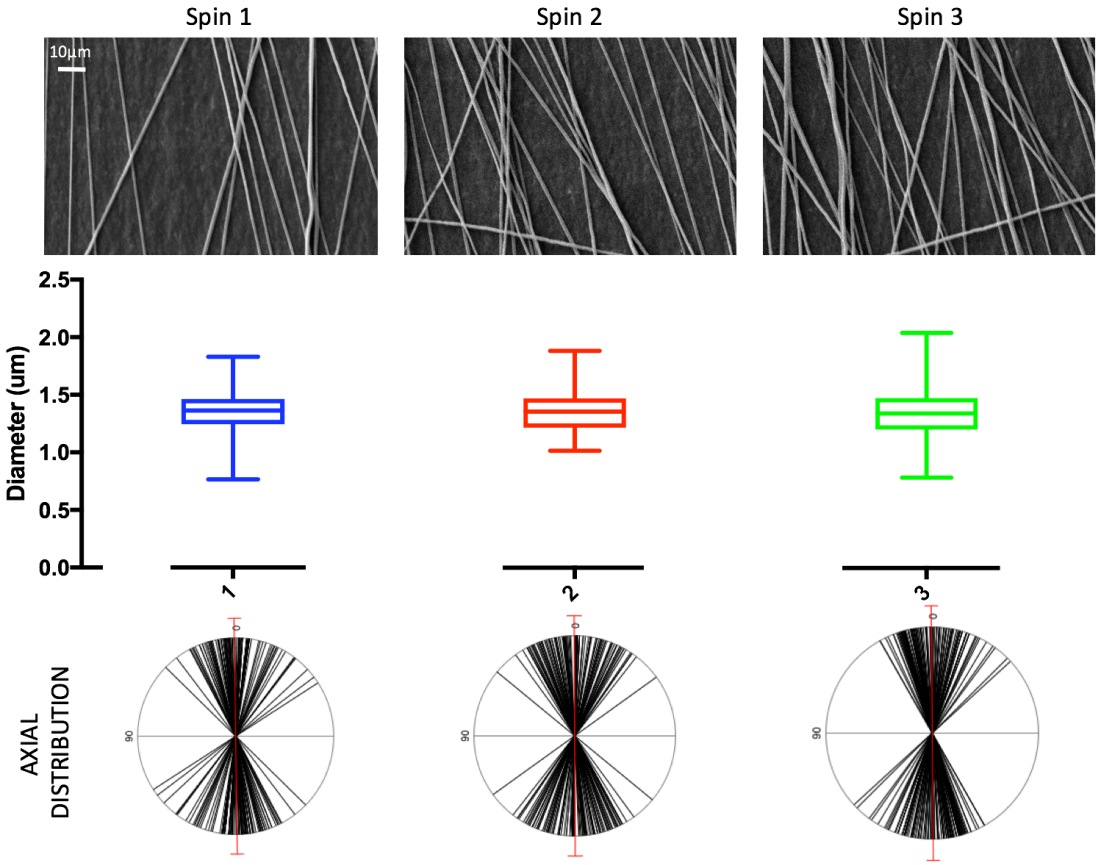
Number of fibres	85	83	62
Diameter (µm) (mean)	1.363	1.332	1.362
Diameter (µm) (standard deviation)	0.1954	0.1831	0.1890
Rayleigh's R	0.8275	0.8273	0.8112
Angular deviation (°)	3.2	3.4	3.6

Figure 2-2. Homogeneity of electrospun fibres from different areas within the same scaffold.

Representative SEM images (2500x magnification, scale bar = 10µm) of electrospun fibres, box and whisker plots of fibre diameter (min-max), axial distributions and summary statistics of the three different areas. There were no significant differences in fibre diameter and alignment between the 3 areas of the same scaffold.

2.6.1.2 Consistency of electrospun scaffolds produced from the same solution over 3 consecutive weeks.

Representative images of the 3 different scaffolds produced over time are presented in Figure 2-3 along with box and whisker plots of fibre diameter, fibre axial distributions and summary statistics. There was no significant difference in the mean diameter of the 3 scaffolds. The angular deviation and Rayleigh's test for uniform direction were also highly consistent across all 3 scaffolds produced at different time points.



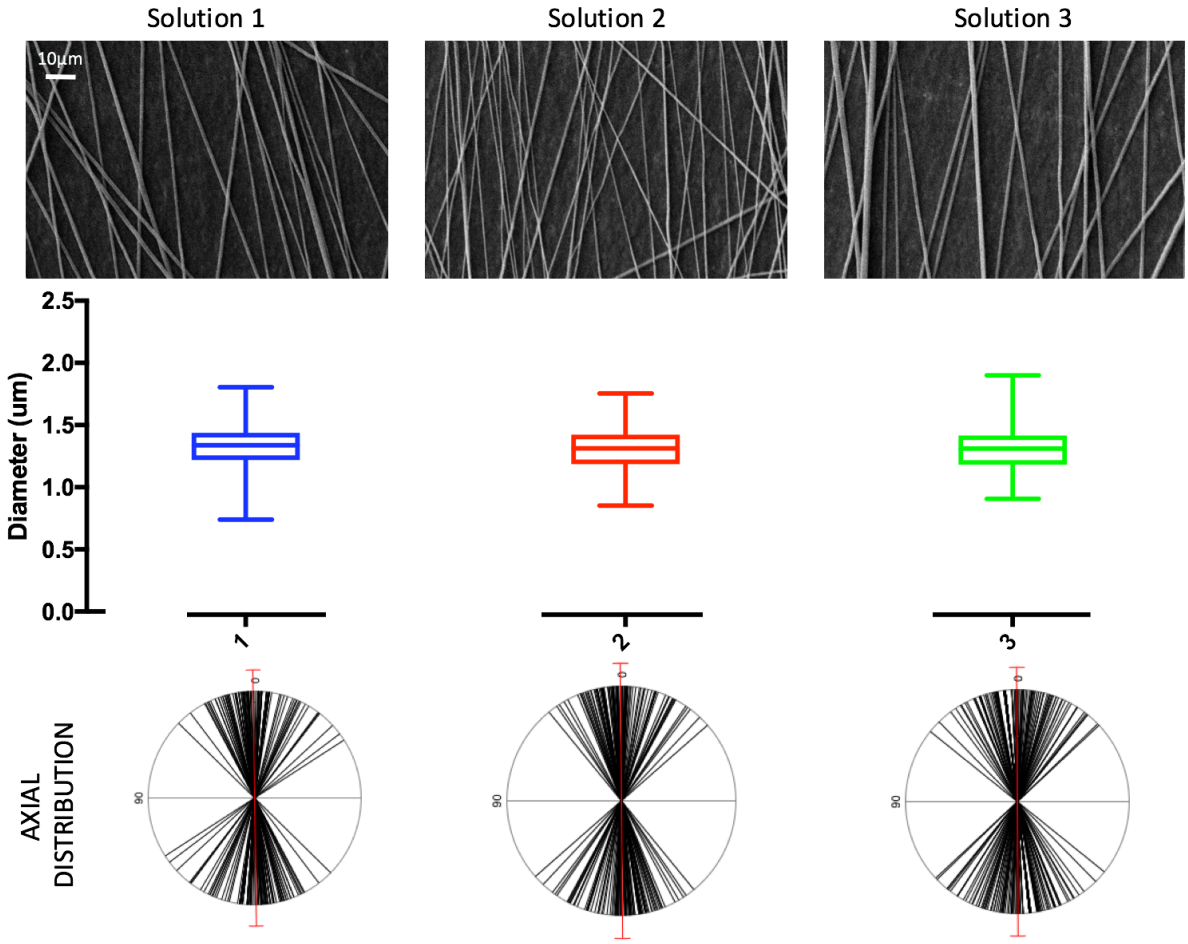
Number of fibres	85	76	83
Diameter (µm) (mean)	1.363	1.363	1.358
Diameter (µm) (standard deviation)	0.1954	0.1853	0.2392
Rayleigh's R	0.8275	0.8009	0.8538
Angular deviation (°)	3.2	3.6	3.0

Figure 2-3. Consistency of electrospun scaffolds produced from the same solution over consecutive weeks.

Representative SEM images (2500x magnification, scale bar = 10μm) of electrospun fibres, box and whisker plots of fibre diameter (min-max), axial distributions and summary statistics of the three different scaffolds produced over 3 weeks. There were no significant differences in fibre diameter in alignment between the 3 scaffolds.

2.6.1.3 Consistency of electrospun scaffolds produced from different PDO solutions of the same concentration

Representative images of the 3 scaffolds produced from 3 different PDO solutions of the same concentration are presented in Figure 2-4 along with box and whisker plots of fibre diameter, fibre axial distributions and summary statistics. There was no significant difference in the mean diameter of the 3 scaffolds. The angular deviation and Rayleigh's test for uniform alignment were also conserved across all 3 scaffolds produced from the 3 solutions.



Number of fibres	85	81	74
Diameter (µm) (mean)	1.363	1.337	1.34
Diameter (µm) (standard deviation)	0.1954	0.1691	0.2008
Rayleigh's R	0.8275	0.8402	0.8130
Angular deviation (°)	3.2	3.3	3.4

Figure 2-4. Consistency of electrospun fibres produced from different PDO solutions of the same concentration.

Representative SEM images (2500x magnification, scale bar = 10µm) of electrospun fibres, box and whisker plots of fibre diameter (min-max), axial distributions and summary statistics of the three different scaffolds produced from 3 different PDO solutions. There were no significant differences in fibre diameter in alignment between these 3 scaffolds.

2.6.2 PDO supplier effects on electrospun scaffolds

PDO resin supply had a notable impact on resultant electrospun fibres (Figure 2-5). Whilst macroscopically producing similar solutions, electrospinning performance was notably different. At the same concentration, Evonik and Polymed polymers were unable to sustain stable electrospinning leading to beading and irregular fibre formation. Increasing concentration to overcome the irregular fibre formation however precluded reliable generation of sub-micron sized fibres. Riverpoint polymer gave much more consistent results and was used subsequently.

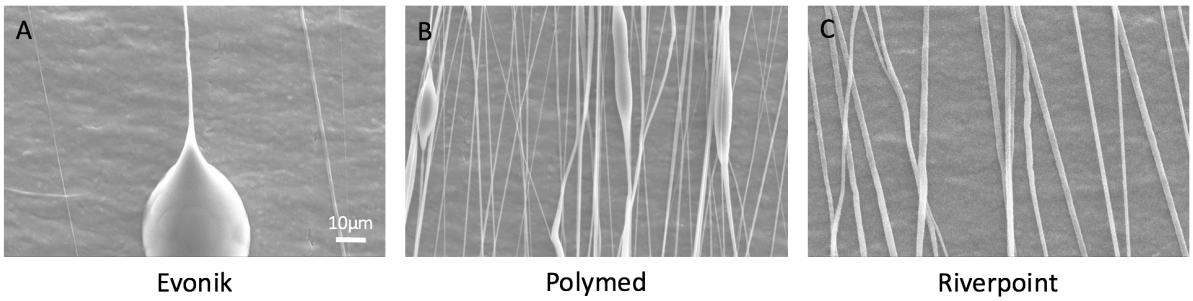


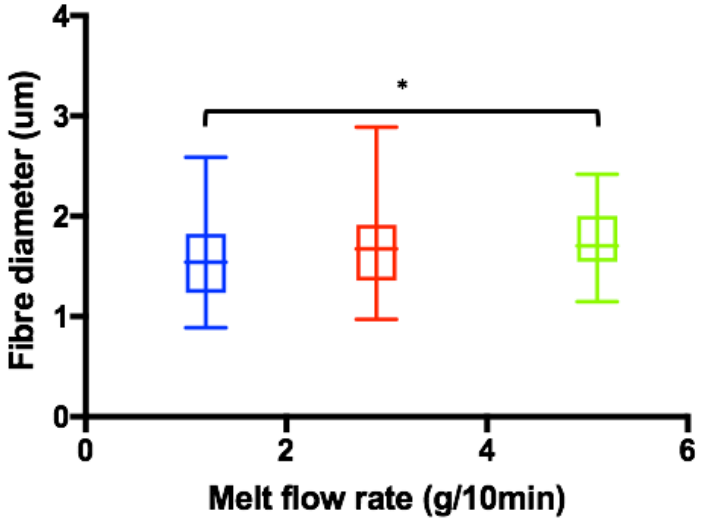
Figure 2-5. Effect of PDO supplier on electrospun fibre fabrication.

Representative SEM images of the scaffolds produced from PDO solutions made from resin from 3 different suppliers showing beading (A), irregular fibre formation (B) and homogenous fibres (C) (2500x magnification, scale bar = 10µm).

2.6.3 PDO batch effects on electrospun scaffold fabrication

The results seen in the use of PDO from different suppliers was likely due to differences in PDO molecular weight. Riverpoint PDO resin is supplied in small aliquots (100g) with a measured melt flow rate (MFR), a surrogate for molecular weight. These ranged from 1.2 to 5.9 g/10min. Electrospinning these solutions under the same conditions showed that the differences between the aliquots could result in significant differences in electrospinning performance as shown in Figure 2-6. Fibre diameter was directly related to MFR with a

significant difference between fibre diameters made from PDO resin with MFRs of 1.2 and 5.9 g/10min (p=0.0243).



MFR (g/10min)	1.2	2.9	5.9
Number of fibres	74	70	64
Diameter (mean)	1.549	1.673	1.743
Diameter (sd)	0.3907	0.402	0.307

Figure 2-6. Effect of PDO batch on electrospun scaffold fabrication.

Box and whisker plot and summary statistics of fibre diameter for electrospun scaffolds produced from PDO resin with different melt flow rates. There was a significant difference (<0.05 (*)) between the scaffolds produced from 1.2 and 5.9g/10min PDO resins.

2.6.4 PDO resin storage condition effects on electrospun fibre fabrication

Storage conditions had surprisingly pronounced effects on electrospinning behaviour. Relative to PDO stored in a solution, storage conditions could increase or decrease the resulting solution viscosity and mean fibre diameter (Figure 2-7). This has significant implications on consistent scaffold fabrication for both laboratory and commercial use. Viscosity data is provided as Figure A-1 in Appendix A.

PDO stored as a solution showed a gradual decrease in electrospun fibre diameter from 1650nm through to 1110nm over 6 months. Smaller reductions in diameter were noted with PDO stored at room conditions, reducing to a 1370nm mean diameter after 6 months, and with PDO stored in a vacuum reducing to 1420nm over the same period. In contrast, PDO stored in an incubator underwent rapid breakdown with sufficient degradation over 1 month to preclude bead free electrospinning. Conversely, PDO stored in the freezer resulted in an increased mean fibre diameter (1760nm after 6 months). This is a difference of over 600nm, or on a biological scale, more than the 500nm size of the collagen fibrils reported in the literature.

The differences in fibre diameter were pronounced from the earliest time point. From 1 month through to the end of the experiment, all storage conditions had statistically significant effects on fibre diameter compared to storage as a solution except for vacuum stored PDO at one month. Additionally, no fibres were produced from incubator stored PDO so this has been excluded from analysis. Effects on fibre alignment were not assessed as part of this experiment but not evident macroscopically. The effects on viscosity follow largely the same trends as described for fibre diameter. From baseline (1218+/- 24.76 cP), viscosity rose for solutions made from PDO stored in a freezer (1371+/- 32.32 cP) over 6 months, and dropped for PDO stored as a solution (940 +/- 15.78 cP), in room temperature (665+/- 29 cP) and in a vacuum (1047+/- 29.50). The viscosity for PDO solutions made from resin stored in the incubator were significantly lower at 1 month (15+/- 1.0 cP) and after 6 months, equal (10.17+/- 0.58 cP) to that of plain HFIP (9.4 +/- 0.29 cP) consistent with complete breakdown of PDO polymer chains.

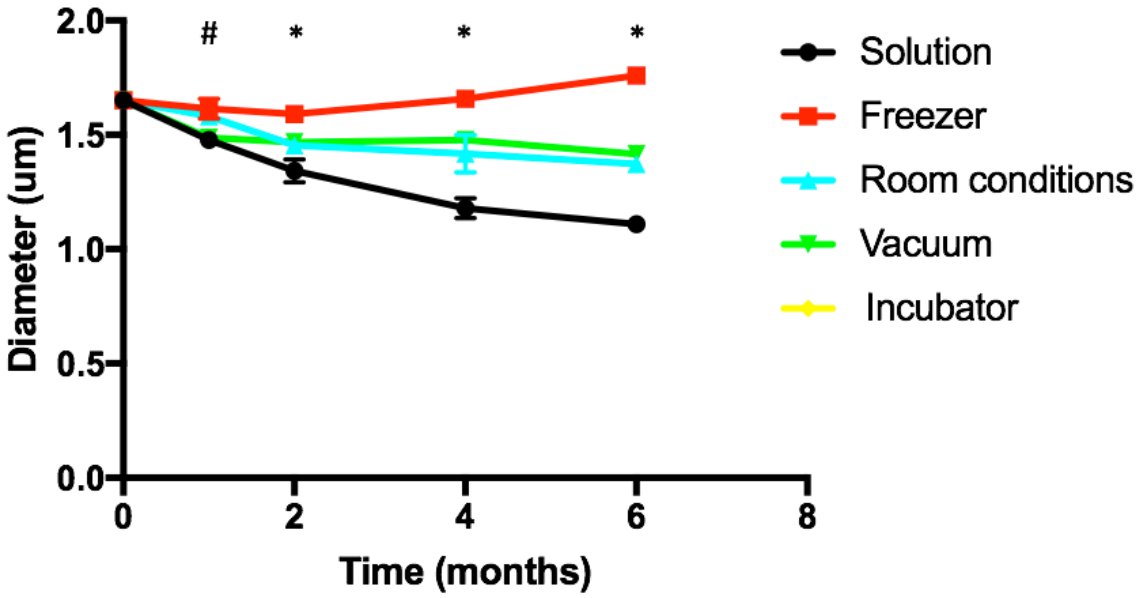


Figure 2-7. The effects of resin storage conditions over time on electrospun fibre diameter.

The mean diameter and standard deviations of solutions prepared from PDO resin stored in different conditions for 6 months. Compared to solution storage as a control condition, the mean diameter was statistically significantly higher for all conditions at all time points (denoted by *, $p<0.05$), except for vacuum storage after 1 month (denoted by #). Electrospinning of incubator stored PDO resin was not possible in the used experimental set up so cannot be included in this figure.

Control PDO solutions of 0, 3, 6, 7, 9, 12, 15% revealed mean fibre diameters (A) and viscosities (B) as shown in Figure 2-8. Measurement of viscosity throughout this range of solutions required alteration to the protocol, specifically the speed of the rotating mandrel. This needed to be decreased from 20rpm to 5rpm to capture the viscosity of 12 and 15% solutions. The performance of these control solutions are important to contextualise the effects of degradation. In this experiment, degradation over relatively short periods had the same effect on fibre diameter as altering PDO solution concentration by 1g/ml.

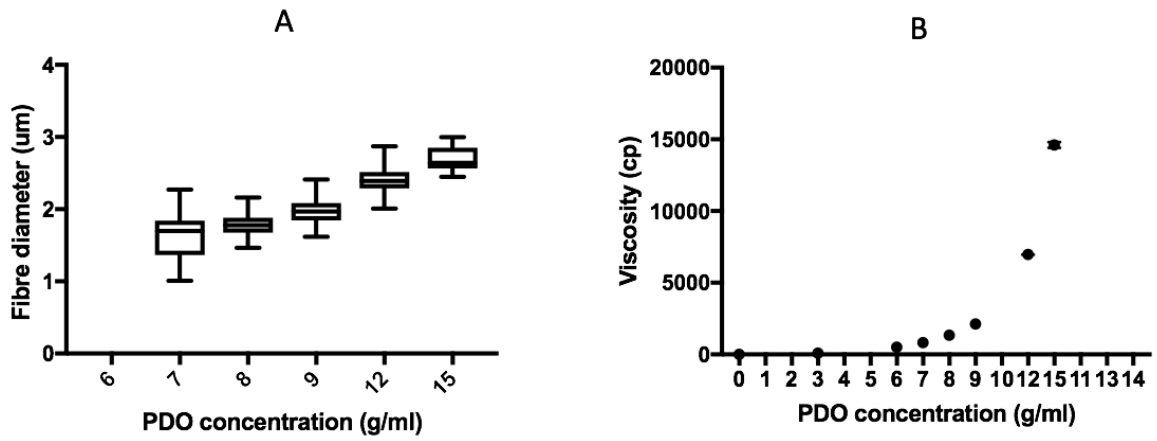


Figure 2-8. The relationship between PDO concentration with diameter and viscosity of control solutions.

These graphs show the relationship between the concentration of PDO and fibre diameter (A) and viscosity (B). The relationship between PDO concentration and viscosity is exponential in contrast to the more linear relationship with fibre diameter. The difference in fibre diameter was statistically significant ($p<0.05$) for all PDO concentrations except between 7 and 8 g/ml, 8 and 9g/ml, and 12 and 15g/ml. The difference in viscosity was significantly different ($p<0.05$) between all concentrations except 3 and 6 g/ml and 6 and 7g/ml.

Storage condition had significant effects on PDO crystallinity after 1 month with this continuing out to 6 months (Figure 2-9). The crystallinity of PDO stored in solution dropped significantly from 55% to 36% at 1 month before stabilising at this level for the remainder of the experimentation period. Subsequent experimentation showed this decrease in crystallinity occurred immediately after dissolution and seems to be a function of dissolution rather than degradation of the PDO polymer (data not shown). Comparing other storage conditions effects on crystallinity to this control was not deemed appropriate accordingly. Storage in a freezer, a vacuum or under room conditions had little effect on PDO crystallinity compared to each other over the 6 months.

PDO storage in an incubator however lead to significant and rapid increases in crystallinity (78%) over the first month before plateauing at a similar level for the next 5 months (85%) compared to PDO stored in a freezer, a vacuum or under room conditions. This may reflect the hydrolytic degradation of the amorphous regions of the polymer occurring more rapidly

than in crystalline regions leading to a relative increase in crystallinity, not an increase in the crystallinity. These results suggest that changes in crystallinity do not underlie the changes in viscosity and effects on electrospinning behaviour.

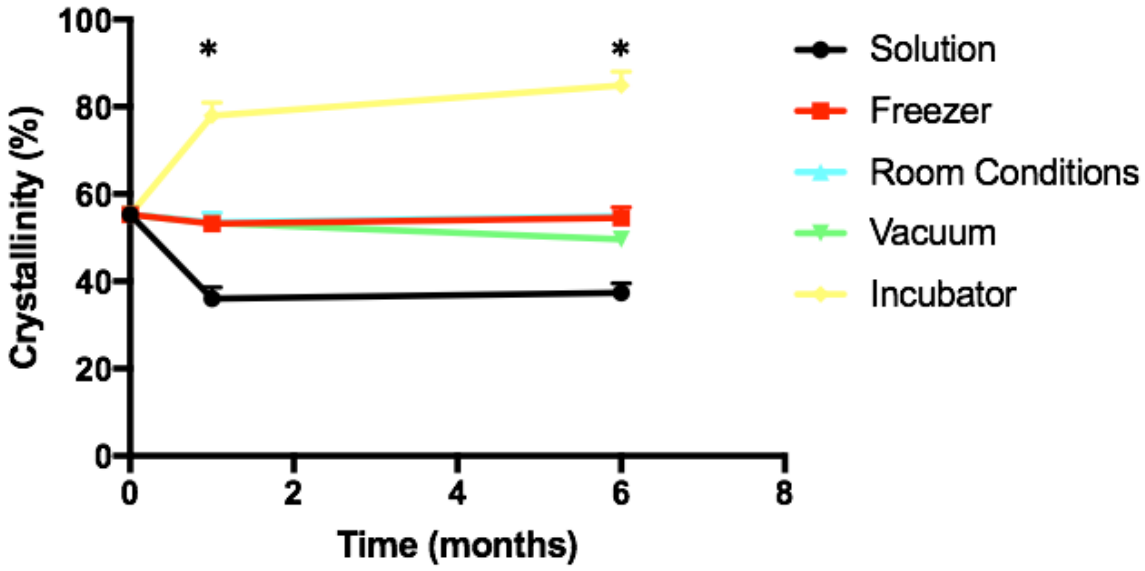


Figure 2-9. Change in PDO crystallinity of PDO resin stored in different conditions over 6 months.

Storage condition had significant effects on PDO crystallinity. Dissolution of PDO as a solution caused an immediate decrease in crystallinity but remained stable thereafter. As this is an effect of HFIP not storage, these results have been excluded from statistical testing. PDO storage in an incubator lead to rapid increases in crystallinity over the first month and a gradual increase thereafter. The crystallinity of PDO was statistically significantly higher compared to freezer, room conditions and vacuum stored PDO at 1 and 6 months (*, $p<0.05$). Storage in freezer, vacuum and room conditions had little effect on PDO crystallinity over the 6 month time course of this experiment with no statistical differences at 6 months.

2.6.5 Fibre diameter optimisation

The effect of various system and process parameters on electrospun fibre diameter were assessed. The most important relationships were found between PDO solution concentration, flow rate, collector speed, collector distance and voltage (Figure 2-10). PDO concentration had the greatest effect on fibre diameter (A), followed by flow rate (B), collector speed (C), and voltage (D). The summary data is included for each parameter in Appendix A as Table A-1.

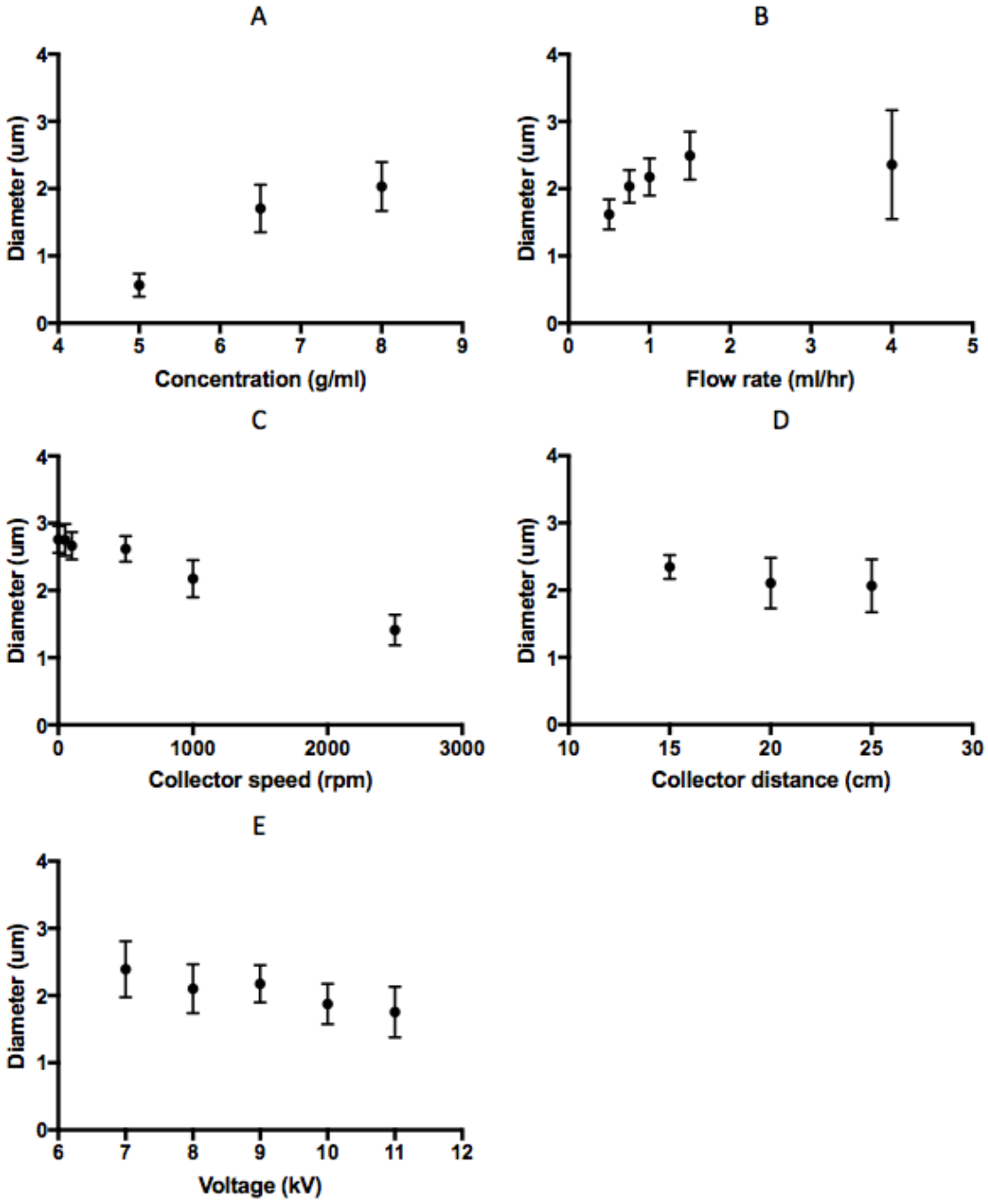


Figure 2-10. Effect of selected influential parameters on electrospun fibre diameter.

Mean and standard deviation of electrospun fibre scaffolds made with varied PDO concentration (A), flow rate (B), collector speed (C), collector distance (D) and voltage (E). Statistical testing was not performed between individual measurements of these parameters as the application was of trends associated with each parameter.

Other parameters that had significant effects on fibre diameter included temperature and humidity (Figure 2-11). Summary data is included in Appendix A as Table A-1

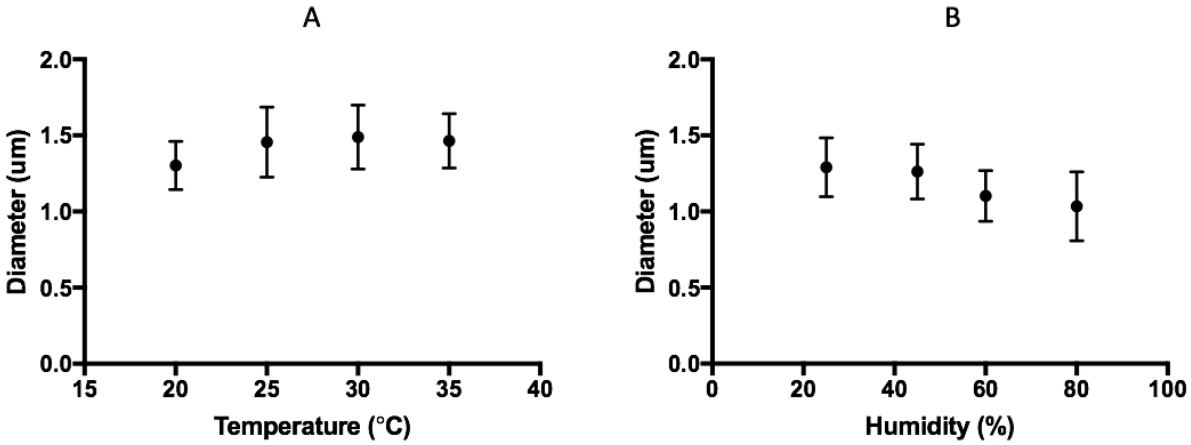


Figure 2-11. Effect of temperature and humidity on electrospun fibre diameter.

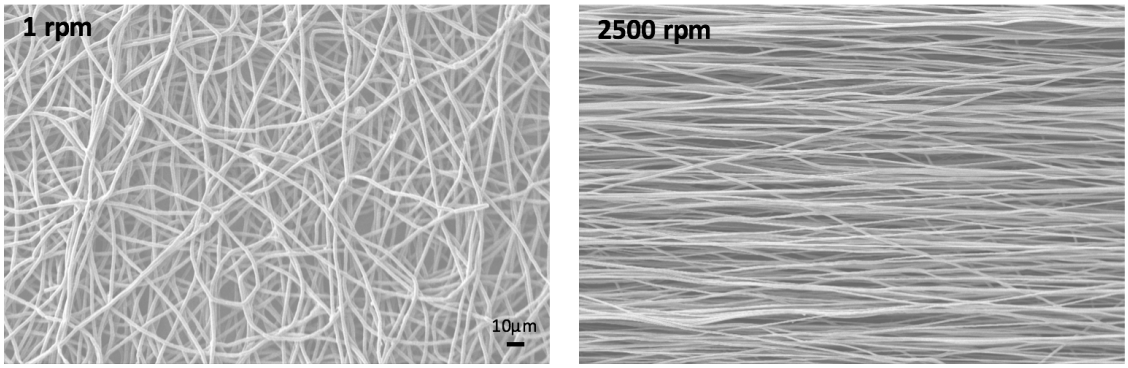
Mean and standard deviation of electrospun fibre scaffolds fabricated at different temperatures (A) and relative humidity (B).

2.6.6 Fibre alignment optimisation

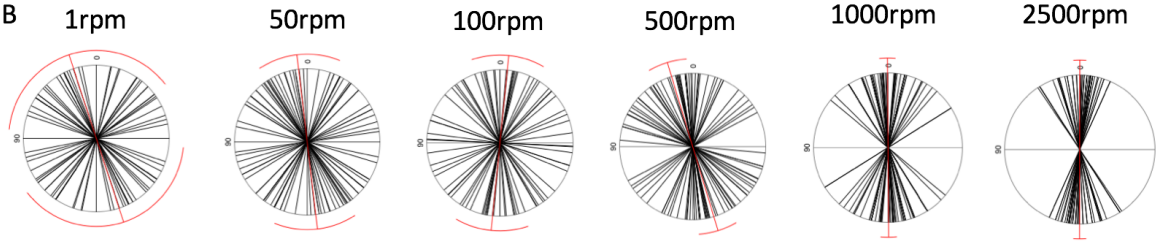
Fibre alignment was an important factor to be able to control in a targeted way. Random morphologies were required to to represent a more tendinopathic ECM matrix, compared to highly aligned fibres representing healthy tendon matrix.

Collector speed had the greatest propensity to influence fibre alignment of the parameters assessed. This parameter alone allowed for the production of random scaffolds through to highly aligned scaffolds. Figure 2-12 shows how increasing collector speed promotes fibre alignment with a reduction in angular deviation and increase in trend to uniform fibre angle distribution.

A



B



C

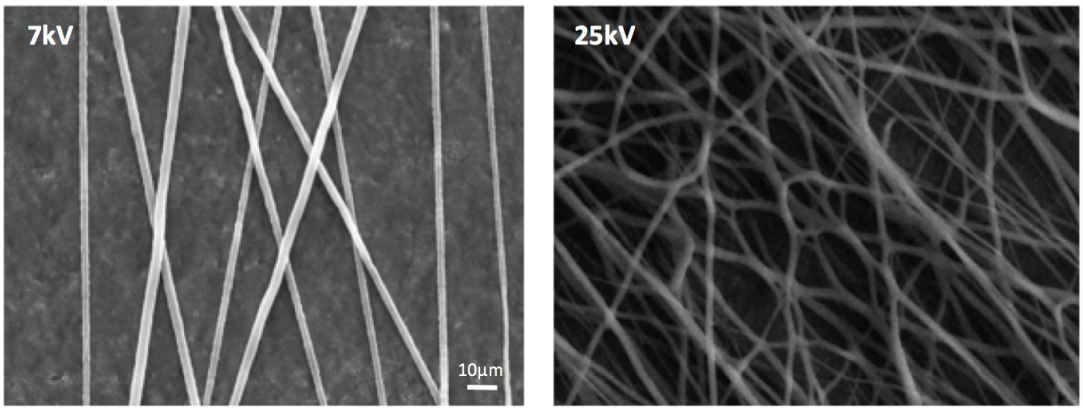
Collector speed (rpm)						
	1	**50**	**100**	**500**	**1000**	**2500**
Number of fibres	49	57	43	54	68	48
Rayleigh's R	0.1010	0.2204	0.2710	0.4142	0.7577	0.8795
Angular deviation	45	28	18	13	5.0	4.0

Figure 2-12. Effect of collector speed on fibre alignment.

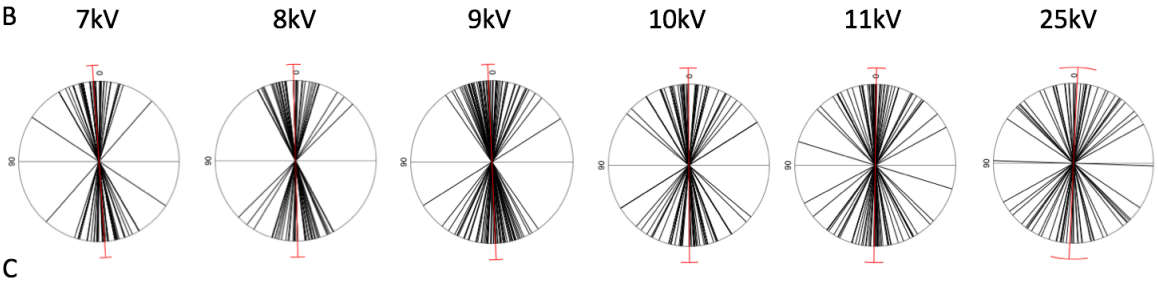
Representative SEM images (500x magnification, scale bar = 10µm) of random and aligned electrospun fibres (A), fibre angle distributions (B) and summary statistics (C) for electrospun scaffolds produced with different collector speeds. The increase in Rayleigh's R and decrease in angular deviation show the correlation between fibre alignment and collector speed.

Using voltage to reduce diameter induced obvious differences in fibre alignment when assessing fibre diameter. Consequently, the effect on alignment was quantified. This revealed that increasing voltage had a detrimental effect on fibre alignment (Figure 2-13). Furthermore, higher voltages induced more branching and cross-linking of fibres (not quantified), creating potential differences in the microscopic topography presented to cell populations.

A



B



C

Voltage (kV)						
	7	**8**	**9**	**10**	**11**	**25**
Number of fibres	67	63	63	68	61	39
Rayleigh's R	0.8698	0.8447	0.8394	0.7577	0.7263	0.5465
Angular deviation	3.5	4.0	4.0	5.5	6.0	12.0

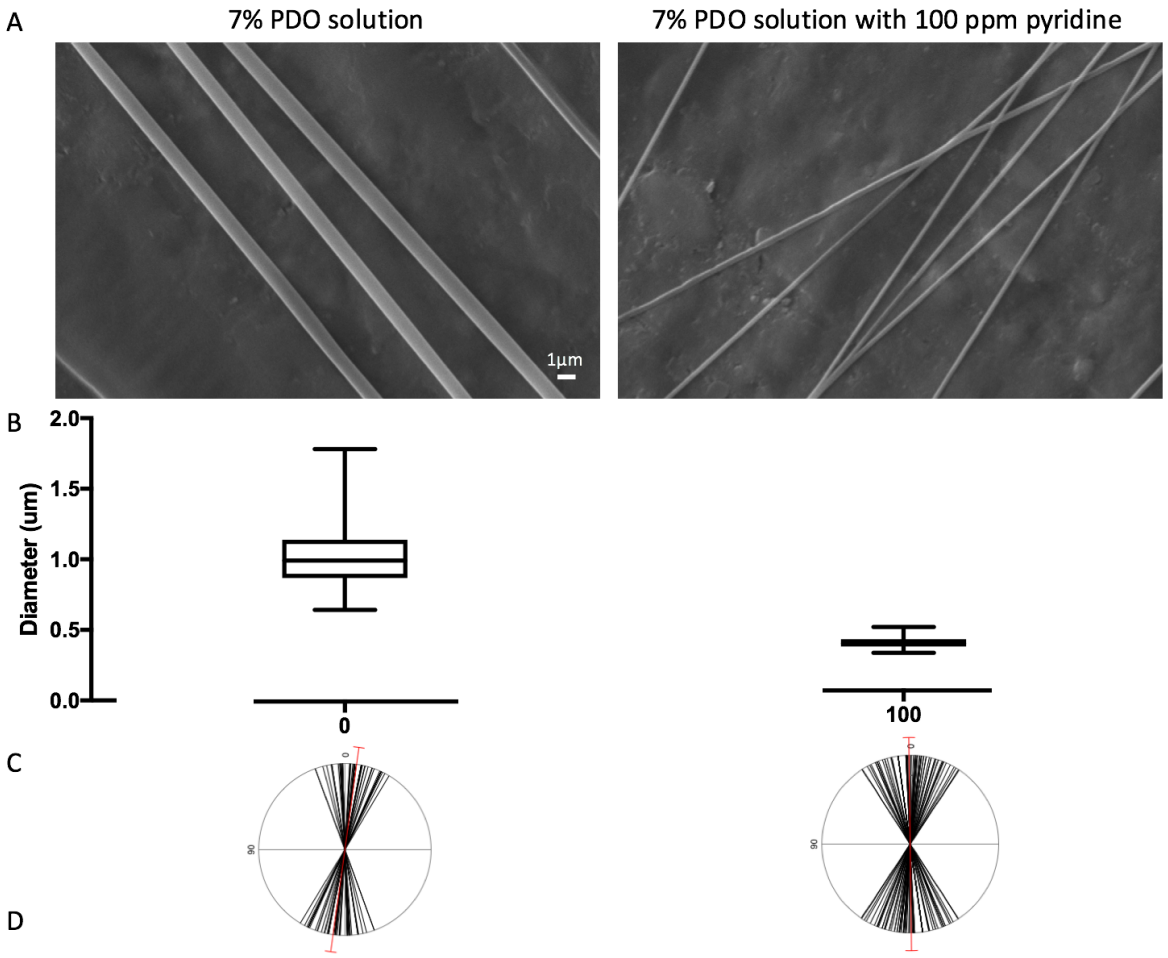
Figure 2-13. Effect of voltage on electrospun fibre alignment.

Representative SEM images (2500x magnification, scale bar = 10µm) of electrospun fibres (A), fibre angle distributions (B) and summary statistics (C) for electrospun scaffolds produced with different voltages. The decrease in Rayleigh's R and increase in angular deviation show the inverse relationship between voltage and fibre alignment. The more branched, irregular morphology from unstable high voltage electrospinning is notable in the SEM images.

2.6.7 Pyridine effect on electrospun scaffold fabrication

The inclusion of pyridine at 100ppm to a 7% PDO solution led to significant changes in electrospinning behaviour (Figure 2-14). When electrospun at a flow rate of 1ml/hr, most of the solution just dripped from the nozzle with a very small Taylor cone being maintained throughout this process. The size of the fibres was however statistically significantly reduced from 1034nm to 340nm ($p<0.0001$). There was no significant difference in the alignment of the

scaffolds produced with and without pyridine. Pyridine also increased the deposition width of electrospun fibres (10.2cm) on the collector by nearly 250% compared to plain PDO solutions (3.9cm).



Number of fibres	72	51
Diameter (µm) (mean)	1.03	0.34
Diameter (µm) (standard deviation)	0.23	0.040
Rayleigh's R	0.9077	0.8629
Angular deviation (°)	3.1	5.2

Figure 2-14. Effect of pyridine on electrospun fibre diameter, alignment and distribution width.

Representative SEM images of electrospun fibres ((A) 10,000x magnification, scale bar 1µm), fibre diameter distributions (B), fibre alignment (C) and summary statistics (D) for electrospun scaffolds produced from 7% PDO solutions with and without 100ppm pyridine. Fibre diameter is significantly reduced with a minimal effect on fibre alignment.

Repeat testing at lower flow rates (0.25ml/hr) eliminated the dripping and increased stability of the cone. Eliminating the dripping is important as observation of the cone is the only visible aspect of the electrospinning process to assess stability throughout production. Dripping also induces episodic surging in the length and thickness of the Taylor cone potentially affecting the consistency of fibres. Repeat testing with pyridine concentrations of 10, 100 and 200ppm revealed a dose-dependent response (Figure 2-15), however the effects of increased pyridine concentration were minimal on fibre diameter but had other effects on alignment and morphology. Based on these results, a pyridine concentration of 100ppm was selected for fabrication of collagen fibril range electrospun fibres balancing lower diameters, with adverse reduction in alignment and crosslinking associated with higher pyridine concentrations.

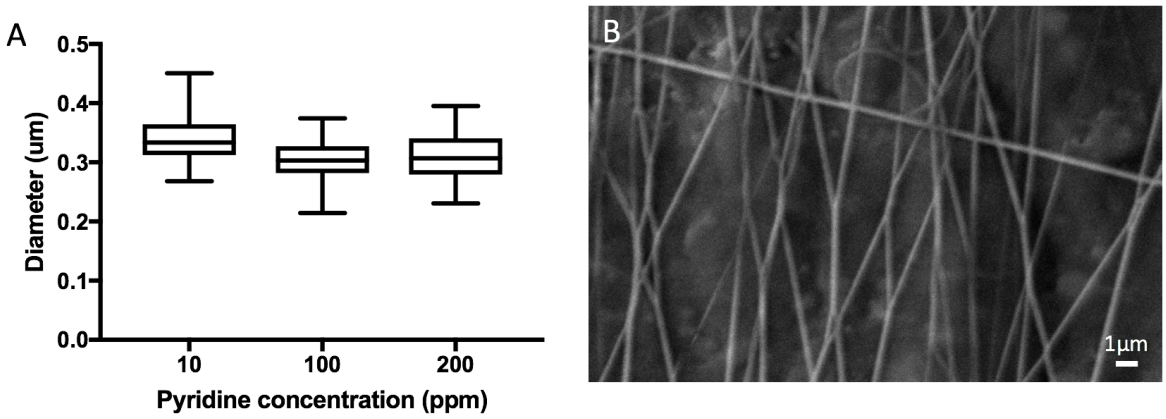


Figure 2-15. Effect of pyridine concentration on electrospun fibre diameter and scaffold morphology.

Pyridine concentration has a dose response relationship with electrospun fibre diameter (A). 200ppm pyridine concentrations were associated with increased branching of fibres and reduction in alignment ((B) SEM image at 10,000x magnification, scale bar = 1µm).

The addition of pyridine had no effect on viscosity at 100ppm but significantly increased conductivity ($p<0.001$). PDO solution without pyridine had a conductivity of 0.062uS/cm, pyridine addition at 100ppm increased this to .98uS/cm. Detailed investigation of these effects

has been undertaken in conjunction with other researchers in the group and is currently undergoing patent review prior to publication.

2.6.8 Biomimetic electrospun scaffolds used for *in vitro* experiments

The targeted 5 scaffolds (aligned: 300nm, 1000nm, 2000nm, 4000nm and random: 1000nm) are shown in Figure 2-16.

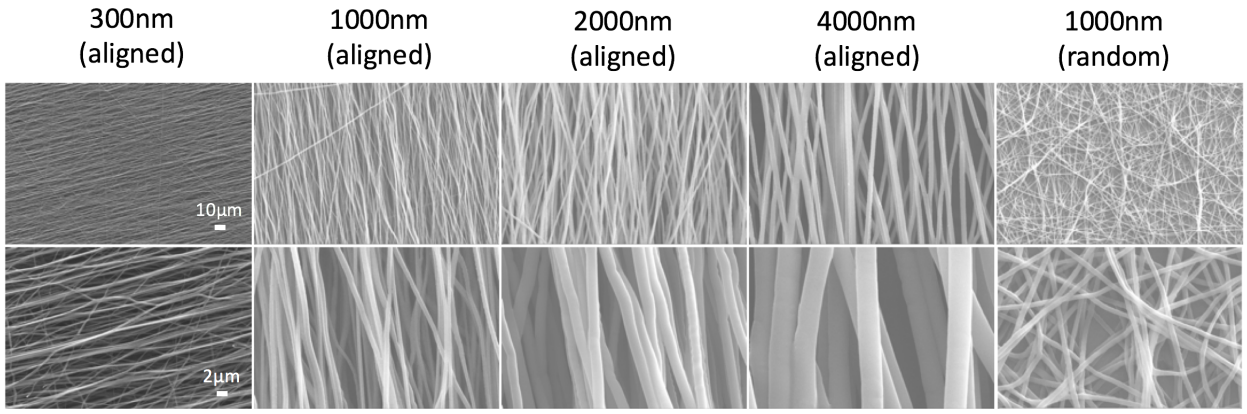


Figure 2-16. The 5 scaffolds produced for subsequent *in vitro* experiments.

SEM images show representative low ((top) 1000x magnification, scale bar = 10µm) and high ((bottom) 2500x magnification, scale bar = 10µm) SEM images of the aligned 300nm, 1000nm, 2000nm and 4000nm scaffolds, and the randomly orientated 1000nm fibre scaffold.

Over the course of the thesis to generate fresh scaffolds for the *in vitro* experiments, up to 6 cycles of matched scaffold production occurred. The mean fibre diameters and distributions are shown in Figure 2-17. There was no significant difference in diameter of the scaffolds used at any time within each scaffold type. The distribution of fibres in 4000nm scaffolds is much higher than other diameter sizes but was consistent. There were also no significant differences in alignment with trends towards alignment as assessed by Rayleigh's R values (>0.90 for all aligned and <0.1 for all random scaffolds) similar across repeats of each scaffold type. Pyridine introduction decreased the tendency to alignment so for 300nm scaffolds, alignment was considered achieved at R>0.85.

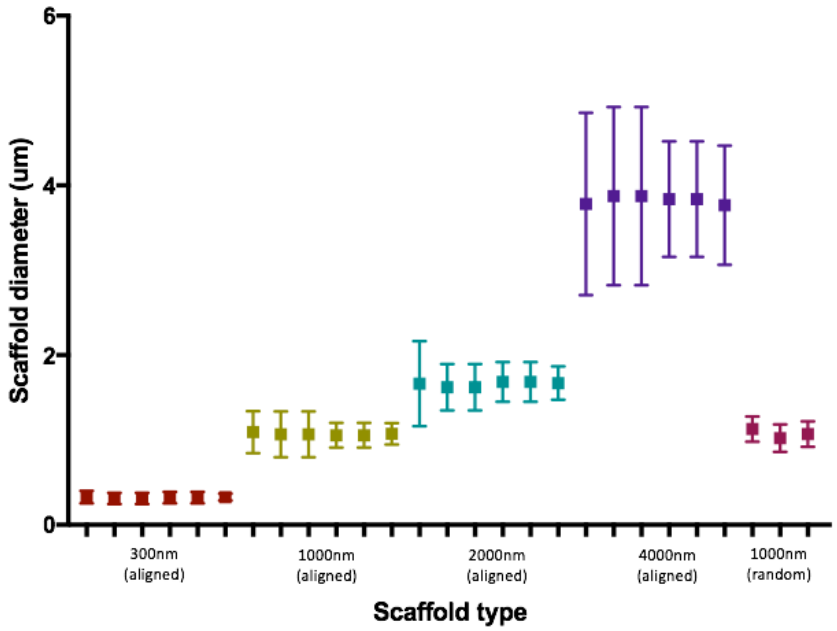


Figure 2-17. Reproducibility of the 5 scaffolds produced over 3 years for *in vitro* evaluations.

The mean and standard deviation for each iteration of each diameter scaffold are plotted to show relative consistency throughout the experiments. No significant difference was observed in mean diameter.

2.6.9 Evaluation of electrospun fibre roughness and local mechanical properties

Measuring fibre roughness and local mechanical properties was unreliable. Efforts to gather this data were exhaustive, using three different AFM providers at institutions affiliated with the University of Oxford. The implications of this are considered in the discussion, both from a cell biology view point, as well as translating these properties as deliberate biomaterial strategies to influence tendon healing.

2.6.10 Scaffold porosity and pore size characterisation

The data generated from porosity and pore size measurement proved too inconsistent for meaningful analysis. To gain adequate data, 80mg of material was required. Fitting this amount of electrospun scaffold into the penetrometer was challenging. The mechanical manipulation involved in doing this likely contributed to data inconsistencies with relative

compression from the required folding. Multiple repeats of 80mg of material also limited other experimentation possible through consumption of material.

2.7 Discussion

This discussion will centre on interpretation of the results from this chapter in the context of this thesis as well as the wider scope of electrospun materials. It is broken into 5 sections. The first section focuses on issues around the consistent production of homogenous electrospun scaffolds. Secondly, the effect of electrospinning parameters in this specific purpose-built electrospinning set up are analysed. The third area assesses the role of pyridine in electrospun scaffolds. Fourthly, the production of the targeted scaffolds is discussed. Finally, the limitations of the experiments and the results of this chapter are considered.

2.7.1 Consistency and homogeneity of electrospun scaffolds

The electrospinning conducted for this thesis was the first to occur with newly acquired purpose-built equipment. This required characterisation of this electrospinning set up and investigation of how parameter changes would affect electrospun fibres. Previous work had been completed within the group in a smaller, self-built set up. Early experiments showed that electrospun fibres were homogenous and could be produced in a repeatable fashion. Additionally, given the purpose-built machine allowed for more accurate and defined electrospinning through stable parameters compared to the old system, more detailed investigations were possible.

Previous differences in electrospun fibre results were assumed to be due to less exact control of voltage, collector speed, temperature and humidity. Precise control over all parameters, however, showed that PDO supplier, batch effects from single suppliers and degradation of PDO resin can have significant effects on electrospinning behaviour, specifically fibre diameter. It is possible these effects also affect alignment, roughness, local mechanical

properties and other electrospun scaffold characteristics not examined as a key aim in this thesis.

Whilst it is expected for PDO from different suppliers to vary in molecular weight, the effects of these differences on electrospun fibres were stark, with production ranging from unusable beaded fibres through to homogenous fibre populations. Depending on supplier, PDO resin is delivered in aliquots or single larger quantities. These aliquots may be characterised and tested individually or not. In one delivery from a single supplier, MFR ranged from 1.2 up to 5.9g/10min. When electrospun in an identical system, these different PDO resins resulted in significantly different mean fibre diameters, 1.549µm and 1.743µm respectively. A 200nm difference could result in significant differences in electrospun material properties and consequent cell-material interactions if not accounted for during production.

Electrospinning projects are often long-term endeavours, requiring production of identical scaffolds at repeated intervals over time. Differences in raw PDO resin supplied could potentially restrict this repetition or at the very least, as encountered in this thesis, require frequent re-characterisation and optimisation of electrospinning parameters to ensure defined characteristics are maintained at comparable values.

Preparation of larger quantities of polymer resin could help to overcome these issues and was investigated accordingly. Large solution volumes (up to 100mls) were trialled to ensure identical solution could be introduced repeatedly into the electrospinning system over time. However, it was noted that (generally around 3 months from dissolution of PDO into HFIP), the resultant electrospun fibres from these solutions were no longer the same as at baseline. This raised the issue of how PDO storage can affect electrospun fibres.

Long term storage in a variety of recommended storage conditions (-8 ˚C), under vacuum and at room temperature), and as a solution were tested in addition to a positive control. This showed that over a 6 month period, there was a significantly different change in viscosity and

fibre diameter depending on the storage condition of PDO. As expected, PDO stored in an accelerated ageing condition suffered significant degradation. The speed of this degradation was however startling with PDO no longer compatible with electrospinning after less than 1 month. Such rapid degradation would suggest that hydrolytic breakdown is occurring very quickly. This is important for two reasons. Firstly, if PDO resin is so sensitive to hydrolytic breakdown, storage and use must be carefully monitored. Secondly, this rapid breakdown of electrospun fibres will also occur *in vivo*, presumably even faster given the surface area to volume ratios of electrospun fibres compared to PDO resin beads. This may affect how long the topography of the implanted material lasts *in vivo* in a conformation to provide the desired biophysical cues, as well as any load bearing capability.

Storage as a solution, in a vacuum and at room temperature led to significant reductions in fibre diameter over time consistent with hydrolytic breakdown of polymer chains. Conversely, storage of PDO at -8 ˚C promoted an increase in viscosity and fibre diameter. This is unlikely to be due to chance or solution preparation error as the trend is continuous over time. Physically however, storage at lower temperatures should not increase molecular chain length. Freeze/thawing cycles have, however, been reported to modulate electrospinning. 3 freeze/thaw cycles were enough to promote crystallinity and significant changes in the mechanical properties of PVA nanofibres [281]. The PDO aliquots in this study, would have undergone 4 freeze/thaw cycles prior to electrospinning at 6 months, potentially affecting the crystallinity of the PDO. If crystalline regions do act as internal cross links and promote mechanical strength, this could explain the increase in viscosity and fibre diameter.

Changes at the molecular level of PDO brought about by storage conditions were re-enforced through DSC results. The proportion of PDO existing in a crystalline phase increased significantly in incubator storage and not in other conditions. This may reflect hydrolytic degradation occurring in the amorphous region of the PDO polymer. These areas are less tightly bound and subject to more rapid breakdown than occurs in crystalline regions. This

phenomenon would lead to a relative increase in crystallinity, not a promotion of crystal formation, even as the PDO is concurrently degrading in the crystalline regions. The observed changes in crystallinity of PDO stored at room temperature, in a freezer and in a vacuum, did not correlate with the observed changes in viscosity and electrospinning behaviour.

However, DSC thermal analysis also showed changes in peak size and location for PDO resin stored in different conditions at 1 and 6 months. These differences suggest changes in the mobility of the polymer chains [282]. PDO stored in the incubator demonstrated a wider melting range and larger re-crystallisation consistent with hydrolytic degradation causing increased chain mobility. Higher chain mobility facilitates re-crystallization upon heating and cooling. In contrast, PDO stored in the freezer showed a narrower and sharper melting peak indicating a narrower range of crystal structures compared to PDO stored in other conditions and reflecting reduced chain mobility. The differences in chain mobility would correlate with the increased viscosity of frozen PDO compared with the other samples. For a more mechanistic investigation of these changes, future work could employ a more detailed structural analysis technique such as X-Ray Powder Diffraction (XRD) or Fourier Transformation Infra-Red spectroscopy (FT IR).

It is surprising more research has not been published into storage condition effects on polymers and electrospinning. This is even more startling given the effects of hydrolytic breakdown are well documented and considered in the storage and sterilisation of polymer biomaterials following fabrication. Unpublished data from within the group has shown storage of electrospun fibres in room conditions compared to inside a desiccator results in significantly gross mechanical properties (tensile strength) within 14 days. One previous publication, however, has looked at long-term storage effects on the viscosity of polylactide and poly(lactide-co-glycolide) over 2 years. It is possible, the results from these polymers have been extrapolated more generally to other polymers. Whilst these are two biodegradable

polymers, degradation of different polymers can vary from days to years, potentially explaining the differences observed with faster degrading PDO.

ISO standards have been developed to ensure the permeability of packaging to water is as low as possible. Packaging often also occurs in nitrogen saturated environments to further limit the effects of water vapour. With new EMA/FDA regulations of biomaterials requiring consideration of biomaterial products and their breakdown products at all stages of their life cycle, attention may also need to be focused upstream, prior to production, to ensure biomaterials are being fabricated from comparable polymer sources to begin with.

Before more complicated aspects of electrospinning have been considered, simple issues around the base PDO resin are apparent. The ramification of these issues (different suppliers, different aliquots from the same suppliers, and different storage conditions) could introduce significant differences into electrospun fibres and subsequent cell responses. These considerations are also important when considering upscaling production and process capacity of a commercial product.

Admittedly, it is possible to adjust for changes in polymer chemistry to conserve fibre diameter. The effects on fibre alignment have not been exhaustively investigated but do not seem to be affected by degradation. However, the effects on other biophysical parameters remain uncharacterised. This is because characterisation of surface roughness and local mechanical properties, where we might expect differences in polymer chemistry to have a more pronounced affect, was not possible. This work also falls outside the scope of this thesis. In the context of biomaterial development, however, it remains to be seen if such differences in polymer chemistry reach a high enough threshold in a biophysical parameter, topographical or mechanical, or surface chemistry which would change any subsequent cell-material interaction and have a biological effect.

Particular attention is focused on electrospun fibre diameter and alignment as biophysical properties for affecting the cell populations involved in tendon healing and biomaterial response. This is likely multifactorial. However, two reasons stand out. Firstly, under the principles of biomimicry, recreating these characteristics of healthy tendon matrix is an obvious requirement. Secondly, these properties are easily to quantify and manipulate. Fibre diameter and fibre alignment have not, however, been shown to be the only biophysically relevant biomaterial properties.

This thesis aimed to examine and quantify in a robust methodological way, the effects of fibre diameter, fibre alignment and fibre stiffness. The ultimate aim was to combine the optimised individual parameters together to create a more functional biomaterial. The limitations of this research raises two issues. Firstly, to be able to examine the effects on cell response, a protocol to consistently and economically measure electrospun fibre stiffness must be generated. Further research and technical development is needed to allow assessment of this important biomaterial property and where it lies in the spectrum of biophysical influence. Secondly, in a commercial setting, production consistency is validated using selected parameters. If fibre stiffness is an important determinant of cell response, then as fibre diameter and alignment are controlled for, stiffness must also be assessed.

2.7.2 Parameter effects on electrospun scaffolds in a purpose-built electrospinning set up

Manipulation of electrospinning parameters had effects in line with the cited literature mentioned in Table 2-1. As this chapter set out to create electrospun fibres ranging from collagen fibrils (<500nm) through to collagen fibres (4000nm), parameter effects on fibre diameter were evaluated. Various combinations of individually favourable parameter settings were trialled without successfully consistently producing electrospun fibres of this size. Operating at the extremes of what PDO solutions could produce in this system often lead to

beading. While these were often connected by ultra narrow fibres (<100nm), beading has been shown to have adverse effects on cell attachment [283]. Furthermore, ensuring the beading was consistent would be hard to quantify to ensure scaffolds produced at different times were homogenous.

Some favourable parameters for reducing electrospun diameter could not be used in this system. Collector distance showed an ability to reduce fibre diameter (by around 100nm) and promote alignment, however when scaling up to use a translocating nozzle, tubes were catching and occasionally being pulled out of position. Over long duration spinning cycles, this interruption could induce aberrations in the electrospun fibres interfering with interpretation of cell-material interactions. The absolute effect of the increased distance was also much reduced when operating at the lower end of the fibre diameter spectrum.

Temperature and humidity changes are known to have considerable effects on the surface topography of the electrospun fibres [203,204]. These parameters have been used to induce deliberate topographical changes. However, as this thesis aims to tightly control all potential biophysical cues, using temperature and humidity would have led to changes in surface topography between scaffold types, limiting interpretation of results. This decision was also taken in conjunction with the effects of hydrolytic breakdown witnessed with PDO storage. Increasing humidity would result in increased incorporation of water molecules into the scaffolds. Despite storage in a desiccator prior to use, this water could instigate degradation leading to changes in topography and local mechanical properties.

2.7.3 Pyridine effect on electrospun scaffold fabrication

Pyridine addition allowed fabrication of continuous electrospun fibres at the diameter required to approximate collagen fibrils (<500nm). Pyridine is a small, volatile, cyclic organic compound miscible in HFIP. Pyridine has previously been reported in the literature as an adjunct to achieve low-diameter electrospun fibres but not with PDO [176, 284]. Pyridine is also

used in the pharmaceutical industry and has FDA approval so inclusion as an adjunct is unlikely to introduce barriers limiting successful translation.

Pyridine addition reduced fibre diameter in a dose-dependent relationship. Pyridine addition, however, decreased fibre alignment and induced a more branched scaffold morphology. These changes were due to significant increases in conductivity of the PDO solutions without changing viscosity. Increasing the collector speed could restore fibre alignment.

The increased fibre distribution width was not deemed detrimental to the consistency or homogeneity of electrospun scaffolds. The increased fibre branching did, however, introduce another topographical change and potential biophysical cue to influence cell biology. Efforts were made to reduce this through altered voltages, flow rates, concentrations but this effect persisted. The degree of crosslinking, albeit on a more molecular level, in biological scaffolds [285], as well as in electrospun fibres [286] has been shown to affect cell function. Further work could be undertaken to assess the influence if cross linking on a higher topographical order induced by pyridine addition also changes cell response.

2.7.4 Final biomimetic scaffold production

The 5 scaffolds required to test hypotheses about cell-material function were successfully produced. The specific parameters used (Table 2-4) were chosen to allow as few differences in the electrospinning process as possible. More changes in parameters could result in more changes, detectable or not, in polymer biophysical properties. Given the demonstrated effects of alterations in hydrophobicity and charge on cell behaviour, addition of pyridine introduces the potential for variation in biological activity through more pathways than diameter changes alone. However, not using pyridine precluded the generation of scaffolds of the physical scale required to allow biomimicry of collagen fibrils.

The production of these scaffolds was achieved at multiple times over 3 years suggesting these same scaffolds can be reproduced repeatedly for further material, biological or other

experiments. Admittedly, these scaffolds were characterised as homogenous based on fibre diameter and fibre alignment. Whilst it was planned to ensure these scaffolds were also consistent across surface roughness, local mechanical properties, porosity, pore size and thickness, this was not possible. Further work is required to ensure protocols are developed to reliably investigate these changes.

Scaffold thickness is an additional important factor to control for to allow comparison of electrospun scaffolds in different *in vitro* experiments. To ensure consistency between scaffolds produced with different electrospinning parameters, it was planned to spin the same amount of PDO by weight. For the 4000nm scaffold, the shortest amount of time to produce a scaffold which could support a fluid column to allow for cell adhesion was 1 hour. 1 hour spinning of 13g/100ml PDO at 3ml/hr equates to 3.9g of PDO deposited. If this is translated to the 7g/100ml PDO solution with pyridine used to produce the 300nm scaffold at 0.3ml/hr, electrospinning would need to occur for more than 24 hours. Whilst this would be possible, the scaffold thickness would not be compatible with our *in vitro* culture system, physically stopping crown closure as well as drawing fluid through capillary action over the high surface area that cell suspensions would dry out before adhesion could occur. Furthermore, long term electrospinning can lead to inconsistencies as relative insulation of the collector increases with accumulated polymer. The surface layers could consequently have different morphologies to the deeper fibres, making interpretation of cell response difficult.

As a result, electrospinning duration was decided by the shortest time required to produce an electrospun scaffold that could support a fluid column for 4 hours to allow cell attachment, the longest period of time used for cell adhesion in the *in vitro* experiments detailed subsequently in this thesis.

2.8 Conclusions

Electrospinning produces homogenous PDO scaffolds with varied alignments and diameters. These can be fabricated consistently at different times and from different solutions. However, PDO supplier, batch and storage conditions all have significant effects on electrospun fibre diameter. This can be mitigated through altering electrospinning parameters at the expense of potentially introducing unintended surface material effects.

Pyridine has significant effects on electrospinning of PDO fibres through modulation of solution conductivity. This leads to thinner, less aligned fibres. Collector speed increase can rescue fibre alignment. However, the increased branching seen with pyridine addition, a topographical feature with biological consequences could not be circumvented. The addition of a conductive molecule may affect the surface charge, hydrophobicity or chemistry of electrospun fibres resulting in altered biological activity separately from the diameter changes.

Targeted scaffold diameters and alignments representing different tendon ECM states were produced. However, characterisation of these scaffolds over the intended full range of biophysical properties was not possible.

Characterisation of local mechanical properties, surface roughness, porosity and pore size were not possible in a reliable, time efficient way. Given these material properties can affect cell phenotype, differentiation and matrix expression, and ultimately tendon healing, future work should be directed to develop protocols and systems to reliable assess these parameters to ensure biomaterials fabricated for research and clinical use are controlled across all biophysical parameters which may influence cell-material interaction and tendon healing.

What was known	What this adds
Electrospun fibrous scaffolds have previously been produced from various polymers with deliberate effects on surface topography, diameter and alignment.	This is the first description of consistent fibrous PDO scaffold generation on a scale approximating collagen fibrils. The incorporation of pyridine into PDO electrospinning will allow fabrication of biomimetic medical devices from a well-established, clinically proven polymer.
The biomaterial life cycle is often evaluated from fabrication through to degradation in vivo.	The effects of polymer storage on electrospinning behaviour has direct effects on fabrication of electrospun scaffolds. These changes in polymer structure may have direct biological effects. Furthermore, the parameter manipulation required to maintain target fibre diameters may also introduce altered biophysical properties and surface modification which affects cell-material interaction. Consideration of upstream aspects of clinical and laboratory production may be necessary to ensure homogenous biomaterial activity.

Chapter 3 Biophysical effects of electrospun fibres on tendon fibroblast and peripheral blood mononuclear cell biology

3.1 Abstract

3.1.1 Background

Biomimetic electrospun materials can guide cell biology. In the context of rotator cuff repair, this guidance could induce favourable healing outcomes from tendon fibroblasts and immune cell populations. However, the response of tendon fibroblasts from diseased rotator cuff tissue to such materials has not been assessed. This experiment sought to characterise and compare the responses of fibroblasts from diseased tendon with healthy tendon. As immune cell populations form the initial host response to biomaterials upon implantation, the response of peripheral blood mononuclear cells was tested on the same scaffolds.

3.1.2 Materials and methods

Tendon fibroblasts were isolated from healthy hamstring and diseased rotator cuff tendons. Peripheral blood mononuclear cells were isolated from leukocyte cones. Biomimetic electrospun scaffolds were fabricated to represent collagen fibrils, collagen fibres and morphologies not encountered in native tendon ECM. Cell populations were cultured on scaffolds for up to 21 days with attachment, metabolic activity, morphology and gene expression assessed.

3.1.3 Results

Tendon fibroblasts derived from diseased tendon demonstrate significantly different attachment, metabolic activity, morphology and gene expression when cultured on electrospun scaffolds compared to fibroblasts from healthy tendon. Electrospun fibres supported tendon fibroblast attachment, proliferation and matrix gene expression. However, changes in electrospun fibre diameter did not drive significant differences in these responses within either population. In contrast, peripheral blood mononuclear cells attach in notably different profiles to electrospun scaffolds of different diameters.

3.1.4 Conclusions

The response of fibroblasts from diseased tendon to electrospun scaffolds is markedly different to that of healthy tendon fibroblasts. Biomimetic fibre diameters did not induce differences in diseased tendon fibroblast function over the ranges and assays used in this thesis more than other fibre diameters. Peripheral blood mononuclear cells are also sensitive to altered fibre diameter. Electrospun biomaterials could play an immunotherapy role in tendon healing upon implantation, in addition to supporting fibroblast function.

3.2 Introduction

Tendon fibroblasts are sensitive to electrospun scaffold-derived biophysical cues, including fibre alignment, diameter and stiffness, as described in section 1.12.1 (Tendon fibroblast

responses to electrospun fibres). Manipulation of these properties could help engage intrinsic biological pathways to promote the cell responses involved in tendon healing.

When manipulating tendon fibroblast response to scaffolds it is important to appreciate the underlying differences between tendon fibroblasts derived from healthy tendon and those from patients with tendon disease. Section 1.5 (Rotator cuff tendinopathy and tears) detailed how tendon fibroblasts from tendinopathic and torn tissue exhibit a truncated morphology, secrete matrix components in altered ratios, produce a less aligned and weaker matrix, and have dysregulated inflammatory profiles compared to tendon fibroblasts from healthy tissue. Given the altered phenotype of tendon fibroblasts from diseased tissue [75], it is likely their response to external stimuli is also different to that observed in tendon fibroblasts from healthy tissue. Kendal et al assessed the biomaterial-elicited response of tendon fibroblasts from healthy and diseased tissue and showed both phenotypes could adhere to and elongate along electrospun fibres. However, there were differences in response with diseased fibroblasts proliferating faster, elongating more slowly and increasing type I:III collagen mRNA expression [289]. Adding to the complexity of response by tendon fibroblasts from diseased tissue, there is a spectrum of disrupted biology within the stages of tendinopathy [40,55,57,79].

Directing the biological activity of tendon fibroblasts in diseased tendons using biophysical cues could promote the structural and functional healing of tendon repair away from fibrosis. Given the differences between healthy and diseased tendon matrix, specifically fibre diameter, alignment and stiffness, scaffolds designed to mimic native tendon ECM could re-program diseased cells towards a 'healthier' phenotype.

The response of peripheral mononuclear cells (PBMCs) is also an important *in vitro* assessment of biomaterials. For example, the porcine SIS grafts discussed in section 1.7.1 (Biologic patches) that were recalled for adverse outcomes, also showed inflammatory

activation in *in vitro* studies [99, 256]. Optimising the biophysical cues for tendon fibroblast response may have negative effects on PBMC and other cell populations or vice versa. Conversely, such changes may also have beneficial or synergistic effects. Given tendon healing is a tissue response combining all these cell populations and inter-population effects, assessment of PBMC response to biophysical properties is also investigated in this chapter.

3.3 Aims

The aims of this chapter are to:

1. Investigate the effect of fibre alignment on tendon fibroblasts derived from healthy tendons
2. Identify and compare the effect of fibre diameter on the activity of fibroblasts from healthy and diseased tendons
3. Characterise and compare the effect of local mechanical properties on fibroblasts derived from healthy and diseased tendons
4. Determine the effect of fibre diameter on the attachment and activity of PBMCs.

3.4 Hypotheses

This work hypothesises that electrospun fibre alignments and diameters that mimic native tendon tissue will induce favourable responses for tendon healing in tendon fibroblasts and PBMCs. Specifically:

1. Aligned fibre scaffolds will support tendon matrix gene expression and morphology more than randomly oriented fibre scaffolds.
2. Fibre diameters approximating collagen fibrils (300nm) and collagen fibres (4000nm) will stimulate tendon fibroblast attachment, increase metabolic activity, promote normal morphology, upregulate tendon matrix gene expression and downregulate

inflammatory gene expression more than fibre diameters not found in natural collagen hierarchy (1000nm and 2000nm).

3. When seeded on biomimetic scaffolds (aligned 300nm and 4000nm scaffolds), tendon fibroblasts derived from diseased tissue will exhibit responses more consistent with healthy tendon fibroblasts
4. Tendon fibroblasts from healthy tendon tissue will be more responsive to biophysical stimuli than tendon fibroblasts from diseased tissue.
5. Fibre diameters approximating collagen fibrils (300nm) and collagen fibres (4000nm) will induce lower levels of expression of inflammatory genes in PBMCs than fibre diameters not found in the natural hierarchy of collagen (1000nm and 2000nm).

3.5 Materials and methods

3.5.1 Electrospun scaffold fabrication and preparation

Electrospun scaffolds were produced and characterised in line with the protocols described in Chapter 2 (Fabrication of biomimetic electrospun scaffolds). Fresh scaffolds with the appropriate alignment and diameter were produced for each experiment and stored in a desiccator for no more than 7 days before use.

1.5cm x 1.5cm sections were cut from scaffolds, sprayed with ethanol to facilitate lifting and mounted on 24 well plate sized cell crowns (Scaffdex, Tampere, Finland). Informal pressure testing was performed to identify any defective scaffolds that may have affected a scaffold's ability to support a cell suspension for the duration of cell attachment. Visual inspection was also undertaken to identify any twisted or altered scaffold tensioning that may have changed the topography and biophysical cues presented to cell populations. Defective scaffolds were not used in experiments.

On the morning of cell seeding, mounted crowns were sterilised in ethanol for 60 minutes and air dried for 2 hours. Scaffolds were then washed twice in Phosphate Buffered Saline (PBS, Sigma-Aldrich, Dorset, UK) and left to air dry. Macroscopic inspection of the scaffold surface was repeated at this stage to remove damaged scaffolds.

Mounted scaffolds were then submerged in 2250µl D10 culture media (Dulbecco's Modified Eagle Medium: Nutrient Mixture F-12 (DMEM/F12) (Lonza, Slough, UK) supplemented with 10% Fetal Bovine Serum (FBS) (Labtech, Uckfield, UK) and 1% penicillin-streptomycin (PS) (ThermoFisher Scientific, Waltham, MA, USA)) in 24 well plates for 1 hour at 37 ^{o}C to facilitate serum protein adsorption. Crowns were removed, rinsed 3 times with PBS with any remaining solution removed from scaffolds prior to cell seeding. Care was taken to ensure scaffolds did not dry out between serum adsorption and cell seeding as pilot experiments had shown this lead to cracking of the electrospun scaffolds.

3.5.2 Tendon fibroblast acquisition, expansion and assessment

3.5.2.1 Human tendon sample procurement

Tendon was acquired from healthy and diseased donors. Healthy tendon fibroblasts were isolated from residual healthy tendon from patients undergoing anterior cruciate ligament reconstruction with autologous hamstring grafts. Diseased tendon fibroblasts were derived from tendon removed during the debridement and repair of large/massive rotator cuff tears. These tissues were collected with informed consent compliant with the Declaration of Helsinki. Ethical approval for collecting these samples was through Oxford Musculoskeletal Biobank (REC 09/H0606/11) in agreement with National and Institutional requirements. At the time of surgery, tissue samples were transferred into sterile tubes containing D10 culture media for transport from the operating theatre to the laboratory.

3.5.2.2 Tendon fibroblast isolation and expansion

Under sterile conditions, tendon tissue was divided with a scalpel into roughly 2mm x 2mm x 2mm explants using a scalpel and forceps, trying to minimise compression of the tendon substance. 6-8 explants were then transferred into 6 well plates. 100µl of D50 culture media (DMEM/F12 media supplemented with 50% FBS and 1% PS) was dripped on to each section. After 24 hours, 2ml of the D50 culture media was added to each well. This media was replaced every 3-4 days.

After 7 to 10 days, when tendon fibroblasts could be seen migrating out of the tendon onto the 6 well plate under phase contrast microscopy, the tendon tissue explants were removed. At this point culture medium was changed to D10 culture media. Media changes continued every 3-4 days. On reaching 80% confluence, cells were lifted mechanically with a cell scraper, and cultured in 10cm dishes (Griener, Frickenhausen, Germany). Cells were expanded and passaged when reaching 80% confluence in 10cm dishes out to passage 3 prior to use in experiments.

3.5.2.3 Tendon fibroblast seeding and culture

For seeding, tendon fibroblasts were counted using a TC20 automated cytometer (Bio-Rad, Hertfordshire, UK) and diluted to 800,000 cells/ml in D10 media. For electrospun scaffolds, 100µl of cell suspension was then placed on to the top surface of mounted scaffolds held in a 24 well tissue culture plate (TCP, Corning Inc, Corning NY, USA). The area of the scaffold in a cell crown is 0.79cm^2, equating to a seeding density of 100,000 cells/cm^2. Cells were left for 2 hours to attach to the scaffold before transfer into D10 media in a fresh 24 well plate. After 24 hours, mounted crowns were transferred to new 24 well plates with fresh media. Media changes were performed using new plates every 3/4 days for the duration of the experiment. To avoid washing off cells and damaging scaffolds during media addition, mounted scaffolds were gently lowered into 24 well plates prefilled with 1750µl of fresh D10 culture media. 500µl

of D10 media was then also carefully added into the cell crown to ensure adequate coverage of cells and scaffold.

For some experiments, tendon fibroblasts were also cultured in 24 well plates and 8 well chamber slides (Nunc Lab-Tek II, ThermoFisher Scientific, Waltham, MA, USA). Seeding densities for these surfaces were maintained at 100,000 cells/cm^2. Tendon fibroblasts were left for 2 hours to adhere before the addition of supplemental D10 media. Media was added into 24 well plate wells to equal the 2250µl volumes used with electrospun scaffolds. 700µl was added to chamber slides because of chamber volume restrictions. Media was refreshed on the same 3-4 day schedule.

3.5.2.4 Tendon fibroblast attachment

Cell attachment was determined at 24 hours unless otherwise stated. To do this, scaffolds on crowns were transferred into 24 well plates containing 1750µl of 10% AlamarBlue (Invitrogen, Paisley, UK) in D10 media. 500µl more of this solution was added into the crowns. This volume was added directly into TCP control wells. Crowns were incubated in 10% AlamarBlue solution for 4 hours. After this time, crowns were lifted and placed in a new 24 well plate. A pipette was used to carefully aspirate any solution suspended on the scaffold and mixed back into the original well. Care was taken to not puncture or damage the scaffolds.

The fluorescence of each solution was then measured in triplicate on a FluoStar Optima microplate reader (BMG Labtech, Ortenberg, Germany) with an excitation of 485nm and an emission of 520nm. The fluorescence readings of scaffolds were then compared to the fluorescence reading of tendon fibroblasts seeded on TCP to determine what proportion of cells had adhered to the scaffolds.

3.5.2.5 Tendon fibroblast metabolic activity

The AlamarBlue assay was also performed according to the protocol from section 3.5.2.4 (Tendon fibroblast attachment) at media changes for the duration of experiments. The fold increase in fluorescence from baseline was calculated at each time point.

3.5.2.6 Tendon fibroblast morphology

Immunostaining was performed to determine the morphology and examine the cytoskeletal arrangement of tendon fibroblasts seeded on scaffolds. Scaffolds and chamber slide wells were washed with 1000µl PBS twice prior to fixation in 10% formalin for 60 minutes. Scaffolds and slides were washed and stored in PBS at 4^{o}C prior to staining.

Cells were permeabilised with 0.5% Triton-X (ThermoFisher Scientific, Loughborough, UK) for 15 minutes. Specimens were then stained with 1 unit of Alexa Fluor ™ 488 Phalloidin (ThermoFisher Scientific, Loughborough, UK) in 200µl PBS for 60 minutes at room temperature in the dark. Nuclear counter staining was performed with 200µl of 300nM DAPI (Molecular Probes, Eugene, Oregon, USA) for 60 minutes at room temperature in the dark. Scaffolds and wells were washed and stored in PBS.

Images were captured at 40X magnification using a Zeiss LSM710 confocal microscope (Carl Zeiss AG, Oberkochen, Germany).

3.5.2.7 Tendon fibroblast gene expression

Scaffolds were rinsed with 1ml PBS, removed from crowns and placed in Eppendorf tubes. 400µl TRIzol (Invitrogen, Paisley, UK) was added and care taken to ensure complete submersion of the scaffolds in the TRIzol solution. mRNA was extracted using the manufacturer's protocol for the Direct-Zol RNA Microprep kit (Zymo Research, Irvine, CA, USA). An on-column DNA treatment was performed with DNAse (ThermoFisher Scientific, Loughborough, UK). mRNA concentration and quality was checked using an ND1000 Nanodrop Spectrophotometer (Nanodrop Technologies, Willington, DE, USA). cDNA was

synthesised using a High Capacity cDNA Reverse Transcription Kit (Applied Biosystems, Waltham, MA, USA) with cDNA diluted to 1.25ng/µl for subsequent use.

For RT-qPCR 4µl (5ng) of cDNA was used in a 10µl reaction with Fast SYBR Green Master Mix (Applied Biosystems, Waltham, MA, USA). Reactions were run using an Applied Biosystems ViiA7 Real-time PCR system (Life Technologies, Carlsbad CA, USA). Primers were used according to manufacturer protocols. The primers and suppliers used for each experiment are listed in subsequent experimental details. Within an experiment, the same primers were used for consistency across analysis. Some changes in primer supplier were necessary in different experiments potentially affecting direct comparisons. *GAPDH*, *TBP* or *ACTB* were used as endogenous reference genes with gene expression calculated based on a comparative CT method. Figures and results are shown normalised to *GAPDH* unless otherwise stated. *ACTB* was not used as cytoskeleton and cell morphology was deliberately targeted with electrospun scaffolds, potentially biasing results. Results performed within the laboratory group using the geNorm Housekeeping Gene Selection Kit (Primer Design) showed *GAPDH* to be more suitable than TBP for tendon fibroblasts cultured on electrospun scaffolds and TCP.

3.5.3 Effect of fibre alignment on healthy tendon fibroblasts

This experiment set out to define the response of healthy tendon fibroblasts to differences in electrospun fibre alignment. This experiment assessed cell attachment, proliferation, morphology and gene expression changes compared to tissue culture plastic over 7 days culture using the protocols outlined in section 3.5.2 (Tendon fibroblast acquisition, expansion and assessment). QuantiTect primers were used for *COL1A1, COL3A1, COL5A1, ACAN, TNC, DCN, SCX-B, TBP* and *GAPDH* (Qiagen, Hilden, Germany). This experiment was conducted in triplicate using cells from healthy hamstring (2 male, 1 female, average age 18.3 years). The time points and numbers of repeats used for this experiment are outlined in Table 3-1.

Table 3-1. Assays used to assess the effects of alignment on healthy tendon fibroblasts.

Assay technique	Number of experimental repeats per time point	Time points
Attachment - AlamarBlue	3	2 hours
Metabolic activity - AlamarBlue	3	1, 3 , 7 days
Morphology – Confocal fluorescence microscopy	2	2 hours and 7 days
Gene Expression - RTqPCR	3	2 hours and 7 days

3.5.4 Effect of fibre diameter on tendon fibroblasts derived from healthy and diseased tendon

This experiment set out to define the response of tendon fibroblasts from healthy and diseased tendon to differences in electrospun fibre diameter. This experiment investigated cell attachment, proliferation, morphology and gene expression changes over 21 days culture using the protocols outlined in section 3.5.2 (Tendon fibroblast acquisition, expansion and assessment). Tendon fibroblasts were isolated from 3 healthy hamstring tendons (2 male, 1 female, average age 18.3 years) and 3 diseased rotator cuff tendons with large/massive tears (2 male, 1 female, average age 65.6 years). The time points and numbers of repeats used for this experiment are outlined in Table 3-2.

Table 3-2. Assays used to assess the effects of diameter on tendon fibroblasts isolated from healthy and diseased tendon.

Assay technique	Number of experimental repeats per time point	Time points
Attachment - AlamarBlue	3	1 day
Metabolic activity - AlamarBlue	3	3, 7, 10, 14, 17 and 21 days
Morphology – Confocal fluorescence microscopy	2	1, 7, 14 and 21 days
Gene Expression – RTqPCR	3	1, 7, 14 and 21 days

QuantiTect primers were used for *COL1A1, COL3A1, COL5A1, ACAN, TNC, DCN, SCX-B, ACTB, PTGS2, IA1, IA2, IA4, IA5, IAV, IB1, IB2, IB3, CD44, CADN2, PTK2, GAPDH* and *TBP* (Qiagen, Hilden, Germany). Primer Design primers were used for *IL6, IL8, TGFB1, HIF1A, DKK3, PTGS2* and *PDPN* (Primer Design, Southampton, UK).

3.5.5 Peripheral Blood Mononuclear Cell response to electrospun scaffold diameter

3.5.5.1 Scaffold preparation

300nm, 1000nm, 2000nm and 4000nm aligned electrospun scaffolds were prepared and mounted as per section 3.5.1 (Electrospun scaffold fabrication and preparation). A 1.1ml/hr flow rate was used for the manufacture of the 2000nm scaffold in this batch of scaffold production to separate the mean fibre diameter further from the 1000nm scaffold for reasons discussed later in section 3.7.2 (Tendon fibroblast response to electrospun fibre diameter is more dependent on disease phenotype than diameter change).

The scaffolds were pre-adsorbed with human serum to avoid potential antigenicity related to xenogeneic tissue from FBS. Human serum was obtained from healthy volunteers (3 males, average age 29) under informed consent and ethics (REC11/H0711/7). Mounted scaffolds were placed on 24 well plate lids and 100µl of serum placed onto the scaffold. Plates were

sealed and placed in an incubator at 37 ºC for 60 minutes. Crowns were then washed 3 times with 2ml PBS to remove any residual serum and unbound protein from the scaffolds.

3.5.5.2 PBMC isolation

The PBMC isolation protocol has been adapted from Martinez 2012 [290]. PBMCs were isolated from leukocyte cones (National Health Service Blood and Transplant, John Racliffe Hospital, Oxford, UK). Leukocyte cones were mixed gently with cold Roswell Park Memorial Institute 1640 (RPMI (Sigma Aldrich, Dorset, UK)) media. The cell suspension was carefully layered on top of 15ml Histopaque 1077 (Sigma Aldrich, Dorset, UK) in a 50ml falcon tube. The solution was centrifuged for 20 minutes at 820G at 4 ºC with minimal acceleration and deceleration settings. The PBMC layer was removed into 3ml cold RPMI media and mixed before resuspension with a further 27ml cold media. PBMCs were pelleted and re-suspended in warm, complete RPMI (cRMPI (RPMI supplemented with 10% FBS, 1% PS and 2mM L-glutamine (Life Technologies, Paisley, UK). PBMCs were frozen down in a 1:1 dilution with freezing media (20% Dimethyl sulfoxide, 50% Human Serum Albumin in RPMI) at 1x10^8 cells per ml using a Mr Frosty Freezing Container (ThermoFisher Scientific, Paisley, UK)

3.5.5.3 PBMC seeding

PBMCs were thawed, re-suspended and rested for 2 hours prior to use. PBMCs were counted with a TC20 ™ automated cell counter before seeding. 3 scaffolds were used for each condition with 1x10^6 viable PBMCs seeded per scaffold in a 100µl volume. This seeding density was maintained across the larger surface area of a 24 well plate for control wells. PBMCs were left to adhere for 1 hour prior to transfer into 24 well plates prefilled with 1750µl complete RPMI media before addition of another 500µl culture media. For control wells, cells were suspended in 24 well plates with additional media added directly into the well.

3.5.5.4 PBMC Gene expression

Gene expression was performed to investigate potential inflammatory activation differences between biomimetic and foreign diameter scaffolds. This was done at the time of seeding to establish baseline PBMC gene expression profiles and repeated on PBMCs cultured on electrospun scaffolds and in 24 well plates at 4 hours and 24 hours. Following gentle PBS washing to remove unattached PBMCs, scaffolds were transferred to eppendorfs and mixed in 400µl TRIzol. In control wells, media was removed prior to a rinse with PBS to remove non-adherent cells before the addition of TRIzol directly into the well. mRNA extraction, cDNA synthesis and RT-qPCR performed as described in section 3.5.2.7 (Tendon fibroblast gene expression). Gene expression data in this experiment is for adherent PBMCs only.

QuantiTect primers were used for *GAPDH*. In house designed primers were used for *TNFA, TGFB1, IL1B, IL6, IL8, IL10, IL12, CD206* and *PTGS2*. The primer sequences are listed in Appendix B as Table B-1.

3.5.5.5 PBMC flow cytometry

Flow cytometry was performed at baseline prior to seeding (0 hours), and after 4 hours and 24 hours in 24 well plates for control cells. For PBMCs seeded on scaffolds this occurred at 4 and 24 hours.. For cells on scaffolds, crowns were rinsed twice in 1ml PBS to remove non-adherent cells before incubation in 1ml Accutase (ThermoFisher Scientific, Waltham, MA, USA) for 10min at 37 ^{o}C. Scaffolds were then rinsed thoroughly with 7ml cold cRPMI to further dissociate cells. For control wells, media was removed prior to the addition of Accutase and incubation in the same conditions as scaffolds. Lifted PBMCs were then transferred into 7ml cold cRPMI.

Lifted PBMC populations were centrifuged, re-suspended and washed twice in 250µl cell staining buffer (BioLegend, London, UK) before staining in 50µl staining master mix in a 96 well plate for 15 minutes. The master mix was made up according to Table 3-3 along with

viability dye eF780 used at a 1:1000 dilution. All antibodies were used at 1:50 dilutions for staining except anti-CD8a, which was used at 1:100. Cells were cleaned once in cell staining buffer before suspension in flow fix solution (cell staining buffer supplemented with 2% paraformaldehyde).

Table 3-3. Antibodies used for PBMC flow cytometry experiments.

Antibody	Supplier	Isotype	Clone	Subset marker of PBMCs for
anti-CD3 BV785	BioLegend	Mouse IgG1; k	UCHT1	T cells
anti-CD4 APC	BioLegend	Mouse IgG1; k	RPA-T4	T Helper cells
anti-CD8a BV510	BioLegend	Mouse IgG1; k	RPA-T8	Cytotoxic T cells
anti-CD14 PeCy7	BioLegend	Mouse IgG2a; k	M5E2	Monocytes
anti-CD45 RA BV421	BD	Mouse IgG1; k	OX33	Naïve T cells
anti-CD56 BV710	BD	Mouse IgG1; k	NCAM16.2	NK cells
anti-TCRVG2 PE	BioLegend	Mouse IgG1; k	B6	Gamma Delta T cells
viability dye eF780	eBiosciences	NA	NA	Live/dead cells

Flow cytometry was performed using a BD LSR Fortessa (BD Biosciences, Berkshire, UK) calibrated with a BD cytometer set up and tracking bead protocol. All PBMC populations were run at the same time with the same set up. Analysis of cell populations was performed with FlowJo v10 (FlowJo LLC, Ashland, Oregon, USA).

3.5.6 Statistical analyses

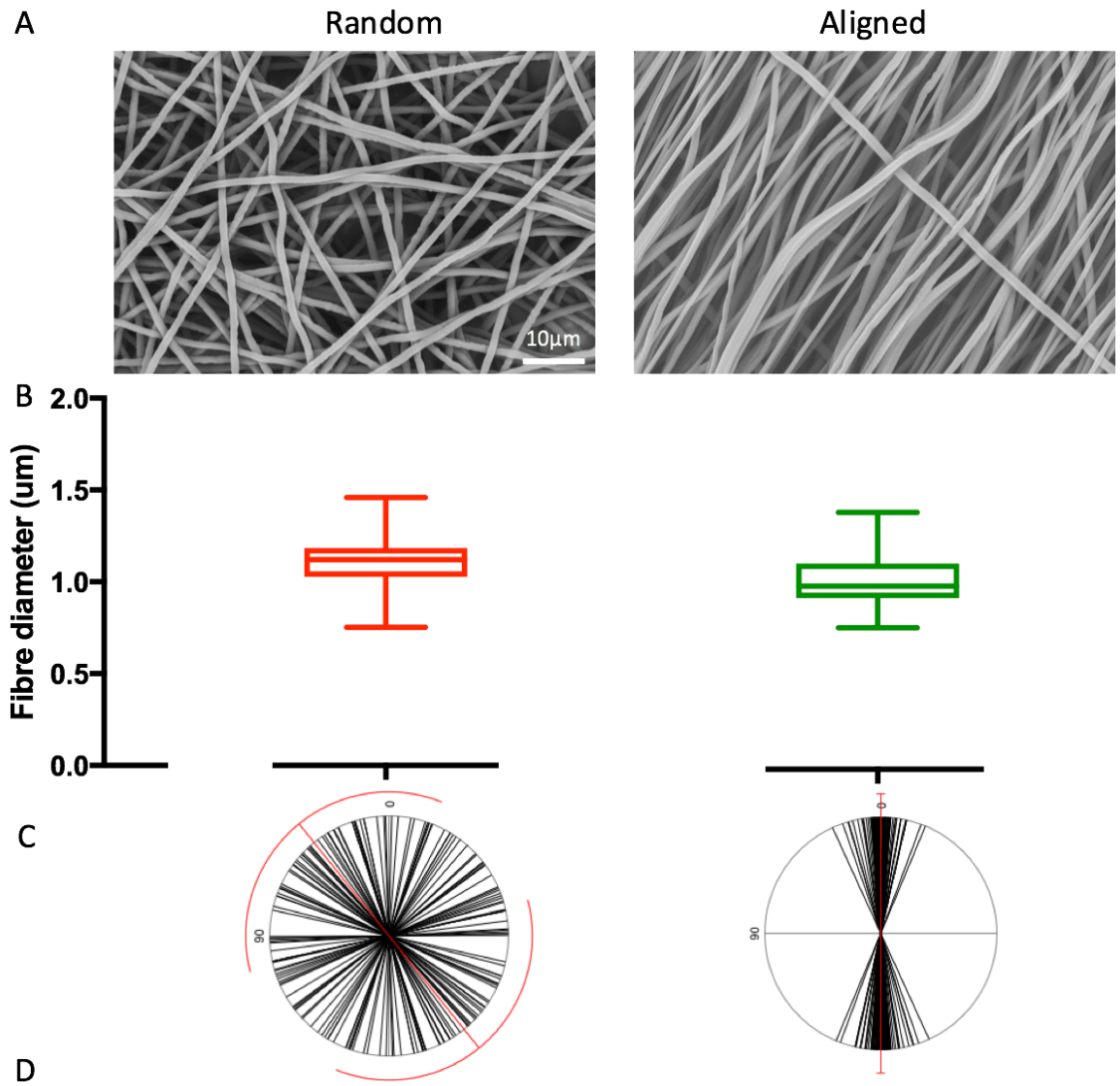
Scaffold analysis was performed using GraphPad Prism software as previously described in section 2.5.14 (Scaffold statistical analysis). The number of repeats in the cell-scaffold experiments was too low to test for normality so non-parametric testing was performed. GraphPad Prism was also used to analyse cell attachment, Accutase lifting efficacy and cell morphology using a one-way ANOVA with post hoc Tukey's testing at the stipulated time point. Gene expression and metabolic activity were analysed using a repeated measures two-way ANOVA with post hoc Tukey's testing. Analysis of PBMC attachment was conducted using a two-way ANOVA with post hoc Tukey's testing. Statistical significance was determined at $p<0.05$.

3.6 Results

3.6.1 Effect of fibre alignment on tendon fibroblasts from healthy tendon

3.6.1.1 Scaffold characterisation

The scaffolds used in this experiment were significantly different in their alignment, but not different in their diameter. Representative images (A), box and whisker plots (B), angle distributions (C) and summary statistics (D) are shown in Figure 3-1. The difference in alignment is evident in the SEM images but also quantified with Rayleigh's test for angular uniformity (aligned, $R>0.9$ and random, $R<0.1$). Scaffolds had normally distributed fibre populations. The mean diameter of the random scaffold was 1103nm compared to 1038nm for the aligned scaffold ($p=0.0795$). The distribution of fibre diameters was also similar between random and aligned scaffolds.



Number of fibres	88	76
Diameter (mean) (um)	1.103	1.038
Diameter (sd) (um)	0.1471	0.1613
Rayleigh's R	0.0974	0.9629
Angular deviation (°)	44	1.7

Figure 3-1. Electrospun scaffolds with random and aligned fibres were fabricated with conserved mean fibre diameters.

Representative SEM images ((A) 2500x magnification, scale bar = 10µm), box and whisker plots ((B) min/max), axial distributions (C) and summary statistics (D) of the aligned and random scaffolds. There were no significant differences in fibre diameter but significant differences in alignment.

3.6.1.2 Attachment of fibroblasts from healthy tendon to random and aligned scaffolds

Tendon fibroblast attachment (Figure 3-2) is displayed as a function of the mean AlamarBlue fluorescence of the same number of cells seeded on TCP. Attachment rates compared to TCP were notably different on random scaffolds (63%, p=0.054) and significantly different on aligned scaffolds (58%, p=0.02). There was no significant difference between random and aligned scaffolds (p=0.55).

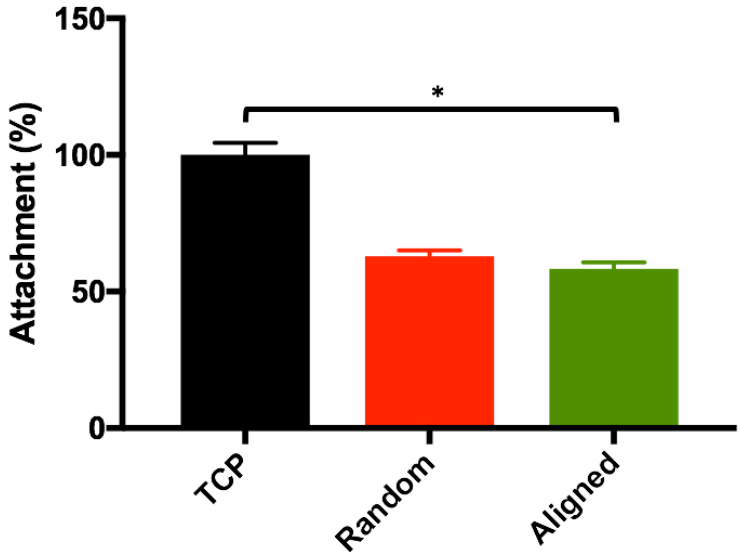


Figure 3-2. Healthy fibroblast attachment rates to random and aligned electrospun scaffolds were similar but notably lower compared to TCP.

Mean percentage attachment to random and aligned scaffolds was calculated as a percentage of TCP adherent cells at 24 hours. There was a significantly lower difference in attachment to aligned scaffolds (*, p=0.02) and a trend towards significance on random scaffolds (p=0.054). No difference was noted between random and aligned scaffold attachment (p=0.55).

3.6.1.3 Metabolic activity of fibroblasts from healthy tendon to random and aligned scaffolds

Metabolic activity increased for fibroblasts cultured on all surfaces from baseline through to 7 days in culture (Figure 3-3). Cells seeded on electrospun scaffolds showed increased metabolic activity compared to those seeded on TCP. Cells seeded on aligned scaffolds had

more strongly increased metabolic activity than random scaffolds. This difference was significant for aligned scaffolds compared to TCP at day 1 ($p=0.045$), day 4 ($p=0.0076$) and day 7 ($p=0.0040$). At day 7, there was also a significant difference in metabolic activity of fibroblasts cultured on aligned scaffolds compared to random scaffolds ($p=0.041$). There was no difference between random scaffolds and TCP at any time point.

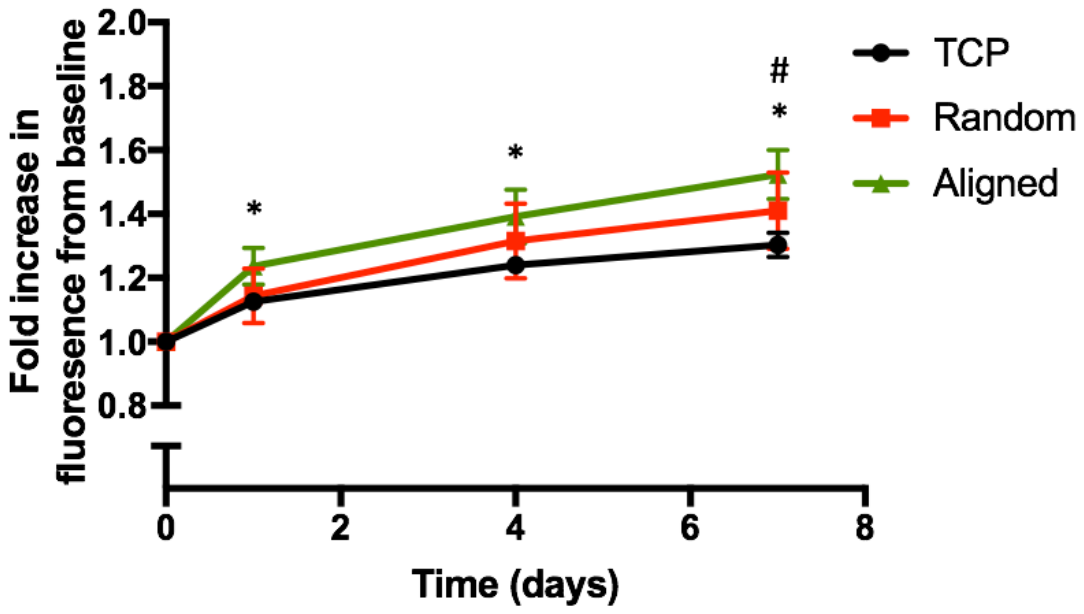


Figure 3-3. Metabolic activity increased for healthy tendon fibroblasts cultured on random and aligned scaffolds more than on TCP.

Metabolic activity increased across all culture conditions. This effect was greatest on aligned scaffolds with significant differences compared to TCP over the entire 7 days (*, $p<0.05$). This increased metabolic activity was also statistically significantly higher compared to random electrospun scaffolds at 7 days (#, $p<0.05$). No significant difference was noted between random scaffolds and TCP at any time point.

3.6.1.4 Morphology of fibroblasts from healthy tendon to random and aligned scaffolds

Aligned scaffolds had a significant effect on cell morphology. Representative images of tendon fibroblasts following 7 days of culture on TCP (A), random scaffolds (B) and aligned scaffolds (C) are shown in Figure 3-4. Aligned scaffolds induced elongation of healthy tendon

fibroblasts compared to cells seeded on TCP. This effect was less profound on tendon fibroblasts seeded on random electrospun fibre scaffolds.

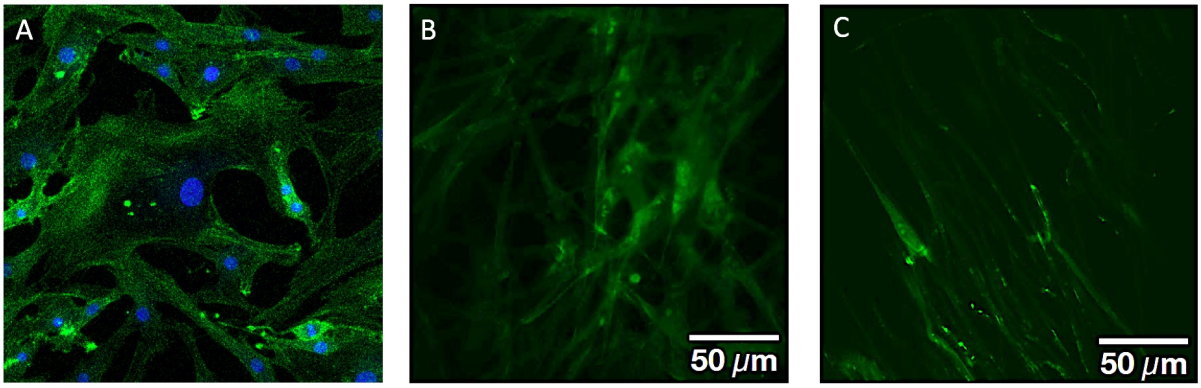


Figure 3-4. Aligned electrospun scaffolds promote an elongated morphology more than random scaffolds and TCP after 7 days culture.

Representative confocal images of healthy tendon fibroblasts cultured on tissue culture plastic (A), random (B) and aligned (A) electrospun scaffolds after 7 days. Cells on TCP adopt a flattened morphology not seen in native tissue in health or disease. Aligned scaffolds promote fibroblast elongation as seen in tendon. Random scaffolds do not induce these same cell shape changes. (Blue = DAPI nuclear stain, green = phalloidin actin stain, scale bar = 50μm)

3.6.1.5 Tendon fibroblast gene expression

Scaffold fibre alignment induced differences in the expression of tendon matrix related genes after 7 days of culture. These differences are shown as the fold change in expression from 24 hours, following 7 days culture on random and aligned scaffolds for tendon fibroblasts in Figure 3-5. *COL3A1, ACAN, DCN* and *TNC* gene expression was increased on both random and aligned fibres, whilst *SCX* expression was decreased. Random scaffolds reduced *COL1A1* and *COL5A1* expression while these were upregulated on aligned fibres. This data shows that there were also differences in the magnitudes of response between scaffold types. However, none of these differences in magnitude were statistically significant.

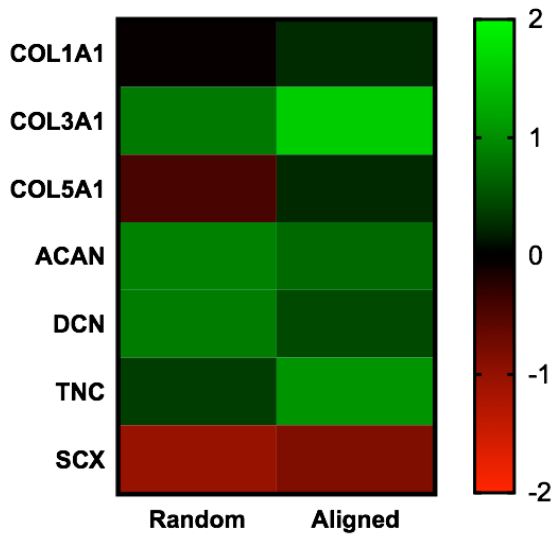


Figure 3-5. Fold change in gene expression differs for tendon fibroblasts cultured on random and aligned electrospun fibres for 7 days.

This heat map shows the differences in gene expression dependent on scaffold fibre alignment. Change in gene expression occurred in the same direction (up or down regulation) in 5 of the selected genes and was opposite for 2 genes (*COL1A1* and *COL5A1*). Mean fold change in expression from 24 hours, following 7 days culture for each condition, log10 scale.

3.6.2 Effects of fibre diameter on tendon fibroblasts derived from healthy and diseased tendon

Fibre diameter was next investigated to determine if this biophysical parameter, specifically biomimetic fibre sizes (300nm and 4000nm), could induce differential tendon fibroblast responses. This experiment was performed in triplicate for tendon fibroblasts derived from both healthy and diseased tendon. Matched repeats were performed in 3 sequential experiments with cells from one healthy and one diseased tendon in each wave as the size of the experiment precluded running the 6 separate experimental repeats at once.

3.6.2.1 Scaffold analysis

The fibre diameters and fibre alignments of the 3 scaffolds for each scaffold type used in this experiment are shown in Figure 3-6. Within each scaffold type (referred to as 300nm, 1000nm, 2000nm and 4000nm) there were no statistically significant differences in mean diameter (A)

or alignment (B). Angular deviation is presented as the mean and the angular deviation in this figure to allow easier appreciation of alignment conservation across scaffold types. Representative images of these scaffolds are included in section 2.6.8, Figure 2-16 (Biomimetic electrospun scaffolds used in *in vitro* experiments).

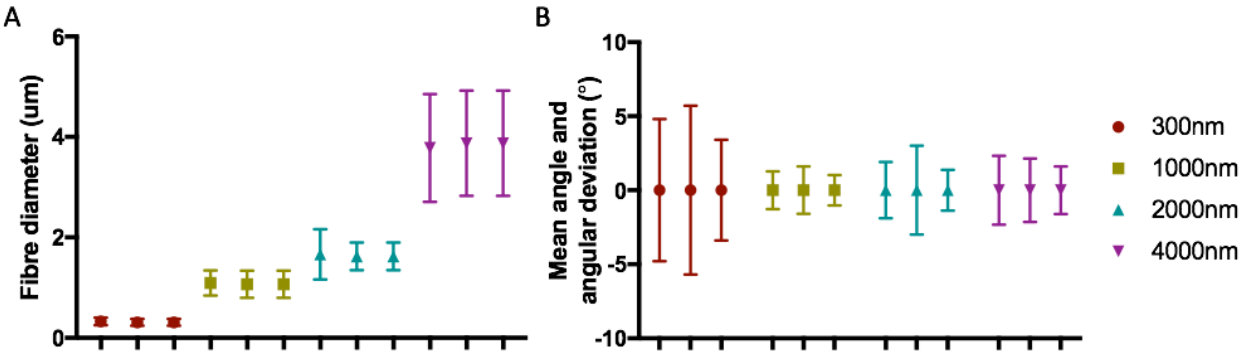


Figure 3-6. Fibre diameter and alignment were conserved across the 3 scaffolds used to assess healthy and diseased tendon fibroblast response to changes in diameter.

Fibre diameter (A, mean and standard deviation) was consistent within each scaffold type. Fibre alignment (B, mean angle and angular deviation) was also consistent within each scaffold with Rayleigh's test for tendency to uniformity revealing R values all greater than 0.9 for 1000, 2000 and 4000nm scaffolds and >0.85 for 300nm scaffolds, the cut off used to determine alignment in this thesis.

3.6.2.2 Fibroblasts from diseased tendon show reduced attachment to electrospun scaffolds

Fibroblasts from healthy compared to diseased tendon displayed altered attachment at 24 hours after seeding (Figure 3-7). When attachment data for all 4 different diameter electrospun scaffolds is considered together, healthy tendon fibroblasts from healthy tendon showed a 72% attachment rate whilst those from diseased tendon showed a 41% attachment ($p<0.0001$). However, when considering the effects of diameter on fibroblasts from healthy and diseased tendon, there were no statistically significant differences and attachment was not dependent on fibre diameter over the range tested.

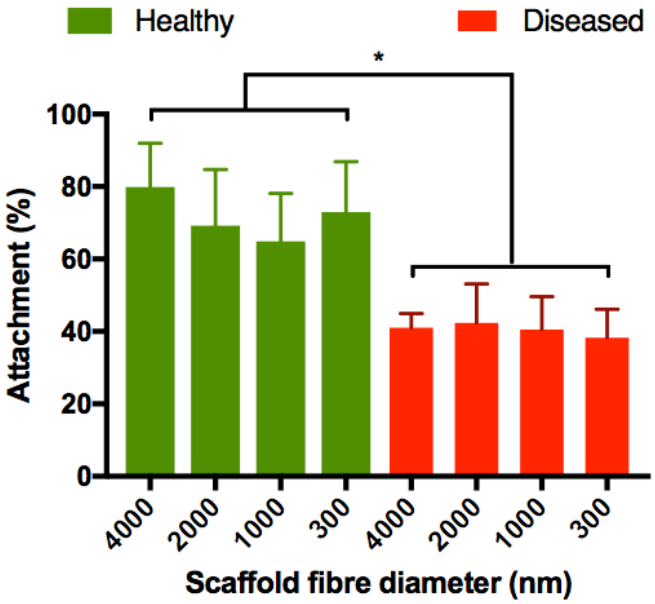


Figure 3-7. Attachment to electrospun scaffolds is dependent on fibroblast disease phenotype but not fibre diameter.

Tendon fibroblasts from healthy tendon were more adherent to electrospun fibre scaffolds than tendon fibroblasts from diseased tendon ($p<0.0001$). Within each cell phenotype, electrospun fibre diameter did not statistically affect attachment. This graph shows the mean and standard deviation calculated relative to the respective cell types seeded on TCP.

3.6.2.3 Fibroblasts from diseased tendon show increased metabolic activity compared to those from healthy tendon

Fibroblasts from both healthy tendon and diseased tendon displayed a sustained increase in metabolic activity over the 21 day culture period as shown in Figure 3-8. When diameters are considered together, fibroblasts from diseased tendon exhibited a significantly greater increase (4.55 fold compared to baseline) in metabolic activity than fibroblasts from healthy tissue (1.97 fold). These differences were apparent throughout the entire culture period reaching significance at day 14 ($p<0.05$) and continuing at day 17 ($p<0.001$) and day 21 ($p<0.001$). There was more variation in the diseased fibroblast response than observed in healthy fibroblast responses. This increased metabolic activity and greater variation were also

seen in fibroblasts from diseased tendon compared to healthy tendon when cultured on TCP (Appendix B.2, Figure B-1).

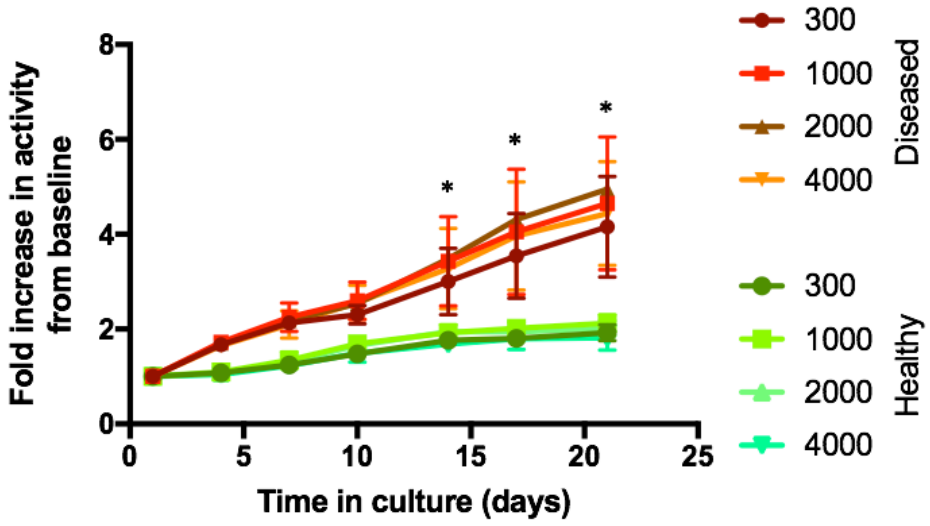


Figure 3-8. Metabolic activity increased significantly over 21 days culture for fibroblasts derived from diseased tendon compared to healthy tendon on electrospun scaffolds irrespective of fibre diameter.

Fibroblasts from diseased tendon exhibited significantly greater increases in metabolic activity than tendon fibroblasts from healthy tendon across the range of electrospun fibre diameters tested (300nm, 1000nm, 2000nm and 4000nm). Within both phenotypes, no significant differences were induced by different electrospun fibre diameters over the tested range. Diseased tendon fibroblasts however had much greater variation in their response. Mean fold increase in fluorescence and standard deviation from baseline.

3.6.2.4 Fibroblast morphology is dependent upon electrospun fibre diameter

Culture of healthy and diseased tendon fibroblasts on electrospun fibres induced an elongated morphology as shown in Figure 3-9. When assessed across all electrospun scaffolds, healthy tendon fibroblasts displayed a slightly higher degree of elongation than diseased tendon fibroblasts. There was an insignificant trend to increasing elongation with increasing diameter from 1000nm to 4000nm in tendon fibroblasts from healthy tissue. The 300nm scaffold did not follow this trend, potentially because of the cross linking and branched morphology interfering with cell shape adoption.

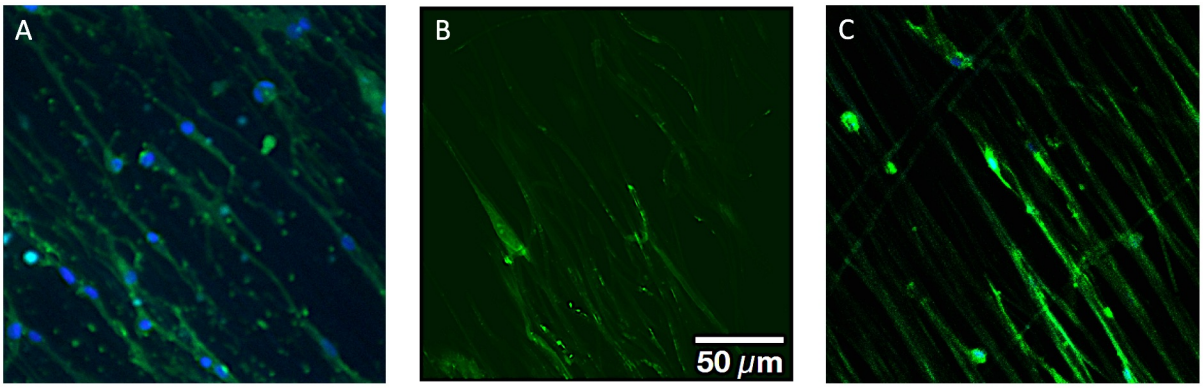


Figure 3-9. Morphology of fibroblasts from healthy tendon after 14 days culture on electrospun fibre scaffolds of 300nm, 1000nm and 4000nm diameters.

Tendon fibroblasts adopted an elongated morphology on electrospun scaffolds of 300nm (A), 1000nm (B) and 4000nm (C). This elongation was greatest on 4000nm scaffolds. The morphology on the 300nm scaffold revealed more irregular cell shapes potentially reflecting the branching fibres. (Blue = DAPI nuclear stain, green = phalloidin actin stain, scale bar = 50μm)

3.6.2.5 Fibroblasts from diseased and healthy tendons show differential gene expression responses to electrospun scaffolds

The effect of scaffold diameter on gene expression was determined by the fold change in expression for each cell population from 24 hours following 14 days culture on the different diameter scaffolds. The effect of scaffold diameter on gene expression was examined using a panel of genes representing tendon matrix, inflammation and resolution, and angiogenesis markers.

The gene expression responses of healthy and diseased fibroblasts across the 4 scaffolds are pooled together for comparison in Figure 3-10. Five genes (*COL5A1, ACAN, IL6, HIF1A* and *PDPN*) showed opposing gene expression responses between the disease states. *COL5A1* expression was increased in fibroblasts from diseased tendon in response to electrospun scaffolds whilst it was decreased in fibroblasts from healthy tendon. *ACAN, IL6, HIF1A* and *PDPN* expression was decreased in fibroblasts from diseased tendons and increased in those

from healthy tendons. Within the other genes assessed, the direction of the gene expression response was consistent but the magnitude of this change differed. These gene expression changes in fibroblasts from healthy versus diseased tendons in response to electrospun fibre diameters did not reach statistical significance. A similar differential response was also noted between responses of fibroblasts from healthy and diseased tendon to TCP (Appendix B.3, Figure B-2), re-enforcing the importance of cell phenotype in driving cell response to biomaterials.

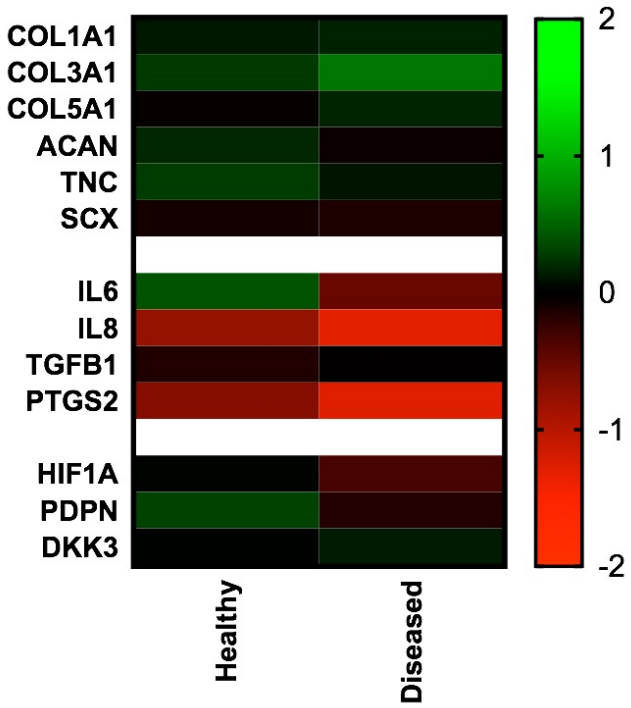


Figure 3-10. Fold change in gene expression for tendon fibroblasts after 14 days culture on electrospun scaffolds is different for fibroblasts derived from healthy compared to diseased tendon.

Tendon fibroblasts from healthy and diseased tendon do not exhibit the same gene expression responses to the same biophysical stimuli provided by electrospun fibres (A) or TCP (B). Mean fold change in expression from 24 hours, following 14 days culture for each cell population on electrospun scaffolds, log10 scale.

Within disease states, electrospun fibre diameter did not consistently regulate expression of the genes analysed. This is shown in Figure 3-11 where the average change is almost equal for each gene across the 4 diameters of both healthy (A) and diseased fibroblasts (B).

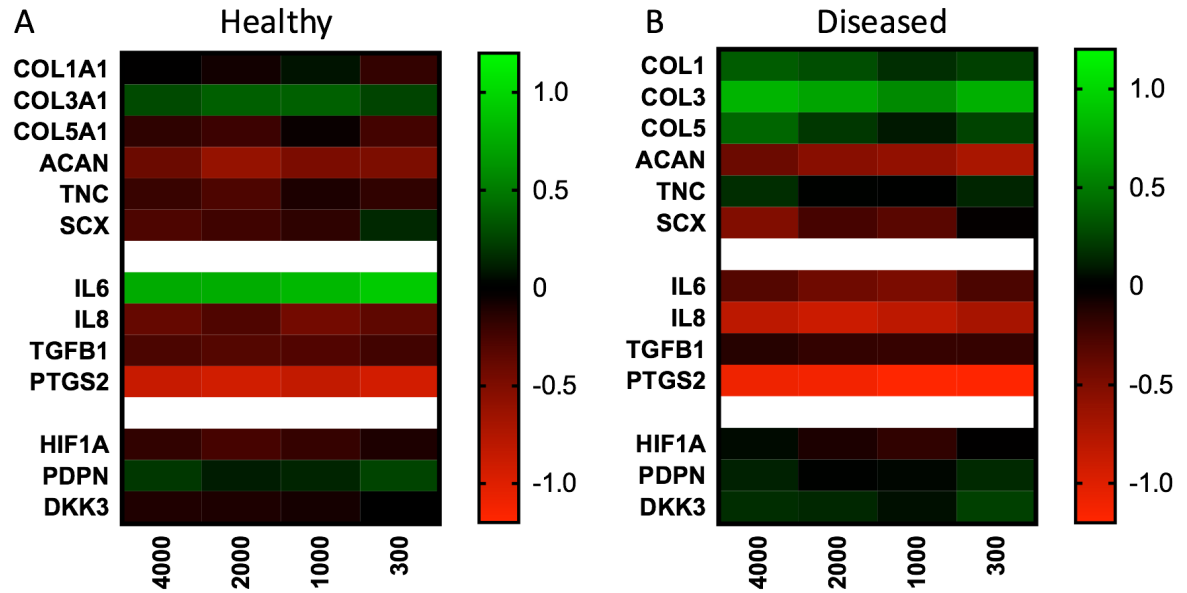


Figure 3-11. Fold change in gene expression changes after 14 days for healthy and diseased tendon fibroblasts cultured on electrospun fibres of different diameters.

Gene expression changes of healthy (A) and diseased (B) fibroblasts cultured on electrospun scaffolds of different diameters. Within disease populations, fold changes in gene expression were congruent and not significantly different. Mean fold change in expression from 24 hours, following 14 days culture for each cell population on different diameter electrospun scaffolds, log10 scale.

The expression profile of *IL6* (Figure 3-12) is shown as a representative example to further illustrate these findings. Firstly, the time course shows that maximal fold changes were reached at 14 days of culture in tendon fibroblasts from both healthy (blues) and diseased tendon (reds). Secondly, the consistent difference in response to the same biophysical stimuli is evident between fibroblasts from healthy and diseased tendon. This data also shows that whilst response to fibre diameters is not significantly different, there may be more subtle effects. The same graphs are provided as Appendix B.4, Figure B-3 for the entire tendon fibroblast gene expression panel.

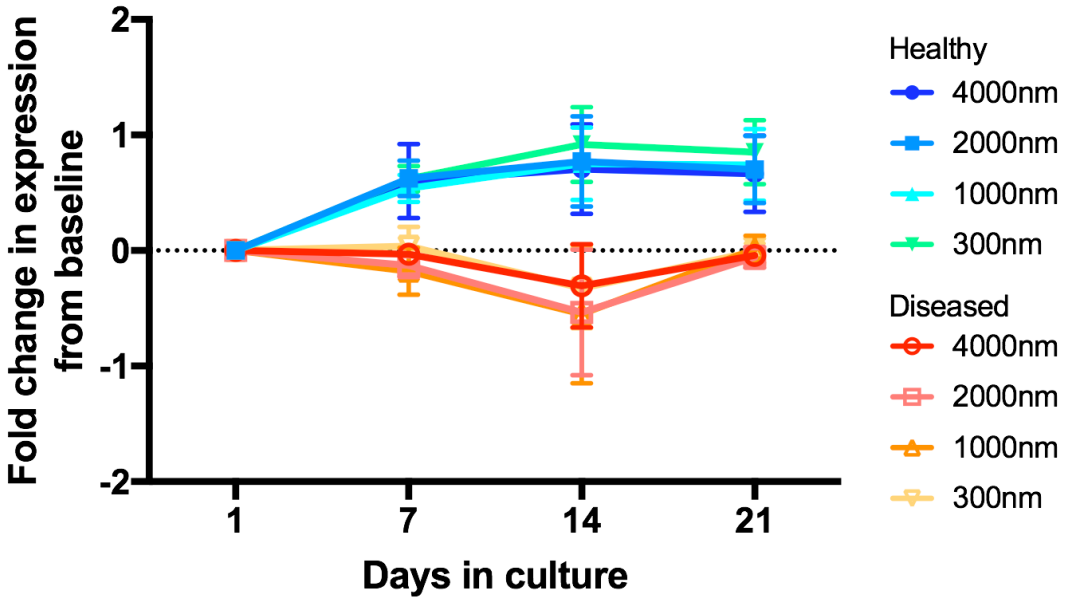


Figure 3-12. *IL6* fold change in expression for tendon fibroblasts derived from healthy versus diseased tendon over 21 days culture on different diameter electrospun scaffolds.

Maximal upregulation and down regulation of *IL6* is seen at day 14, irrespective of cell phenotype and fibre diameter. This plot also highlights the discordance between fibroblasts isolated from healthy and diseased tendon. Mean fold change, and standard deviation, in expression from 24 hours for each cell population at various time points following culture on electrospun scaffolds of different diameters, log10 scale.

To ascertain whether differential attachment of fibroblasts from healthy versus diseased tendons was driven by altered cell-surface proteins, integrin gene expression for each cell disease state was assessed after 14 days culture across the 4 tested diameters. There was also no difference in gene expression change dependent on cell disease state or across this range of fibre diameters. However, changes in integrin expression over this time period would not cover the cell attachment period which occurs within 24 hours of seeding.

To examine changes over a more appropriate time point, a repeat experiment was completed with cells harvested at the time of seeding (0 hours), and seeded cells cultured for 24 hours on 1000nm electrospun fibres. This showed large changes in integrin expression from the time of seeding (up to 10 fold reduction in IA2) in response to electrospun fibres for both healthy and

diseased fibroblasts. However, the pattern of integrin and cell adhesion expression between healthy and diseased fibroblast response was similar (Figure 3-12).

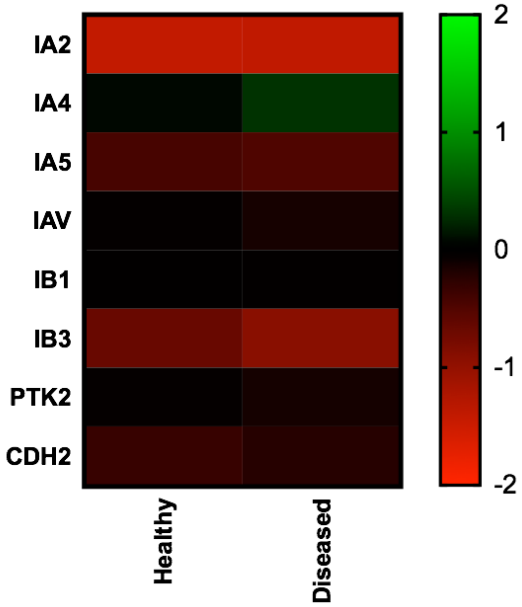


Figure 3-13. Fold changes in the expression of selected cell attachment genes was similar for healthy and diseased fibroblasts cultured on electrospun scaffolds for 24 hours.

Healthy and diseased fibroblast cell attachment gene expression profiles show similar patterns after culture on electrospun scaffolds for 24 hours. Mean change in expression at 24 hours compared to cells at the time of lifting (0 hours) for each cell phenotype, log10 scale.

3.6.3 Effects of fibre diameter on PBMCs

3.6.3.1 Scaffold analysis

The fibre diameters and alignments of the scaffolds utilised for PBMC attachment and gene expression studies are shown in Table 3-4. Each scaffold had the targeted fibre diameter and alignment.

Table 3-4. Summary statistics of the fibre diameter and alignment of the electrospun scaffolds used to assess PBMC responses to electrospun scaffolds.

	300nm	1000nm	2000nm	4000nm
n	37	31	33	31
Mean diameter (um)	0.325	1.02	2.04	4.45
Standard deviation (um)	0.066	0.16	0.26	0.47
Rayleigh's R	0.9021	0.9393	0.9362	0.9204
Fibre angular deviation (°)	5.0	3.2	3.3	4

3.6.3.2 PBMC Gene expression

PBMC gene expression in response to different electrospun fibre diameters was assessed at 4 and 24 hours. This revealed an upregulation in the expression of 7 of the 9 selected inflammatory genes (*TNFA, IL1B, IL6, IL8, IL10, IL12B,* and *CD206*) compared to cells prior to seeding (t=0 hours). TGFB expression remained relatively stable and PTGS2 expression was markedly reduced. This pattern of response was consistent over the 4 diameters tested with no significant differences between the fibre diameters at 4 hours (data not shown) or 24 hours. The 4 and 24 hour time points were selected for two reasons. Firstly, pilot data had shown that 4 hours incubation was a threshold for PBMC attachment to supply sufficient mRNA for gene expression analysis. The 24 hour time point was selected as this experiment was designed to examine the initial PBMC response. This has been linked to long term biomaterial outcomes with future work intended to examine more detailed characteristics of monocyte differentiation and macrophage polarisation.

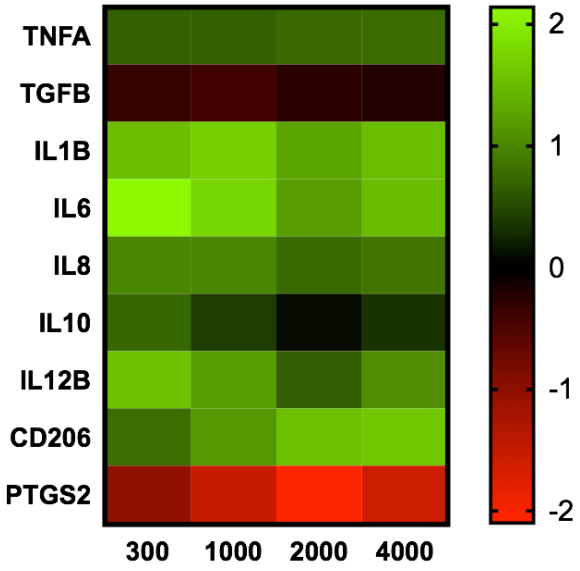


Figure 3-14. Fold change in inflammatory gene expression was not significantly influenced by diameter for PBMCs seeded on electrospun scaffolds for 24 hours.

The fold change in PBMC inflammatory gene expression at 24 hours compared to baseline was not influenced by electrospun fibre diameter. Mean fold change in expression following 24 hours culture compared to the time of seeding, log 10 scale.

3.6.3.3 Flow cytometry

Targeting PBMC responses to implanted electrospun materials could open the potential for biomaterials to adopt an immunomodulatory role in addition to supporting tendon fibroblasts. Accordingly, identification of PBMC sub populations could give insights into which populations are more adherent and govern the interaction with implanted electrospun fibres.

Flow cytometry of scaffold-adherent PBMCs demonstrated diameter dependent effects on the proportion of key PBMC populations. Representative gating strategies are shown in Figure 3-14. The PBMC populations were first sorted to select live single cells only (A-C). These cells (D) were divided based on CD3+ expression. CD3+ cells were divided into populations based on CD4 (T Helper cell), CD8 (Cytotoxic T cell) (E) and TCR GD expression (Gamma delta T

cells) (F). CD3- cells were split into CD14+ cells (monocytes) (G) and CD56+ cells (NK cells) (H).

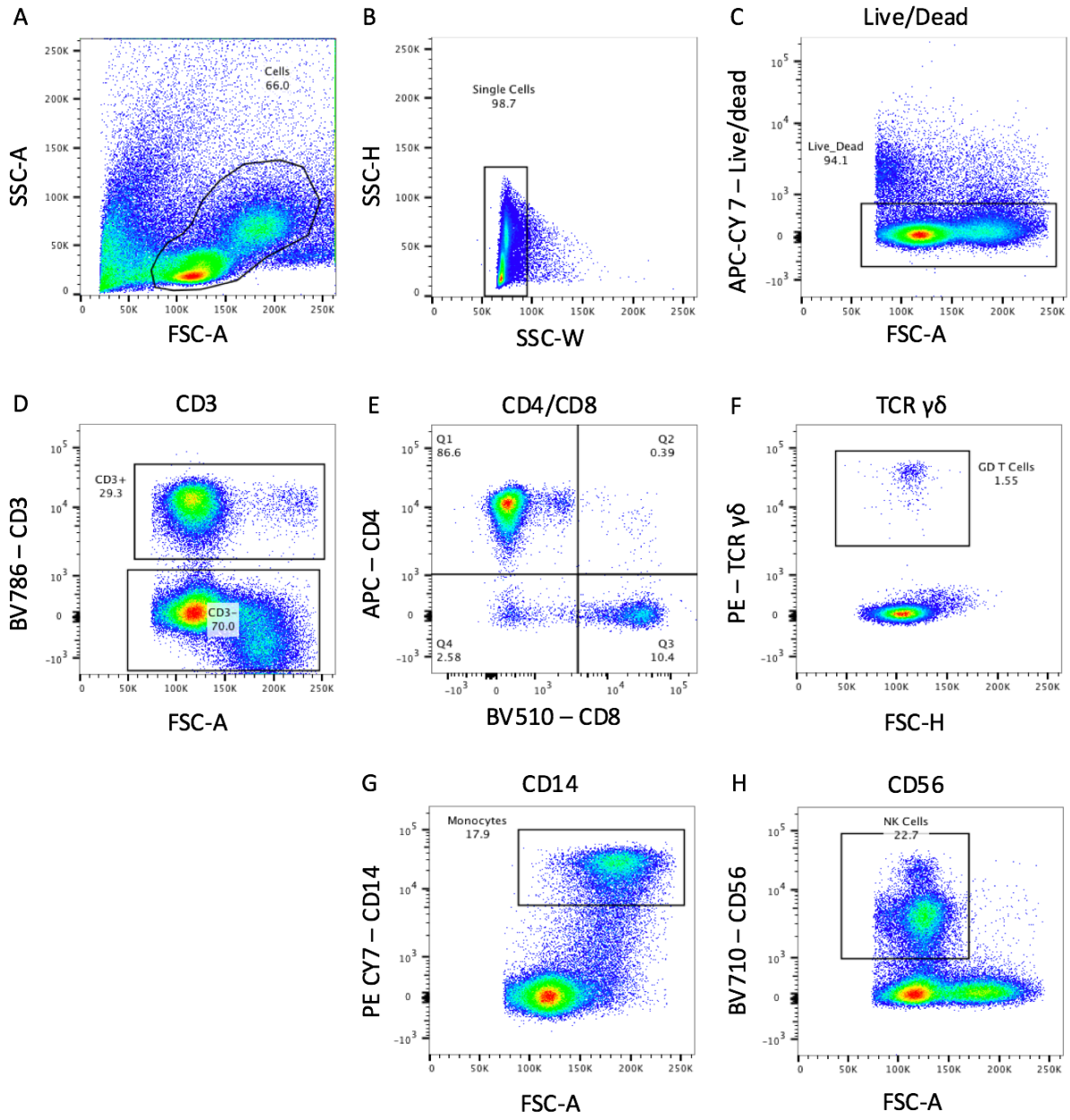


Figure 3-15. PBMC flow cytometry gating strategy.

These representative plots show the gating strategy used to identify immune cell populations of interest after culture on electrospun scaffolds. Gating was informed by isotype controls. Cell population selection (A), single cell selection (B), live cell selection (C). This live, single cell population was split based on CD3 expression (D). CD3+ cells were further analysed to show CD4/CD8 expression (E) and GD T cells (F). CD3- cells were then split based on CD14 expression (G) and CD56 expression (H).

This analysis showed notable changes in the populations of adherent PBMCs in response to the different diameter electrospun scaffolds. Firstly, the results grouped based on diameter. The 300nm and 1000nm responses were congruent, as were the 2000nm and 4000nm scaffold responses were also congruent. Secondly, these changes increased in magnitude over time from the 4 hour to the 24 hour time point.

Specifically, relative to cells in TCP, the proportion of CD3+ cells on 300 and 1000nm scaffolds increased and the proportion of CD3+ cells on 2000nm and 4000nm scaffolds decreased significantly (Figure 3-15A) at 4 and 24 hours. The proportion of CD4+ cells dropped on all diameter scaffolds compared to control cells (Figure 3-15B) at 4 and 24 hours. The proportion of CD4-/CD8- cells increased initially on all scaffolds (4 hours), but at 24 hours this was only maintained on 2000nm and 4000nm scaffolds (Figure 3-15C). The proportion of CD14+ monocytes increased greatly on only the 2000nm and 4000nm scaffolds compared to control cells and the 300nm and 1000nm scaffolds (Figure 3-15E). The proportion of NK cells dropped over all electrospun scaffolds compared to control PBMC populations, however this was greater in the 2000nm and 4000nm scaffolds than the 300nm and 1000nm scaffolds (Figure 3-15F). Restrictions in biological fluid prevented 3 repeats for each condition and each time point to allow for formal statistical testing of significance.

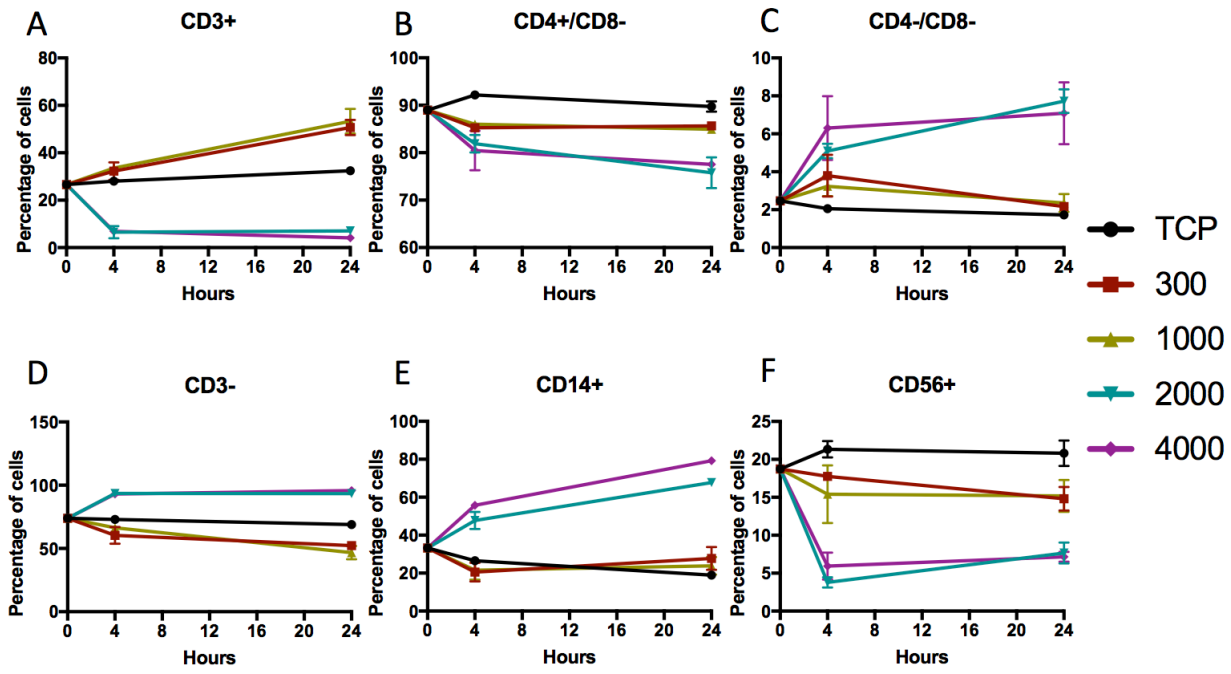


Figure 3-16. Graphs of selected PBMC populations showing fibre diameter dependent cell attachment of PBMCs over 24 hours.

Changes in CD3+ cell populations (A) after culture on electrospun scaffolds of different diameters and the CD4+/CD8- (B) and CD4-/CD8- (C) proportion of the CD3+ cells. The change in proportion of CD3- (D) PBMCs and the proportions of CD14+ cells (E) and CD56+ cells (F) are shown below. CD3 used for T cell identification, CD4 for T Helper cell identification, CD8 for Cytotoxic T cell identification, CD14 for monocyte identification, CD56 for NK identification.

3.7 Discussion

This chapter aims to investigate the effect of fibre alignment on healthy tendon fibroblasts, compare the effect of fibre diameter on tendon fibroblasts from healthy and diseased tissue and investigate the effect of fibre diameter on peripheral blood mononuclear cells. There were 3 main findings from this work. Firstly, different cell lineages, PBMCs and tendon fibroblasts, display altered sensitivities to the same changes in fibre diameter. Secondly, with tendon fibroblasts, disease phenotype governs the response to altered fibre diameter. Thirdly, fibre diameter effects were able to significantly modulate PBMC biology but tendon fibroblasts, particularly when isolated from healthy tendon, were relatively inert.

3.7.1 Fibre alignment supports tendon fibroblast proliferation, morphology and matrix gene expression

The effects of fibre alignment were assessed on tendon fibroblasts from healthy tendon using a random scaffold and an aligned scaffold. The difference in alignment was marked, however, a mean fibre diameter of 1000nm was conserved across these scaffolds. These scaffolds were deliberately fabricated using the same solution with as few adjustments in electrospinning parameters as possible (only collector speed and flow rate). This was to minimise any unintended differences in other biophysical properties, including hydrophobicity, charge, local mechanical properties, scaffold porosity and scaffold pore size.

Unintended effects on these biophysical properties, particularly hydrophobicity and charge, can affect cell response and the protein corona. This is reviewed in detail in chapter 4. Altered concentrations and conformations of proteins in the corona may then drive biological responses, in addition to those induced from altered fibre alignment. Whilst discussed in more detail in the next chapter, mass spectrometry data showed there were no significant differences in relative abundance of any of the over 800 proteins adsorbed to 1000nm random and aligned electrospun scaffolds following incubation in human serum. However, the mass spectrometry techniques used cannot establish if the protein conformations were altered. Hence, it is likely that individual protein concentrations in the protein corona on the scaffolds used in this experiment were also consistent, even if functionalised with FBS not the human serum the mass spectrometry experiments were performed on. Thus, the observed results are likely attributable to the effect of fibre alignment rather than protein adsorption.

Fibre alignment did not have a significant impact on healthy fibroblast attachment. As the AlamarBlue assay is an assay of metabolic activity and cell viability, and does not directly count cell number, there are caveats to this assessment. The premise of this thesis is that electrospun fibres create a biomaterial niche that directly influences cell biology. As the

control population was seeded on TCP, a surface designed for maximal cell attachment, the metabolic activity of fibroblasts may be relatively up or down regulated due to differences in the material surfaces. However, the main question of this experiment was to compare the attachment to random and aligned scaffolds, not comparison of these scaffolds to TCP. Any up or down regulation of fibroblast metabolic activity would have been similar on both electrospun scaffolds suggesting a genuine lack of difference in attachment rate to these scaffolds.

The same AlamarBlue assay was used to assess changes in metabolic activity longitudinally for 7 days as a proxy of proliferation. Aligned scaffolds promoted a more pronounced increase in metabolic activity than random fibre scaffolds, reaching statistical significance after 7 days. Future work should quantify fibroblast numbers using microscopy or another technique.

The change in metabolic activity observed over the entire 7 day culture period also has inferences for the cell attachment results discussed previously. Over the 7 day culture period, the maximal absolute change in fluorescence for cells cultured on electrospun fibres compared to TCP was 20%. In the attachment analysis after a 2 hour period, a 40% reduction in fluorescence was observed in both aligned and random scaffolds for the same fibroblasts seeded on the same scaffolds. This much greater change in fluorescence over only 2 hours suggests that the reduction in fluorescence in these attachment experiments reflects a reduction in cell number, not a hyper acute change in cell metabolic activity.

Interpretation of cell number results must be considered within the context of rotator cuff repair. One of the characteristics of tendinopathic tissue is hyper-cellularity. It may be that scaffolds that can reduce fibroblast proliferation are preferable for the deposition of ECM more representative of healthy tendon. Presently, there is no available literature linking *in vitro* tendon fibroblast proliferation with clinical outcomes. There is some evidence, however, that cell invasion throughout the thickness of the scaffold is important for tissue formation,

with *in vitro* invasion correlating with improved tissue mechanical properties for biomaterials implanted in animal models [210,211]. In the context of this experiment, increasing cell number on scaffolds over time may suggest increased invasion of tendon fibroblasts into the scaffold.

Using microscopy to assess cell invasion may be a useful biomaterial metric. Whilst, confocal microscopy allows calculations of exact cell numbers, in addition to cell morphological changes (as shown in this thesis,) it is time consuming and expensive. Accordingly, protocols were developed in pilot experiments for spinning-disc microscopy to enable such analysis in the future. Scaffold thickness variation and inconsistent Z-axis positioning with cell crowns limits full automation and high throughput analysis. Variable scaffold staining also affects automated image analysis. Despite these restrictions, for future experiments spinning disc microscopy could allow accurate cell counts, in addition to the assessment of cell invasion and cell morphology on a scale to generate meaningful statistical analysis.

Gene expression changes of healthy and diseased tendon fibroblasts showed some potential benefits of aligned electrospun scaffolds compared to random fibre scaffolds. Specifically aligned scaffolds lead to upregulation of *COL1A1*, *COL3A1* and *COL5A1* gene expression, all important markers of tendon matrix deposition. Aligned fibre scaffolds also lead to lower upregulation of *ACAN* and *DCN* expression. One of the molecular features of diseased tendon matrix is increased proteoglycan content. These trends were not statistically significant and the differences in fold changes are relatively low. However, this was a short time course of 7 days. Given these gene expression changes on aligned fibres suggest improved matrix quality, consistent with the literature [140,236,242], further exploration of aligned scaffold effects on tendon fibroblasts is warranted.

Fibre alignment was not evaluated in tendon fibroblasts derived from diseased tissue as following the principles of biomimicry and results in this experiment, it is unlikely random fibres would assist in improving diseased fibroblast response. Formally characterising the

response of fibroblasts from diseased tendon to alignment and comparison with the observed healthy fibroblast responses, could however re-enforce the notion of disease phenotype dependent biomaterial responses. If future work is conducted in this area, using a range of alignments could be an interesting way to strengthen our understanding of alignment effects. Such work could elucidate whether there is a dose-response to increasing alignment or if changes in biological response are threshold dependent.

3.7.2 Tendon fibroblast response to electrospun fibre diameter is more dependent on disease phenotype than fibre diameter

This thesis is primarily interested in influencing the biology of diseased tendon fibroblasts to improve rotator cuff tear repair outcomes. However healthy fibroblast samples are more abundant and often used for biomaterial analysis. Critically, this experiment shows that tendon fibroblasts from diseased tissue display different responses to fibre alignment compared with fibroblasts from healthy tendon. Furthermore, these results show that fibroblasts from healthy tendon are relatively inert, making evaluation of responses to biomaterials more challenging.

There was no statistically significant difference between the batches of scaffolds produced for these experiments. However, one issue relating to these scaffolds, was the slightly lower mean diameter of the 2000nm scaffold than what was intended due to equipment challenges. The mean diameter was only 1700nm. However, one third of the experiment had been completed at the time of discovery and the decision taken to continue with the reduced diameter. The mean diameter (1700nm) was statistically significantly different to the 1000nm scaffolds used (1000nm). However, it is unknown if this difference would also be of biological significance. Consideration was given to pooling the 1000nm and 2000nm scaffolds together as a single scaffold type as the distributions did overlap, however the mean difference was 700nm, significantly greater than the 35nm threshold which fibroblasts react to [252], potentially leading

to different responses. Furthermore, the 1000nm and 2000nm scaffolds were not targeting specific native collagen structure diameters like the 300nm (fibrils) and 4000nm (fibres) scaffolds. Accordingly, being slightly under 2000nm did not result in the scaffold failing to replicate a targeted biological structure.

The most interesting results of these experiments were the differences observed between tendon fibroblasts derived from healthy and diseased tendon in response to the same changes in fibre diameter. These fibroblast populations showed different attachment rates, changes in metabolic activity, changes in cell morphology and changes in gene expression to the same electrospun scaffolds depending on disease state. Re-enforcing this differential response, fibroblasts from healthy and diseased tendon also exhibited altered responses to TCP for these same metrics.

This work shows that rotator cuff tendon fibroblasts from diseased tendon respond differently when compared with tendon fibroblasts from healthy hamstring cultured on the same biomaterial stimuli. Therefore, using healthy tendon fibroblasts to assess biomaterials for potential implantation will not give researchers the most accurate prediction of *in vivo* response for biomaterials used in rotator cuff tears.

Admittedly, there are differences between the cell types in addition to disease state, which may account for some of the observed variance. These include donor age and the site of origin. Tendon fibroblasts from healthy tendon were isolated from patients with an average age over 40 years younger. They have also come from hamstring tendon, not rotator cuff tendon. Interestingly, fibroblasts from diseased tendon showed greater variation in response between patients than the healthy fibroblasts, giving weight to a spectrum of disease existing within rotator cuff tears.

The healthy cells used in this experiment showed similar attachment rates (70%) to the healthy cells seeded in the fibre alignment experiment (63%) discussed in section 3.7.1 (Fibre

alignment supports tendon fibroblast proliferation, morphology and matrix gene expression). Fibroblasts from diseased tendon again showed significantly lower attachment rates (40%). The reasons for this reduced attachment are not clear. The fold changes in integrin expression between fibroblasts from diseased and healthy tendon were not notably different, however, mRNA expression does not correlate with protein levels. More functional analysis of the differences in the adhesome of healthy and diseased fibroblasts may reveal changes in protein expression and pathway function related to cell attachment.

Another potential reason for reduced adhesion is the altered cytoskeletal function of diseased fibroblasts. Diseased fibroblasts are less dynamic and exhibit different morphologies than healthy cells, as discussed later and as shown in the literature [289]. Fibroblasts need to form sufficient adhesion contacts to survive. Therefore, reduced cytoskeletal mechanics may reduce the area diseased cell filopodia can explore to establish focal adhesions to scaffolds over the attachment period, with media addition potentially washing off non or less adherent fibroblasts. This ability to attach may be influenced by disease chronicity or severity. As has been shown in cancer metastasis research, increasing mutations lead to cancer cells that are no-longer anchorage dependent for survival.

This lower attachment has implications for biomaterials research. Biomaterials aim to increase tendon fibroblast attachment and invasion through the depth of the scaffold, testing in healthy cells may suggest a biomaterial does encourage cell attachment. In reality however, diseased fibroblasts may not demonstrate the same attachment profile to this material and altering surface biophysical properties may be beneficial to improve this. Future research should investigate this further.

If only 40% of diseased fibroblasts are attaching to scaffolds, there is a significant proportion that must be non-adherent or washed off more easily. These cells could be collected in the flow through left in the original TCP wells. Characterising the differences between the

adherent and non-adherent fibroblast populations may reveal insights about fibroblast sub populations. These sub populations may have different roles to play in biomaterial outcome. Furthermore, selection of this population *in vitro* may bias longitudinal experiments, not resembling the whole population of tendon fibroblasts which will interact with the biomaterial *in vivo*.

Longitudinal change in metabolic activity again revealed differences in the diseased and healthy tendon fibroblast response. Diseased cells showed a nearly 5 fold increase in activity from baseline compared to the 2 fold increase in activity of healthy fibroblasts. This difference likely reflects the underlying cell biology. Healthy cells are a relatively dormant cell population, slowly turning over tendon matrix. Tendinopathic tissue is characterised by hypercellularity, increased proliferation rates and increased matrix turnover.

If we are trying to reprogram diseased cells towards a healthy phenotype, then a reduction in increase in metabolic activity may be advantageous. However, within diseased cells, electrospun fibre diameter did not have a significant effect or suggest a strong effect of fibre diameter on metabolic activity. This was also true for healthy fibroblasts. These results contrast with findings reported in the literature where lower fibre diameters increased healthy fibroblast proliferation [140]. This may be due to the outputs assessed. This thesis has used a metabolic activity assay as a surrogate for proliferation compared to the nucleic acid quantification through a PicoGreen assay used by Erisken et al.

Assessment of morphology was consistent with previous research showing relatively truncated diseased fibroblast morphology compared to healthy fibroblasts over the fibre diameter range evaluated [289]. There were however suggestions of a diameter dependent response to cell shape consistent with previous research [239]. Higher fibre diameters elicited more elongated morphologies in both healthy and diseased fibroblasts. However, the number of measurements in this assessment are low, limiting potential inferences and detection of

more subtle differences. As previously outlined, high throughput microscopy techniques could improve the sensitivity for detecting changes in cell shape, cell invasion and cell number. However, future work should first ensure cell morphology is a useful metric to correlate *in vitro* outcomes with *in vivo* results and clinical outcomes.

The gene expression data displays a similar pattern to that discussed in the sections relating to attachment and proliferation. Specifically, marked differences between healthy and diseased responses but no notable differences within the responses of these cell types seeded over different fibre diameter scaffolds. As previously mentioned, the disease state dependent gene expression response has implications for *in vitro* biomaterial assessment, where using cells from diseased tissue may give more accurate information on subsequent host responses and outcomes. The data presented in the results section of this thesis is the fold change in gene expression after 14 days culture. Similar results were observed after 7 and 21 days. The fold changes seemed to peak in magnitude at day 14 before plateauing and decreasing. This is consistent with research from within the group and may be a function of fibroblasts taking some time to react and develop to a mature final phenotype before losing phenotype or being influenced by other cells when reaching confluence over the scaffold surfaces at longer time points.

One important limitation in the gene expression data of this experiment is that the baseline values were obtained 24 hours after initial seeding. Whilst it may take a period of time to mature to a final phenotype, cell morphology changes occur within hours. If gene expression changes also occur in this initial period, the comparison of subsequent expression to that at 24 hours will not reflect the genuine fold change which may be observed if compared to the cells at the time of lifting or in their native tendon matrix. Using cells at the time of seeding for comparison would likely amplify the evaluation of changes in gene expression. However, this is still a less than ideal comparison, given the phenotypic drift associated with culture on TCP compared to native tissue.

Future research in this area could maximise precious cell and material resources by assessing changes in gene expression at a single time point. This time point would ideally be determined through correlation with *in vivo* outcomes. This is important as within the experimental set up, there is considerable variation in cell response between patients and variation in some degree between the scaffolds. Future research could also utilise microarray or RNAseq technologies. Whilst the genes of interest in this thesis relate to tendon matrix, inflammation and angiogenesis, all key pathways in tissue healing, these may not be the most sensitive to biophysical cues. With the biomaterial response, tendon healing and remodelling extending over months to years, there may be other markers which exhibit responses earlier in this time course for easier *in vitro* assessment. There is a need to identify key markers and metrics for *in vitro* assessment that correlate with *in vivo* responses.

As mentioned in section 3.7.1 (Fibre alignment supports tendon fibroblast proliferation, morphology and matrix gene expression), changes to other biophysical properties may have occurred as a consequence of the altered parameters required to manufacture PDO scaffolds over the targeted diameter range. For the 300nm scaffold, PDO solutions included pyridine. Pyridine has profound effects on electrospinning behaviour as detailed in section 2.6.7 (Pyridine effect on electrospun scaffold fabrication). It is also important to again highlight the increased branching seen in 300nm scaffolds through the introduction of pyridine potentially introduces another variable to influence cell response. Whilst the effect of such branching has not been assessed in the literature, another change in fibre uniformity, beading, has shown considerable effects on fibroblast attachment [139,248]. To generate the 4000nm scaffold, much greater flow rates and PDO concentrations were used than for other scaffolds.

As a result of the different parameter configurations to produce the different scaffolds, surface material properties may be altered, in addition to the fibre diameter changes. It is possible that the different bound corona underlies some of the observed effects. This is discussed in Chapter 4. The differences in the protein coronas between scaffold diameters, does not

interfere with the assessment of disease phenotype affecting cell response. Comparing cell populations over one scaffold diameter controls for the differences in protein corona but still shows tendon fibroblast response is notably different depending on whether tendon fibroblasts were isolated from diseased tendon or healthy tendon.

3.7.3 Electrospun fibre diameter affects PBMC sub-population attachment

This experiment was conducted using aligned scaffolds of varying diameters. As this was separate from the previous experiment examining fibroblast phenotype, the 2000nm scaffold mean fibre diameter is 2040nm. A deliberate decision was made to not include a random scaffold for comparison. However, whilst PBMC responses to aligned fibres are relevant, as aligned fibres seem to be beneficial for the tendon fibroblast response and are likely to compose part of future electrospun biomaterials, the response of PBMCs to random fibre scaffolds could also be important. If random fibres can influence the initial macrophage and immune cell response to instigate a beneficial inflammatory profile, a transient, fast degrading random fibre layer could be incorporated into biomaterial surfaces. This would then give way to the aligned fibres suited for tendon fibroblast invasion and matrix deposition.

Differences in fibre diameter did not elicit notable differences between PBMC gene expression over 4 hours or 24 hours relative to baseline. This is surprising given the flow cytometry results showing significant changes in cell subpopulation proportions. This may be due to cell lifting issues as shown in Appendix B.4 (Accutase lifting efficacy of PBMCs from electrospun scaffolds). Accutase treatment is only lifting half of the adherent PBMCs from scaffolds. The remaining adherent cells would be included on immersion of the scaffolds in trizol and could account for a lack in gene expression difference.

Flow cytometry showed diameter dependent effects in PBMC sub-populations that attached to scaffolds. The 300nm and 1000nm scaffolds induced similar changes in attached PBMC sub-populations and the 2000nm and 4000nm scaffolds also induced consistent differences.

Between these two groupings of scaffolds, there were marked differences to the changes observed in PBMC responses. Again these groupings, suggest the hypothesis about precise biomimetic fibre diameters being more important in governing cell response, is not necessarily true.

The most striking difference detected in flow cytometry was the changed CD14+ monocyte attachment between the two scaffold groupings, with much higher monocyte proportions found on larger diameters. This may reflect that large diameters extend larger surface areas for cells to attach to. However, these are a key cell population in determining the inflammatory response. There were also relatively more CD4-/CD8- cells and less CD4+ T helper cells on larger diameter scaffolds. The role of these cell populations in biomaterial outcomes is not well characterised and warrants further investigation.

The increasing presence of CD14+ monocytes is interesting but needs further analysis to determine biological significance. This research did not attempt to further stratify the macrophage population. Whether, over longer time periods, these adherent monocytes become activated towards macrophages with a more M2-like phenotype consistent with other research [265,291], and are secreting an anti-inflammatory cytokine profile needs assessment. Pooled cell gene expression results did not suggest this had occurred at 24 hours but differentiation is a longer process. Additionally, it is the cross talk between tendon fibroblasts and immune cells reacting to a biomaterial, not a response in isolation that will govern the long term host-material response and tissue outcome.

Another, limitation of this work is the efficacy of Accutase. Flow cytometry can only be performed on the cells which are lifted from the electrospun scaffolds. This research showed that after Accutase treatment, over 30% of the seeded cells remained on the scaffolds. This leaves a significant proportion of PBMCs attached. It is not known if Accutase treatment removes adherent PBMCs in a non-selective manner, or if particular subsets are more

amenable to the action of Accutase. If the more adherent cells are a particular subset, or the cells with stronger interactions are more important in governing the cell-material response, analysis of these populations are critical and may require alternative treatments than Accutase to be studied. Future research should examine these differences in detail.

3.8 Conclusions

This work demonstrates a marked difference between tendon fibroblast response to biophysical stimuli dependent on isolation from diseased rotator cuff tendon or healthy hamstring tendon.

Attachment, proliferation, morphology and gene expression are dependent on the disease state of the tendon from which fibroblasts are isolated. This has implications for biomaterial evaluation. Fine tuning of biomaterials in response to observations made using healthy fibroblasts may have opposite or unwanted effects on diseased tendon fibroblasts upon implantation *in vivo*.

Fibre alignment as a biophysical property induced minor changes in healthy tendon fibroblast biology. Fibre diameter did not induce significant differences in healthy or diseased biology in the metrics used in this thesis. Biomimetic cues from fibre diameter and fibre alignment may not be powerful enough stimuli to assist in reprogramming diseased tendon fibroblast phenotypes sufficiently to influence host-material outcomes. Local mechanical properties remain uncharacterised biophysical stimuli which could influence tendon fibroblast response.

PBMCs showed marked sensitivity to fibre diameter, in contrast to tendon fibroblasts. Sub-population attachment, notably monocytes, to scaffolds was strongly dependent on fibre diameter. Using biophysical cues to target these sub-populations and ultimately the inflammatory response may therefore be a more potent method of influencing tendon healing and improving patient outcomes.

Biomimetic fibre diameters and alignments did not induce more favourable biological changes. In addition, consistent production and minimising fibre variation of PDO scaffolds with mean diameters of 300nm and 4000nm is more challenging than producing mid-range fibre diameters. Given, consistent production capacity is a crucial factor to consider in the development of an ideal biomaterial and the lack of observed biological influence of these harder to achieve diameters, focusing on mid-range fibre scaffolds may be more productive biologically and technically easier.

However, even if biomimetic fibre alignments and diameters have less biological influence on tendon fibroblasts than hypothesised, electrospun scaffolds still hold considerable potential as a biomaterial strategy. The porosity, pore size, potential for surface functionalisation and drug delivery that come with electrospun scaffolds are all conducive to improving cell-material interaction. Manipulating other biophysical properties or functionalising electrospun scaffolds in another way may be able to induce stronger biological changes while also harnessing the benefits of electrospun materials.

What was known	What this adds
Tendon fibroblasts isolated from healthy tendon are responsive to biophysical cues.	Fibroblasts from diseased tendon are also responsive to biophysical cues. The responsive of fibroblasts from diseased tendon to the same biomaterial stimuli is different from the response of fibroblasts from healthy tendon. This differential response has implications for biomaterial design and evaluation.
Fibre diameter and alignment have increased tendon matrix gene and protein expression *in vitro* and *in vivo*.	Electrospun scaffolds with biomimetic diameters and alignments approximating collagen fibrils and collagen fibres did not have a greater biological influence than other scaffold morphologies on tendon fibroblasts derived from healthy or diseased tendon tissue.
Macrophages are receptive to biophysical properties including stiffness, diameter, alignment and topography. Macrophage differentiation and activation can be influenced by biophysical cues. This response to biomaterial stimuli is linked to foreign body responses and long term biomaterial outcomes.	PBMC sub population attachment to electrospun scaffolds is diameter dependent, particularly that of monocytes to larger fibre diameters. Biophysical stimuli could drive the differentiation of these monocytes down macrophage lineages to generate a local response more conducive to tendon healing in a novel immunomodulatory role for electrospun biomaterials

Chapter 4 Functionalisation of electrospun scaffolds through modulation of the adsorbed protein corona

4.1 Abstract

4.1.1 Background

The local response to biomaterial implants will be determined by cell responses to both biochemical and biophysical cues. Optimisation of the biochemical cues through surface protein functionalisation could further modulate cell-biomaterial interactions to improve material outcomes. This chapter examined two aspects of protein adsorption; firstly, how different fibre diameters and alignments affect protein adsorption from serum and secondly, if incubating the same scaffold with different biological fluids altered the protein corona.

4.1.2 Materials and methods

In the first arm of the experiment aligned 300nm, 1000nm, 2000nm and 4000nm diameter scaffolds and a random 1000nm diameter fibre scaffold were incubated in human serum. Secondly, aligned 1000nm scaffolds were treated with matched human blood, serum, plasma and synovial fluid from 3 donors. Protein coronas were isolated and analysed with mass spectrometry. Scaffolds were then seeded with tendon fibroblasts or PBMC populations to assess cell response.

4.1.3 Results

Fibre alignment made no difference to the adsorption of serum proteins to electrospun surfaces. Fibre diameter affected the binding of 11 proteins leading to significantly different intensities over the 4 diameters tested. Treatment with different biological fluids led to differences in over 125 protein species over the same 1000nm, aligned scaffold morphology. Biological fluid functionalisation had significant effects on tendon fibroblast activity and gene expression as well as PBMC gene expression and sub-population attachment.

4.1.4 Conclusions

Changing scaffold diameters results in slightly different corona composition. For the purposes of interpreting cell-material interaction, this means there are biophysical and biochemical differences guiding cell response with diameter changes. These biochemical cues can be significantly manipulated by treatment with different biological fluids to influence tendon fibroblast and PBMC interactions with electrospun biomaterials.

4.2 Introduction

This chapter has two main objectives. The first is to investigate whether changes to fibre alignment and fibre diameter alter the composition of proteins that adsorb on to electrospun scaffolds. The second component is to examine whether the composition and conformation of

this adsorbed protein corona can be deliberately manipulated to create a more biologically supportive adsorbed protein coating.

Biomaterials adsorb a protein layer to their surface immediately upon contact with biological fluids, as discussed in section 1.9.1 (Mechanisms of cell-material interaction) [219,292]. Protein adsorption precedes recruitment and attachment of immune and stromal cells. This protein coating is often referred to as the protein corona or niche. The proteins drawn into this corona and their adopted conformation are influenced by the material surface properties, specifically surface chemistry, hydrophobicity and charge [293]. These underlying properties have not historically been considered in the assessment of electrospun biomaterials despite the significant effects hydrophobicity [131,225,226], charge [233,234] and surface chemistry have on fibroblast attachment as well as protein binding [223] and bound protein conformation [224]. However, the adsorbed protein interface is emerging as an important mechanism for manipulating and improving cell-material interactions for a particular biological need [292].

Chapter 3 highlighted how process and system parameters must be manipulated to create electrospun scaffolds of altered alignment and diameter from the same polymer. These changes may have unintended secondary effects on other important biomaterial properties, including hydrophobicity, charge or roughness. In the context of this thesis, the variable electrospinning parameters used to change fibre alignment or diameter, may have caused such secondary differences, obscuring the true relationship between cell response and the intended biophysical property. To investigate this, the protein coronas of electrospun fibre scaffolds used in this thesis were analysed to determine whether the concentration of individual proteins differed between scaffolds of altered alignment and diameter.

Proteins from blood adsorb to biomaterials when they are surgically implanted. This blood-based corona could be replaced through pre-adsorption in serum, plasma or synovial fluid from the patient, potentially functionalising scaffold surfaces in order to maximise host-

material interaction. Functionalising electrospun fibres surfaces with bioactive molecules is a common theme in the literature [172]. However, inclusion of bioactive molecules into an electrospun scaffold to promote biological activity increases development cost and time as the biomaterial is no longer regulated as a scaffold but as a medical device [120]. Using a patient's own blood or other biological fluid to functionalise a scaffold at the time of surgery avoids this complexity.

Consequently, the second set of experiments in this chapter characterised the differences in protein corona formed through adsorption of different biological fluids and how these changes affected tendon fibroblast and PBMC responses to the same biomaterial. Fluids which are readily available at the time of surgery include blood, blood derivatives and synovial fluid. This thesis will explore the effects of whole blood, serum, plasma and synovial fluid. Given serum and plasma derive from whole blood and differ in proteins relating to coagulation, the protein coronas of these fluid are likely to be more similar to each other, than to synovial fluid. In this experiment, synovial fluid was taken at the time of joint replacement from patients undergoing surgery for osteoarthritic knees. Osteoarthritis has an inflammatory component with synovial fluid shown to have elevated inflammatory cytokines including TNF-α, IL-6, IL-15, IL-17 IL-21 [294-296]. Whilst the nature of inflammation and tissue damage in knee osteoarthritis is different to that of tendon rotator cuff disease to replicate the diseased shoulder joint, it is more readily available from patients to allow collection in quantities that facilitate experiments on a reasonable scale without pooling of samples.

4.3 Aims

This chapter aims to

1. Evaluate the composition of protein coronas formed on electrospun materials varying in fibre alignment or diameter and determine if these altered protein coronas may underlie observed cell-material responses.
2. Evaluate if incubation of electrospun scaffolds in different biological fluids can change the composition of the formed protein corona.
3. Assess whether an altered protein corona can modulate PBMC and tendon fibroblast response to the same biomaterial.

4.4 Hypotheses

1. Electrospun scaffolds varying in alignment and diameter will absorb similar protein coronas upon incubation to the same fluid.
2. Electrospun scaffolds with the same biophysical properties will create distinct protein coronas when incubated in blood, serum, plasma and synovial fluid.
3. Protein coronas formed from different biological fluids will induce altered responses from tendon fibroblasts and PBMC cells. Synovial fluid will result in a different cell response compared to that of blood, serum and plasma.

4.5 Materials and methods

4.5.1 Electrospun fibre diameter and alignment effects on protein corona formation

4.5.1.1 Electrospun scaffold fabrication and characterisation

300nm, 1000nm, 2000nm and 4000nm aligned electrospun scaffolds and 1000nm randomly orientated fibre scaffolds were produced and characterised as outlined in section 2.5.11 (Final electrospun biomimetic scaffold production parameters). The 2000nm scaffold was prepared using the 1.1ml/hr flow rate. The 4000nm scaffold was prepared using the 14% PDO solution.

4.5.1.2 Electrospun scaffold functionalisation

Electrospun scaffolds were mounted, sterilised and washed as detailed in section 3.5.1 (Electrospun scaffold fabrication and preparation). Following mounting, scaffolds were soaked in 100µl of human serum (3 males, average age 29 - collected with appropriate ethical approval (REC11/H0711/7)) followed by incubation for 1 hour at 37 ^{o}C. These scaffolds were rinsed twice with 2ml of PBS to remove unbound serum proteins.

4.5.1.3 Mass spectrometry protocol for analysis of adsorbed protein corona and original biological fluid composition

Scaffolds were removed from crowns and placed in to 2ml PBS with gentle agitation on a plate shaker for 5 minutes. This washing step was repeated to fully remove any serum or loosely bound protein that may influence mass spectrometry analysis. Scaffolds were then clasped in a Lo Bind eppendorf tube (Eppendorf AG, Hamburg, Germany) before brief centrifugation to remove any remaining PBS and unbound protein from the scaffold. Bound protein was removed and digested from the washed scaffolds using 500ng trypsin (Promega, Southampton, UK) in 50mM ammonium bicarbonate at 37 ^{o}C overnight. Samples were then

processed by research staff at the Target Discovery Institute (University of Oxford, UK) using adapted in house protocols.

The resulting peptides were purified using SOLA C18 HRP desalting cartridges. Eluted peptides were dried, re-suspended in 2% acetonitrile, 0.1% trifluoroacetic acid and stored at -20 ^{o}C prior to analysis. Protein was also precipitated from the original serum using a methanol/chloroform/water extraction method [297] prior to digestion using the same trypsin protocol. This created a reference protein library for each biological fluid to compare the bound proteome with.

Peptides were detected by nano-UPLC-MS/MS over a 60 min gradient of 0.1% formic acid in 5% DMSO to 0.1% formic acid to 35% acetonitrile in 5% DMSO using a Dionex Ultimate 3000 nano-UPLC with an EASY-Spray column (75 µm x 500 µm, 2µm particle size (ThermoFisher Scientific, Waltham, MA, USA) coupled to an Orbitrap Fusion Lumos TriBrid Mass Spectrometer (ThermoFisher Scientific, Waltham, MA, USA). MS1 spectra were acquired in the Orbitrap between 375-1500m/z with a resolution of 120,000. MS2 spectra of CID fragmented precursors were acquired in the linear ion trap in rapid scan mode. Selected precursors were excluded from repeated analysis for 30s.

Raw MS data files were analysed using MaxQuant [298]. Post-processing evaluation, principal component analyses and statistical analyses were performed in Perseus [299] and R (R Core Team 2018). The fragment ion spectra were searched against the 2017 UNIPROT human reference proteome along with a common protein contaminant database provided through MaxQuant. Oxidation of methionine was allowed as a variable modification and a false discovery rate of 1% was allowed for both peptides and proteins. Trypsin, with a maximum of 2 missed cleavages, was used as the enzyme specificity. Proteins were quantified with MaxFLQ within MaxQuant. The 'match between runs' option was utilised and all other settings left as default.

4.5.2 Characterisation of protein coronas formed through functionalisation of electrospun fibres with different biological fluids

4.5.2.1 Electrospun scaffold preparation and functionalisation

1000nm aligned electrospun scaffolds were produced and characterised as outlined in section 2.5.11 (Final electrospun biomimetic scaffold production parameters). Electrospun scaffolds were mounted and sterilised as detailed in section 3.5.1 (Electrospun scaffold fabrication and preparation). Following mounting, scaffolds were soaked in either 100µl of human blood, serum, plasma or synovial fluid from three patients undergoing total knee arthroplasty (1 male, 2 females, average age 67) through Oxford Musculoskeletal Biobank (REC 09/H0606/11). These were then incubated, washed and processed as described in section 3.5.1 (Electrospun scaffold fabrication and preparation).

4.5.2.2 Mass Spectrometry characterisation of the adsorbed protein corona

Mass spectrometry was performed as detailed in section 4.5.1.3 (Mass spectrometry protocol for analysis of adsorbed protein corona and original biological fluid composition) in conjunction with the Target Discovery Institute. Again, neat aliquots of each of the biological fluids incubated on scaffolds were analysed to generate comparison reference proteomes.

4.5.3 Tendon fibroblast response to electrospun fibres functionalised through biological fluid treatment

4.5.3.1 Electrospun scaffold fabrication, characterisation and functionalisation

1000nm diameter, aligned electrospun scaffolds for this experiment were prepared as described in section 2.5.11 (Final electrospun biomimetic scaffold production parameters). The scaffolds used in this experiment were from the same round of manufacturing as those used for experiment 4.5.2.

These scaffolds also underwent incubation with 100µl of blood, serum, plasma and synovial fluid using the previously described protocol. In this experiment, the biological fluids for incubation were obtained from 3 patients undergoing total knee arthroscopy (2 females, 1 male, average age 71). These are different patients to those used in experiment 4.5.2. After the washing steps to remove excess biological fluid and unbound protein, mounted cell crowns were seeded with tendon fibroblasts. Uncoated controls were also included with incubations occurring in PBS, not protein containing fluid.

4.5.3.2 Tendon fibroblast seeding

Tendon fibroblasts from healthy hamstring tendon (male, 20 years old) and diseased rotator cuff tendon (male, 72 years old) were obtained and expanded for use in line with sections 3.5.2.1 (Human tendon sample procurement) and 3.5.2.2 (Tendon fibroblast isolation and expansion). These were seeded at 100,000 cells/cm^2 in 100µl of media on the electrospun scaffolds pre-adsorbed with blood, serum, plasma, synovial fluid or PBS alone. Cells had a 2 hour attachment period as described in section 3.5.2.3 (Tendon fibroblast seeding and culture). Control cell populations of each disease phenotype were also seeded into 24 well plates.

4.5.3.3 Tendon fibroblast attachment

Assessment of tendon fibroblast attachment was performed using an AlamarBlue assay after 24 hours as described in experiment 3.5.2.4 (Tendon fibroblast attachment analysis). This was performed with experimental repeats for each condition.

4.5.3.4 Tendon fibroblast metabolic activity

Metabolic activity was also assessed at day 4 and day 7 as described in experiment 3.5.2.5, also in triplicate. This measure of metabolic activity was used as a surrogate indicator of proliferation as previously discussed.

4.5.3.5 Tendon fibroblast gene expression

Tendon fibroblast gene expression was examined for cells from both healthy and diseased tendons at the time of seeding and at day 7 as outlined in experiment 3.5.2.7 to calculate fold change over time. As mentioned in the discussion of Chapter 3, comparisons to fibroblasts seeded on scaffolds for 24 hours may mask the real change in gene expression occurring from baseline with changes potentially occurring within 24 hours. As a result, the change in gene expression at 7 days has been calculated compared to gene expression of fibroblasts at the time of seeding for this experiment.

4.5.4 PBMC response to electrospun fibres functionalised through biological fluid treatment

4.5.4.1 Electrospun scaffold fabrication, characterisation and functionalisation

The scaffolds for this experiment were prepared from the same electrospinning production cycle as those used in experiment 4.5.3. These scaffolds were also functionalised using the same biological fluids from the same patients (2 females, 1 male, average age 71) following the same protocols.

4.5.4.2 PBMC isolation and seeding

PBMCs used in this experiment were acquired as detailed in 3.5.5.2 and seeded as described in 3.5.5.3. Simply, 100µl of viable PBMCs (1x10^7/ml) were seeded on to aligned, 1000nm mounted scaffolds with an attachment period of 1 hour before transfer to 24 well plates containing 1750µl of cRPMI with a further 500µl added into the crown. For TCP control wells, PBMCs were seeded in the same density in 24 well plates with media added directly.

4.5.4.3 PBMC gene expression

PBMC gene expression was performed as outlined in section 3.5.5.4 (PBMC gene expression). Inflammatory genes (*TNFA, TGFB, IL1B, IL6, IL8, IL10, IL12B, CD206* and *PTGS2*) were compared to *GAPDH* and *ACTB* (data is shown normalised to *GAPDH*) at 4 hours and 24

hours following seeding compared to 0 hours. Gene expression was performed in triplicate at baseline on the PBMC populations. This was repeated for the 3 patients for all 4 fluid types with technical repeats at the 4 hour and 24 hour time points owing to restrictions in the amount of synovial fluid collected from each patient. Control PBMCs were cultured in TCP wells in the same numbers. This inflammatory gene panel is the same as that used in PBMC experiments from Chapter 3, with suppliers and sequences for these primers included as Appendix B, Table B-1.

4.5.4.4 PBMC flow cytometry

Flow cytometry was performed using the same protocols described in section 3.5.5.5 (PBMC flow cytometry) with technical repeats. Given the proportion of adherent cells remaining after Accutase treatment, as discussed in Appendix B.4 (Accutase lifting efficacy of PBMCs from electrospun scaffolds), the incubation time was increased to 15 minutes, the longest recommended period for cell lifting by the manufacturer. Antibody concentrations and suppliers were the same as provided in Table 3-3 (Antibodies used for flow cytometry experiments).

4.5.5 Statistical analysis

Statistical analysis was performed using GraphPad Prism software. Scaffold analysis was performed in line with the protocols described in section 2.5.14 (Scaffold statistical analysis). An unpaired, two-tailed t test with Welch's correction was used was used for assessing differences between the random and aligned scaffolds to ensure diameter was conserved. Rayleigh's test for uniformity was also performed to ensure differences in alignment were adequate and compliant with pre-determined criteria ($R<0.1$ for random fibres and $R>0.9$ for aligned fibres of 1000nm, 2000nm and 4000nm scaffolds, and $R>0.85$ for aligned 300nm scaffolds).

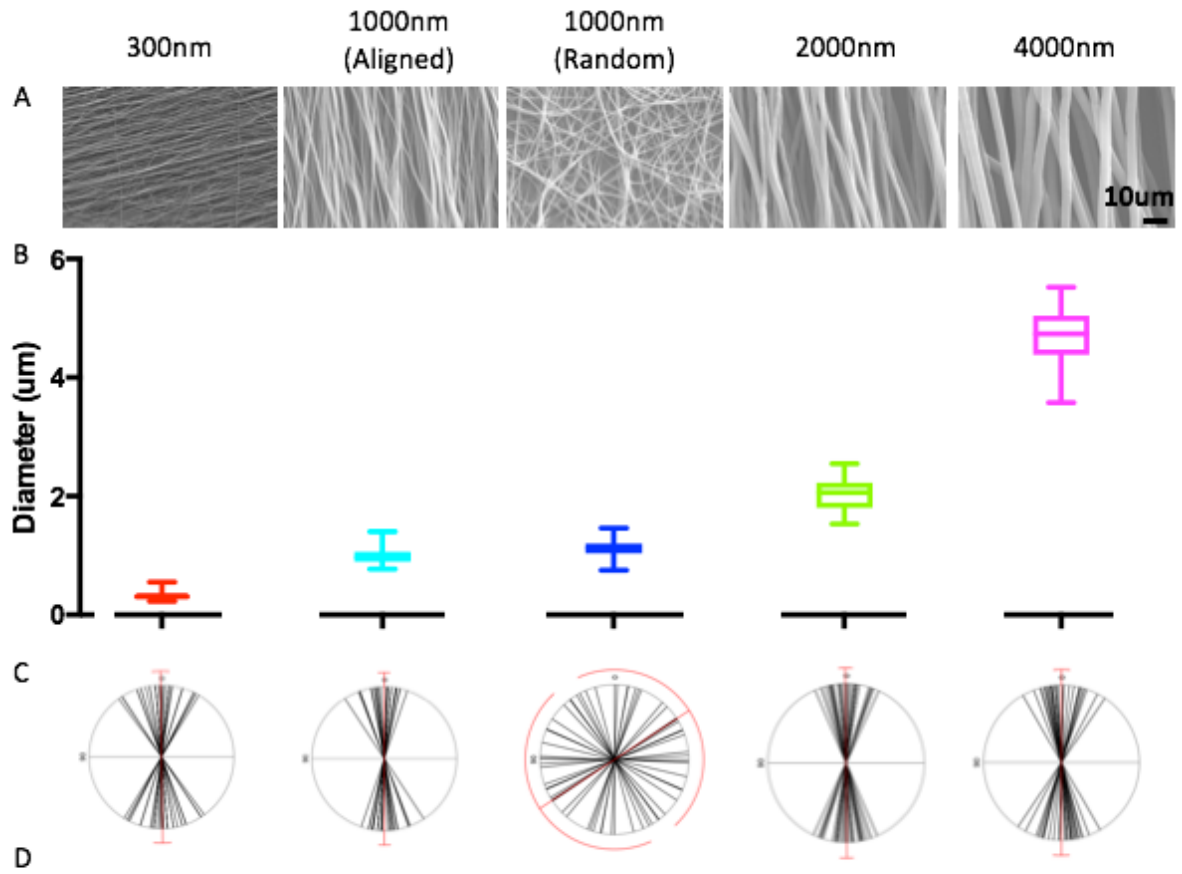
To assess the difference in attachment of healthy and diseased fibroblasts to electrospun scaffolds coated in different biological fluids, a one-way ANOVA with post hoc Tukey's testing was performed on the percentage attachment compared to TCP. To test, the metabolic activity over time a repeated measures two-way ANOVA with post hoc Tukey's testing was used. The fold change in gene expression was tested using a one-way ANOVA with post hoc Tukey's testing. Assessment of PBMC gene expression and flow cytometry results was evaluated with a repeated measures two-way ANOVA with post hoc Tukey's test.

4.6 Results

4.6.1 Electrospun fibre diameter and alignment effects on protein corona formation

4.6.1.1 Scaffold characterisation

Representative images, box and whisker plots, axial distributions and summary statistics of the electrospun scaffolds used in this experiment are detailed in Figure 4-1. For the 1000nm scaffolds used to assess alignment effects on protein adsorption, there is no significant difference in fibre diameter but the differences in alignment were within the range stipulated for this thesis ($R>0.9$ for the aligned scaffold and $R<0.1$ for the random scaffold).



Number of fibres (n)	35	31	31	33	31
Diameter (mean) (um)	0.33	1.021	1.12	2.04	4.70
Diameter (sd) (um)	0.066	0.16	0.15	0.27	0.47
Rayleigh's R	0.8622	0.9225	0.07	0.9153	0.8791
Angular deviation (°)	6.2	4.0	45.0	4.1	5.2

Figure 4-1. Electrospun scaffolds used to examine fibre diameter and alignment effects on protein corona formation.

Representative SEM images ((A) 2500x magnification, scale bar = 10µm), box and whisker plots (min-max (B)), axial distributions (C) and summary statistics (D) of the 300nm, 1000nm (aligned), 1000nm (random), 2000nm and 4000nm scaffolds used in this experiment.

For the scaffolds used to test whether differences in diameter altered protein adsorption, mean diameters were significantly different ($p<0.001$) whilst conserving alignment. For the 300nm scaffold, the Rayleigh's test indicates an R of 0.8622, less than the >0.9 set out as a criteria for

alignment in Chapter 2. This is similarly the case for the 4000nm scaffold where the R value is 0.8791. Slightly lower alignment had already been accepted in the 300nm scaffold as an effect of pyridine and the morphological trade off to achieve collagen fibril sized electrospun fibres. Attempts were made to fabricate 4000nm scaffolds with greater alignment. However, this proved challenging with fibre stacking occurring in 4000nm scaffolds (Figure 4-2). The biological significance of discrete fibres with slight reductions in alignment were deemed less important than more aligned stacked fibre scaffolds. Additionally, using an absolute value of >0.9 also means two scaffolds could satisfy the criteria for alignment but have R values of 0.90001 and 0.9999. This would be a greater difference in alignment than between the scaffolds used in this experiment yet still fulfil criteria stipulated for alignment in this thesis.

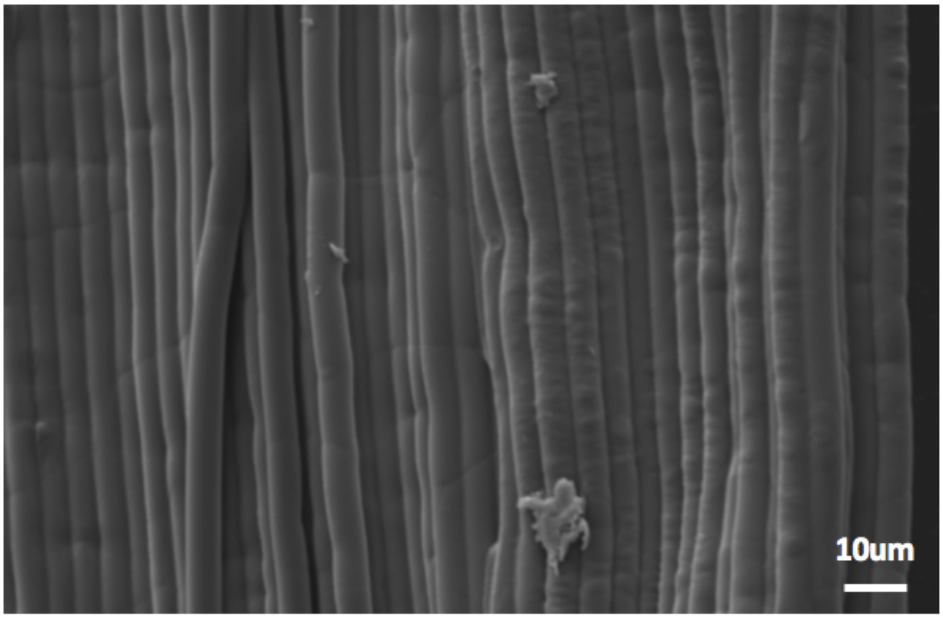


Figure 4-2. Stacking of electrospun fibres distorts scaffold morphology.

SEM image showing stacked electrospun fibres deposited in contact with each other creating grooved or ridged sheets, not discrete fibres. Whilst this is an extreme example, the same phenomenon often occurred to lesser extents when trying to produce 4000nm scaffolds for this experiment. This was a new challenge, not encountered with previous scaffold fabrication cycles. No protocol correction could be found to explain the phenomenon (2500x magnification, scale bar = 10µm).

4.6.1.2 Validation of mass spectrometry data validity

In these experiments, there are two hypotheses to test. Firstly, do biophysical properties affect the formation of protein coronas, and secondly can the composition of this corona be manipulated through incubation with different biological fluids.

Protein detection by mass spectrometry detection depends not only on the concentration of proteins but on the relative abundance of these proteins. Abundant proteins can prevent the detection of less abundant peptides. Removal of these more abundant proteins is referred to as depletion.

In the context of these experiments, the protein corona which formed on electrospun fibres was compared to the raw fluids the fibres were incubated with. This could examine if specific proteins were enriched, relatively depleted, or absent in the local protein niche adsorbed to the electrospun scaffolds. However, this introduces a potential bias. As the scaffolds adsorb only a small amount of the total protein from a biological fluid solution, with washing removing the remainder, compared to the original fluid there be a relative depletion of the more abundant proteins. Removal of abundant proteins by washing would therefore allow detection of the less abundant protein species on the scaffolds but not in the neat fluids leading to incorrect interpretation of enrichment.

More proteins were detected in the serum-derived coronas adsorbed on to the scaffolds than from the neat serum. To examine whether depletion was causing this phenomenon, the 678 detected proteins from the serum adsorbed scaffolds in this experiment were plotted against a known deep reference database of 960 serum proteins (Figure 4-3). This database is compiled with a protocol to maximise detection of all available proteins. The proteins are ranked in their intensity across the X-axis (most abundant on the left through to least abundant on the right) with the Y-axis depicting the absolute intensity for individual proteins. In this figure, reference proteins are grey and detected proteins from the scaffold coronas are red.

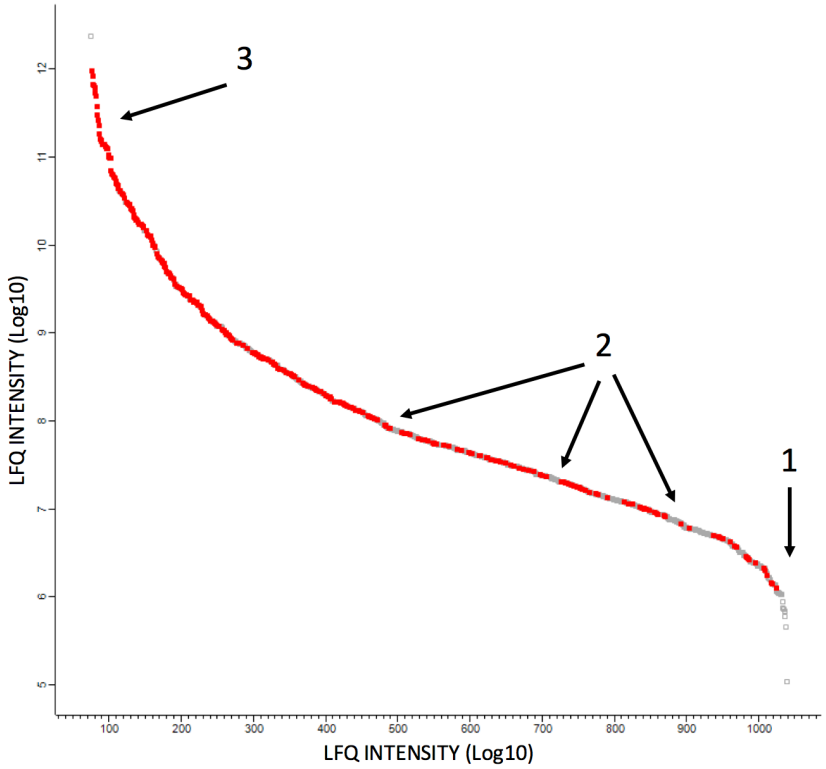


Figure 4-3. Overlay of the intensity of proteins detected on serum adsorbed aligned, 1000nm electrospun scaffold and a reference protein database.

Proteins detected from a serum-adsorbed 1000nm aligned electrospun fibre protein corona (red) compared with reference database proteins (grey). Individual proteins are plotted from most abundant to the least abundant on the right based on their intensity during detection. There are three things to note. 1) There is no relative shift to the less intense range of the proteins detected in this experiment which would imply detection is related to depletion. 2) There is non-specific depletion of certain proteins over the range detected on the electrospun scaffolds suggesting the corona is distinct from the original fluid. 3) There are proteins at higher intensity levels in the corona than in the reference database, potentially suggesting relative enrichment.

There are 3 findings of note from this data. Firstly, if the relative depletion of proteins through washing simply opened up detection of less abundant proteins, we would expect to see enrichment of proteins detected at the tail (right end of x-axis) of this plot (1). This is not the case. Secondly, if the scaffolds were binding proteins in a non-specific way, there would be no gaps in the detected protein curve (2). These gaps suggest there is specific depletion of certain proteins in the niche surrounding electrospun fibres. Finally, there is also a suggestion of protein enrichment with protein species being detected at higher intensities (left end of x-

axis) than the reference data base (3). This may also be partially explained by the depletion of proteins in the reference sample to expose the less abundant proteins. Taken together, these findings suggest the detected differences in electrospun scaffold protein coronas are not the result of non-specific binding being revealed through relative depletion from removal of abundant species through washing.

4.6.1.3 Protein corona composition in response to altered electrospun fibre alignment

There were no significant differences between the proteins detected in the aligned fibre corona compared to the corona formed on random electrospun fibres from incubation in serum (data not shown).

4.6.1.4 Protein corona composition in response to altered electrospun fibre diameter

Principal component analysis (PCA) of the proteins detected in the coronas of different mean fibre diameter electrospun scaffolds is shown in Figure 4-4. This shows a clear relationship between fibre diameter and the variation detected in the protein corona on the different scaffolds.

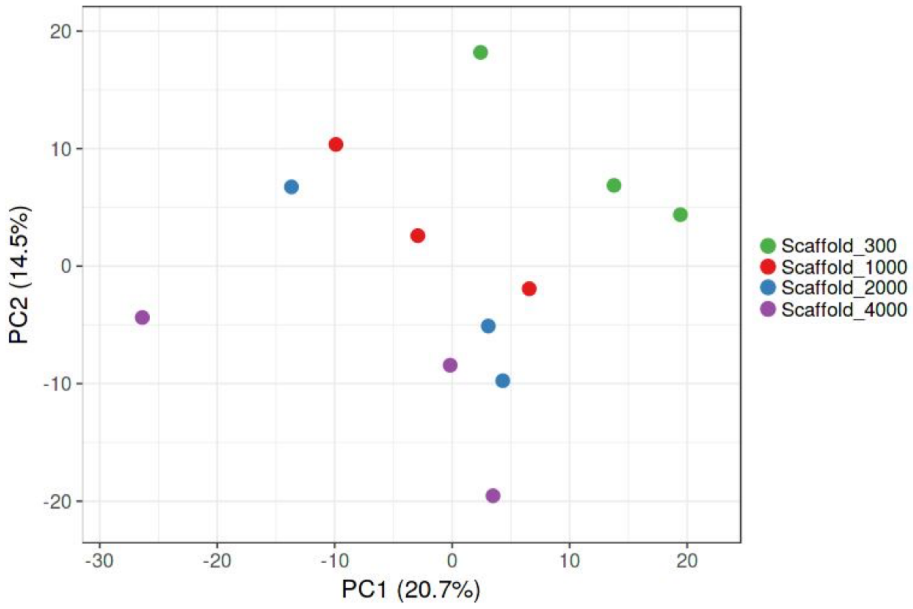


Figure 4-4. Principal component analysis of protein coronas formed on electrospun scaffolds with different mean diameters.

300nm, 1000nm, 2000nm and 4000nm aligned scaffolds were adsorbed in serum for 1 hour before analysis of the adsorbed coronas through mass spectrometry. Principal component analysis separates the adsorbed coronas based on diameter. There is more relative separation of the 300nm scaffolds from the 1000nm diameter scaffold than the separation occurring between the other step changes in fibre diameter.

Analysis of the individual identities of proteins within the coronas, revealed 11 proteins with significantly different intensities in the coronas formed on the different diameter electrospun scaffolds (Figure 4-5). Whilst this is a low fraction of the total proteins detected (2%), statistical analysis allowed for a false-discovery rate of 1%. Further evidence that these observations are not due to chance is that these proteins group in an interesting way. The top 4 proteins are enriched with decreasing diameter whereas, the bottom 7 proteins are increased with increasing diameter. Secondly, within scaffold diameters, the trends are highly conserved across the 3 different sera used. Finally, complement proteins are intrinsically adherent to enable their role in opsonisation and the immune response. The fact that biologically linked complement (C1R and C1S, C4BPA and C4BPB) or complement related (SERPING1 and PROS1) species cluster contiguously is more plausibly due to a biological interaction with electrospun scaffolds than a chance effect across highly related proteins.

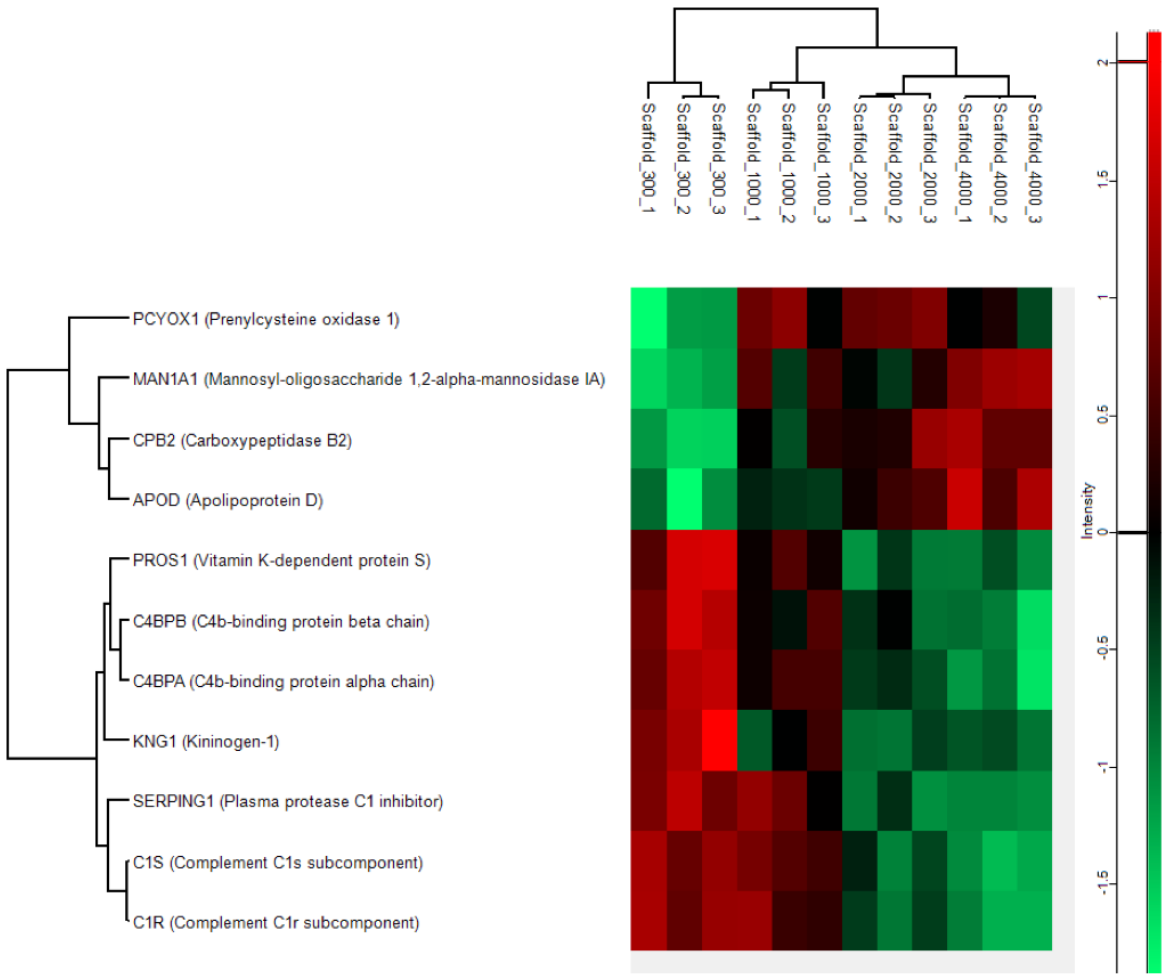


Figure 4-5. Heat map of proteins detected at significantly different intensities in protein coronas formed on electrospun scaffolds of different mean diameters.

Electrospun scaffolds of 300nm, 1000nm, 2000nm and 4000nm diameters were incubated for 1 hour in sera prior to mass spectrometry analysis of the bound protein. 11 of the 678 proteins detected in serum-adsorbed protein coronas showed significantly different intensities. These proteins showed consistent diameter dependent responses. However, these responses grouped in two ways, either increasing intensity with decreasing fibre diameter (top), or increasing intensity with increasing diameter (bottom). Intra-scaffold variation between the three different serums was relatively minimal suggesting consistency of effect. Log10 scale, with red representing increased intensities and green reduced intensities.

In this experiment, 5 of the 11 proteins displaying altered corona concentrations are related to the complement cascade with potential effects on immune cell attraction, attachment and activation with implications for the initial immune response. The most significant differences are also seen between the 300nm scaffold compared to any other diameter. This scaffold is

fabricated using pyridine and with more extreme changes in electrospinning parameters, possibly underlying surface changes which affect protein-scaffold interaction.

4.6.2 Biological fluid treatment effects on protein corona formation

4.6.2.1 Scaffold characterisation

1000nm aligned electrospun fibre scaffolds were used in this experiment. These were produced in the same batch as the equivalent scaffold used in the experiments detailed in section 4.6.1 (Electrospun fibre diameter and alignment effects on protein corona formation) with images and summary data presented in Figure 4-1.

4.6.2.2 Corona composition analysis through mass spectrometry

Principal component analysis was performed on the proteins isolated from the original biological fluids used to functionalise the electrospun scaffolds as well as on the proteins derived from the resulting protein coronas (Figure 4-6). This analysis shows that there is more separation between the protein composition of the coronas compared to the differences between the composition of the neat, original fluids. The niche created from protein adsorption to electrospun scaffolds from a biological fluid is distinct from the composition of the original fluid.

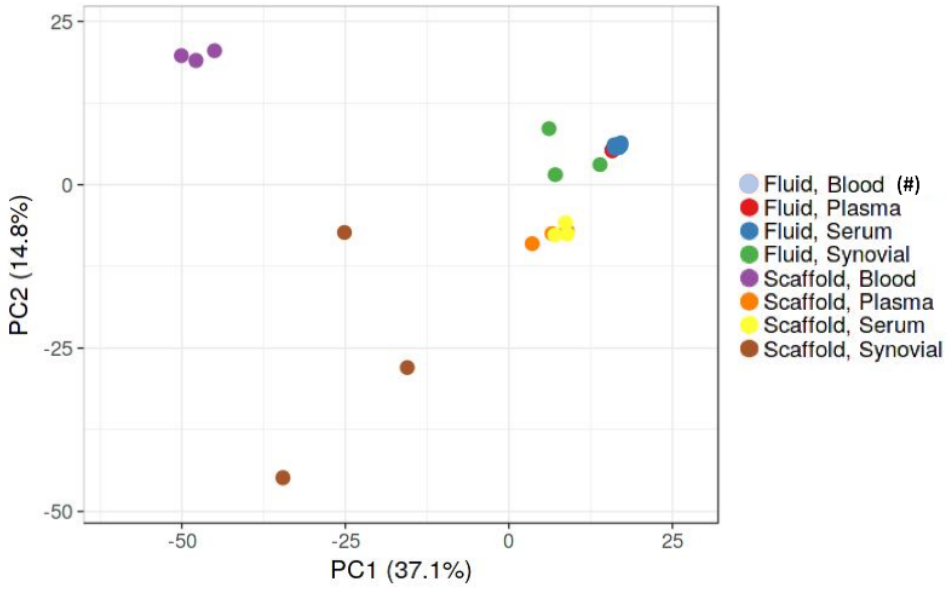


Figure 4-6. Principal component analysis of proteins from blood, serum, plasma and synovial fluid and the resultant protein coronas formed on adsorption to identical 1000nm, aligned electrospun fibre scaffolds.

1000nm, aligned electrospun scaffolds were treated with blood, serum, plasma and synovial fluid for 1 hour prior to analysis of the adsorbed corona through mass spectrometry. Principal component analysis of the detected proteins shows 3 notable findings. Firstly, the protein composition of neat serum, plasma and synovial fluid is relatively similar, especially between serum and plasma. Blood is not compatible with the mass spectrometry set up used in this experiment (#) so cannot be compared to the other neat fluids. Secondly, there are pronounced differences between the coronas adsorbed from the different biological fluids to the same 1000nm scaffolds. Again, the serum and plasma corona protein groupings are similar to each other. Synovial fluid and blood however show greater differences. Thirdly, the groupings between the three experimental repeats are similar, apart from the synovial fluid repeats.

Detailed investigations of these proteins revealed 125 proteins from blood, serum, plasma and synovial fluid exhibited statistically significant differences in adsorption to electrospun fibres (Figure 4-7). Detailed images with protein names are provided in Appendix C, Figure C-1. From this heat map, there are 3 interesting observations. Firstly, for each fluid type, there is both relative enrichment and depletion of proteins in the coronas formed on electrospun scaffolds, suggesting pre-adsorption does change the surface protein composition. Secondly, serum and plasma induced coronas are very similar, with synovial fluid and blood being distinct, as reflected in the PCA. Thirdly, for each fluid type, the protein changes are largely

consistent, except for coronas formed from incubation in synovial fluid which display marked heterogeneity, again as reflected in the PCA plot.

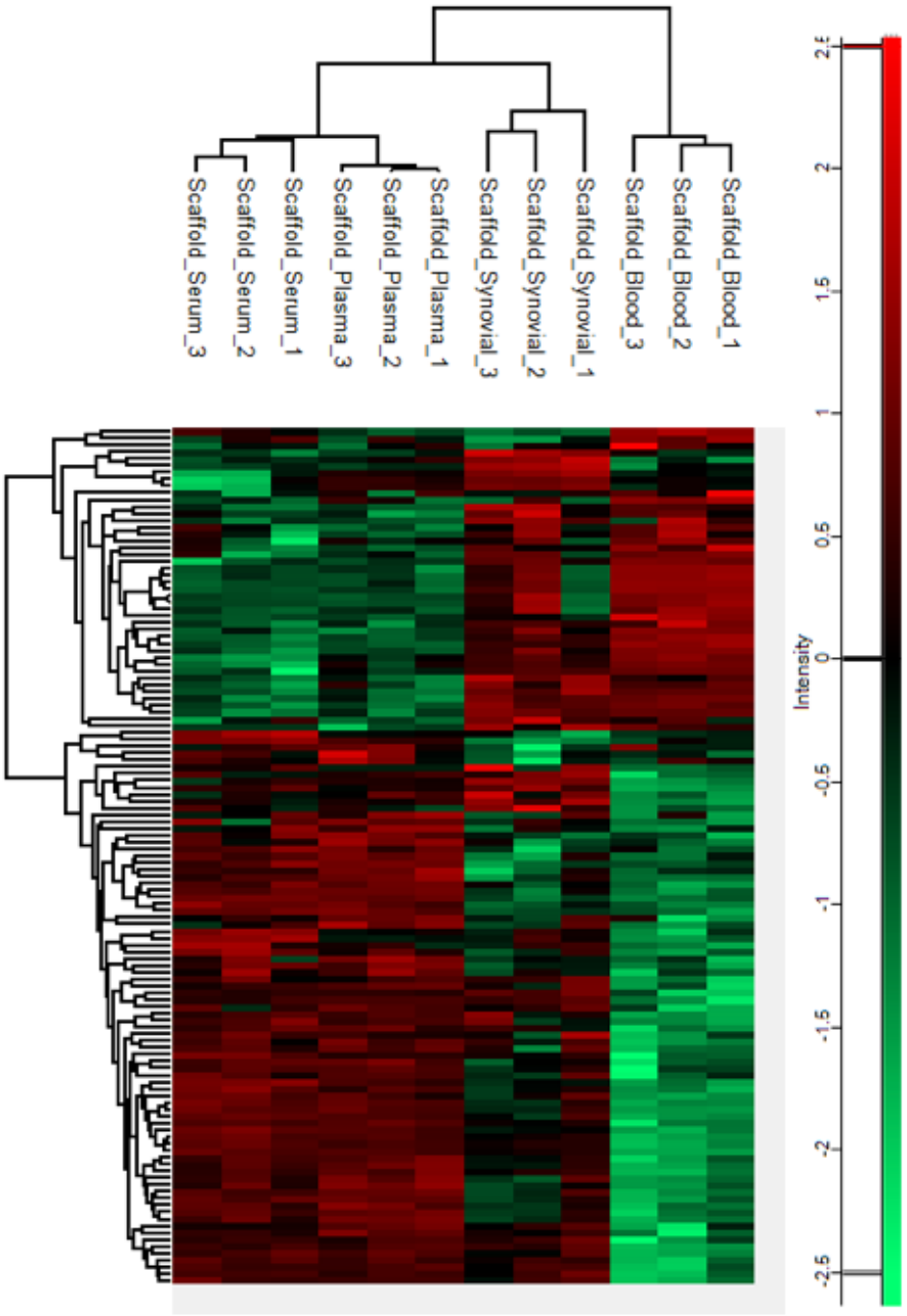


Figure 4-7. Heat map of proteins detected at statistically different intensities in the coronas formed through incubation of electrospun scaffolds in biological fluids.

This heat map shows the 125 proteins present at statistically different intensities across the coronas formed from blood, serum, plasma and synovial fluid after adsorption on aligned,

1000nm scaffolds. These proteins separate in 3 patterns. Firstly, some proteins are relatively enriched while others are relatively depleted. Secondly, the proteins in serum and plasma coronas display more consistent intensities compared to synovial fluid or blood. Thirdly, the differences in intensity between the 3 synovial fluid coronas is the most heterogeneous of the 4 fluid types. Log10 scale, with red indicating increased abundance and green reduced abundance.

4.6.3 Biological fluid functionalisation effects on healthy and diseased tendon fibroblasts

4.6.3.1 Attachment

Tendon fibroblasts from healthy tendon showed increased attachment rates compared to tendon fibroblasts from diseased tendon (Figure 4-8). This was conserved across all electrospun fibre fluid treatments as well as the uncoated control scaffolds. Pooling tendon fibroblasts into healthy or diseased phenotypes showed statistically lower attachment of tendon fibroblasts from diseased tendon versus healthy tendon (48% and 95% respectively, ($p=0.0079$)), consistent with previous results detailed in section 3.6.2.2 (Fibroblasts from diseased tendon show reduced attachment to electrospun scaffolds). The different protein coronas generated through incubation in serum, plasma, blood or synovial fluid did not induce significant differences in attachment rates of fibroblasts from healthy or diseased tendon.

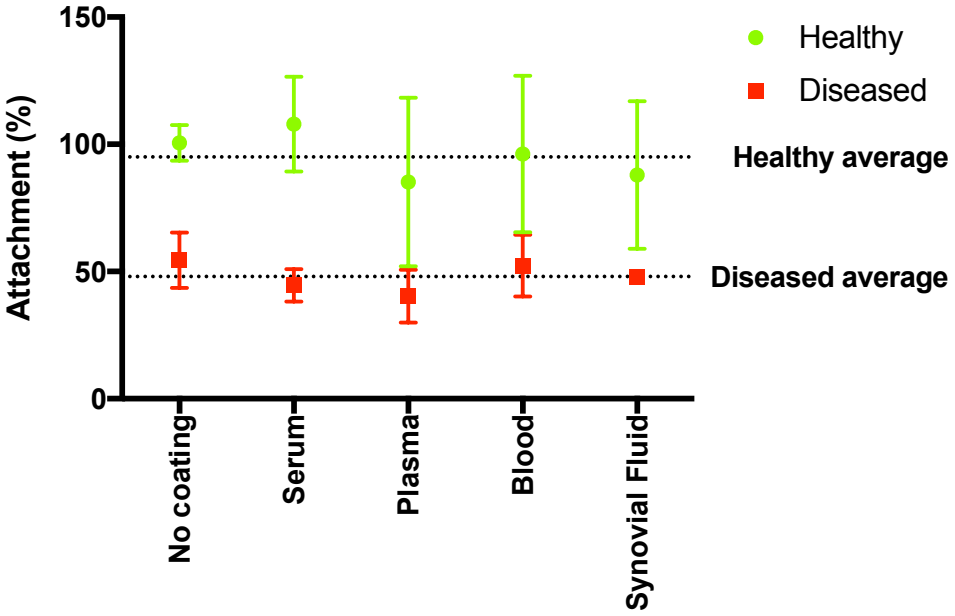


Figure 4-8. Attachment rates of tendon fibroblasts from healthy and diseased tendon to electrospun scaffolds functionalised with coronas adsorbed from different biological fluids.

Mean and standard deviation attachment percentages for tendon fibroblasts from healthy tendon (green) showed higher attachment rates than tendon fibroblasts from diseased tendon (red) consistent with previous results. There were no differences in attachment to scaffolds functionalised with biological fluids for either tendon fibroblast disease phenotype.

4.6.3.2 Metabolic activity

Fibroblasts from healthy and diseased tendon were cultured on scaffolds functionalised with different biological fluids with metabolic activity assessed for one week. Fibroblasts from diseased tendon exhibit significantly greater increases (3.5 fold average at 7 days) in metabolic activity than their counterparts derived from healthy tendon (1.4 fold over the same time period) (Figure 4-9, $p<0.001$). This is consistent with previous results (3.6.2.3).

Functionalisation through pre-adsorption with biological fluids altered the metabolic activity of tendon fibroblasts from diseased tendon. At day 4, significant differences were observed between the uncoated control scaffolds and scaffolds adsorbed in serum ($p=0.0276$), plasma ($p=0.0076$) and synovial fluid ($p=0.0255$). At day 7, significant increases were noted in

scaffolds adsorbed in blood (p=0.0479), serum (p=0.0005), plasma (p<0.0001) and synovial fluid (p=0.0008) compared to uncoated controls. The increase in metabolic activity was significantly less in blood adsorbed scaffolds compared to those incubated with plasma (p=0.0016). These data suggest the adsorbed protein coronas can modulate metabolic activity of diseased tendon fibroblasts over time but have less effect on those derived from healthy fibroblasts. Again, the relatively blunted response observed in fibroblasts from healthy compared to diseased tendon is similar to what was observed in the responses in previous experiments.

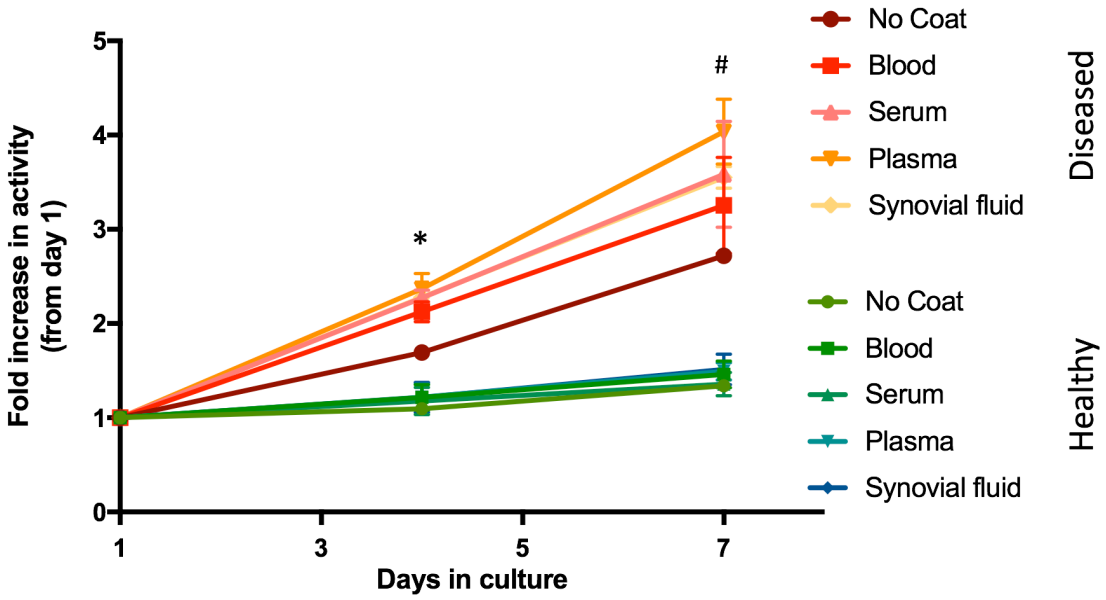


Figure 4-9. Metabolic activity of tendon fibroblasts isolated from healthy tendon and diseased tendon on electrospun scaffolds functionalised with coronas adsorbed from different biological fluids.

Fold increase in metabolic activity for tendon fibroblasts from healthy tendon (green) and diseased tendon (red) over 7 days. Fibroblasts from diseased tendon showed a greater increase in metabolic activity. These increases were modulated by the biological fluid that scaffolds were functionalised with. Significant differences were noted between uncoated scaffolds and serum, plasma and synovial fluid at day 4 (*) and between uncoated scaffolds and all other scaffolds at day 7 (#). There was also a significant difference between metabolic activity of fibroblasts cultured on plasma absorbed scaffolds compared to blood adsorbed scaffolds at day 7. Mean fold increase and standard deviation compared to day 1.

4.6.3.3 Tendon fibroblast gene expression

The expression of 10 genes was measured in tendon fibroblasts cultured on scaffolds that had been pre-adsorbed in with blood, serum, plasma, synovial fluid as well as an uncoated control. These genes were divided into three groups important for tendon repair; tendon matrix components (*COL1A1, COL3A1* and *ACAN*); cell attachment markers (*IA2, IA4* and *IB3*); and inflammation/resolution markers (*PDPN, IL6, IL8* and *PTGS2*). These genes were chosen based on our previous data indicating these genes were sensitive to biophysical cues. In this experiment, the fold change at 7 days is calculated based on the expression of cells from the time of seeding (scaffold naïve cells), not from cells cultured on scaffolds for 24 hours as discussed in section 3.6.2.5 (Fibroblasts from diseased healthy tendons show different gene expression responses to electrospun scaffolds).

The data from this experiment supports earlier results in this thesis showing distinct differences between the response to scaffold-based cues of fibroblasts from healthy and diseased tendon (Figure 4-10). Within tendon matrix genes, there were more increases in gene expression in tendon fibroblasts derived from healthy tendon than observed in those from diseased tendon. The opposite was observed in the inflammatory markers with relatively larger increases in the expression of *IL6* and *IL8*, and down regulation of *PTGS2* in tendon fibroblasts derived from diseased compared to healthy tendon. There was also a lesser but relative down regulation of integrins in tendon fibroblasts from diseased tendon.

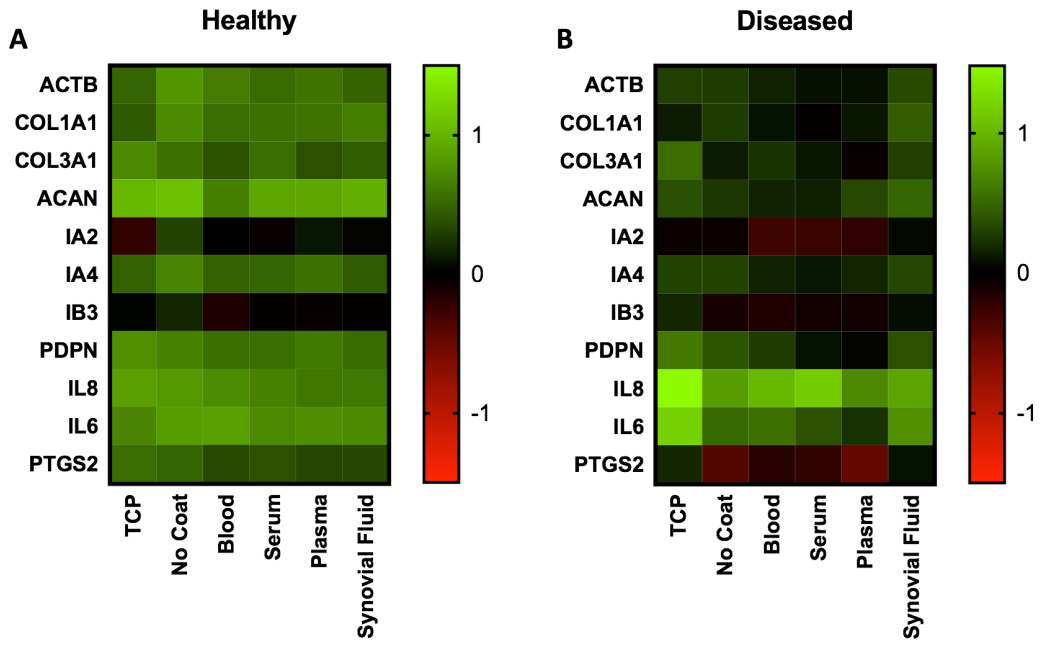


Figure 4-10. Fold changes in gene expression of tendon fibroblasts cultured for 7 days on electrospun scaffolds functionalised with coronas adsorbed from different biological fluids.

Tendon fibroblasts from healthy (A) and diseased tendon (B) were cultured on TCP, uncoated electrospun scaffolds and scaffolds functionalised with blood, serum, plasma or synovial fluid for 7 days. These heat maps show the fold change in gene expression from the original cell population at the time of seeding (0 hours). The pattern of change is different between healthy and diseased tendon derived fibroblasts. Within a tendon fibroblast population, treatment with biological fluids does not significantly modulate gene expression. Mean fold change in gene expression at 7 days compared to time of seeding, green depicts increasing expression, red reduced expression, log10 scale.

Within the response of tendon fibroblasts from healthy tendon, functionalisation of the corona through incubation in different biological fluids did not induce obvious changes in the fold expression of the selected genes over 7 days culture. The gene expression response of tendon fibroblasts from diseased tendon was relatively heterogeneous in response to the same fluid functionalised scaffolds. Compared to untreated control scaffolds, there were also no statistically significant differences in either matrix, adhesion or inflammatory gene expression across the different scaffolds. Of note, the responses to the serum and plasma adsorbed scaffolds was the most consistent of the different functionalised scaffolds. While the response

of fibroblasts to synovial fluid incubated scaffolds was the most different compared to the other fluid treated scaffolds.

4.6.4 Biological fluid functionalisation effects on PBMC populations

4.6.4.1 Scaffold characterisation

The 1000nm aligned electrospun scaffolds used in this experiment were manufactured and prepared from the same batch as described in experiment 4.6.1.

4.6.4.2 Gene expression

PBMC gene expression after culture on electrospun scaffolds functionalised with various fluid treatments was calculated as a fold change from baseline at 4 hours and 24 hours. Figure 4-11 (A) shows the fold changes in gene expression of PBMCs cultured on TCP, uncoated electrospun scaffolds and the pooled response to scaffolds treated with biological fluids at 24 hours (4 hour data is similar and shown as Appendix C, Figure C-2). The pattern of change for untreated and treated electrospun fibres is different to that of TCP suggesting that PBMC changes in gene expression are sensitive to the biochemical stimuli of different protein coronas. PBMC expression of the inflammatory genes *IL1B, IL6, IL8,* and *IL10* are modulated by culture on electrospun scaffolds compared to culture in suspension in TCP wells. This finding was also true of non-coated scaffolds suggesting biophysical stimuli also have a role in modulating the expression of these genes.

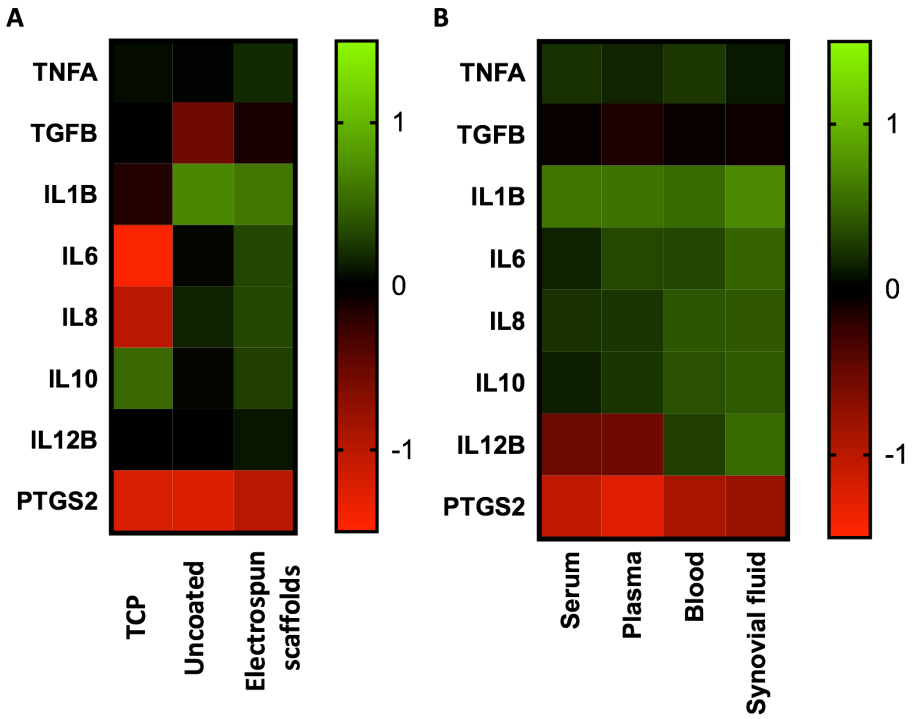


Figure 4-11. Fold changes in gene expression of PBMCs cultured for 24 hours on electrospun scaffolds functionalised with biological fluids.

PBMC fold change in gene expression after 24 hours culture on electrospun scaffolds functionalised with blood, serum, plasma and synovial fluid, untreated scaffolds or TCP from PBMCs at the time of seeding (0 hours). To highlight the effect of biophysical scaffold cues, fold changes for PBMCs cultured on TCP are compared against uncoated scaffolds and the pooled responses to of electrospun scaffolds treated with biological fluids (A). Functionalisation of scaffolds with biological fluids also modulated gene expression (B) most notably in *IL12B* but with a general reduction in upregulation for serum and plasma treated scaffolds compared to blood and synovial fluid treated scaffolds. Mean fold change in gene expression at 24 hours compared to time of seeding, green depicts increasing expression, red reduced expression, log10 scale.

Altered corona composition also had an effect on PBMC gene expression, particularly in the inflammatory genes *IL1B, IL6, IL8,* and *IL10* (Figure 4-11 (B)). Fold changes in PBMC gene expression of these markers are similar on electrospun fibres treated with serum and plasma. However, this shared response is distinct to the fold changes induced from blood or synovial fluid treated scaffolds. Firstly, *IL12B* gene expression was decreased on plasma and serum-adsorbed scaffolds, whilst it was increased in synovial fluid and blood based coronas. There was no change in *IL12B* expression in PBMCs seeded on uncoated scaffolds or TCP. Secondly,

the upregulation of *IL6, IL8* and *IL10* in serum and plasma treated scaffolds was lower on serum and plasma treated scaffolds than blood and synovial fluid adsorbed scaffolds but more than occurred in uncoated control scaffolds.

4.6.4.3 Flow cytometry

Analysis of adherent PBMC subpopulations that attached to the functionalised electrospun fibres are presented in Figure 4-12. The gating strategy and antibodies used in this experiment are the same as previously described and discussed in experiment 3.6.3.3.

PBMC sub population proportions varied on uncoated electrospun fibres compared to control cell populations, highlighting that electrospun materials have direct effects on PBMC attachment profiles. This is clearly shown in the monocyte (E) and NK cell plots (F).

PBMC response to the electrospun fibres was further affected by functionalisation with different biological fluids. These differential responses fell into 2 groups; the PBMC response to serum and plasma functionalised scaffolds; and the PBMC response to the uncoated, blood and synovial fluid coated scaffolds. These effects are particularly evident in the CD3- (D), monocyte (E) and NK cell plots (F).

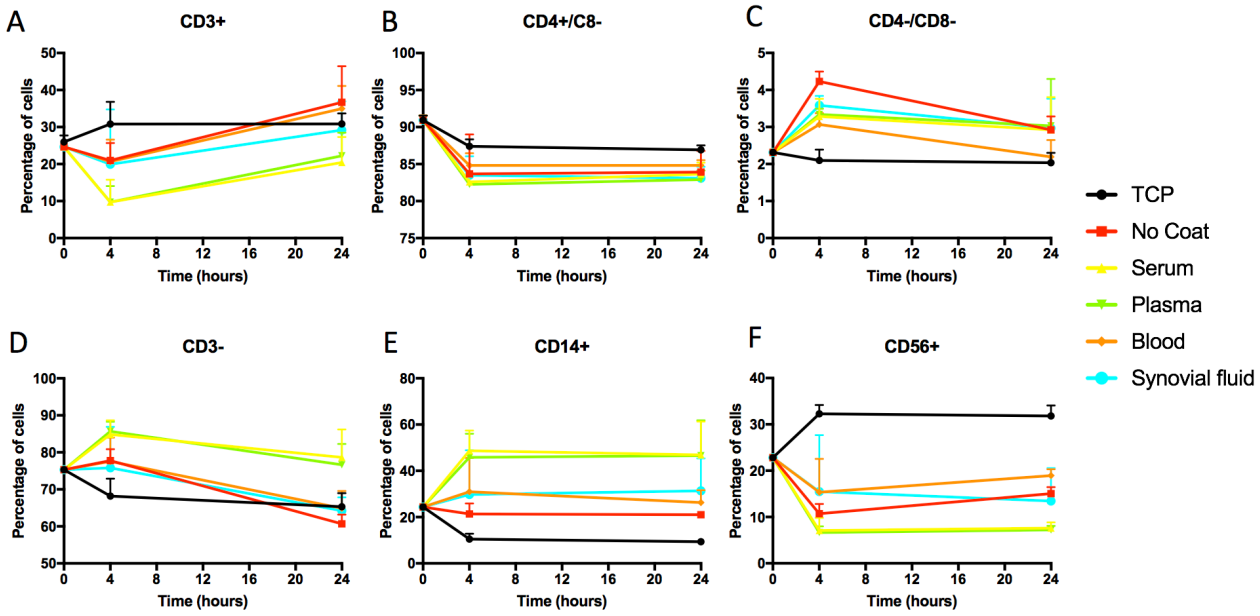


Figure 4-12. Plots of selected PBMC populations following culture on electrospun scaffolds functionalised with biological fluids over 24 hours.

Graphs of selected PBMC sub populations following culture on electrospun scaffolds for 24 hours. Compared to control cell populations in TCP, serum and plasma treated electrospun scaffolds promoted increased CD3- cell attachment (D), particularly CD14+ monocytes (E) and reduced CD56+ NK cells (F). The sub population formation was highly consistent between serum and plasma treated scaffolds. This grouping was different to blood, synovial fluid and uncoated controls.

The proportion of CD3+ cells was significantly lower on serum ($p=0.0018$) and plasma ($p=0.0018$) functionalised scaffolds than control cells at 4 hours but not at 24 hours. There were no significant differences across all conditions of CD4+/CD8- cells. At 4 hours CD4-/CD8- cell number was significantly higher on uncoated ($p<0.0001$), serum ($p=0.0433$), plasma ($p=0.0310$), synovial fluid ($p=0.0060$) and a trend to significance for blood ($p=0.1481$) coated scaffolds than control. However, these differences had regressed by 24 hours.

CD3- cells also revealed fluid-dependent effects. The proportion of CD3- cells was significantly higher on serum ($p=0.0008$) and plasma ($p=0.0004$) adsorbed scaffolds at 4 hours but not significant at 24 hours compared to control cells. At 24 hours the proportion of CD3- cells was also significantly higher on serum and plasma treated scaffolds compared to

uncoated (serum, p=0.0003, plasma, p=0.0014), blood (serum, p=0.0077, plasma, p=0.0312) and synovial fluid (serum, p=0.0046, plasma, p=0.0196) conditioned scaffolds.

This increased attachment of CD3- cells corresponds with an increased attachment of CD14+ monocytes. Again the differences were most pronounced between serum and plasma coated scaffolds with significantly higher monocyte proportions at 4 hours (p=0.0001, p=0.0004 respectively) and at 24 hours (p=0.0001, p=0.0002) compared to control cells. This was also true of serum and plasma treated scaffolds compared to uncoated electrospun fibres at 4 hours (p=0.0084, p=0.0229) and 24 hours (p=0.0139, p=0.0156).

The number of CD56+ NK cells is also significantly reduced on all electrospun fibre scaffolds compared to control cells at 4 hours (serum (p<0.0001, plasma (p<0.0001), blood (p=0.001), synovial fluid (p=0.001), uncoated (p<0.0001)) and at 24 hours (serum (p<0.0001, plasma (p<0.0001), blood (p=0.0039), synovial fluid (p<0.0001), uncoated (p=0.001)). Furthermore, the proportion of NK cells on serum (p=0.0146) and plasma (p=0.0103) treated scaffolds was significantly lower than blood treated scaffolds at 24 hours but not compared to other scaffold conditions.

4.7 Discussion

This chapter had two main aims. The first was to investigate whether changing the biophysical properties of electrospun scaffolds, specifically fibre alignment and diameter, resulted in altered corona protein composition. The second was examining if this corona could be deliberately manipulated through incubation in different biological fluids, functionalising the scaffolds to influence and improve cell-material interaction.

Altered fibre alignment and diameter had limited effects on the adsorbed corona of electrospun scaffolds. Exposing electrospun scaffolds to serum, plasma, blood and synovial fluid lead, however, lead to 125 proteins differing significantly in intensity in the adsorbed

coronas. These altered coronas had effects on tendon fibroblast metabolic activity and gene expression. These coronas also induced significant differences in the attachment of PBMC sub populations. This discussion will review how altering the protein corona through biological fluid functionalisation changes tendon fibroblast and PBMC material interactions in the context of rotator cuff repair.

4.7.1 Protein corona formation on electrospun fibres is affected by mean fibre diameter

As described, biomaterials adsorb a surface layer of proteins, electrolytes and other molecules immediately upon exposure to biological fluids. Cells then invade the scaffold in response to how the bound proteins are held in space, their conformation and their relative concentrations.

In this thesis, and in the literature, fibrous scaffolds are considered based on their fibre diameter and fibre alignment. However, the production strategies used to create these differences in biophysical characteristics likely impart effects on other material properties. It may be that these material properties dictate altered corona formation and biological effects, not just the altered biophysical stimuli. Changing the hydrophobicity, charge and roughness of other biomaterial surfaces, not electrospun fibres, has been shown to alter protein binding, as well as conformation [224,300]. Measuring these aspects of electrospun fibres are not routine, potentially explained by the challenges of dealing with fibres in a nanometre range.

Removal of abundant proteins allows detection of less abundant species in mass spectrometry analysis. We sought to verify the changes detected were real and not false positives in the relative concentration due to a depletion effect. The identities and intensities of the serum proteins adsorbed to scaffolds compared to a reference database showed there was specific depletion and enrichment of proteins, not simply a detection of the lower level proteins made visible by depletion. Additional data to support specific protein-fibre interactions include the

correlation between increased or decreased abundance with increasing diameter. These results demonstrate that the protein binding cannot just be a function of an increase in exposed fibre surface area promoting relatively higher adsorption on larger diameter fibres than narrower fibres. Additionally, the clustering of proteins from the complement cascade is unlikely to be a chance finding but likely a biological response from this part of the innate immune system evolved to facilitate cell interaction with foreign material. Further validity is garnered through pilot experiment data. This showed showed similar findings in the number and particular species that bound differently, including complement, to the data presented in this thesis.

The observed differences in protein corona formation from serum to different electrospun scaffolds offer insights into the effects of altered electrospinning parameters and scaffold surface properties. There were no differences in corona composition between scaffolds with identical diameters but different alignments. However, there were differences between scaffolds with different mean diameters but the same alignments. If one considers how these scaffolds are made, the magnitude of change in electrospinning parameters mirrors these observations. Between random and aligned scaffolds, there are small changes in flow rate and collector speed. Between diameters, there are more significant changes in polymer concentration, inclusion of an additional molecule (pyridine) and more significant changes in flow rate. These more pronounced parameter changes are more likely to affect the surface properties of resulting electrospun fibres, whilst changing fibre diameter.

Furthermore, mass spectrometry in this form is unable to detect the conformation of absorbed proteins. Protein function is regulated by conformation with altered isoforms of fibronectin being more or less supportive of cell interaction and attachment [224]. Consequently, on the scaffolds used to test the response of cell types to different fibre diameters, there are biophysical differences as well as biochemical differences, and potentially bioactivity

differences from altered protein conformations, which may underlie the observed differences in fibroblast and PBMC response.

Identifying that electrospun fibres can adsorb differential protein coronas poses the possibility of deliberately manipulating the corona. Incubation in different biological fluids prior to implantation is a safe, affordable and acceptable way for patients and clinicians to potentially functionalise electrospun biomaterials to improve cell-material interactions and encourage activation of pathways that promote tissue healing. This work shows that functionalisation using serum, plasma, blood and synovial fluid leads to enrichment and depletion of over 100 different proteins in the electrospun fibre corona. This corona is relatively similar between serum and plasma but notably different compared to blood. The fact serum and plasma are the most similar fits biologically as they are derived from blood, with plasma containing coagulation proteins. Synovial fluid displays an altered corona pattern in comparison to serum and plasma, again fitting biologically with synovial fluid derived from synoviocytes for a specialised function. Synovial fluid for this experiment was obtained from patients undergoing total knee arthroplasty. Macroscopically, the synovial fluids had different colours, viscosities and some degree of blood staining. This greater heterogeneity between donors was shown in the PCA and intensity analysis where more variation is noted compared to that within the serum, plasma, and blood repeats.

Irrespective of whether protein adsorption is affected by direct changes in electrospun fibre diameter or unintended changes in surface material properties, differential protein corona formation occurs. Additionally, utilising different biological fluids can amplify the differences in proteins adsorbed to the same electrospun scaffold. Furthermore, the pattern of protein binding or depletion to electrospun scaffolds is a specific, not random, process dependent on protein concentrations in the original fluid and on the properties of the biomaterial scaffold. These differences may provide a mechanism to deliberately influence the tissue-material response and integration of scaffolds with tissue *in vivo*.

4.7.2 Diameter dependent protein corona results in the context of previous tendon fibroblast and PBMC experiments

The results from this chapter show that protein adsorption is dependent on electrospun scaffold fibre diameter. This has applications to results from Chapter 3, specifically the tendon fibroblast and PBMC interactions with electrospun scaffolds of different fibre diameters. These experiments were conducted before the relationship between electrospun fibre diameter and alignment on protein corona formation were investigated.

There are, however, caveats to considering these data together. The data from the mass spectrometry data was obtained on scaffolds fabricated at different times, albeit with high concordance in fibre diameter, fibre alignment and production procedures. This data was also generated looking at the incubation of scaffolds in human serum compared to the 10% FBS, D10 media in the tendon fibroblast experiments. However, it is likely that similar differential binding of small numbers of fetal bovine serum proteins would occur. For tendon fibroblasts from healthy tendon, there were marked effects noted in morphology and gene expression on the different fibre alignments where differential binding did not occur but limited differences in response to fibre diameter where differential protein binding did occur. The combination of these findings supports that tendon fibroblasts from healthy tendon are sensitive to biophysical cues.

Secondly, there were differences in tendon fibroblast morphology on scaffolds, irrespective of disease state and fibre diameter, as well as between protein coronas and fibre diameter. Thus, the observed differences in morphology could be a result of the altered fibre diameter, the altered corona, or both. It is not possible to attribute the relative effects of these two phenomenon on cell biology.

Finally, the differences observed in corona protein composition correlate more strongly with the composition of the PBMC sub populations that attached to different diameter aligned

electrospun fibres (Figure 3-15). The mass spectrometry data shows the 300nm scaffold corona were most similar to the 1000nm scaffolds and significantly different in composition to that of the 2000nm and 4000nm scaffolds. Thus, there are two groupings of scaffolds based on differences in protein corona, one comprising the 300nm and 1000nm scaffolds, and the other consisting of the 2000nm and 4000nm scaffolds (Figure 4-5). The flow cytometry data shows similar groupings across the CD3+/CD3- split, CD4+ T Helper cell, CD4-CD8- T cell, CD14+ monocyte and CD56+ NK cell sub populations (Figure 3-15). Of these cell types, monocytes showed the most significant changes (almost 60% more on the higher diameter grouping than the lower diameter grouping).

This has important implications given the link between macrophages, inflammation and biomaterial outcomes. When the identities of the proteins that define the differences in corona on each diameter grouping are considered, the data becomes even more interesting. Five of the proteins are directly related to the complement cascade, an important chemoattractant for monocytes and macrophage differentiation. These proteins are relatively increased on the 300nm and 1000nm scaffolds which showed less monocyte adhesion. This suggests that there is another factor, in addition to the different composition, influencing monocyte binding, potentially the spatial arrangement induced by different diameters or a difference in the conformation of these proteins induced on the different surfaces of electrospun scaffolds. The larger diameters may provide large enough fibres to support monocytes while they sense out cites for adhesion not falling through the scaffold like on smaller fibres, acting as a net with a resultant increased adhesion. *In vivo* invasion would occur in a different perfusion environment than the seeding model used in this experiment potentially limiting extrapolation. If, however, larger fibres are important for facilitating monocyte attachment and invasion, given monocytes are much smaller than fibroblasts (12µm and round, compared to 100µm long and up to 30µm wide), larger fibres may be important to facilitate monocyte

attachment if biomaterials are to form an immunomodulatory role with deliberately tailored biophysical properties.

4.7.3 Electrospun scaffold biological fluid functionalisation effects on tendon fibroblast and PBMC populations

The response of tendon fibroblasts seeded on electrospun scaffolds is a holistic reaction to both biophysical and biochemical stimuli. Different fibre diameters, and their corresponding coronas, were unable to manipulate tendon fibroblast biology sufficiently *in vitro* to suggest such a modification in an implanted biomaterial would result in significant changes to *in vivo* outcomes. From the literature however, we know fibroblasts from diseased tendon are responsive to other cues, particularly inflammatory stimuli [40,55], and must have an ability to react if given the right stimulation. Accordingly, finding different mechanisms to influence tendon fibroblast biology may be possible.

Scaffold functionalisation with bioactive molecules is one approach. Direct incorporation of bioactive molecules during the production process of scaffolds raises barriers to regulation and development. However, pre-adsorbing biomaterials in fluids to modify corona formation at the time of implantation could induce different coronas with subsequent effects on tendon fibroblast function. As any surgically implanted biomaterial will be invaded by PBMCs before fibroblast infiltration, the effects of biological fluid functionalisation on PBMCs must also be tested. This is important as the tendon response to an implanted biomaterial will be a function of all cell populations and their interactions with the biomaterial's biochemical and biophysical stimuli. This section will firstly review more practical aspects of using biological fluids to functionalise electrospun scaffolds. The focus then shifts to the relationship between tendon fibroblasts and functionalised fibres. The following section explores the same relationship with PBMCs. The section concludes by examining more detailed concepts related to corona formation and future work.

Any fluid used to functionalise a biomaterial must be affordable, available and acceptable to patients and surgeons. Serum, plasma, blood and synovial fluid treatments, as autologous treatments taken at the time of surgery, fulfil these criteria. These fluids induced biologically distinct coronas on 1000nm aligned electrospun scaffolds with significant differences in nearly 10% of the proteins detected in the coronas formed on electrospun fibres.

There was minimal difference between the neat serum and plasma samples prior to scaffold treatment. This translated into very similar corona compositions in fluids functionalised with these 2 fluids. The coronas were, however, distinct from the original fluids. This suggests the adsorbed corona creates a novel protein niche from each fluid type in a specific manner according to the fluid. Blood as an untreated fluid is not compatible with the mass spectrometry set up used in this thesis so cannot be compared in the same way.

Within a fluid type (serum, plasma or blood), the induced coronas from 3 individual donors were very similar. This reliability is important if such functionalisation using a fluid type is to be used clinically. In contrast, the synovial fluids and coronas formed from synovial fluids were much more variable. Consequently, the use of synovial fluids as an augmentation strategy to functionalise biomaterials is likely to elicit more inconsistent cell-material interactions than blood, serum or plasma pre-treatment limiting potential applications.

The 3 donors used in these experiment were undergoing treatment for knee osteoarthritis with synovial fluid isolated from the osteoarthritic knees at the time of surgery. This means the synovial fluid may comprise inflammatory signals or even inflammatory cells from a diseased joint, potentially perpetuating a compromised immune state upon implantation. This would also be true of synovial fluid isolated from diseased shoulder joints undergoing treatment for rotator cuff tears. However, whilst both inflammatory conditions, there is likely to be differences in the cytokine and fluid composition between the two diseased joint fluids.

The response to pre-adsorption in healthy synovial joint fluid may be significantly different and should be tested as synovial fluid from uninflamed joints may provide molecular cues to reduce inflammation and promote healing. However, access to such healthy synovial fluid would require accessing another joint at the time of surgery, increasing chances of post-operative morbidity and raising patient concerns. Furthermore, the amount of synovial fluid in healthy joints is limited and may be unreliable as a treatment adjunct.

Functionalisation of electrospun scaffolds with serum, plasma, blood and synovial fluid did not impact upon attachment of tendon fibroblasts isolated from healthy or diseased tendon. Again, however, fibroblasts from diseased tendon showed the same significantly reduced attachment compared to fibroblasts from healthy tendon. Biological fluid functionalisation did, however, have significant effects on the metabolic activity of tendon fibroblasts from diseased tendon. After 4 and 7 days culture, the activity of fibroblasts on serum and plasma adsorbed fibres was higher than the activity on blood, synovial fluid and uncoated control fibres. This grouping of serum and plasma induced metabolic activity replicates the grouped protein corona composition of serum and plasma adsorbed scaffolds.

The gene expression response of the tendon fibroblasts from diseased tendon was again markedly different compared to fibroblasts from healthy tendon (Figure 4-10). However, within each phenotype, biological fluid treatment failed to induce significant differences in fold changes in gene expression after 7 days culture. Whilst not significant, culture on serum, plasma and blood adsorbed scaffolds, induced more differences in gene expression compared to uncoated scaffolds suggesting an effect of functionalisation. Comparison to synovial fluid is less valid, given the considerable variation between donors, as discussed.

Whilst only a 7 day culture period, functionalisation of electrospun fibres has led to differences in tendon fibroblast response. When compared with earlier results, the effects on metabolic activity and gene expression from biological fluid functionalised fibres is greater

than the effects of altered fibre diameter. This suggests fluid functionalisation may provide a greater stimulus to influence tendon fibroblast function *in vivo* than changes in fibre diameter.

PBMCs were also responsive to differences in protein corona composition formed through biological fluid adsorption. The gene expression response to biological fluid functionalised fibre scaffolds showed a significant difference compared to scaffold-naïve PBMCs and PBMCs seeded on uncoated scaffolds (Figure 4-11 (A)). Within the 4 fluid types, only *IL12B* expression was significantly affected, with a decrease in expression on serum and plasma fibres but an increase on blood and synovial fluid samples. Again, we see a similar cell response between serum and plasma scaffolds, consistent with the similar protein coronas induced by these fluids. IL-12 is produced from activated macrophages to induce Th1 cells [301]. Increases in *IL12* production on blood and synovial fluids coronas could be an early indicator of a biasing of PBMC responses to a macrophage led inflammatory reaction.

Flow cytometry revealed significant differences in PBMC subpopulation attachment to electrospun scaffolds functionalised with different fluids. Again, a similar response was evident between serum and plasma treated scaffolds, compared to blood and synovial fluid treated fibres. Specifically, serum and plasma coated samples induced greater monocyte attachment. The increase in monocyte attachment on serum and plasma treated fibres could be significant for influencing the local response to implanted scaffolds, depending on where these monocytes differentiate to on the M1 or M2 macrophage spectrum. Biasing this population towards an M2 spectrum may help lay the foundation for a favourable biomaterial-immune response, improved resolution, as well as relationships with other cell populations involved in tendon healing [302]. Future work should specifically investigate this monocyte sub-population in detail, looking into markers of activation and cytokine production.

Common to all these assessments of the protein corona is the complexity of this adsorbed interface. In these experiments, wash steps have deliberately tried to remove unbound protein. In reality on top of this bound corona sits a layer of other protein and molecular species, termed the soft corona. It is unknown whether the hard corona or soft corona are more influential in determining cell outcomes. In this thesis, all scaffolds used for cell response as well as for corona assessment underwent the same initial washing so this should not be a major factor in data interpretation and comparison between experiments. Whilst less sensitive silver stains on proteins from the wash steps (data not included) showed no obvious differences to each other between these layers, mass spectrometry could be performed to characterise these layers and evaluate their relative contribution to tendon fibroblast and PBMC response. Cross linking of the adsorbed proteins could reveal inferences about the spatial arrangement of proteins and sub structure formation. This cross linking work can also give information about the conformation of proteins. This is important as biological activity is a function of conformation and concentration. Work has commenced on optimising a cross-linked mass spectrometry protocol to allow generation of this data.

Future work could also explore how the protein corona forms on a single scaffold type formed using extremes of the production process. It is possible to manufacture a 1000nm aligned scaffold using multiple combinations of parameters. In this study 8% solution was electrospun at 0.5ml/hr, 7kV, 1500rpm. Within the setup outlined in Chapter 2, for proof of principle (data not included) it has been possible to produce consistent scaffolds with the same alignment and diameter using a 16% PDO solution with 100ppm pyridine, a 12% solution at 0.2ml/hr, a 10% solution at 11kV and 2500rpm collector speed, amongst other combinations. Characterisation of how these changed electrospinning parameters effect the hydrophobicity, charge and the subsequent corona formation may give insight into which properties could be used to selectively bind protein corona components form a particular biological fluid. This research could also have regulatory implications. Establishing the importance of surface

property changes and corona formation may lead to the need for increased compliance testing of these surface properties during production for clinical use.

4.8 Conclusions

Electrospun scaffolds of different diameters result in distinct protein corona formation upon incubation with human serum. This differential, specific binding may be a result of the topography of the scaffold, the surface properties of the scaffold or both. The greatest differences in protein composition were induced on the 300nm scaffolds. These findings suggest tendon fibroblast and PBMC responses cannot be attributed to solely fibre diameter changes, but also protein adsorption differences.

Functionalisation of electrospun fibres through biological fluid adsorption induces significant differences in corona composition. These in turn induce changes in the metabolic activity and gene expression of tendon fibroblasts isolated from diseased tendon. Fibroblasts isolated form healthy tendon show much less variation in response to these corona biochemical stimuli.

Functionalisation through corona formation has important effects on PBMC subpopulation attachment to electrospun biomaterials. Serum and plasma adsorbed scaffolds were able to induce significantly higher monocyte adherence than other fluids or control samples.

Protein corona composition can have effects on tendon fibroblast and PBMC cell populations. PBMCs are highly sensitive to these changes, opening a potential novel pathway to host-material response through immunomodulation in addition to tendon fibroblast support.

What was known	What this adds
Upon interaction with biological fluids, biomaterials adsorb a protein corona and associated molecules. The composition of this corona can influence cell biology through changes in protein concentration and protein conformation.	Electrospun scaffolds with different diameters promoted specific adsorption of protein species from serum, leading to significant alterations in the composition of the bound corona. This response could be due to the spatial arrangement of the fibres or due to altered surface properties deriving from alterations in the electrospinning parameters.
Functionalisation of biomaterials with bioactive molecules induces altered cell function. Inclusion of a bioactive molecule raises regulatory challenges.	The protein corona can be greatly influenced by treatment with different biological fluids. This altered corona can have significant effects on tendon fibroblasts and PBMCs populations, particularly PBMC sub-population attachment and gene expression.
The foreign body response to biomaterials can promote chronic inflammation, resulting in fibrosis rather than tissue healing.	Functionalisation with autologous blood components may offer an immunomodulatory mechanism to better direct the initial immune and foreign body response towards healing, particularly of monocyes.

Chapter 5 Discussion

5.1 Overview

This section will start by reviewing the aims and hypotheses set out at the beginning of this thesis. The discussion will then revisit the significance of rotator cuff tears and the requirement for novel biomaterials tailored for tendon tissue to improve surgical repair outcomes. The remaining discussion will explore how the findings in this thesis contribute to the development of such materials. This will centre around the fabrication of electrospun scaffolds, adsorbed protein coronas and the response of tendon fibroblast and PBMC cell populations.

5.2 Thesis aims and hypotheses

The overarching aim of this thesis was to identify key scaffold parameters that could influence tendon cell populations to improve the biomaterial driven repair of torn rotator cuff tendons. To achieve this, we first aimed to generate a range of reproducible, biomimetic electrospun scaffolds that varied in fibre diameter and fibre alignment. To investigate how these biophysical properties could improve tendon healing, the biological response of key cell populations involved in tendon healing, namely tendon fibroblasts and peripheral blood mononuclear cells (PBMCs), were assessed. Furthermore, the effect of electrospun scaffold biological fluid functionalisation on tendon fibroblast and PBMC populations was investigated.

The key aims and hypotheses, as outlined in Chapter 1, are:

5.2.1 Aims

1. Generate a range of biomimetic scaffolds to approximate different hierarchical levels of tendon structure to provide biophysical cues similar to native tendon ECM.
2. Compare and contrast the response of fibroblasts from healthy and diseased tendon to the same biomimetic scaffolds.
3. Determine if a particular scaffold type provides biophysical cues to promote tendon fibroblasts from diseased tendon to adopt a profile more similar to fibroblasts from healthy tendon.
4. Investigate the attachment and response of PBMCs to biomimetic scaffolds to determine if scaffold types influence inflammatory response.
5. Investigate whether functionalisation of biomaterials through biological fluid exposure can modify the PBMC and tendon fibroblast response to scaffolds.

5.2.2 Hypotheses

1. Tendon fibroblast populations will attach, proliferate and produce more tendon matrix on electrospun fibres approximating those of native collagen fibrils and fibres.
2. Diseased tendon fibroblasts will revert to a more 'healthy' phenotype as assessed by changes in gene expression favouring tendon matrix production and reduced inflammation when exposed to biomimetic biophysical cues.
3. Peripheral blood mononuclear cells will demonstrate increased expression of inflammatory genes when cultured on electrospun fibres not replicating native ECM components.
4. Functionalisation of electrospun fibres through adsorption with biological fluids will moderate tendon fibroblast and PBMC attachment and gene expression.

5.3 The significance of rotator cuff tendon tears

Rotator cuff tendon tears cause considerable pain and disability to patients, utilise limited surgical resources and place a significant economic burden on health systems [1]. The magnitude of these impacts is only set to increase with an ageing population [6] expecting effective medical treatments [13,14]. Presently, there is no prevention strategy for rotator cuff tears, nor is there an early intervention which can prevent progression of rotator cuff disease or tear size. As the understanding of rotator cuff tendon disease pathophysiology expands, these may develop in time. However, for the thousands of people currently undergoing surgery annually, a 40% failure rate within 12 months of operating is unacceptable [8]. Even with advances in surgical technique and biomaterials over the last 30 years, patients still face the same poor surgical outcomes, operative risks and rehabilitation periods [12], despite the increasingly significant investment for each operation [7].

Rotator cuff repair outcomes could be improved in a number of ways. We could stratify patients to identify those more likely to receive a lasting benefit from the operation [303]. Operating on those who are most likely to benefit from current surgical best practice, will reduce unnecessary risk and health care expenditure. It will not, however, help the more than 60% of patients suffering from the pain and disability of a torn rotator cuff deemed unsuitable for surgical repair. To help these patients, a novel range of biomaterials and treatment strategies must be developed to help guide tendon tissue repair and regeneration.

A biomaterial for rotator cuff repair must be safe, effective, affordable and acceptable to patients [120]. Given the lack of clinical success of current biomaterials for tendon repair, novel materials must do more than provide mechanical support to the repair site as healing progresses [93,96,102]. Biomaterials must employ biophysical and biochemical properties to regulate cell function [132] and degrade at a rate matching tissue formation to enable appropriate tissue maturation and remodelling of the deposited tendon tissue [67,103]. This is a complex set

of requirements requiring a deliberate design process engaging biological, engineering and clinical principles.

The biomaterials commercially available for tendon repair have, however, all been repurposed from other tissue types and clinical uses. This repurposing has occurred without consideration of the specialised requirements for successful structural and functional repair of tendon [100,101,244]. The incongruity between biomaterial design and clinical use is reflected in the persistent high failure rates of rotator cuff repair and lack of improvement in surgical outcomes despite new iterations of surgical scaffolds [12].

5.4 The potential of electrospun scaffolds as biomaterials for rotator cuff repair

Electrospun materials hold considerable promise as a novel biomaterials technology for tendon repair. Electrospun fibres can replicate the biological structures of native tendon ECM, in particular the alignment and hierarchical divisions of collagen structure. The biophysical cues provided by biomimetic structures are biologically powerful stimuli, controlling biological processes ranging from stem cell differentiation [133,138] through to tendon fibroblast ECM deposition [242]. This can occur through direct effects as well as through epigenetic changes. Such epigenetic changes are less well characterised but potentially important tools to ensure more lasting changes in cell populations involved in biomaterial interaction at the site of implantation [133, 304, 305].

Electrospun fibres can be functionalised with biologically active molecules [172] or topographical features [204,205] to further influence cell behaviour. Furthermore, they can have super-structural elements to facilitate cell-material interaction including pores to allow cell invasion [211] and porosity to allow matrix deposition [208,209]. This potential biological activity and the ease of fabrication, has seen development of a number of electrospun materials for

applications in the repair of different tissues including, bone [156], cardiac muscle [154], cornea [152], and nerve tissue [306]. However, large, well-designed clinical trials of these materials are needed to prove the promise of biomimetic electrospun materials and demonstrate superiority over other types of biomaterials.

Developing and testing a novel biomaterial for rotator cuff repair is challenging. Presently, there are no accepted *in vitro* or *in vivo* criteria or metrics with which to determine the performance of a biomaterial designed for use in rotator cuff tear repair. Furthermore, the correlation between *in vitro* and *in vivo* outcomes remains unexplored and unproven. This is complicated by an incomplete understanding of the biology of rotator cuff disease and of healthy tendon. Historically, attempts have focused on using scaffolds to structurally augment repair. Where biological augmentation has been considered the target cell population has been tendon fibroblasts. The focus on tendon fibroblasts is driven by their ability to synthesise ECM, replacing that of damaged tendon. Using scaffolds to effect tendon fibroblasts assumes they are responsive to scaffold based cues. Of concern, the ability of tendon fibroblasts from diseased tendon to respond to biomaterials has not been comprehensively evaluated. This is true of both older generations of biomaterials adopted into use for rotator cuff repairs, and for newer materials under development and reported in the literature.

The results from this thesis suggest the tendon fibroblast reaction to biophysical cues alone may not be sufficient to exact a difference in end stage tendon disease healing. With an increased appreciation of the role of inflammation and dysregulated resolution in tendinopathy [55,69,307], biomaterials may be able to adopt an immunomodulatory role in order to help 'reset' the tissue response from chronic inflammation and fibrosis towards tendon repair. However, in accepting that more than one cell type contributes to the tissue response to an implanted biomaterial, the effect of a biomaterial must be tested against all contributing cell populations. Additionally, the significant cross-talk between tendon fibroblasts,

macrophages, and endothelial cells, means the local response to a biomaterial implant is synergistic and needs to be considered in a co-ordinated manner, not in isolation.

This thesis deepens the understanding of the utility of electrospun biomaterials in tissue repair. Results have established that PDO, a polymer with a long history of safe use in biomedical applications, can be electrospun to create homogenous scaffolds in a reproducible fashion. However, the effects of both supplier and, critically, batch variation from the same supplier introduce variability into the electrospinning process. Storage conditions of PDO resin further increase variability. This thesis has shown that these effects can be controlled for through minor changes in electrospinning parameters. The effects of these minor changes may induce differences in surface material properties which alter the concentration or conformation of adsorbed proteins. In this thesis, deliberate changes in electrospinning parameters to change fibre diameter resulted in changes in the adsorption of only 11 proteins. It is likely that the subtle changes in electrospinning parameters to account for batch and storage effects would have less impact on the number of proteins bound at different intensities. However, the biological consequences of altered protein concentrations, and potentially conformations, could be significant even at minor levels.

Beyond tuning biophysical properties alone, it has been shown that altering charge and surface chemistry can functionalise scaffolds to modulate protein and cell attachment [233-235]. Deliberately changing the charge and surface chemistry of a specific scaffold could further functionalise the basal electrospun scaffold bioactivity. In order to achieve this more specific analysis of electrospinning parameter effects on scaffolds, protocols must be developed to allow accurate assessment of local mechanical properties, hydrophobicity and charge on electrospun fibre materials ranging into the hundreds of nanometres.

This thesis identifies pyridine as a simple adjunct to scaffold manufacture that induces significant effects on electrospinning of PDO solutions. Pyridine reduces fibre diameter while

preserving alignment and does not induce cytotoxicity. It also improves the stability of electrospinning at low PDO concentrations enabling more consistent electrospinning, improving both scaffold homogeneity and the duration stable electrospinning of low diameter PDO fibres can be maintained. Improved stability and scaffold homogeneity is a significant step to achieve in upscaling from laboratory production to meet stringent clinical production criteria. This research has been submitted for publication in conjunction with other researchers from the Carr group (Polymer, submitted).

5.5 Biophysical parameters of electrospun fibre scaffolds can regulate cell biology but this regulation is dependent on cell type and cell disease state

Electrospun fibres are intrinsically bioactive, inducing increased metabolic activity, morphological transformations and gene expression changes from tendon fibroblasts, as well as attachment effects and gene expression differences from PBMCs. Whilst, the literature around tendon fibroblast responses to fibrous scaffolds is contradictory, findings in this thesis are similar to previous descriptions, including aligned fibres (compared to random fibres) promoting tendon fibroblast proliferation [238], altering matrix gene expression [236,242] and inducing a more elongated morphology of tendon fibroblasts [238-240]. The effects of fibre diameter were less consistent with previous literature but this may be related to the range of fibres tested in the literature being more variable (ranging from tens of nanometres to tens of micrometres) than a discrete, more definable aligned or random characteristic. Fibre diameters used in this study did not have as significant effects on healthy fibroblast function as previously reported [140], nor did different diameters induce markedly different gene expression responses in this study unlike some reports [140,243]. These findings go against the

hypothesis that biomimetic fibre diameters will induce greater responses in tendon fibroblast attachment, proliferation and matrix gene expression.

The comparison of tendon fibroblasts derived from healthy and diseased tendon in response to biomaterials contributes new information to the literature. There is only one previous study, also from the Carr group, which compares the response of these two cell populations [289]. This study does not however look at differences in response to fibre alignment or diameter but rather the density of electrospun fibres. In general, the findings of this thesis suggest tendon fibroblasts isolated from diseased and healthy tendon are minimally responsive to the changes in fibre diameter over the tested range. More interestingly, and importantly for biomaterial development, is that the responses of these fibroblasts populations to the same biophysical stimuli are distinctly different. Demonstrating the difference in response to biomaterials raises questions about *in vitro* biomaterial evaluation practices. Biomaterials being developed for rotator cuff repair are going to be implanted into diseased rotator cuff tendons, consequently, *in vitro* investigation using tendon fibroblasts from diseased rather than healthy tendon, will increase the likelihood of successful biomaterial translation and concordance between *in vitro* and *in vivo* outcomes.

However, access to tendon fibroblasts from diseased tendon is limited and is only accessible to certain centres. Whilst collaboration and improved awareness of the need for disease-specific testing will assist in generating access to tendon fibroblasts from diseased tendon, the use of such cells still has limitations. Tears are usually classified as small, medium, or large/massive, a categorical system that does not capture the true biological nature of the underlying disease. Additionally, there is a spectrum of donor variability between patients within each class of tear. Development of a model to induce changes in the phenotype of fibroblast from healthy tendon, or a cell line that recapitulates the phenotype of fibroblasts derived from diseased tendon, may generate a more homogenous cell population for initial biomaterial evaluation.

PBMCs are more sensitive to scaffold-based biophysical cues than tendon fibroblasts, perhaps best shown by the differences in cell attachment for PBMC sub-populations in response to altered fibre diameters. This sensitivity of PBMC populations to biophysical cues fits with previous literature [143,266,267,291]. PBMC sensitivity to biomaterial stimuli is understandable from an evolutionary perspective, having evolved as part of the innate immune system to probe and react to foreign materials as a foreign body/infection control mechanism. Given the links between immune response and biomaterial outcomes [42,259,260], the responsiveness of PBMCs to scaffold based cues and dominance in abundance immediately upon implantation, optimising the parameters of an electrospun material to play an immunomodulatory role may be a promising avenue to improve host-material response and ultimately promote tendon healing.

To further examine the immunomodulatory potential of fibre diameter on PBMC behaviour, the monocyte-derived populations must be characterised. Monocyte attachment from experiments in this thesis showed higher attachment with increased fibre diameters. This was not however, a graduated response with the lower (300nm and 1000nm fibres) and higher (2000nm and 4000nm fibres) diameter fibres clustering together. These findings suggest there may be a threshold response of monocytes and possibly other immune cells which could be utilised in biomaterial design.

Having adhered to scaffolds, monocytes will differentiate, initiating the foreign body response. The foreign body response is the immune system attempting to wall off harmful foreign material. As part of this, macrophages fuse to form Foreign Body Giant cells, a cell type known to drive chronic inflammatory states. Higher numbers of monocytes observed on larger diameter fibres could be positive or negative depending on their differentiation into macrophages and what activation phenotype they adopt [259]. There is conflicting research about the effect of fibre diameter on monocyte differentiation and function with reports of smaller fibre diameters promoting both M1 [291] and M2 phenotypes [143,267]. This may be because

of other biophysical [266] and biochemical [263] features of the electrospun fibres contributing to this differentiation.

This thesis did not examine the effects of random fibre alignment on PBMCs. The justification for this approach is that a biomaterial must contain aligned fibres for collagen biomimicry to promote tendon fibroblast responses and guide ECM deposition. However, *in vivo* these responses occur later so a surface coating or sacrificial fibre population could be included to guide the initial immune cell interaction and modulate the early foreign body response before transitioning into a more matrix promoting form. This also applies to fibre diameter, where a short-lived surface coating could be optimised for immune cell response before degrading to expose fibre diameters more amenable to tendon fibroblast function and ECM deposition.

Regulating PBMC and tendon fibroblast function through biomaterials must not be considered in isolation. The tissue response to a biomaterial is a function of the interaction between various cell populations. This thesis has examined tendon fibroblasts and PBMCs separately. An increasing volume of literature has examined the more synergistic effects between immune and stromal populations on biomaterials [74,276]. This is an important area for future development, alongside the incorporation of the angiogenic response [272,273] from endothelial cells and the potential interaction of tendon progenitor stem cells [39].

5.6 Biological fluid adsorption creates unique protein coronas on electrospun scaffolds capable of modulating tendon fibroblast and PBMC-scaffold interactions

Changing fibre diameter altered the adsorption of proteins from biological fluids on to electrospun scaffolds. In this thesis, proteins including important components of the complement cascade, were bound at significantly different levels over the 4 fibre diameters of scaffolds. This means there is not only a spatial difference to how the proteins available for

cell interaction are displayed, but a different protein composition. Furthermore, whilst not explored in this thesis, changes to electrospinning parameters and biophysical parameters can also affect the conformation of the bound proteins. Changes in biomaterial surface have been shown to alter the integrin binding sites of fibronectin with subsequent effects on proliferation and differentiation [224,300]. The protein corona is thus a manipulable biomaterial property which could be used to influence cell-material interactions upon implantation.

One way to manipulate the protein corona composition, without increasing the regulatory barriers, is treatment with different biological fluids that are available at the time of surgery. The different protein coronas formed from serum, plasma, blood and synovial fluid on electrospun scaffolds with identical biophysical properties were able to influence both tendon fibroblast and PBMC activity. These differences were more notable than those induced by biophysically active changes of fibre diameters.

Tendon fibroblasts from diseased tendon showed greater changes in metabolic activity and gene expression to altered protein corona composition than tendon fibroblasts from healthy tendon. In the context of rotator cuff disease, this suggests the protein corona composition has the potential to induce significant biological changes in tendon fibroblast response in conjunction with biophysical cues. This increased sensitivity of tendon fibroblasts from diseased tendon to the protein niche may relate to primed inflammatory signatures. Reports have shown that fibroblasts isolated from patients with tendon disease respond profoundly to inflammatory stimulation compared to fibroblasts derived from healthy tendons [55]. This immune memory is emerging as an important feature of stromal cell populations, not just as an immune system specific response [308]. If an implanted material triggers this inflammatory memory, it may propagate a continued chronic inflammation and fibrosis cycle. Utilising protein adsorption, in addition to biophysical cues, to reduce the stimulation of tendon fibroblasts may help generate a local response more conducive to tendon healing than fibrosis.

The composition of the scaffold protein corona also has direct effects on the immune response, notably altering the relative proportion of monocytes that adhere to scaffold surfaces upon seeding with PBMCs. However, as previously discussed, the differentiation and function of these monocytes needs assessment before these findings can be utilised in biomaterial applications.

The protein corona will also change over the life cycle of an implant with ramifications for cell-material interaction. How long pre-adsorbed corona effects are sustained also needs examination. They may contribute only to the initial PBMC response and not be important for tendon fibroblast interaction for a number of reasons. Firstly, pre-adsorbed biomaterials will be encapsulated within a blood clot, potentially competing with and displacing bound proteins. Secondly, as the fibrin clot is phagocytosed, the interstitial fluid bathing biomaterials imparts a different series of proteins to displace or modify the adsorbed corona. This means by the time tendon fibroblasts invade the material, the corona may be sufficiently altered that the pre-adsorbed proteins no longer remain to influence tendon fibroblast responses. In this case, pre-adsorption can be tailored to maximise effects on immune cell interaction and establishing a beneficial local immune response independent of effects on tendon fibroblast biology. Furthermore, the time taken for a biomaterial to degrade is dependent on the polymer chemistry and scaffold architecture. This degradation will change the surface chemistry and protein adsorption properties of a scaffold. Additionally, cells will also deposit a matrix to replace the polymer, again changing the local protein niche.

This experiment considered interactions with bound proteins, the hard corona. In reality, the interface which cells interact with is more complex with proteins pulling in secondary proteins and molecules to form the soft corona. Assessment of the entire corona, formation and transition over time *in vivo,* must be considered in future research.

5.7 Limitations

The important limitations of each experiment have been discussed in each chapter where appropriate. There are, however, three main limitations to this thesis.

The first limitation is the ability to fully characterise the fabricated biomimetic scaffolds. Whilst the targeted parameters of fibre alignment and fibre diameter were reliably and repeatedly manufactured, other biophysically active aspects of the electrospun scaffolds could not be reliably tested. These include local mechanical properties, hydrophobicity, charge, porosity, pore size and scaffold thickness, all properties capable of effecting cell biology. Not measuring these properties potentially confounds attribution of the observed results to fibre diameter and alignment alone. Measurement of these properties will be needed to ensure longitudinal consistency in experiments and specific quality control criteria for clinical production as manipulation of one biophysical parameter of an electrospun scaffold is likely to affect others.

The second major limitation in this study is the low number of experimental repeats for each experiment. Having triplicates allows for statistical testing but given the heterogeneity of biological samples is often insufficient to formally test hypotheses. A cell line or model may reduce this variability to improve the reliability of initial testing.

Further to donor variation, the effects of cell culture on cell biology are pronounced. This thesis has examined cell interactions with materials in isolation *in vitro*. In reality, biomaterials will be implanted *in vivo,* where cell responses will be dependent on complicated interactions with other cell types, over longer periods, and on biomaterials that are degrading with alterations in topography and protein interface. These effects will introduce significant differences between biomaterial outcomes observed *in vitro* from what are seen *in vivo*.

This thesis also only characterised changes in gene expression, not protein expression. Given the effects of biophysical epigenetic regulation occur at both the nuclear and cytoplasmic level,

biophysical effects could have greater impacts on the translation of gene to functional protein than those detected in upstream gene expression analysis.

The difference between tendon fibroblast response to biophysical stimuli depending on isolation from diseased or healthy tendon also has caveats. Firstly, healthy tendon was derived from hamstring, not rotator cuff tendon. Differences in cell phenotype between tendon locations could explain some of the observed difference. Secondly, healthy tendon is isolated from younger patients with potential phenotypic differences compared to older tendon, not disease state. However, consistent access to tendon from elderly rotator cuff patients without rotator cuff diseases is not possible, consequently this cannot be used as a control tissue accounting for location and age differences.

5.8 Future work

Developing a biomaterial to improve patient outcomes for rotator cuff repair will involve coordinated collaboration across all disciplines of medical research. An area of particular focus should be developing a set of *in vitro* metrics which can be used to predict *in vivo* outcomes across research groups. Currently, research groups use a variety of methods to evaluate innovative biomaterials, reporting on cell attachment, proliferation, gene and protein expression without knowing what a desired response in each outcome is, or at which time point these evaluations should occur.

Related to this, is the choice of appropriate cell types with which to test these chosen metrics. Evaluation of biomaterials against tendon fibroblasts alone is inappropriate given the sensitivity of PBMC and other cell populations to biophysical properties and their contributions to host-material response and long term healing outcomes. Development of a cell line or model to stimulate fibroblasts towards a phenotype resembling fibroblasts from

diseased rotator cuff tendons is important to ensure the results of *in vitro* work are generalizable to *in vivo* applications.

The communication between all cell populations in diseased tendon that interact with an implanted biomaterial needs to be investigated, particularly with the potential immunomodulatory role of biomaterials. Over the life cycle of an implant, the relative importance of specific cell types to successful tendon repair will change. Furthermore, with a transition from non-degradable to degradable polymer materials, the effects of degradation become important as protein adsorption will change and breakdown products will affect cell-material interaction. Future work must consider how cell-material interaction changes through the life cycle of the biomaterial and how this can be optimised to promote tendon healing.

5.9 Implications of this thesis

This thesis contributes to the growing field of biomaterials for rotator cuff tendon repair, and in a broader context, tissue engineering and regenerative medicine.

The main implication of this thesis is that the disease phenotype of tendon fibroblasts plays a significant role in how fibroblasts respond to biomaterial stimuli. Continuing to evaluate biomaterials for tendon repair with fibroblasts derived from healthy tendon will not give an accurate depiction of how a material will function upon implantation into diseased rotator cuff tendon *in vivo*.

PBMCs showed greater sensitivity to biophysical stimuli than tendon fibroblasts. This sensitivity opens the possibility of an immunomodulatory role for electrospun biomaterials in rotator cuff tendon disease. This is an increasingly important aspect of biomaterial research given the importance of breaking the chronic inflammatory cycle that perpetuates rotator cuff tendon disease.

Functionalisation of biomaterials with biological fluids also holds potential to further modulate the tendon fibroblast and PBMC interactions to biophysical stimuli.

Electrospun materials can be fabricated and functionalised to influence the biology of cell populations found in diseased tendon following scaffold implantation, including fibroblasts and PBMCs, offering an ability to co-ordinate synergistic responses to improve tendon healing.

5.10 Summary

The need to develop a biomaterial to improve rotator cuff tear surgical outcomes is acute. Electrospun biomaterials are a promising technology to meet this burden as they are biomimetic structures capable of providing biophysical cues to influence local cell biology. Electrospun materials are also well suited to surface functionalisation for further targeting of cell biology through integrated biochemical stimuli. Improved understanding of the pathophysiology and inflammatory nature of rotator cuff tendinopathy will allow tuning of these properties in directions to target the appropriate cell types with appropriate stimuli at appropriate time points through the healing process after implantation.

Collaboration to define common *in vitro* metrics which correlate with *in vivo* outcomes will increase the speed and chance of successful translation of tendon biomaterials to have clinical impact for patients. Further evaluation of the effects of biomaterial degradation, immune-fibroblast interactions and the responses of tendon-progenitor stem cell and endothelial cell populations will paint a more complete picture of the tendon-material response and important aspects of tendon healing.

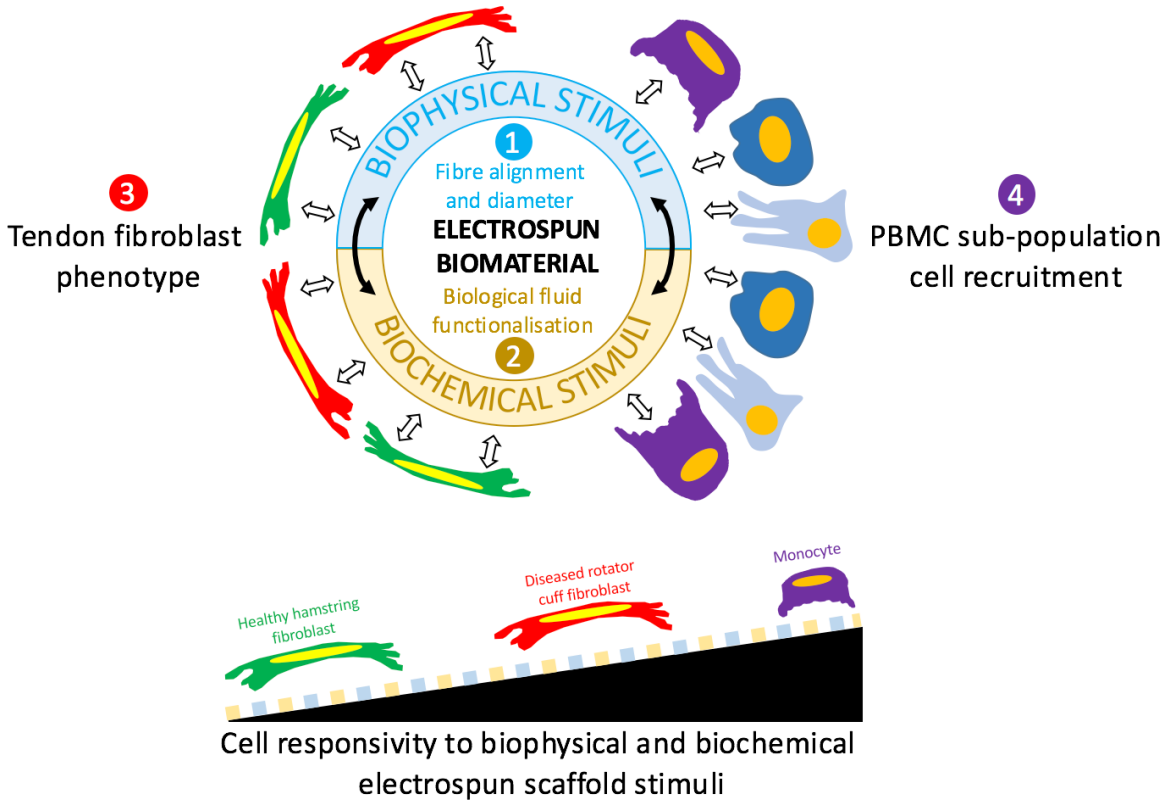


Figure 5-1. Rotator cuff tendon response to implanted electrospun biomaterials is dependent on biophysical cues, biochemical stimuli and multiple cell populations.

The response of rotator cuff tendon to an implanted material is a global response from multiple cell populations to multiple stimuli, all of which will change over the life cycle of the implant. This thesis has explored how biophysical parameters ((1) fibre alignment and fibre diameter) and biochemical stimuli ((2) biological fluid functionalised protein coronas), affect tendon fibroblast and PBMC populations. This thesis has also demonstrated that tendon fibroblast responses to biomaterial stimuli are dependent on their origin from healthy hamstring or diseased rotator cuff tendon (3). Furthermore, the results show that manipulation of the biophysical and biochemical stimuli of electrospun materials can alter PBMC recruitment, particularly monocytes (4).

Future work should consider the cross-talk between cell populations and how this moderates response to biomaterial stimuli, the effects of biomaterial degradation on local cell and protein interaction, and further characterise monocyte differentiation and activation, as well as other immune cell populations including T Cell, NK cell and dendritic cell responses.

Chapter 6 References

1. Aurora, A., McCarron, J., Iannotti, J. P. & Derwin, K. Commercially available extracellular matrix materials for rotator cuff repairs: State of the art and future trends. *J. Shoulder Elb. Surg.* **16,** S171–S178 (2007).

2. Judge, A., Murphy, R. J., Maxwell, R., Arden, N. K. & Carr, A. J. Temporal trends and geographical variation in the use of subacromial decompression and rotator cuff repair of the shoulder in England. *Bone Joint J.* **96–B,** 70–74 (2014).

3. Thangarajah, T. *et al.* Augmentation of Rotator Cuff Repair With Soft Tissue Scaffolds. *Orthop. J. Sport. Med.* **3,** 2325967115587495 (2015).

4. Minagawa, H. *et al.* Prevalence of symptomatic and asymptomatic rotator cuff tears in the general population: From mass-screening in one village. *J. Orthop.* **10,** 8–12 (2013).

5. Kohl 3rd, H. W. *et al.* The pandemic of physical inactivity: global action for public health. *Lancet* **380,** 294–305 (2012).

6. Vos, T. *et al.* Years lived with disability (YLDs) for 1160 sequelae of 289 diseases and injuries 1990-2010: A systematic analysis for the Global Burden of Disease Study 2010. *Lancet* **380,** 2163–2196 (2012).

7. Thorpe, A., Hurworth, M., O'Sullivan, P., Mitchell, T. & Smith, A. Rising trends in surgery for rotator cuff disease in Western Australia. *ANZ J. Surg.* **86,** 801–804 (2016).

8. Carr, A. *et al.* Effectiveness of open and arthroscopic rotator cuff repair (UKUFF). *Bone Joint J.* **99–B,** 107–115 (2017).

9. Galatz, L. M., Gerstenfeld, L., Heber-Katz, E. & Rodeo, S. A. Tendon regeneration and scar formation: The concept of scarless healing. *J. Orthop. Res.* **33,** 823–831 (2015).

10. Sugaya, H., Maeda, K., Matsuki, K. & Moriishi, J. Repair integrity and functional outcome after arthroscopic double-row rotator cuff repair. A prospective outcome study. *J. Bone Joint Surg. Am.* **89,** 953–960 (2007).

11. Bayliss, L. E. *et al.* The effect of patient age at intervention on risk of implant revision after total replacement of the hip or knee: a population-based cohort study. *Lancet* **389,** 1424–1430 (2017).

12. McElvany, M. D., McGoldrick, E., Gee, A. O., Neradilek, M. B. & Matsen, F. A. Rotator Cuff Repair: Published Evidence on Factors Associated With Repair Integrity and Clinical Outcome. *Am. J. Sports Med.* **43,** 491–500 (2014).

13. Sullivan, R. *et al.* Delivering affordable cancer care in high-income countries. *Lancet Oncol.* **12,** 933–980 (2011).

14. Kim, M., Blendon, R. J. & Benson, J. M. How interested are Americans in new medical technologies? A multicountry comparison. *Health Aff.* **20,** 194–201 (2001).

15. McPherson, E. J., Friedman, R. J., An, Y. H., Chokesi, R. & Dooley, R. L. Anthropometric study of normal glenohumeral relationships. *J. Shoulder Elb. Surg.* **6,** 105–112 (1997).

16. HUMAN. BioDigital Human Visualization Platfrom. (2018). Available at: https://human.biodigital.com. (Accessed: 1st June 2018)

17. Yamamoto, A. *et al.* The impact of faulty posture on rotator cuff tears with and without

symptoms. *J. Shoulder Elb. Surg.* **24,** 446–452 (2015).

18. Keating, J. F., Waterworth, P., Shaw-Dunn, J. & Crossan, J. The relative strengths of the rotator cuff muscles. A cadaver study. *J. Bone Joint Surg. Br.* **75,** 137–140 (1993).

19. Kannus, P. Structure of the tendon connective tissue. *Scand. J. Med. Sci. Sport.* **10,** 312–320 (2000).

20. Franchi, M., Trire, A., Quaranta, M., Orsini, E. & Ottani, V. Collagen structure of tendon relates to function. *ScientificWorldJournal.* **7,** 404–420 (2007).

21. Shoulders, M. D. & Raines, R. T. Collagen structure and stability. *Annu. Rev. Biochem.* **78,** 929–958 (2009).

22. James, R., Kesturu, G., Balian, G. & Chhabra, A. B. Tendon: biology, biomechanics, repair, growth factors, and evolving treatment options. *J. Hand Surg. Am.* **33,** 102–112 (2008).

23. O'Brien, M. Structure and metabolism of tendons. *Scand. J. Med. Sci. Sports* **7,** 55–61 (2007).

24. Riley, G. The pathogenesis of tendinopathy. A molecular perspective. *Rheumatology (Oxford).* **43,** 131–42 (2004).

25. Harvey, R. *Lippincott Illustrated Reviews: Biochemistry, 7th edition*. (Philadelphia : Wolters Kluwer Health, [2011] ©2011, 2011).

26. Kjaer, M. Role of extracellular matrix in adaptation of tendon and skeletal muscle to mechanical loading. *Physiol. Rev.* **84,** 649–698 (2004).

27. O'Brien, M. Structure and metabolism of tendons. *Scand. J. Med. Sci. Sports* **7,** 55–61 (1997).

28. Wang, J. H.-C. Mechanobiology of tendon. *J. Biomech.* **39,** 1563–82 (2006).

29. Dvir, T. *et al.* Nanowired three dimensional cardiac patches. *Nat. Nanotechnol.* **6,** 720–725 (2011).

30. Chansky, H. A. & Iannotti, J. P. The vascularity of the rotator cuff. *Clin. Sports Med.* **10,** 807–822 (1991).

31. Clark, J. M. & Harryman, D. T. 2nd. Tendons, ligaments, and capsule of the rotator cuff. Gross and microscopic anatomy. *J. Bone Joint Surg. Am.* **74,** 713–725 (1992).

32. Kastelic, J., Galeski, A. & Baer, E. The Multicomposite Structure of Tendon. *Connect. Tissue Res.* **6,** 11–23 (1978).

33. Frantz, C., Stewart, K. M. & Weaver, V. M. The extracellular matrix at a glance. *J. Cell Sci.* **123,** 4195 LP-4200 (2010).

34. Kalamajski, S. & Oldberg, Å. The role of small leucine-rich proteoglycans in collagen fibrillogenesis. *Matrix Biol.* **29,** 248–253 (2010).

35. Tozer, S. & Duprez, D. Tendon and ligament: development, repair and disease. *Birth Defects Res. C. Embryo Today* **75,** 226–236 (2005).

36. Alexander, S. *et al.* Tenocyte responses to mechanical loading in vivo: A role for local insulin-like growth factor 1 signaling in early tendinosis in rats. *Arthritis Rheum.* **56,** 871–881 (2007).

37. McNeilly, C. M., Banes, A. J., Benjamin, M. & Ralphs, J. R. Tendon cells in vivo form a three dimensional network of cell processes linked by gap junctions. *J. Anat.* **189 (Pt 3,** 593–600 (1996).

38. Thorpe, C. T. *et al.* Aspartic Acid Racemization and Collagen Degradation Markers Reveal an Accumulation of Damage in Tendon Collagen That Is Enhanced with Aging. *J. Biol. Chem.* **285,** 15674–15681 (2010).

39. Bi, Y. *et al.* Identification of tendon stem/progenitor cells and the role of the extracellular matrix in their niche. *Nat. Med.* **13,** 1219–1227 (2007).

40. Dakin, S. G. *et al.* Inflammation activation and resolution in human tendon disease. **7,** 1–14 (2015).

41. Kawamura, S., Ying, L., Kim, H.-J., Dynybil, C. & Rodeo, S. A. Macrophages accumulate in the early phase of tendon–bone healing. *J. Orthop. Res.* **23,** 1425–1432 (2005).

42. Xia, Z. & Triffitt, J. T. A review on macrophage responses to biomaterials. *Biomed. Mater.* **1,** R1-9 (2006).

43. Gaut, L. & Duprez, D. Tendon development and diseases. *Wiley Interdiscip. Rev. Dev. Biol.* **5,** 5–23 (2016).

44. Benjamin, M. *et al.* Where tendons and ligaments meet bone: attachment sites ('entheses') in relation to exercise and/or mechanical load. *J. Anat.* **208,** 471–490 (2006).

45. Liu, R. W., Lam, P. H., Shepherd, H. M. & Murrell, G. A. C. Tape Versus Suture in Arthroscopic Rotator Cuff Repair: Biomechanical Analysis and Assessment of Failure Rates at 6 Months. *Orthop. J. Sport. Med.* **5,** 2325967117701212 (2017).

46. Rothrauff, B. B. *et al.* The Rotator Cuff Organ: Integrating Developmental Biology, Tissue Engineering, and Surgical Considerations to Treat Chronic Massive Rotator Cuff Tears. *Tissue Eng. Part B. Rev.* **23,** 318–335 (2017).

47. Apostolakos, J. *et al.* The enthesis: a review of the tendon-to-bone insertion. *Muscles, Ligaments and Tendons Journal* **4,** 333–342 (2014).

48. Serhan, C. N. & Savill, J. Resolution of inflammation: the beginning programs the end. *Nat. Immunol.* **6,** 1191–1197 (2005).

49. Peacock, E. Physiology of tendon repair. *Am. J. Surg.* **109,** 283–286 (1965).

50. Howell, K. *et al.* Novel Model of Tendon Regeneration Reveals Distinct Cell Mechanisms Underlying Regenerative and Fibrotic Tendon Healing. *Sci. Rep.* **7,** 45238 (2017).

51. Fenwick, S. A., Hazleman, B. L. & Riley, G. P. The vasculature and its role in the damaged and healing tendon. *Arthritis Res. Ther.* **4,** 252 (2002).

52. Gelberman, R. H., Vande Berg, J. S., Lundborg, G. N. & Akeson, W. H. Flexor tendon healing and restoration of the gliding surface. An ultrastructural study in dogs. *J. Bone Joint Surg. Am.* **65,** 70–80 (1983).

53. Voleti, P. B., Buckley, M. R. & Soslowsky, L. J. Tendon Healing: Repair and Regeneration. *Annu. Rev. Biomed. Eng.* **14,** 47–71 (2012).

54. Dyment, N. A. *et al.* Lineage Tracing of Resident Tendon Progenitor Cells during Growth and Natural Healing. *PLoS One* **9,** e96113 (2014).

55. Dakin, S. G. *et al.* Persistent stromal fibroblast activation is present in chronic tendinopathy. *Arthritis Res. Ther.* **19,** 16 (2017).

56. Rees, J. D., Stride, M. & Scott, A. Tendons – time to revisit inflammation. *Br. J. Sports Med.* (2013).

57. Dean, B. J. F., Dakin, S. G., Millar, N. L. & Carr, A. J. Review: Emerging concepts in the pathogenesis of tendinopathy. *Surgeon* **15,** 349–354 (2017).

58. Neer, C. S. 2nd. Impingement lesions. *Clin. Orthop. Relat. Res.* 70–77 (1983).

59. Jeong, J. Y. *et al.* Location of Rotator Cuff Tear Initiation: A Magnetic Resonance Imaging Study

of 191 Shoulders. *Am. J. Sports Med.* **46,** 649–655 (2018).

60. Rathbun, J. B. & Macnab, I. The microvascular pattern of the rotator cuff. *J. Bone Joint Surg. Br.* **52,** 540–553 (1970).

61. Matthews, T. J. W., Hand, G. C., Rees, J. L., Athanasou, N. A. & Carr, A. J. Pathology of the torn rotator cuff tendon. Reduction in potential for repair as tear size increases. *J. Bone Joint Surg. Br.* **88,** 489–495 (2006).

62. September, A. V, Schwellnus, M. P. & Collins, M. Tendon and ligament injuries: the genetic component. *Br. J. Sports Med.* **41,** 241–246 (2007).

63. Harvie, P. *et al.* Genetic influences in the aetiology of tears of the rotator cuff. Sibling risk of a full-thickness tear. *J. Bone Joint Surg. Br.* **86,** 696–700 (2004).

64. Gwilym, S. E. *et al.* Genetic influences in the progression of tears of the rotator cuff. *J. Bone Joint Surg. Br.* **91,** 915–917 (2009).

65. Seitz, A. L., McClure, P. W., Finucane, S., Boardman, N. D. 3rd & Michener, L. A. Mechanisms of rotator cuff tendinopathy: intrinsic, extrinsic, or both? *Clin. Biomech. (Bristol, Avon)* **26,** 1–12 (2011).

66. Glazebrook, M. A., Wright, J. R. J., Langman, M., Stanish, W. D. & Lee, J. M. Histological analysis of achilles tendons in an overuse rat model. *J. Orthop. Res.* **26,** 840–846 (2008).

67. Christensen, B. *et al.* Effects of long-term immobilization and recovery on human triceps surae and collagen turnover in the Achilles tendon in patients with healing ankle fracture. *J. Appl. Physiol.* **105,** 420–426 (2008).

68. Codman, E. A. *The shoulder; rupture of the supraspinatus tendon and other lesions in or about the subacromial bursa.* ([T. Todd Company, printers], 1934).

69. Mosca, M. J. *et al.* Trends in the theory that inflammation plays a causal role in tendinopathy: a systematic review and quantitative analysis of published reviews. *BMJ Open Sport Exerc. Med.* **4,** (2018).

70. Abrams, G. D. *et al.* Association of synovial inflammation and inflammatory mediators with glenohumeral rotator cuff pathology. *J. Shoulder Elb. Surg.* **25,** 989–997 (2016).

71. Cook, J. L., Rio, E., Purdam, C. R. & Docking, S. I. Revisiting the continuum model of tendon pathology: what is its merit in clinical practice and research? *Br. J. Sports Med.* **50,** 1187 LP-1191 (2016).

72. Dean, B. J. F., Gettings, P., Dakin, S. G. & Carr, A. J. Are inflammatory cells increased in painful human tendinopathy? A systematic review. *Br. J. Sports Med.* **50,** 216–220 (2016).

73. Hansen, P. *et al.* Micromechanical properties and collagen composition of ruptured human achilles tendon. *Am. J. Sports Med.* **41,** 437–443 (2013).

74. Stolk, M. *et al.* New insights into tenocyte-immune cell interplay in an in vitro model of inflammation. *Sci. Rep.* **7,** 9801 (2017).

75. Dean, B. J. F., Franklin, S. L. & Carr, A. J. A systematic review of the histological and molecular changes in rotator cuff disease. **1,** 158–166 (2012).

76. Scott, A., Backman, L. J. & Speed, C. Tendinopathy: Update on Pathophysiology. *J. Orthop. Sport. Phys. Ther.* **45,** 833–841 (2015).

77. Arya, S. & Kulig, K. Tendinopathy alters mechanical and material properties of the Achilles tendon. *J. Appl. Physiol.* **108,** 670–675 (2010).

78. Brukner, P. & Khan, K. *Clinical Sports Medicine*. (McGraw-Hill, 2007).

79. Dean, B. J. F. *et al.* Differences in glutamate receptors and inflammatory cell numbers are associated with the resolution of pain in human rotator cuff tendinopathy. *Arthritis Res. Ther.* **17,** 176 (2015).

80. Yamaguchi, K. *et al.* Natural history of asymptomatic rotator cuff tears: a longitudinal analysis of asymptomatic tears detected sonographically. *J. shoulder Elb. Surg.* **10,** 199–203 (2001).

81. Ainsworth, R. & Lewis, J. S. Exercise therapy for the conservative management of full thickness tears of the rotator cuff: a systematic review. *Br. J. Sports Med.* **41,** 200–210 (2007).

82. Serhan, C. N. Resolution Phase of Inflammation: Novel Endogenous Anti-Inflammatory and Proresolving Lipid Mediators and Pathways. *Annu. Rev. Immunol.* **25,** 101–137 (2007).

83. Chechik, O. *et al.* Timing matters: NSAIDs interfere with the late proliferation stage of a repaired rotator cuff tendon healing in rats. *Arch. Orthop. Trauma Surg.* **134,** 515–520 (2014).

84. Chen, M. R. & Dragoo, J. L. The effect of nonsteroidal anti-inflammatory drugs on tissue healing. *Knee Surg. Sports Traumatol. Arthrosc.* **21,** 540–549 (2013).

85. Gialanella, B. & Prometti, P. Effects of corticosteroids injection in rotator cuff tears. *Pain Med.* **12,** 1559–1565 (2011).

86. Green, S., Buchbinder, R., Glazier, R. & Forbes, A. Systematic review of randomised controlled trials of interventions for painful shoulder: selection criteria, outcome assessment, and efficacy. *BMJ* **316,** 354–360 (1998).

87. Dean, B. J. F., Franklin, S. L., Murphy, R. J., Javaid, M. K. & Carr, A. J. Glucocorticoids induce specific ion-channel-mediated toxicity in human rotator cuff tendon: a mechanism underpinning the ultimately deleterious effect of steroid injection in tendinopathy? *Br. J. Sports Med.* **48,** 1620–1626 (2014).

88. Dean, B. J. F. *et al.* The risks and benefits of glucocorticoid treatment for tendinopathy: A systematic review of the effects of local glucocorticoid on tendon. *Semin. Arthritis Rheum.* **43,** 570–576 (2014).

89. Beck, J., Evans, D., Tonino, P. M., Yong, S. & Callaci, J. J. The Biomechanical and Histologic Effects of Platelet-Rich Plasma on Rat Rotator Cuff Repairs. *Am. J. Sports Med.* **40,** 2037–2044 (2012).

90. Ellera Gomes, J. L., da Silva, R. C., Silla, L. M. R., Abreu, M. R. & Pellanda, R. Conventional rotator cuff repair complemented by the aid of mononuclear autologous stem cells. *Knee Surgery, Sport. Traumatol. Arthrosc.* **20,** 373–377 (2012).

91. Carr, A. J. *et al.* Platelet-Rich Plasma Injection With Arthroscopic Acromioplasty for Chronic Rotator Cuff Tendinopathy: A Randomized Controlled Trial. *Am. J. Sports Med.* **43,** 2891–2897 (2015).

92. Hudgens, J. L. *et al.* Platelet-Rich Plasma Activates Proinflammatory Signaling Pathways and Induces Oxidative Stress in Tendon Fibroblasts. *Am. J. Sports Med.* **44,** 1931–1940 (2016).

93. Cole, B. J. *et al.* Arthroscopic rotator cuff repair: prospective functional outcome and repair integrity at minimum 2-year follow-up. *J. shoulder Elb. Surg.* **16,** 579–585 (2007).

94. Moraes, V. Y., Lenza, M., Tamaoki, M. J., Faloppa, F. & Belloti, J. C. Platelet-rich therapies for musculoskeletal soft tissue injuries. *Cochrane Database Syst. Rev.* (2014). doi:10.1002/14651858.CD010071.pub3

95. Youngstrom, D. W., Barrett, J. G., Jose, R. R. & Kaplan, D. L. Functional characterization of

detergent-decellularized equine tendon extracellular matrix for tissue engineering applications. *PLoS One* **8,** e64151 (2013).

96. Smith, R. D. *et al.* The response of tenocytes to commercial scaffolds used for rotator cuff repair. *Eur. Cell. Mater.* **31,** 107–118 (2016).

97. Zimmer. Durable Reinforcement implant consisting of an acellular scaffold of. (2012).

98. Walton, J. R., Bowman, N. K., Khatib, Y., Linklater, J. & Murrell, G. a C. Restore orthobiologic implant: not recommended for augmentation of rotator cuff repairs. *J. Bone Joint Surg. Am.* **89,** 786–791 (2007).

99. Malcarney, H. L., Bonar, F. & Murrell, G. a C. Early inflammatory reaction after rotator cuff repair with a porcine small intestine submucosal implant: a report of 4 cases. *Am. J. Sports Med.* **33,** 907–911 (2005).

100. Zargar, N. & Carr, A. The regulatory ancestral network of surgical meshes. *PLoS One* **13,** e0197883 (2018).

101. Heneghan, C. J. *et al.* Trials of transvaginal mesh devices for pelvic organ prolapse: a systematic database review of the US FDA approval process. *BMJ Open* **7,** (2017).

102. Chaudhury, S., Holland, C., Thompson, M. S., Vollrath, F. & Carr, A. J. Tensile and shear mechanical properties of rotator cuff repair patches. *J. shoulder Elb. Surg.* **21,** 1168–1176 (2012).

103. Galloway, M. T., Lalley, A. L. & Shearn, J. T. The role of mechanical loading in tendon development, maintenance, injury, and repair. *J. Bone Joint Surg. Am.* **95,** 1620–1628 (2013).

104. Shea, K. P. *et al.* Human Tendon Cell Response to 7 Commercially Available Extracellular Matrix Materials: An In Vitro Study. *Arthroscopy* **26,** 1181–1188 (2010).

105. Xu, H. *et al.* Implantation of a porcine acellular dermal graft in a primate model of rotator cuff repair. *J. Shoulder Elb. Surg.* **21,** 580–588 (2012).

106. Ide, J. *et al.* Reconstruction of large rotator-cuff tears with acellular dermal matrix grafts in rats. *J. shoulder Elb. Surg.* **18,** 288–295 (2009).

107. Adams, J. E., Zobitz, M. E., Reach, J. S. J., An, K.-N. & Steinmann, S. P. Rotator cuff repair using an acellular dermal matrix graft: an in vivo study in a canine model. *Arthroscopy* **22,** 700–709 (2006).

108. Lederman, E. S. *et al.* A prospective, multicenter study to evaluate clinical and radiographic outcomes in primary rotator cuff repair reinforced with a xenograft dermal matrix. *J. shoulder Elb. Surg.* **25,** 1961–1970 (2016).

109. Gupta, A. K., Hug, K., Boggess, B., Gavigan, M. & Toth, A. P. Massive or 2-Tendon Rotator Cuff Tears in Active Patients With Minimal Glenohumeral Arthritis: Clinical and Radiographic Outcomes of Reconstruction Using Dermal Tissue Matrix Xenograft. *Am. J. Sports Med.* **41,** 872–879 (2013).

110. Barber, F. A., Burns, J. P., Deutsch, A., Labbe, M. R. & Litchfield, R. B. A prospective, randomized evaluation of acellular human dermal matrix augmentation for arthroscopic rotator cuff repair. *Arthroscopy* **28,** 8–15 (2012).

111. Holzapfel, B. M. *et al.* How smart do biomaterials need to be? A translational science and clinical point of view. *Adv. Drug Deliv. Rev.* **65,** 581–603 (2013).

112. O'Brien, F. J. Biomaterials & scaffolds for tissue engineering. *Mater. Today* **14,** 88–95 (2011).

113. Anderson, J. M. Biological Responses to Materials. *Annu. Rev. Mater. Res.* **31,** 81–110 (2001).

114. Lysaght, M. J., Jaklenec, A. & Deweerd, E. Great expectations: private sector activity in tissue engineering, regenerative medicine, and stem cell therapeutics. *Tissue Eng. Part A* **14,** 305–315 (2008).

115. Langer, R. & Vacanti, J. P. Tissue engineering. *Science (80-.).* **260,** 920–926 (1993).

116. Leeper, N. J., Hunter, A. L. & Cooke, J. P. Stem cell therapy for vascular regeneration: Adult, embryonic, and induced pluripotent stem cells. *Circulation* **122,** 517–526 (2010).

117. Fairchild, P. J. The challenge of immunogenicity in the quest for induced pluripotency. *Nat. Rev. Immunol.* **10,** 868–875 (2010).

118. Beeson, D. & Lippman, A. Egg harvesting for stem cell research: medical risks and ethical problems. *Reprod. Biomed. Online* **13,** 573–579 (2006).

119. Richards, M., Fong, C.-Y., Tan, S., Chan, W.-K. & Bongso, A. An efficient and Safe Xeno-Free Cryopreservation Method for the Storage of Human Embryonic Stem Cells. *Stem Cells* **22,** 779–789 (2004).

120. Stace, E., Dakin, S., Mouthuy, P.-A. & Carr, A. Translating Regenerative Biomaterials Into Clinical Practice. *J. Cell. Physiol.* **231,** 36–49 (2015).

121. Qu, F., Holloway, J. L., Esterhai, J. L., Burdick, J. A. & Mauck, R. L. Programmed biomolecule delivery to enable and direct cell migration for connective tissue repair. *Nat. Commun.* **8,** 1780 (2017).

122. Ignatious, F., Sun, L., Lee, C.-P. & Baldoni, J. Electrospun nanofibers in oral drug delivery. *Pharm. Res.* **27,** 576–588 (2010).

123. Daghighi, S., Sjollema, J., van der Mei, H. C., Busscher, H. J. & Rochford, E. T. J. Infection resistance of degradable versus non-degradable biomaterials: an assessment of the potential mechanisms. *Biomaterials* **34,** 8013–8017 (2013).

124. Guilak, F. *et al.* Control of Stem Cell Fate by Physical Interactions with the Extracellular Matrix. *Cell Stem Cell* **5,** 17–26 (2009).

125. Pashuck, E. T. & Stevens, M. M. Designing regenerative biomaterial therapies for the clinic. *Sci. Transl. Med.* **4,** 160sr4 (2012).

126. Hench, L. L. *New Materials and Technologies for Healthcare.* (Imperial College Press, 2012).

127. Hinderer, S., Layland, S. L. & Schenke-Layland, K. ECM and ECM-like materials — Biomaterials for applications in regenerative medicine and cancer therapy. *Adv. Drug Deliv. Rev.* **97,** 260–269 (2016).

128. Chiquet, M., Gelman, L., Lutz, R. & Maier, S. From mechanotransduction to extracellular matrix gene expression in fibroblasts. *Biochim. Biophys. Acta* **1793,** 911–920 (2009).

129. Geiger, B. & Bershadsky, A. Assembly and mechanosensory function of focal contacts. *Curr. Opin. Cell Biol.* **13,** 584–592 (2001).

130. Wei, J. *et al.* Influence of surface wettability on competitive protein adsorption and initial attachment of osteoblasts. *Biomed. Mater.* **4,** 45002 (2009).

131. Kim, S. H. *et al.* Correlation of proliferation, morphology and biological responses of fibroblasts on LDPE with different surface wettability. *J. Biomater. Sci. Polym. Ed.* **18,** 609–622 (2007).

132. Burdick, J. a, Mauck, R. L., Gorman, J. H. & Gorman, R. C. Acellular biomaterials: an evolving alternative to cell-based therapies. *Sci. Transl. Med.* **5,** 176ps4 (2013).

133. Downing, T. L. *et al.* Biophysical regulation of epigenetic state and cell reprogramming. *Nat.*

Mater. **12,** 1154–62 (2013).

134. Doyle, A. D. & Yamada, K. M. Mechanosensing via cell-matrix adhesions in 3D microenvironments. *Exp. Cell Res.* **343,** 60–66 (2016).

135. Dalby, M. J., Gadegaard, N. & Oreffo, R. O. C. Harnessing nanotopography and integrin–matrix interactions to influence stem cell fate. *Nat. Mater.* **13,** 558 (2014).

136. Clark, E. A. & Brugge, J. S. Integrins and signal transduction pathways: the road taken. *Science (80-.).* **268,** 233 LP-239 (1995).

137. Rowland, D. *et al.* A comparative evaluation of the effect of polymer chemistry and fiber orientation on mesenchymal stem cell differentiation. *J. Biomed. Mater. Res. Part A* **104,** 2843–2853 (2016).

138. Engler, A. J., Sen, S., Sweeney, H. L. & Discher, D. E. Matrix Elasticity Directs Stem Cell Lineage Specification. *Cell* **126,** 677–689 (2006).

139. Chen, M., Patra, P. K., Warner, S. B. & Bhowmick, S. Role of Fiber Diameter in Adhesion and Proliferation of NIH 3T3 Fibroblast on Electrospun Polycaprolactone Scaffolds. *Tissue Eng.* **13,** 579–587 (2007).

140. Erisken, C., Zhang, X., Moffat, K. L., Levine, W. N. & Lu, H. H. Scaffold Fiber Diameter Regulates Human Tendon Fibroblast Growth and Differentiation. *Tissue Eng. Part A* **19,** 519–528 (2012).

141. Wang, F. *et al.* Urethral reconstruction with tissue-engineered human amniotic scaffold in rabbit urethral injury models. *Med. Sci. Monit.* **20,** (2014).

142. Franz, S., Rammelt, S., Scharnweber, D. & Simon, J. C. Immune responses to implants - a review of the implications for the design of immunomodulatory biomaterials. *Biomaterials* **32,** 6692–6709 (2011).

143. Saino, E. *et al.* Effect of Electrospun Fiber Diameter and Alignment on Macrophage Activation and Secretion of Proinflammatory Cytokines and Chemokines. *Biomacromolecules* **12,** 1900–1911 (2011).

144. Cui, H., Webber, M. J. & Stupp, S. I. Self-assembly of peptide amphiphiles: from molecules to nanostructures to biomaterials. *Biopolymers* **94,** 1–18 (2010).

145. Zhang, S. Fabrication of novel biomaterials through molecular self-assembly. *Nat. Biotechnol.* **21,** 1171 (2003).

146. Di Martino, A., Sittinger, M. & Risbud, M. V. Chitosan: a versatile biopolymer for orthopaedic tissue-engineering. *Biomaterials* **26,** 5983–5990 (2005).

147. Liu, X. & Ma, P. X. Phase separation, pore structure, and properties of nanofibrous gelatin scaffolds. *Biomaterials* **30,** 4094–4103 (2009).

148. Matsuzaki, R. *et al.* Three-dimensional printing of continuous-fiber composites by in-nozzle impregnation. *Sci. Rep.* **6,** 23058 (2016).

149. Guvendiren, M., Molde, J., Soares, R. M. D. & Kohn, J. Designing Biomaterials for 3D Printing. *ACS Biomater. Sci. Eng.* **2,** 1679–1693 (2016).

150. Hakimi, O. *et al.* A layered electrospun and woven surgical scaffold to enhance endogenous tendon repair. *Acta Biomater.* **26,** 124–135 (2015).

151. Gallagher, A. *et al.* A Novel Peptide Hydrogel for an Antimicrobial Bandage Contact Lens. *Adv. Healthc. Mater.* **5,** 2013–2018 (2016).

152. Ortega, I., Ryan, A. J., Deshpande, P., MacNeil, S. & Claeyssens, F. Combined microfabrication and electrospinning to produce 3-D architectures for corneal repair. *Acta Biomater.* **9,** 5511–5520 (2013).

153. Haik, J., Kornhaber, R., Blal, B. & Harats, M. The Feasibility of a Handheld Electrospinning Device for the Application of Nanofibrous Wound Dressings. *Adv. Wound Care* **6,** 166–174 (2017).

154. Li, J. *et al.* Human Pluripotent Stem Cell-Derived Cardiac Tissue-like Constructs for Repairing the Infarcted Myocardium. *Stem Cell Reports* **9,** 1546–1559 (2017).

155. Guoxu, Z., Xiaohui, Z., Jian, L. T. & Feng, X. Recent Advances in Electrospun Nanofibrous Scaffolds for Cardiac Tissue Engineering. *Adv. Funct. Mater.* **25,** 5726–5738 (2015).

156. Yoshimoto, H., Shin, Y. M., Terai, H. & Vacanti, J. P. A biodegradable nanofiber scaffold by electrospinning and its potential for bone tissue engineering. *Biomaterials* **24,** 2077–2082 (2003).

157. Zuo, Y., Yang, F., Wolke, J. G. C., Li, Y. & Jansen, J. A. Incorporation of biodegradable electrospun fibers into calcium phosphate cement for bone regeneration. *Acta Biomater.* **6,** 1238–1247 (2010).

158. Khandaker, M. *et al.* Use of Polycaprolactone Electrospun Nanofibers as a Coating for Poly(methyl methacrylate) Bone Cement. *Nanomater. (Basel, Switzerland)* **7,** (2017).

159. Pandolfi, L. *et al.* A nanofibrous electrospun patch to maintain human mesenchymal cell stemness. *J. Mater. Sci. Mater. Med.* **28,** 44 (2017).

160. Maldonado, M. *et al.* The effects of electrospun substrate-mediated cell colony morphology on the self-renewal of human induced pluripotent stem cells. *Biomaterials* **50,** 10–19 (2015).

161. Brown, G. E. & Khetani, S. R. Microfabrication of liver and heart tissues for drug development. *Philos. Trans. R. Soc. B Biol. Sci.* **373,** (2018).

162. Tucker, N., Stanger, J., Staiger, M. & Hofman, K. The History of the Science and Technology of Electrospinning from 1600 to 1900. *J. Eng. Fiber. Fabr.* (2013).

163. Silva, G. A. Nanotechnology approaches for drug and small molecule delivery across the blood brain barrier. *Surg. Neurol.* **67,** 113–116 (2007).

164. Kumar, G. *et al.* The determination of stem cell fate by 3D scaffold structures through the control of cell shape. *Biomaterials* **32,** 9188–9196 (2011).

165. Haycock, J. *3D Cell Culture: Methods and Protocols*. (Humana Press, 2010).

166. Doshi, J. & Reneker, D. H. Electrospinning process and applications of electrospun fibers. *J. Electrostat.* **35,** 151–160 (1995).

167. Maheshwari, G., Brown, G., Lauffenburger, D. A., Wells, A. & Griffith, L. G. Cell adhesion and motility depend on nanoscale RGD clustering. *J. Cell Sci.* **113,** 1677 LP-1686 (2000).

168. Korff, T. & Augustin, H. G. Tensional forces in fibrillar extracellular matrices control directional capillary sprouting. *J. Cell Sci.* **112 (Pt 1,** 3249–3258 (1999).

169. Roskelley, C. D., Srebrow, A. & Bissell, M. J. A hierarchy of ECM-mediated signalling regulates tissue-specific gene expression. *Curr. Opin. Cell Biol.* **7,** 736–747 (1995).

170. Friedl, P. & Brocker, E. B. The biology of cell locomotion within three-dimensional extracellular matrix. *Cell. Mol. Life Sci.* **57,** 41–64 (2000).

171. Wan-Ju, L., Laurencin, C., Caterson, E., Tuan, R. & Ko, F. Electrospun nanofibrous structure: A novel scaffold for tissue engineering. *J. Biomed. Mater. Res.* **60,** 613–621 (2002).

172. Stace, E. T., Nagra, N. S., Tibrewal, S., Khan, W. & Carr, A. J. The use of novel electrospun scaffolds in musculoskeletal tissue engineering: a focus on the rotator cuff. *Curr. Stem Cell Res. Ther.* (2018). doi:10.2174/1574888X13666180129105707

173. IME Electrospinning. EC-DIG+ promotional material. (2017). Available at: https://www.ime-electrospinning.com/electrospinning-machines/ec-dig-plus/. (Accessed: 1st June 2018)

174. Haider, A., Haider, S. & Kang, I.-K. A comprehensive review summarizing the effect of electrospinning parameters and potential applications of nanofibers in biomedical and biotechnology. *Arab. J. Chem.* (2015). doi:https://doi.org/10.1016/j.arabjc.2015.11.015

175. Ramakrishna, S. *An Introduction to Electrospinning and Nanofibers*. (World Scientific, 2005).

176. Tan, S.-H., Inai, R., Kotaki, M. & Ramakrishna, S. Systematic parameter study for ultra-fine fiber fabrication via electrospinning process. *Polymer (Guildf).* **46,** 6128–6134 (2005).

177. Deitzel, J. M., Kleinmeyer, J., Harris, D. & Beck Tan, N. C. The effect of processing variables on the morphology of electrospun nanofibers and textiles. *Polymer (Guildf).* **42,** 261–272 (2001).

178. Lyons, J., Li, C. & Ko, F. Melt-electrospinning part I: processing parameters and geometric properties. *Polymer (Guildf).* **45,** 7597–7603 (2004).

179. Tan, S.-H., Inai, R., Kotaki, M. & Ramakrishna, S. Systematic parameter study for ultra-fine fiber fabrication via electrospinning process. *Polymer (Guildf).* **46,** 6128–6134 (2005).

180. Zhou, H., Green, T. B. & Joo, Y. L. The thermal effects on electrospinning of polylactic acid melts. *Polymer (Guildf).* **47,** 7497–7505 (2006).

181. Megelski, S., Stephens, J. S., Chase, D. B. & Rabolt, J. F. Micro- and Nanostructured Surface Morphology on Electrospun Polymer Fibers. *Macromolecules* **35,** 8456–8466 (2002).

182. Beachley, V. & Wen, X. Effect of electrospinning parameters on the nanofiber diameter and length. *Mater. Sci. Eng. C* **29,** 663–668 (2009).

183. De Vrieze, S. *et al.* The effect of temperature and humidity on electrospinning. *J. Mater. Sci.* **44,** 1357 (2008).

184. Edmondson, D., Cooper, A., Jana, S., Wood, D. & Zhang, M. Centrifugal electrospinning of highly aligned polymer nanofibers over a large area. *J. Mater. Chem.* **22,** 18646–18652 (2012).

185. Thompson, C. J., Chase, G. G., Yarin, A. L. & Reneker, D. H. Effects of parameters on nanofiber diameter determined from electrospinning model. *Polymer (Guildf).* **48,** 6913–6922 (2007).

186. Brooks, H. & Tucker, N. Electrospinning predictions using artificial neural networks. *Polymer (Guildf).* **58,** 22–29 (2015).

187. Khanlou, H. M. *et al.* Prediction and optimization of electrospinning parameters for polymethyl methacrylate nanofiber fabrication using response surface methodology and artificial neural networks. *Neural Comput. Appl.* **25,** 767–777 (2014).

188. Sheikh, F. A. *et al.* Imaging, spectroscopy, mechanical, alignment and biocompatibility studies of electrospun medical grade polyurethane (Carbothane??? 3575A) nanofibers and composite nanofibers containing multiwalled carbon nanotubes. *J. Mech. Behav. Biomed. Mater.* **41,** 189–198 (2015).

189. Wu, H. *et al.* Electrospun Metal Nanofiber Webs as High-Performance Transparent Electrode. *Nano Lett.* **10,** 4242–4248 (2010).

190. Mouthuy, P.-A., Crossley, A. & Ye, H. Fabrication of calcium phosphate fibres through electrospinning and sintering of hydroxyapatite nanoparticles. *Mater. Lett.* **106,** 145–150 (2013).

191. Liu, J., Bauer, A. J. P. & Li, B. Solvent vapor annealing: An efficient approach for inscribing secondary nanostructures onto electrospun fibers. *Macromol. Rapid Commun.* **35,** 1503–1508 (2014).

192. Lu, H. H. *et al.* Anterior cruciate ligament regeneration using braided biodegradable scaffolds: in vitro optimization studies. *Biomaterials* **26,** 4805–4816 (2005).

193. Berber, E., Horzum, N., Hazer, B. & Demir, M. M. Solution electrospinning of polypropylene-based fibers and their application in catalysis. *Fibers Polym.* **17,** 760–768 (2016).

194. Fang, J., Zhang, L., Sutton, D., Wang, X. & Lin, T. Needleless Melt-electrospinning of Polypropylene Nanofibres. *J. Nanomater.* **2012,** 16:1--16:9 (2012).

195. Mahshid, V., Zaat, S., Smit, T. & Roovers, J.-P. Biomimetic implants for pelvic floor repair. *Neurourol. Urodyn.* **37,** 566–580 (2017).

196. McClellan, P. & Landis, W. J. Recent Applications of Coaxial and Emulsion Electrospinning Methods in the Field of Tissue Engineering. *Biores. Open Access* **5,** 212–227 (2016).

197. Han, D. & Steckl, A. J. Triaxial Electrospun Nanofiber Membranes for Controlled Dual Release of Functional Molecules. *ACS Appl. Mater. Interfaces* **5,** 8241–8245 (2013).

198. Chen, R. *et al.* Preparation and characterization of coaxial electrospun thermoplastic polyurethane/collagen compound nanofibers for tissue engineering applications. *Colloids Surfaces B Biointerfaces* **79,** 315–325 (2010).

199. Townsend-Nicholson, A. & Jayasinghe, S. N. Cell electrospinning: a unique biotechnique for encapsulating living organisms for generating active biological microthreads/scaffolds. *Biomacromolecules* **7,** 3364–3369 (2006).

200. Siang, L. Y., P., L. M. & Joachim, L. S. C. Sustained-release of naproxen sodium from electrospun-aligned PLLA–PCL scaffolds. *J. Tissue Eng. Regen. Med.* **11,** 1011–1021 (2015).

201. Hu, X. *et al.* Electrospinning of polymeric nanofibers for drug delivery applications. *J. Control. Release* **185,** 12–21 (2014).

202. Zhu, J. *et al.* The regulation of phenotype of cultured tenocytes by microgrooved surface structure. *Biomaterials* **31,** 6952–6958 (2010).

203. Fashandi, H. & Karimi, M. Pore formation in polystyrene fiber by superimposing temperature and relative humidity of electrospinning atmosphere. *Polymer (Guildf).* **53,** 5832–5849 (2012).

204. Liu, W., Huang, C. & Jin, X. Tailoring the grooved texture of electrospun polystyrene nanofibers by controlling the solvent system and relative humidity. *Nanoscale Res. Lett.* **9,** 350 (2014).

205. Aragon, J., Navascues, N., Mendoza, G. & Irusta, S. Laser-treated electrospun fibers loaded with nano-hydroxyapatite for bone tissue engineering. *Int. J. Pharm.* **525,** 112–122 (2017).

206. Anandkumar, N. *et al.* A Fast Process for Imprinting Micro and Nano Patterns on Electrospun Fiber Meshes at Physiological Temperatures. *Small* **9,** 3405–3409 (2013).

207. Zhang, C., Gao, C., Chang, M.-W., Ahmad, Z. & Li, J.-S. Continuous micron-scaled rope engineering using a rotating multi-nozzle electrospinning emitter. *Appl. Phys. Lett.* **109,** 151903 (2016).

208. Simonet, M., Schneider, O., Neuenschwander, P. & Stark, W. Ultraporous 3D polymer meshes by low-temperature electrospinning: Use of ice crystals as a removable void template. *Polym. Eng. Sci.* **47,** 2020–2026 (2007).

209. Baker, B. M. *et al.* The potential to improve cell infiltration in composite fiber-aligned

electrospun scaffolds by the selective removal of sacrificial fibers. *Biomaterials* **29,** 2348–2358 (2008).

210. Beason, D. P. *et al.* Fiber-aligned polymer scaffolds for rotator cuff repair in a rat model. *J. shoulder Elb. Surg.* **21,** 245–250 (2012).

211. Yang, C., Deng, G., Chen, W., Ye, X. & Mo, X. A novel electrospun-aligned nanoyarn-reinforced nanofibrous scaffold for tendon tissue engineering. *Colloids Surf. B. Biointerfaces* **122,** 270–276 (2014).

212. Tejeda-Alejandre, R., Lara-Padilla, H., Mendoza-Buenrostro, C., Rodriguez, C. A. & Dean, D. Electrospinning Complexly-shaped, Resorbable, Bifurcated Vascular Grafts. *Procedia CIRP* **65,** 207–212 (2017).

213. Mouthuy, P.-A., Zargar, N., Hakimi, O., Lostis, E. & Carr, A. Fabrication of continuous electrospun filaments with potential for use as medical fibres. *Biofabrication* **7,** 25006 (2015).

214. Samavedi, S., Vaidya, P., Prudhvidhar, G., Whittington, A. & Goldstein, A. Electrospun meshes possessing region-wise differences in fiber orientation, diameter, chemistry and mechanical properties for engineering bone-ligament-bone tissues. *Biotechnol. Bioeng.* **111,** 2549–2559 (2014).

215. Middleton, J. C. & Tipton, A. J. Synthetic biodegradable polymers as orthopedic devices. *Biomaterials* **21,** 2335–2346 (2000).

216. He, X. *et al.* Uniaxially Aligned Electrospun All-Cellulose Nanocomposite Nanofibers Reinforced with Cellulose Nanocrystals: Scaffold for Tissue Engineering. *Biomacromolecules* **15,** 618–627 (2014).

217. Abhari, R. E., Mouthuy, P.-A., Zargar, N., Brown, C. & Carr, A. Effect of annealing on the mechanical properties and the degradation of electrospun polydioxanone filaments. *J. Mech. Behav. Biomed. Mater.* **67,** 127–134 (2017).

218. Luo, X. *et al.* Study on structure, mechanical property and cell cytocompatibility of electrospun collagen nanofibers crosslinked by common agents. *Int. J. Biol. Macromol.* **113,** 476–486 (2018).

219. Wilson, C. J., Clegg, R. E., Leavesley, D. I. & Pearcy, M. J. Mediation of Biomaterial–Cell Interactions by Adsorbed Proteins: A Review. *Tissue Eng.* **11,** 1–18 (2005).

220. Chen, Q.-Z. *et al.* Surface functionalization of Bioglass®-derived porous scaffolds. *Acta Biomater.* **3,** 551–562 (2007).

221. Correia, D. M. *et al.* Superhydrophilic poly(l-lactic acid) electrospun membranes for biomedical applications obtained by argon and oxygen plasma treatment. *Appl. Surf. Sci.* **371,** 74–82 (2016).

222. Duque Sanchez, L., Brack, N., Postma, A., Pigram, P. J. & Meagher, L. Surface modification of electrospun fibres for biomedical applications: A focus on radical polymerization methods. *Biomaterials* **106,** 24–45 (2016).

223. Keselowsky, B. G., Collard, D. M. & Garcia, A. J. Surface chemistry modulates fibronectin conformation and directs integrin binding and specificity to control cell adhesion. *J. Biomed. Mater. Res. A* **66,** 247–259 (2003).

224. Llopis-Hernandez, V., Rico, P., Ballester-Beltran, J., Moratal, D. & Salmeron-Sanchez, M. Role of surface chemistry in protein remodeling at the cell-material interface. *PLoS One* **6,** e19610 (2011).

225. Wan, Y., Yang, J., Yang, J., Bei, J. & Wang, S. Cell adhesion on gaseous plasma modified poly-(L-lactide) surface under shear stress field. *Biomaterials* **24,** 3757–3764 (2003).

226. Wan, Y. *et al.* Characterization of surface property of poly(lactide-co-glycolide) after oxygen plasma treatment. *Biomaterials* **25,** 4777–4783 (2004).

227. Jiao, Y.-P. & Cui, F.-Z. Surface modification of polyester biomaterials for tissue engineering. *Biomed. Mater.* **2,** R24-37 (2007).

228. von Oepen, R. & Michaeli, W. Injection moulding of biodegradable implants. *Clin. Mater.* **10,** 21–28 (1992).

229. Abhari, R. E. *et al.* Using an industrial braiding machine to upscale the production and modulate the design of electrospun medical yarns. *Polym. Test.* **69,** 188–198 (2018).

230. Hakimi, O., Mouthuy, P. A. & Carr, A. Synthetic and degradable patches: An emerging solution for rotator cuff repair. *Int. J. Exp. Pathol.* **94,** 287–292 (2013).

231. Cayenne Medical. BioWick SureLock Implant. (2016). Available at: http://cayennemedical.com/biowick-surelock/. (Accessed: 1st June 2018)

232. Webb, K., Hlady, V. & Tresco, P. Relative importance of surface wettability and charged functional groups on NIH 3T3 fibroblast attachment, spreading, and cytoskeletal organization. *J. Biomed. Mater. Res.* **41,** 422–430 (1998).

233. Hamdan, M., Blanco, L., Khraisat, A. & Tresguerres, I. Influence of Titanium Surface Charge on Fibroblast Adhesion. *Clin. Implant Dent. Relat. Res.* **8,** 32–38 (2006).

234. Schneider, G. B. *et al.* The effect of hydrogel charge density on cell attachment. *Biomaterials* **25,** 3023–3028 (2004).

235. De Rosa, M. *et al.* Cationic polyelectrolyte hydrogel fosters fibroblast spreading, proliferation, and extracellular matrix production: Implications for tissue engineering. *J. Cell. Physiol.* **198,** 133–143 (2003).

236. Lee, C. H. *et al.* Nanofiber alignment and direction of mechanical strain affect the ECM production of human ACL fibroblast. *Biomaterials* **26,** 1261–1270 (2005).

237. Ying, L. *et al.* Effects of fiber orientation and diameter on the behavior of human dermal fibroblasts on electrospun PMMA scaffolds. *J. Biomed. Mater. Res. Part A* **90A,** 1092–1106 (2008).

238. Shaoping, Z. *et al.* An aligned nanofibrous collagen scaffold by electrospinning and its effects on in vitro fibroblast culture. *J. Biomed. Mater. Res. Part A* **79A,** 456–463 (2006).

239. Bashur, C. a, Shaffer, R. D., Dahlgren, L. a, Guelcher, S. a & Goldstein, A. S. Effect of fiber diameter and alignment of electrospun polyurethane meshes on mesenchymal progenitor cells. *Tissue Eng. Part A* **15,** 2435–2445 (2009).

240. Truong, Y. B. *et al.* A comparison of the effects of fibre alignment of smooth and textured fibres in electrospun membranes on fibroblast cell adhesion. *Biomed. Mater.* **5,** 25005 (2010).

241. Kapoor, A., Caporali, E. H. G., Kenis, P. J. a. & Stewart, M. C. Microtopographically patterned surfaces promote the alignment of tenocytes and extracellular collagen. *Acta Biomater.* **6,** 2580–2589 (2010).

242. Delaine-Smith, R. M., Green, N. H., Matcher, S. J., MacNeil, S. & Reilly, G. C. Monitoring Fibrous Scaffold Guidance of Three-Dimensional Collagen Organisation Using Minimally-Invasive Second Harmonic Generation. *PLoS One* **9,** e89761 (2014).

243. Cardwell, R., Dahlgren, L. & Goldstein, A. Electrospun fibre diameter, not alignment, affects mesenchymal stem cell differentiation into the tendon/ligament lineage. *J. Tissue Eng. Regen. Med.* **8,** 937–945 (2012).

244. Chaurey, V. *et al.* Nanofiber size-dependent sensitivity of fibroblast directionality to the methodology for scaffold alignment. *Acta Biomater.* **8,** 3982–3990 (2012).

245. Lo, C.-M., Wang, H.-B., Dembo, M. & Wang, Y. Cell Movement Is Guided by the Rigidity of the Substrate. *Biophys. J.* **79,** 144–152 (2000).

246. Gray, D., Tien, J. & Chen, C. Repositioning of cells by mechanotaxis on surfaces with micropatterned Young's modulus. *J. Biomed. Mater. Res. Part A* **66A,** 605–614 (2003).

247. Solon, J., Levental, I., Sengupta, K., Georges, P. C. & Janmey, P. A. Fibroblast adaptation and stiffness matching to soft elastic substrates. *Biophys. J.* **93,** 4453–4461 (2007).

248. Grier, W. K., Iyoha, E. M. & Harley, B. A. C. The influence of pore size and stiffness on tenocyte bioactivity and transcriptomic stability in collagen-GAG scaffolds. *J. Mech. Behav. Biomed. Mater.* **65,** 295–305 (2017).

249. Wirth, C. *et al.* Nitinol surface roughness modulates in vitro cell response: a comparison between fibroblasts and osteoblasts. *Mater. Sci. Eng. C* **25,** 51–60 (2005).

250. Hallab, N. J., Bundy, K. J., O'Connor, K., Moses, R. L. & Jacobs, J. J. Evaluation of metallic and polymeric biomaterial surface energy and surface roughness characteristics for directed cell adhesion. *Tissue Eng.* **7,** 55–71 (2001).

251. Pennisi, C. P. *et al.* Nanoscale topography reduces fibroblast growth, focal adhesion size and migration-related gene expression on platinum surfaces. *Colloids Surf. B. Biointerfaces* **85,** 189–197 (2011).

252. Loesberg, W. A. *et al.* The threshold at which substrate nanogroove dimensions may influence fibroblast alignment and adhesion. *Biomaterials* **28,** 3944–3951 (2007).

253. Yin, Z. *et al.* The regulation of tendon stem cell differentiation by the alignment of nanofibers. *Biomaterials* **31,** 2163–2175 (2010).

254. Christopherson, G. T., Song, H. & Mao, H. Q. The influence of fiber diameter of electrospun substrates on neural stem cell differentiation and proliferation. *Biomaterials* **30,** 556–564 (2009).

255. da Silva Meirelles, L., Fontes, A. M., Covas, D. T. & Caplan, A. I. Mechanisms involved in the therapeutic properties of mesenchymal stem cells. *Cytokine Growth Factor Rev.* **20,** 419–427 (2009).

256. Iannotti, J. P. *et al.* Porcine small intestine submucosa augmentation of surgical repair of chronic two-tendon rotator cuff tears. A randomized, controlled trial. *J. Bone Joint Surg. Am.* **88,** 1238–1244 (2006).

257. Anderson, J. M., Rodriguez, A. & Chang, D. T. Foreign body reaction to biomaterials. *Semin. Immunol.* **20,** 86–100 (2008).

258. Kavvadias, T., Kaemmer, D., Klinge, U., Kuschel, S. & Schuessler, B. Foreign body reaction in vaginally eroded and noneroded polypropylene suburethral slings in the female: a case series. *Int. Urogynecol. J.* **20,** 1473–1476 (2009).

259. Brown, B. N., Ratner, B. D., Goodman, S. B., Amar, S. & Badylak, S. F. Macrophage polarization: an opportunity for improved outcomes in biomaterials and regenerative medicine. *Biomaterials* **33,** 3792–3802 (2012).

260. Sheikh, Z., Brooks, P. J., Barzilay, O., Fine, N. & Glogauer, M. Macrophages, Foreign Body Giant Cells and Their Response to Implantable Biomaterials. *Mater. (Basel, Switzerland)* **8,** 5671–5701 (2015).

261. Cao, H., Mchugh, K., Sing, C. & Anderson, J. The topographical effect of electrospun nanofibrous scaffolds on the in vivo and in vitro foreign body reaction. *J. Biomed. Mater. Res. Part A* **93A,** 1151–1159 (2009).

262. William, B. *et al.* In vivo leukocyte cytokine mRNA responses to biomaterials are dependent on

surface chemistry. *J. Biomed. Mater. Res. Part A* **64A,** 320–329 (2002).

263. Brodbeck, W. G. *et al.* Biomaterial adherent macrophage apoptosis is increased by hydrophilic and anionic substrates in vivo *Proc. Natl. Acad. Sci.* **99,** 10287 LP-10292 (2002).

264. Murray, P. J. *et al.* Macrophage Activation and Polarization: Nomenclature and Experimental Guidelines. *Immunity* **41,** 14–20 (2014).

265. Garg, K., Pullen, N. a., Oskeritzian, C. a., Ryan, J. J. & Bowlin, G. L. Macrophage functional polarization (M1/M2) in response to varying fiber and pore dimensions of electrospun scaffolds. *Biomaterials* **34,** 4439–4451 (2013).

266. Blakney, A. K., Swartzlander, M. D. & Bryant, S. J. The effects of substrate stiffness on the in vitro activation of macrophages and in vivo host response to poly(ethylene glycol)-based hydrogels. *J. Biomed. Mater. Res. A* **100,** 1375–1386 (2012).

267. Bota, P. C. *et al.* Biomaterial topography alters healing in vivo and monocyte/macrophage activation in vitro. *J. Biomed. Mater. Res. Part A* **95A,** 649–657 (2010).

268. Kou, P. M. & Babensee, J. E. Macrophage and dendritic cell phenotypic diversity in the context of biomaterials. *J. Biomed. Mater. Res. - Part A* **96 A,** (2011).

269. Tony, Y. *et al.* Effects of substrate stiffness on cell morphology, cytoskeletal structure, and adhesion. *Cell Motil.* **60,** 24–34 (2004).

270. Costa, C., Incio, J. & Soares, R. Angiogenesis and chronic inflammation: cause or consequence? *Angiogenesis* **10,** 149–166 (2007).

271. Jackson, J. R., Seed, M. P., Kircher, C. H., Willoughby, D. A. & Winkler, J. D. The codependence of angiogenesis and chronic inflammation. *FASEB J.* **11,** 457–465 (1997).

272. Kusumbe, A. P., Ramasamy, S. K. & Adams, R. H. Coupling of angiogenesis and osteogenesis by a specific vessel subtype in bone. *Nature* **507,** 323 (2014).

273. Rafii, S., Butler, J. M. & Ding, B.-S. Angiocrine functions of organ-specific endothelial cells. *Nature* **529,** 316 (2016).

274. Heath, D., Lannutti, J. & Cooper, S. Electrospun scaffold topography affects endothelial cell proliferation, metabolic activity, and morphology. *J. Biomed. Mater. Res. Part A* **94A,** 1195–1204 (2010).

275. Whited, B. & Rylander, M. The influence of electrospun scaffold topography on endothelial cell morphology, alignment, and adhesion in response to fluid flow. *Biotechnol. Bioeng.* **111,** 184–195 (2013).

276. Schoenenberger, A. D., Foolen, J., Moor, P., Silvan, U. & Snedeker, J. G. Substrate fiber alignment mediates tendon cell response to inflammatory signaling. *Acta Biomater.* **71,** 306–317 (2018).

277. Ali, S. A., Zhong, S. P., Doherty, P. J. & Williams, D. F. Mechanisms of polymer degradation in implantable devices. I. Poly(caprolactone). *Biomaterials* **14,** 648–656 (1993).

278. Ping Ooi, C. & Cameron, R. E. The hydrolytic degradation of polydioxanone (PDSII) sutures. Part I: Morphological aspects. *J. Biomed. Mater. Res.* **63,** 280–290 (2002).

279. Ping Ooi, C. & Cameron, R. E. The hydrolytic degradation of polydioxanone (PDSII) sutures. Part II: Micromechanisms of deformation. *J. Biomed. Mater. Res.* **63,** 291–298 (2002).

280. Ishikiriyama, K. *et al.* Heat capacity of poly-p-dioxanone. *J. Macromol. Sci. Part B* **37,** 27–44 (1998).

281. Lee, H. *et al.* Enhancement of mechanical properties of polymeric nanofibers by controlling

crystallization behavior using a simple freezing/thawing process. *RSC Adv.* **7,** 43994–44000 (2017).

282. Bonnet, M., Rogausch, K.-D. & Petermann, J. The endothermic "annealing peak" of poly(phenylene sulphide) and poly(ethylene terephthalate). *Colloid Polym. Sci.* **277,** 513–518 (1999).

283. Chen, J., Xu, J., Wang, A. & Zheng, M. Scaffolds for tendon and ligament repair: review of the efficacy of commercial products. *Expert Rev. Med. Devices* **6,** 61–73 (2009).

284. Huang, C. *et al.* Electrospun polymer nanofibres with small diameters. *Nanotechnology* **17,** 1558–1563 (2006).

285. Rowland, C. R., Lennon, D. P., Caplan, A. I. & Guilak, F. The effects of crosslinking of scaffolds engineered from cartilage ECM on the chondrogenic differentiation of MSCs. *Biomaterials* **34,** 5802–5812 (2013).

286. Zulkifli, F. H., Jahir Hussain, F. S., Abdull Rasad, M. S. B. & Mohd Yusoff, M. Improved cellular response of chemically crosslinked collagen incorporated hydroxyethyl cellulose/poly(vinyl) alcohol nanofibers scaffold. *J. Biomater. Appl.* **29,** 1014–1027 (2015).

287. Dean, B. J. F., Franklin, S. L. & Carr, A. J. A systematic review of the histological and molecular changes in rotator cuff disease. *Bone Joint Res.* **1,** 158–166 (2012).

288. Dakin, S. G. *et al.* Inflammation activation and resolution in human tendon disease. *Sci. Transl. Med.* **7,** 311ra173 LP-311ra173 (2015).

289. Kendal, A. *et al.* Resorbable electrospun polydioxanone fibres modify the behaviour of cells from both healthy and diseased human tendons. *Eur. Cell. Mater.* **33,** 169–182 (2017).

290. Martinez, F. Analysis of Gene Expression and Gene Silencing in Human Macrophages. *Curr. Protoc. Immunol.* **96,** 14.28.1-14.28.23 (2012).

291. Wang, Z. *et al.* The effect of thick fibers and large pores of electrospun poly(epsilon-caprolactone) vascular grafts on macrophage polarization and arterial regeneration. *Biomaterials* **35,** 5700–5710 (2014).

292. Othman, Z., Cillero Pastor, B., van Rijt, S. & Habibovic, P. Understanding interactions between biomaterials and biological systems using proteomics. *Biomaterials* **167,** 191–204 (2018).

293. Firkowska-Boden, I., Zhang, X. & Jandt Klaus, D. Controlling Protein Adsorption through Nanostructured Polymeric Surfaces. *Adv. Healthc. Mater.* **7,** 1700995 (2017).

294. Scanzello, C. R. *et al.* Local cytokine profiles in knee osteoarthritis: elevated synovial fluid interleukin-15 differentiates early from end-stage disease. *Osteoarthr. Cartil.* **17,** 1040–1048 (2009).

295. Snelling, S. J. B. *et al.* Presence of IL-17 in synovial fluid identifies a potential inflammatory osteoarthritic phenotype. *PLoS One* **12,** e0175109 (2017).

296. Mabey, T. *et al.* Plasma and synovial fluid inflammatory cytokine profiles in primary knee osteoarthritis. *Biomarkers Biochem. Indic. Expo. response, susceptibility to Chem.* **21,** 639–644 (2016).

297. Wessel, D. & Flugge, U. I. A method for the quantitative recovery of protein in dilute solution in the presence of detergents and lipids. *Anal. Biochem.* **138,** 141–143 (1984).

298. Cox, J. & Mann, M. MaxQuant enables high peptide identification rates, individualized p.p.b.-range mass accuracies and proteome-wide protein quantification. *Nat. Biotechnol.* **26,** 1367–1372 (2008).

299. Tyanova, S. *et al.* The Perseus computational platform for comprehensive analysis of (prote)omics data. *Nat. Methods* **13,** 731–740 (2016).

300. García, A. J., Vega, M. D. & Boettiger, D. Modulation of Cell Proliferation and Differentiation through Substrate-dependent Changes in Fibronectin Conformation. *Mol. Biol. Cell* **10,** 785–798 (1999).

301. Mora-Solano, C. & Collier, J. H. Engaging adaptive immunity with biomaterials. *J. Mater. Chem. B. Mater. Biol. Med.* **2,** 2409–2421 (2014).

302. McWhorter, F. Y., Davis, C. T. & Liu, W. F. Physical and mechanical regulation of macrophage phenotype and function. *Cell. Mol. Life Sci.* **72,** 1303–1316 (2015).

303. Rashid, M. S. *et al.* Increasing age and tear size reduce rotator cuff repair healing rate at 1 year: Data from a large randomized controlled trial. *Acta Orthop.* **88,** 606–611 (2017).

304. Li, Y. *et al.* Biophysical Regulation of Histone Acetylation in Mesenchymal Stem Cells. *Biophys. J.* **100,** 1902-1909 (2011).

305. Lv, L *et al.* Biomaterial Cues Regulate Epigenetic State and Cell Functions - A Systematic Review. *Tissue Eng. Part B. Rev.* **24,** 112-132 (2018).

306. Yang, F., Murugan, R., Wang, S. & Ramakrishna, S. Electrospinning of nano/micro scale poly(l-lactic acid) aligned fibers and their potential in neural tissue engineering. *Biomaterials* **26,** 2603–2610 (2005).

307. Millar, N. L., Murrell, G. A. C. & McInnes, I. B. Inflammatory mechanisms in tendinopathy – towards translation. *Nat. Rev. Rheumatol.* **13,** 110 (2017).

308. Crowley, T., Buckley, C. & Clark, A. Stroma: the forgotten cells of innate immune memory. *Clin. Exp. Immunol.* **193,** 24–36 (2018).

A.1 The effects of PDO resin storage conditions on solution viscosity over time

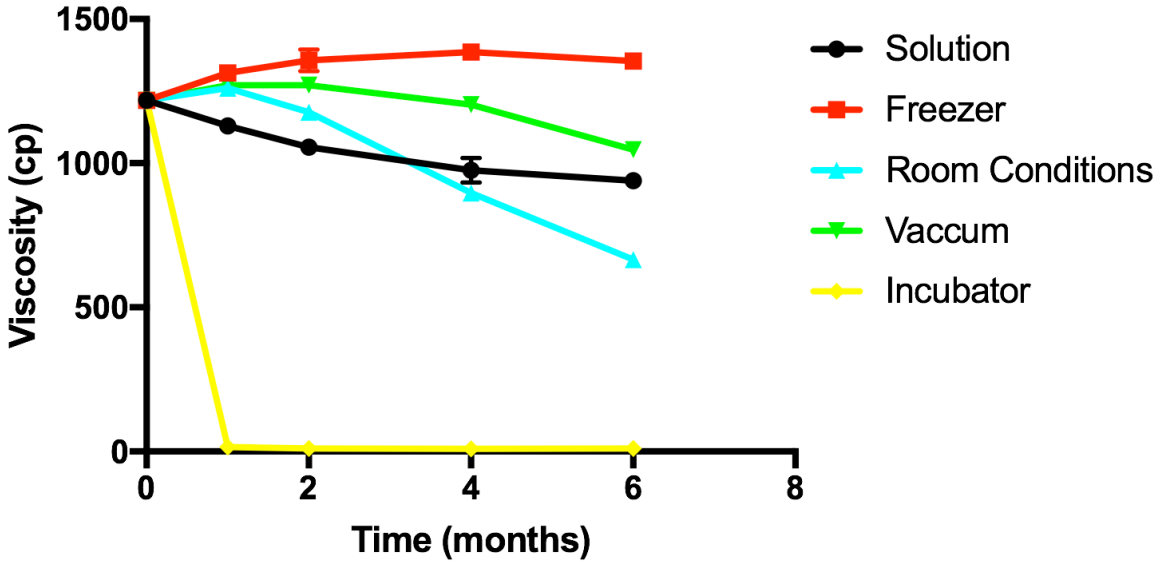


Figure A-1. The effects of PDO resin storage conditions on solution viscosity over time.

This shows the viscosity of solutions prepared from PDO resin after storage in different conditions for 6 months. There are 4 things to note. Firstly, for PDO stored as a solution, there is a gradual decrease in viscosity over the 6 months. Storage of PDO in an incubator quickly induced degradation of PDO, highlighting the sensitivity of PDO resin to hydrolytic breakdown. Thirdly, viscosity of PDO stored in a freezer increased over the time period assessed. Room condition and vacuum storage led to reduction in viscosity at 6 months. (Mean viscosity and standard deviation).

A.2 Fibre diameter optimisation parameter effects

Table A-1. The effects of electrospinning parameters on fibre diameter.

PDO concentration (g/ml)			
	5	**6.5**	**8**
Number (n)	36	32	32
Diameter (mean)	0.57	1.71	2.03
Diameter (SD)	0.17	0.36	0.37

Flow rate (ml/hr)					
	0.5	**0.75**	**1.0**	**1.5**	**4**
Number (n)	24	24	28	26	40
Diameter (mean)	1.62	2.04	2.18	2.49	2.36
Diameter (SD)	0.22	0.24	0.28	0.36	0.81

Collector speed (rpm)						
	1	**50**	**100**	**500**	**1000**	**2500**
Number (n)	29	27	26	29	28	38
Diameter (mean)	2.76	2.75	2.67	2.62	2.18	1.41
Diameter (SD)	0.20	0.24	0.20	0.19	0.28	0.23

Collector distance (cm)			
	15	**20**	**25**
Number (n)	36	38	32
Diameter (mean)	2.34	2.11	2.07
Diameter (SD)	.18	.38	.39

Voltage (kV)					
	7	**8**	**9**	**10**	**11**
Number (n)	23	30	28	31	34
Diameter (mean)	2.39	2.10	2.20	1.88	1.75
Diameter (SD)	0.42	0.36	0.27	0.30	0.38

Temperature (°C)				
	20	**25**	**30**	**35**
Number (n)	23	30	28	31
Diameter (mean)	2.39	2.10	2.20	1.88
Diameter (SD)	0.42	0.36	0.27	0.30

Humidity (%)				
	25	**45**	**60**	**80**
Number (n)	59	84	68	72
Diameter (mean)	1.29	1.26	1.10	1.03
Diameter (SD)	0.19	0.18	0.17	0.23

Appendix B Additional information for Chapter 3

B.1 Primer sequences used for PBMC expression studies

Table B-1. Primer sequences used for gene expression analysis.

GENE	Forward	Reverse
TNFA	GGCCAAGCCCTGGTATGAG	TAGTCGGGCCGATTGATCTC
TGFB1	CAATTCCTGGCGATACCTCAG	GCACAACTCCGGTGACATCAA
IL1B	CACGATGCACCTGTACGATCA	TGGAGAGCTTTCAGTTCATATGGA
IL6	GCAGAAAACAACCTGAACCTT	ACCTCAAACTCCAAAAGACCA
IL8	TGCTAAAGAACTTAGATGTCAGT	TGGTCCACTCTCAATCACTCTCA
IL10	TACGGCGCTGTCATCGATT	GGCTTTGTAGATGCCTTTCTCTTG
IL12B	AGAAGATGGTATCACCTGGACC	GAACCTCGCCTCCTTTGTGAC
PTGS2	CAGGCTTCCATTGACCAGAG	TTTCTCCTGTAAGTTCTTCAAATGAT

B.2 Metabolic activity of tendon fibroblasts cultured on TCP shows a similar increase for fibroblasts from diseased tendon compared to healthy tendon

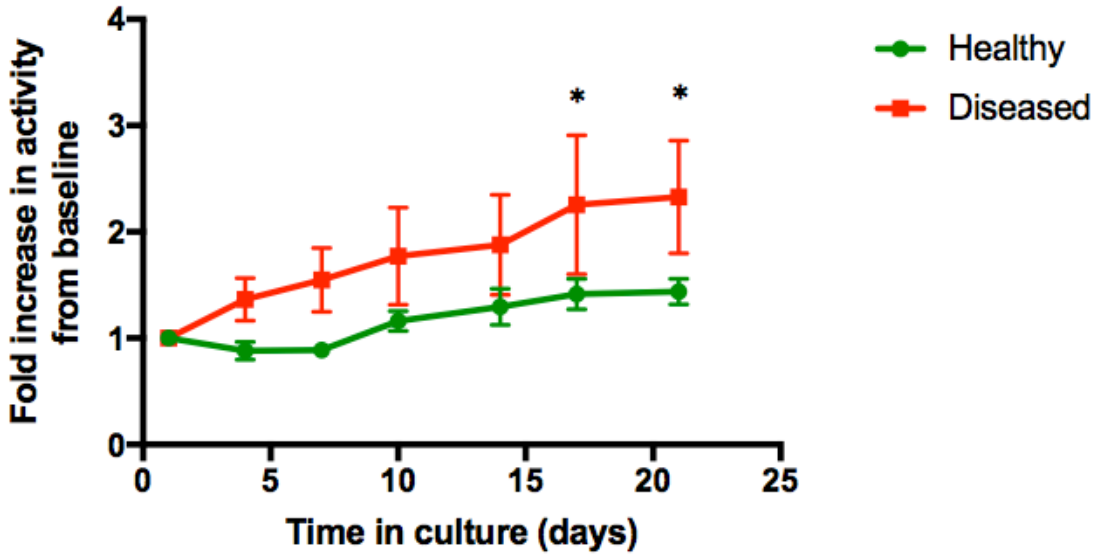


Figure B-1. Tendon fibroblasts derived from diseased tendon display increased metabolic activity when cultured on TCP compared to fibroblasts from healthy tendon.

Fibroblasts from diseased tendon exhibited significantly greater increases in metabolic activity than tendon fibroblasts from healthy tendon. This is consistent with culture on electrospun scaffolds (Figure 3-8). This was significantly different at Day 17 and day 21 (*, $p<0.05$). Diseased tendon fibroblasts however had much greater variation in their response. (Mean fold change with standard deviation relative to baseline).

B.3 Gene expression of tendon fibroblasts cultured on TCP also shows a differential response in tendon fibroblasts from diseased tendon compared to healthy tendon

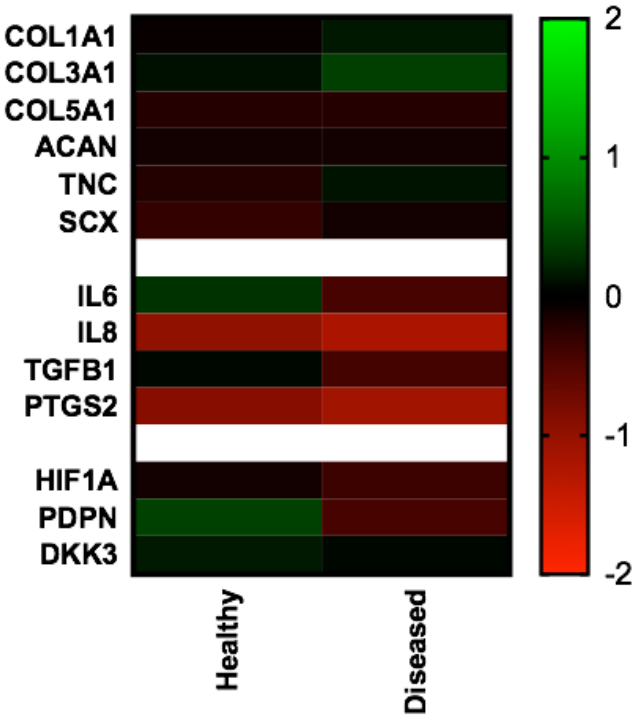


Figure B-2. The fold change in gene expression is different for tendon fibroblasts derived from healthy and diseased tendon on TCP after 14 days culture.

Tendon fibroblasts exhibit changes in gene expression in response to TCP depending on their isolation from healthy or diseased tendon. This is a similar finding to what was seen between the two fibroblast phenotypes when cultured on electrospun fibres where the same biophysical stimuli induced differential gene expression. Heat map of mean fold change from 24 hours following culture for 14 days for each cell phenotype, log10 scale.

B.4 Fibroblasts from diseased and healthy tendons show differential gene expression responses to electrospun scaffolds

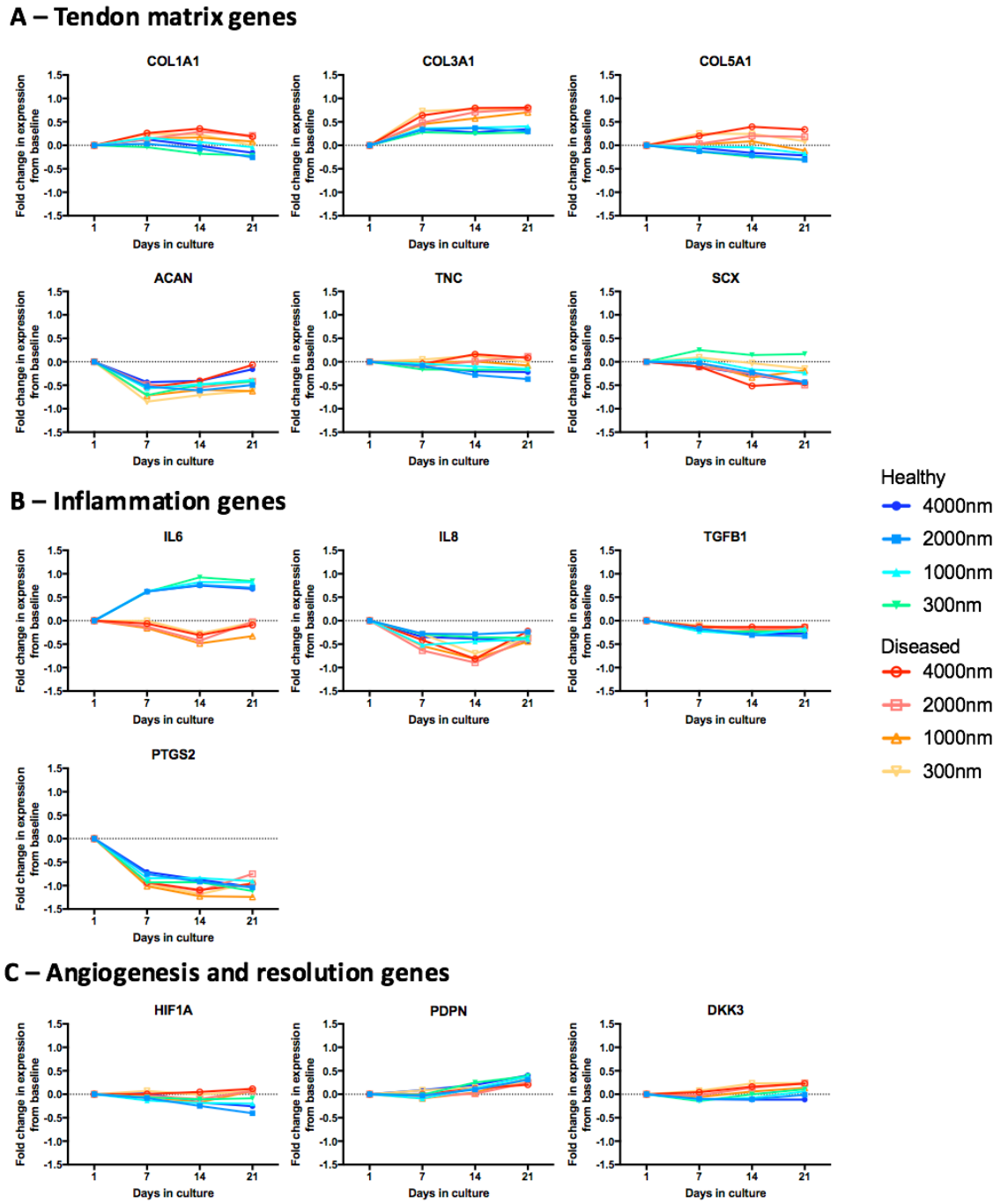


Figure B-3. Gene expression changes for tendon fibroblasts from healthy and diseased tendon cultured for 21 days on different diameter electrospun scaffolds.

Longitudinal data to supplement Figure 3-11, highlighting as discussed firstly, the consistent temporal trends in changes in expression out to 14 days culture, secondly, the differential response between tendon fibroblast populations derived from healthy and diseased tendon, and thirdly, the relatively small effect of mean fibre diameter over the 300nm to 4000nm aligned scaffolds tested. Mean fold change in expression from 24 hours at various time points, Log10 scale.

B.5 Accutase lifting efficacy of PBMCs from electrospun scaffolds

To investigate the effects of Accutase on cell lifting, 8 scaffolds were prepared and seeded and handled as described in section 3.5.5 (Peripheral Blood Mononuclear Cell response to electrospun scaffold diameter) with serum from a single patient (male, 30 years old). After 1 hour for cell adherence, scaffolds were incubated in 2250ul of 10% AlamarBlue in cRPMI for 2 hours. 4 scaffolds then underwent the lifting treatment with Accutase. The remaining 4 scaffolds were washed in the same way with 1ml warmed PBS replacing the Accutase. The AlamarBlue assay was performed again 24 hours after the initial lifting.

The Accutase lifting protocol reduced the fluorescence of scaffolds seeded with PBMC populations to 31% of the original value. Treatment with a control solution (PBS instead of Accutase) reduced this to 60% of the baseline fluorescence (Figure B-3). This was significantly different between the groups (p=0.0016). This data suggests nearly a third of the originally seeded PBMC population remained adherent to the scaffolds and not included in the flow cytometry analysis.

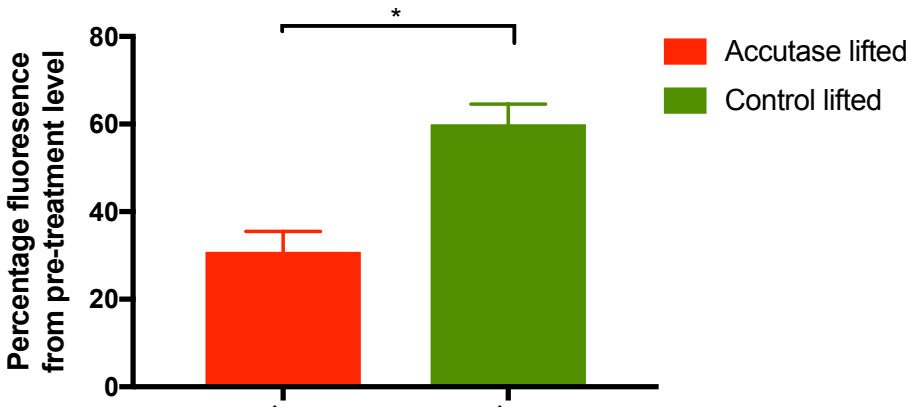


Figure B-4. Accutase lifting efficacy of PBMCs from electrospun fibre scaffolds.

Fluorescence for electrospun scaffolds subjected to cell lifting with active Accutase or a control solution as a percentage of the baseline fluorescence. There is a reduction in fluorescence in both conditions. In the control scaffolds, fluorescence dropped by 40%. In scaffolds treated with Accutase, fluorescence dropped by 70%. This difference was statistically significant (*). Mean fluorescence change and standard deviation from baseline.

C.1 Detailed information of mass spectrometry corona composition analysis

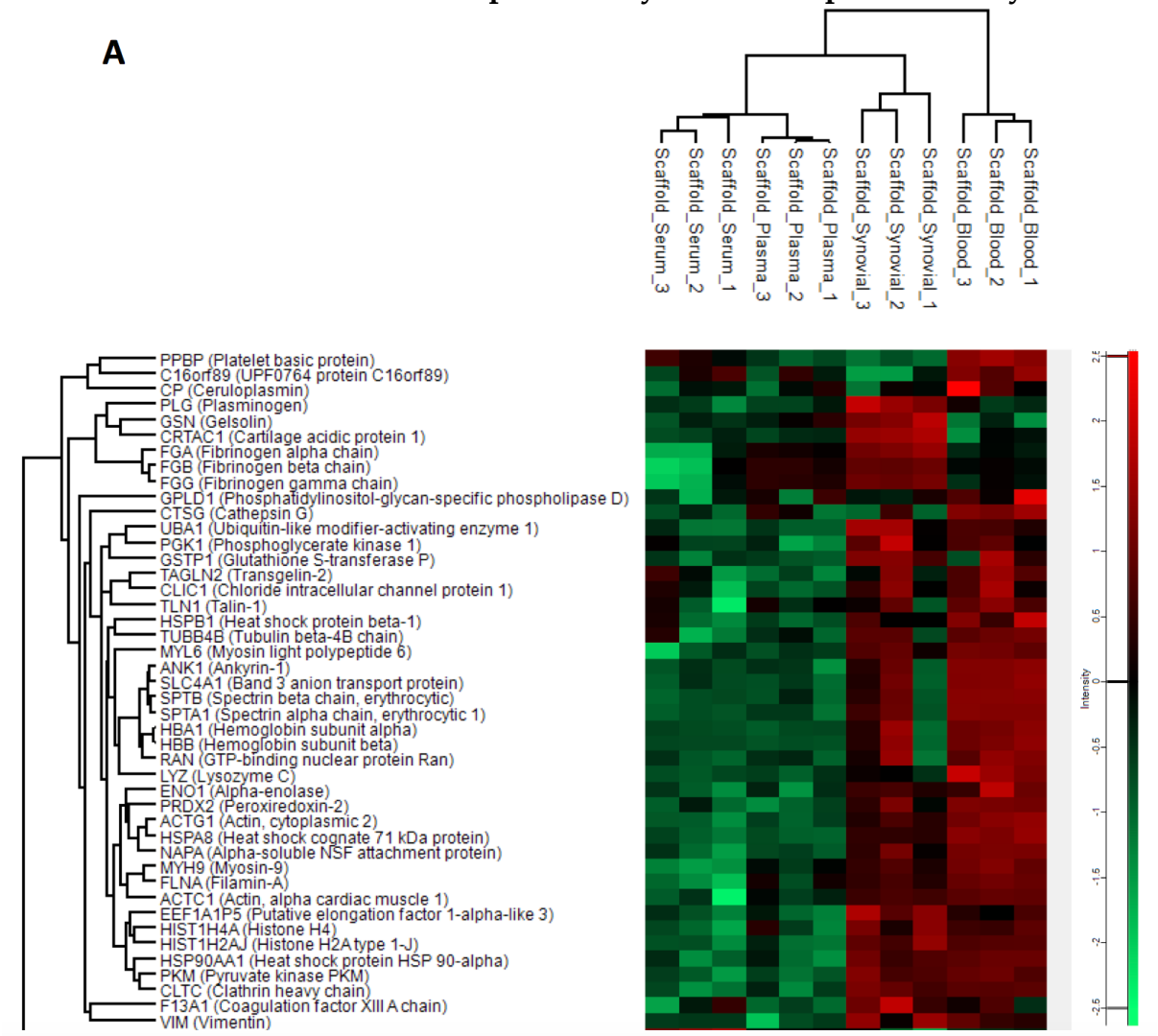


Figure C-1 (1/3). Heat map of proteins detected at significantly different intensities in the coronas formed through treatment of electrospun scaffolds in biological fluids.

This heat map shows the 125 proteins present at statistically different intensities across the coronas formed from blood, serum, plasma and synovial fluid after adsorption on aligned, 1000nm scaffolds. These proteins separate in 3 patterns. Firstly, some proteins are relatively enriched while others are relatively depleted. Secondly, the proteins in serum and plasma coronas display more consistent intensities compared to synovial fluid or blood. Thirdly, the differences in intensity between the 3 synovial fluid coronas is the most heterogeneous of the 4 fluid types. Log10 scale, with red indicating increased abundance and green reduced abundance.

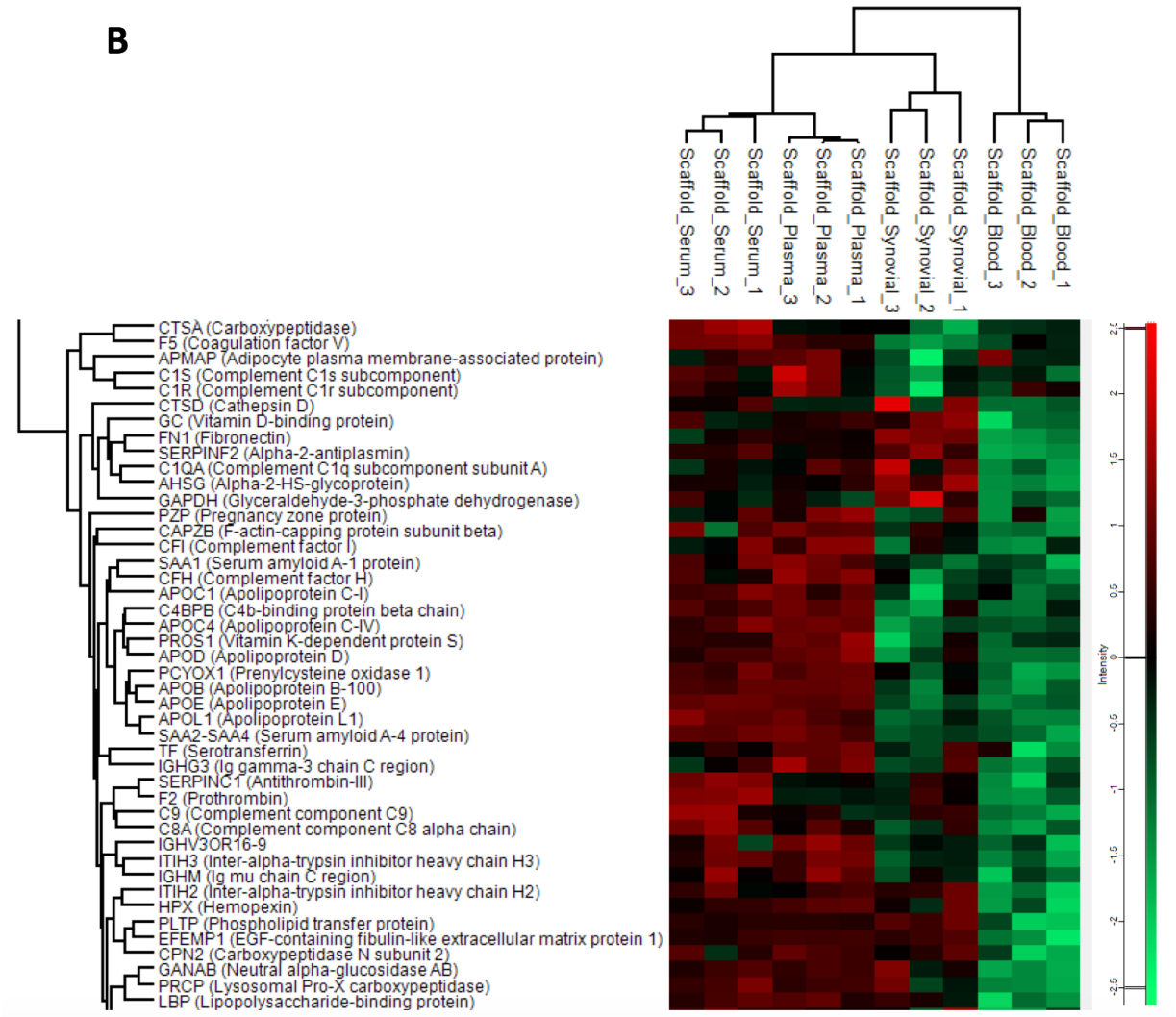


Figure C.1 continued (2/3).

C

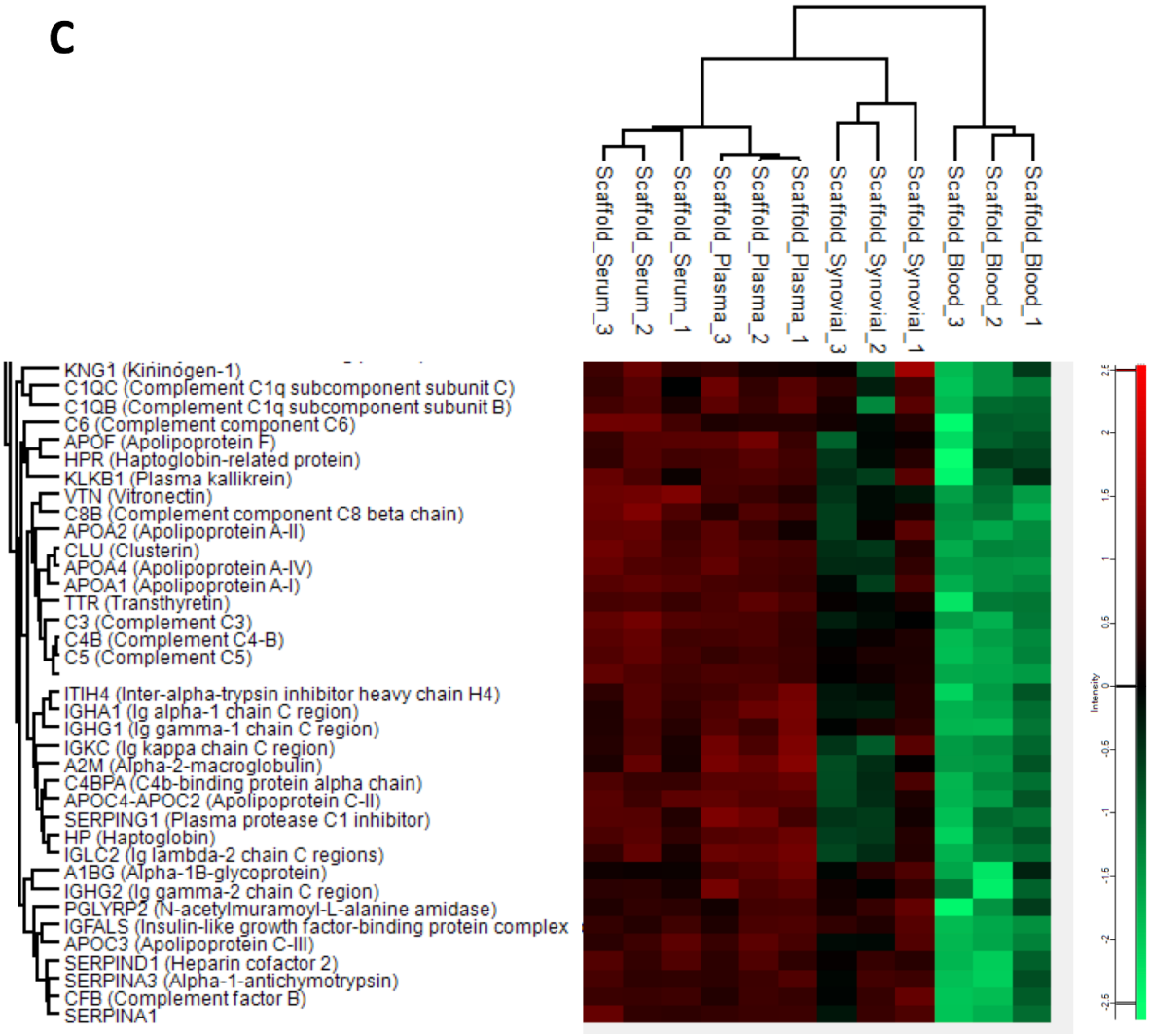


Figure C.1 continued (3/3).

C.2 Functionalisation effects on immune cell population gene expression

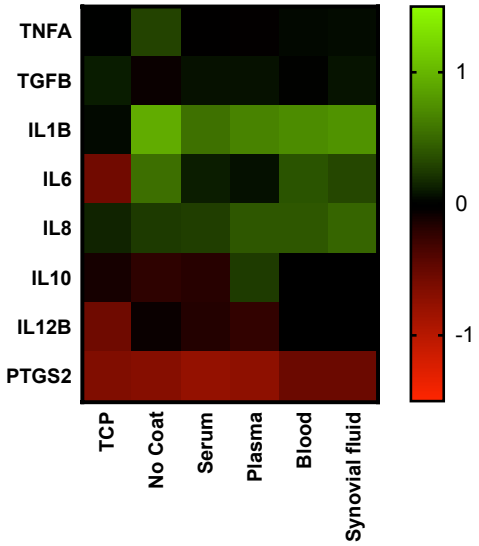


Figure C-2. Fold changes in gene expression of PBMCs cultured on electrospun scaffolds functionalised with biological fluids for 4 hours.

PBMC change in gene expression after 4 hours culture on electrospun scaffolds functionalised with blood, serum, plasma and synovial fluid, untreated scaffolds or TCP. This figure shows changes similar to those described after 24 hours culture and explained in detail in Figure 4-11. Mean fold change at 4 hours from time of seeding, log10 scale.

Appendix D List of suppliers

10cm dishes - Griener, Frickenhausen, Germany
24 well plate - Corning Inc, Corning, NY, USA

AC160TS probe - Olympus, Japan
Accutase - ThermoFisher Scientific, Waltham, MA, USA
AlamarBlue - Invitrogen, Paisley, UK
Alexa Fluor ™ 488 Phalloidin - ThermoFisher Scientific, Loughborough, UK
Aluminium stubs - Agar Scientific, Essex, UK
Applied Biosystems ViiA7 system - Life Technologies, Carlsbad CA, USA
AutoPore IV 9500 mercury porosimeter - Micromeritics Instrument Co, Norcross, GA, USA

BD LSRFortessa – BD Biosciences, Berkshire, UK

Carbon tape - Agar Scientific, Essex, UK
Cell crowns - Scaffdex, Tampere, Finland
Cell staining buffer - Biolegend, London, UK
Chamber slides - Lab-Tek, ThermoFisher Scientific, Waltham, MA, USA

DAPI - Molecular Probes, Eugene, OR, USA
Dionex Ultimate 3000 nano-UPLC with an EASY-Spray column - ThermoFisher Scientific, Waltham, MA, USA
Direct-Zol RNA Microprep kit - Zymo Research, Irvine, CA, USA
DMEMF-12 - Lonza, Slough, UK
DNAse - ThermoFisher Scientific, Loughborough, UK

Ethicon PDO suture – Johnson & Johnson Medical N.V., Beerse, Belgium
EVO LS15 SEM- Zeiss, Oberkochen, Germany

Fast SYBR Green Master Mix - Applied Biosystems, Waltham, MA, USA
Fetal Bovine Serum - Labtech, Uckfield, UK
FluoStar Optima microplate reader - BMG Labtech, Ortenberg, Germany

geNorm House Keeper Selection Kit – Primer Design, Southampton, UK

HFIP - Apollo Scientific Ltd, Cheshire, UK
High Capacity cDNA Reverse Transcription Kit - Applied Biosystems, Waltham, MA, USA
Histopaque 1077 - Sigma Aldrich, Dorset, UK

IME electrospinning machine - IME Technologies, Spaarpot, the Netherlands

L-glutamine - ThermoFisher Scientific, Waltham, MA, USA

Lo Pind eppendorfs - Eppendorf AG, Hamburg, Germany
LSM710 confocal microscope - Carl Zeiss AG, Oberkochen, Germany

MFP-3D Atomic Force Microscope - Asylum Research, High Wycombe, UK

ND1000 Nanodrop - Nanodrop Technologies, Willington, DE, USA

Orbitrap Fusion Lumos TriBrid Mass Spectrometer - ThermoFisher Scientific, Waltham, MA, USA

Penicillin-streptomycin - ThermoFisher Scientific, Waltham, MA, USA
PDO
- Riverpoint Medical, Portland, OR, USA
- Evonik Nutrition and Care GmBH, Essen Germany
- Polymed, Anderson, SC, USA

PHD 2000 syringe pump - Harvard Apparatus, Kent, UK
Phosphate Buffered Saline – Sigma Aldrich, Dorset, UK
Primer Design primers - Primer Design, Southampton, UK
Pyridine – Sigma-Aldrich, Dorset, UK

RPMI-1640 - Sigma Aldrich, Dorset, UK

Q2000-1275 Differential Scanning Calorimeter - TA Instruments, Hertfordshire, UK
QuantiTect primers - Qiagen, Hilden, Germany

SC7620 Mini Sputter Coater - Quorum Technologies, Laughton, UK
SevenCompact S230/InLab741 ISM probe - Mettler Toledo, Leicester, UK
Sigma custom primers - Sigma Aldrich, Dorset, UK
SOLA C18 HRP desalting cartridges - ThermoFisher Scientific, Waltham, MA, USA

TC20 automated cytometer - Bio-Rad, Hertfordshire, UK
Trypsin - Promega, Southampton, UK
Triton-X - ThermoFisher Scientific, Loughborough, UK
TRIzol - Invitrogen, Paisley, UK
TZero aluminium pans - TA Instruments, Hertfordshire, UK

ViscoPad R viscometer - Fungilab, Barcelona, Spain